The Modulation of Tau Aggregation in a Cell Model of Alzheimer's Disease by the Proteasome Adaptor Protein NUB1

Emma Richet

A thesis submitted for the degree of Doctor of Philosophy

March 2012

University College London,

Institute of Ophthalmology

Declaration

I, Emma Richet, confirm that the work presented in this thesis is my own. Where information has been derived from other sources, I confirm that this has been indicated in the thesis.

Abstract

Neurofibrillary tangles (NFT) in Alzheimer's disease (AD) are mainly composed of hyperphosphorylated and aggregated wild-type tau. NFTs are decorated by the ubiquitin-like modifier NEDD8, a protein targeted for proteasomal degradation by the NEDD8 Ultimate Buster 1 (NUB1). NUB1 has been shown to reduce synphilin-1 positive inclusions in a model of Parkinson's disease. Therefore, this study examined the subcellular localisation of NUB1 as well as the effect of NUB1 on tau phosphorylation and aggregation. Furthermore, the effect of reducing NUB1 expression by RNA interference was investigated.

Brain sections from AD patients showed that NUB1 and NEDD8 were expressed in the pyramidal neurons of the hippocampus, where the accumulation of NFTs is most abundant. In rat primary cortical neurons, NUB1 and tau co-localised in neurites and signalling structures such as varicosities, suggesting a functional interaction between them. The upregulation of the tau kinase GSK3β in AD leads to increased tau hyperphosphorylation and accumulation. In SK-N-SH neuroblastoma cells, which lack endogenous tau, ectopic wild-type tau formed inclusions when it was co-expressed with GSK3β, and this was enhanced by proteasome inhibition. NUB1 co-localised with both tau and GSK3β and significantly reduced tau inclusion formation. In neuroblastoma cells, NUB1 could interact with both tau and GSK3β, disrupt their interaction, and decrease the GSK3β-dependent phosphorylation of tau. NUB1 can directly bind synphilin-1 and induce its proteasomal degradation. Therefore, the ability of NUB1 to regulate GSK3β degradation was investigated in neuroblastoma cells. The upregulation of NUB1 accelerated the turnover of GSK3β, and the ubiquitin-associated (UBA) domains of NUB1 were necessary for NUB1 to exert its effect. Conversely, the downregulation of endogenous NUB1 by RNA interference increased the stability of endogenous GSK3β. Thus, NUB1 might have a role in tau inclusion formation by modulating GSK3β levels.

Acknowledgements

I am most grateful to my supervisor, Dr. Jacqueline van der Spuy, for her great support, patience and advice. I am thankful she trusted me enough to give me the opportunity to work on such an interesting project, when I thought “ASAP” was a new laboratory technique. I would like to thank Prof. Mike Cheetham for his great ideas and advice, and Prof. Alison Hardcastle who brilliantly encouraged me for the past three years.

I would like to thank Dr. Diane Hanger and Dr. Marcus Groettrup, who provided essential reagents for this study. I am most grateful to Dr. Teresa Rodriguez and Dr. Amy Pooler, who helped, advised and supported me when I was working at the Institute of Psychiatry.

I am tremendously grateful to all my co-workers, past and present, in particular Dr Monica Aguila, with whom I shared the best of my time inside and outside the laboratory and who never let me down, and Naheed Kanuga, always helpful and comforting. I am delighted to have worked with the great post-docs Dr. John Bett, Dr.Nele Schwarz and Dr. Sergey Novoselov who happily shared their knowledge and never missed an occasion to laugh, and with Dr. David Parfitt and Dr. Caroline Mc Culley who never got tired of my questions about the secrets of the English language. And of course, I am thankful to my co-partners in PhD, Dimitra Athanasiou and Dalila Bevilacqua, who patiently listened to my complaints and to whom I wish the best.

I would like to thank all my friends and family for their unforgettable support and for pushing me when I felt the lowest. I cannot thank enough Amy, Alessia and Monica, who made my time in London an amazing experience. I would also like to thank Vivien, Sarah, Sam, and Nick for their support and incredible friendship.

Je continuerai en français, pour exprimer toute ma gratitude au Dr.Carole Kretz et à son équipe, qui m'a donné le goût de la Science et sans qui je n'aurais jamais pu faire cette thèse. Un immense merci à toute la bande Apoptose, Sacha, Emma, Béa, Yves, Quentin, Chris et Julien, dont les cris de ralliements «Schmou» résonnent encore à mes oreilles et me donne l'envie de continuer. Un grand merci à tous mes amis en France, particulièrement à Marie, Jeanne et Manale, qui sont venues plusieurs fois me faire sourire et me remonter le moral. Je ne remercierai jamais assez ma famille, ma sœur, sans qui je n'aurais pas été une Londonienne avertie, et mon frère, pour son altruisme et son aide plus que bienvenue. Et enfin, je remercie chaleureusement mes parents pour leur aide précieuse, mon père, pour les longues heures à discuter Science et Médecine, et ma mère, pour son soutien incommensurable tout au long de ce long voyage.

Dedication

This thesis is dedicated to my two grandmothers, who suffered from dementia.

Table of contents

List of figures

List of tables

List of abbreviations

AB: Antibody

Aβ: Amyloid-β

AD: Alzheimer's disease

ADAS-Cog: Alzheimer disease assessment scale cognitive

ADP: Adenosine diphosphate

AICD: APP intracellular domain

ALS: Amyotrophic lateral sclerosis

APP: Amyloid precursor protein

APP-BP1: Amyloid precursor protein-binding protein 1

APS: Ammonium persulphate

AR-JP: Autosomal recessive juvenile Parkinsonism

ATP: Adenosine triphosphate

Atx-3: Ataxin-3

BACE: β-site APP cleavage

BCA: Bicinchonitic acid

BO: Beads only

BTS: Blessed test score

BSA: Bovine serum albumin

CaMKII: Calcium/calmodulin-dependent protein kinase II

CAND-1: Cullin-associated and neddylation dissociated-1

CBD: Corticobasal dementia

CDK: Cyclin-dependent kinase

CDR: Clinical dementia rating

CHIP: Carboxy terminus of HSC70-interacting protein

CHX: Cycloheximide

CK1: Casein kinase 1

CNS: COP9 signalosome

CMA: Chaperone-mediated autophagy

CSF: Cerebrospinal fluid

CJD: Creutzfeld-Jacob disease (Prion diseases)

CRL: Cullin-RING E3 ubiquitin ligases

CT: Computer tomography

CUL: Cullin

DAB: 3,3-diaminobenzidine tetrahydrochloride

DAPI: 4',6-diamidino-2-phenylindole

DIV: Days in vitro

DMEM: Dubbelco's modified eagle's medium

DMSO: Dimethyl sulfoxide

DUB: Deubiquitinating enzyme

DYRK1A: Dual specificity tyrosine-phosphorylation-regulated kinase 1A

E: Glutamic acid

EDTA: Ethylenediaminetetraacetic acid

EEG: Electroencephalography

EGTA: Ethylene glycol-bis(2-aminoethylether)-N,N,N′,N′-tetraacetic acid

EPO: Epoxomicin

ER: Endoplasmic reticulum

FAD: Familial AD

FALS: Familial ALS

FAT10 (Ubiquitin D, di-ubiquitin like): F-adjacent transcript 10

FBS: Foetal bovine serum

fMRI: Functional MRI

FTD: Frontotemporal dementia

FTDP-17: Frontotemporal dementia and parkinsonism linked to chromosome 17

FTLD: Frontotemporal lobar degeneration

FRAP: Fluorescence recovery after photobleaching

GDP: Guanosine diphosphate

GSK3: Glycogen synthase kinase 3

GTP: Guanosine triphoshate

HBSS: Hank's balanced salt solution

HBD: Heparin-binding domain

HD: Huntington’s disease

HECT: Homologous to E6-associated protein C terminus

HRP: Horseradish peroxidase

HS: Heat shock

HSP: Heat shock protein

Htt: Huntingtin

ICC: Immunocytochemistry

IDE: Insulin degrading enzyme

IHC: Immunohistochemistry

IMS: Industrial methylated spirit

IP: Immunoprecipitation

IPOD: Insoluble protein deposit

JNK: C-Jun N-terminal kinase

JUNQ: Juxtanuclear quality control

K: Lysine

KO: Knock-out

LCA: Leber congenital amaurosis

LAC: Lactacystin

LB: Luria-Bertani broth

LOAD: Late-onset AD

Lys: Lysine

N/A: Non applicable

M: Mander's coefficient

MARK: Microtubule-affinity regulating kinases

MAP: Microtubule-associated protein

MAPK: Mitogen-activated protein kinases

MBD: Microtubule-binding domain

MCI: Mild cognitive impairment

MG132: Z-Leu-Leu-Leu-al

MMSE: Mini-mental state examination

MonoUb: Monoubiquitin

MRI: Magnetic resonance imaging

MTOC: Microtubule organising centre

NAE: NEDD8 activating enzyme

NEDD8: Neural precursor cell expressed, developmentally down-regulated 8

NEP: Neprisylin

NES: Nuclear export sequence

NFT: Neurofibrillary tangles

NLS: Nuclear localisation signal

NPC: Nuclear-pore complex

NT: Neuropil threads

NUB1: NEDD8-ultimate buster 1

OA: Okadaic acid

O/N: Overnight

PBS: Phosphate buffered saline

PC: Pearson's coefficient

PD: Parkinson's disease

PDPK: Proline-directed protein kinase

PEM: Pipes/EGTA/$MgCl_2$ buffer

PET: Positron emission tomography

PFA: Paraformaldehyde

PHF: Paired-helical filament

PhIC: Phosphatase inhibitor cocktail

PiD: Pick's disease

PIC: Protease inhibitor cocktail

PIM: Proteasome interacting motif

PK: Protein kinase

PKA: cAMP-dependent protein kinase

PKC: Protein kinase C

PLC-γ: Phospholipase C-γ

PolyUb: Polyubiquitin

PolyQ: Polyglutamine

PP1/2A/5: Protein phosphatase 1, 2A and 5

Pro, P: Proline

PrP: Prion protein

PSMD4: Proteasome subunit non-ATPase 4, also called S5a

PS1, 2: Presenilin 1, 2

PSP: Progressive supranuclear palsy

RING: Really interesting new gene

ROS: Reactive oxygen species

RT: Room temperature

SCA-3: Spinocerebellar ataxia type 3

SCF: Skp1-Cullin-F-box

SDS: Sodium monododecyl sulphate

SDS-PAGE: Sodium dodecyl sulphate-polyacrylamide gel electrophoresis

SEM: Standard error of the mean

Ser, S: Serine

SF: Serum free media

siRNA: small interfering RNA

SNP: Single nucleotide polymorphism

SQSTM1: Sequestosome 1 (also called p62)

SR: Serum rich media without antibiotics

SRK: Src-family non-receptor tyrosine kinase

Thr, T: Threonine

Ub: Ubiquitin

UBQLN1/2/3: Ubiquilin1,2 and 3

UCH-L1: Ubiquitin carboxy-terminal hydrolase

UBA: Ubiquitin-associated domain

UBD: Ubiquitin-binding domain

UBL: Ubiquitin-like domain

UDP: UBL-domain proteins

ULM: Ubiquitin-like modifier

UIM: Ubiquitin-interacting motif

UPR: Unfolded protein response

UPS: Ubiquitin-proteasome system

USE1: UBA6-specific E2 enzyme

WB: Western blotting, western blot

Tyr, Y: Tyrosine

Chapter 1
Introduction

1.1. Alzheimer's disease

Dementia is described as a severe impairment of cognitive abilities, which often correlates with ageing. The most common dementia is Alzheimer's disease (AD), discovered in 1907 by Alois Alzheimer, who identified two histopathological hallmarks, neurofibrillary tangles (NFTs) and Amyloid-β (Aβ) plaques, in patients brains affected with the disorder. About 24 million people worldwide are affected by AD, and this number is expected to more than triple by 2040 (Reitz *et al.*, 2011). Therefore, AD is a universal therapeutic challenge. The pathological and molecular mechanisms have been thoroughly studied for the last century, yet the causes and consequences of the disease are not fully understood (Ballard *et al.*, 2011).

1.1.1. Epidemiology, symptoms and diagnosis

1.1.1.1. Epidemiology

Dementia is particularly difficult to classify and to differentiate between neurodegenerative disorders. However, ~ 70% of cases of dementia are thought to be caused by AD. The highest prevalence of people developing AD is in North America, Western Europe and China. AD occurs mainly as a sporadic late-onset disease (LOAD), but also as an early-onset familial disorder (FAD) in less than 10% of cases. Currently, AD diagnosis can only be certain post-mortem with the detection of NFTs and Aβ plaques (Ballard *et al.*, 2011).

1.1.1.2. Symptoms and diagnosis

Cognitive tests. Early symptoms of cognitive decline include deficient memory, language breakdown and disorientation. Cognitive decline is always combined with behavioural changes (social withdrawal, agitation), and often with

depression, anxiety, apathy, insomnia and paranoia (Hort *et al.*, 2010, http://www.aafp.org/afp/2001/0215/p703.html). After detection of the first symptoms, the most common cognitive test physician's use is the Mini-Mental State Examination (MMSE), although it cannot accurately diagnose dementia. To further assess cognitive decline, other tests, such as the Alzheimer Disease Assessment Scale Cognitive (ADAS-Cog) or Blessed test can be performed (www.alzheimersresearchuk.org; www.alzforum.org). With good cognitive tests, it is possible to determine whether the patient is suffering from dementia or not. However, it is still very difficult to precisely diagnose the type of dementia. Therefore, depending on the score, the patient will be subjected to further analysis, such as brain scans, tests for biomarkers in blood and cerebrospinal fluid (CSF) or electroencephalography (EEG) (Hort *et al.*, 2010).

Scans and imaging. Magnetic Resonance Imaging (MRI) or Computer Tomography (CT) brain scans can be used to detect brain shrinkage, hippocampal atrophy, and vascular changes, but are not considered specific markers for AD. Changes in brain cognitive activities occur in AD, and can be measured with a functional MRI (fMRI). However, cognitive abilities are not secluded to one part of the brain, and the impairment of one region of the brain might be compensated by others, thus rendering the diagnosis more difficult to make (Hort *et al.*, 2010; Hampel *et al.*, 2011).

Other diagnostic techniques. A promising way of diagnosing AD might be the analysis of CSF and plasma components. The difficult diagnosis of AD has raised an intensive search for potential early biomarkers of the disease present in the blood and the CSF. Other methods used to diagnose AD include Positron Emission Tomography (PET). However, even with the numerous diagnostic methods available, there is still a pressing need to accurately distinguish between the different dementias in order for the treatment to target the right abnormalities. Nevertheless, great progress has been made in AD diagnostic assessments, providing valuable information on the disease progression.

AD is still an incurable neurodegenerative disease. Neuronal death in the hippocampus and the limbic system induce memory loss and language disorder, before the disease spreads to the neocortex (also called isocortex)

and eventually leads to death. AD is an amyloid-associated disorder, in that it is characterised by the abnormal accumulation of protein in β-cross fibrils, also typified by other neurodegenerative disorders including the Prion diseases (CJD), Parkinson's disease (PD) and Huntington's disease (HD) (Duyckaerts *et al.*, 2009; Finder 2010; Ballard *et al.*, 2011).

1.1.2. Amyloid-β

1.1.2.1. Amyloid-β Precursor Protein

Aβ is produced by the cleavage of the Amyloid Precursor Protein (APP). APP is a transmembrane protein with a large extracellular domain (ectodomain) containing two heparin-binding domains (HBD) and a single small membrane spanning domain, formed by a hydrophobic α-helix (Multhaup, 2006). Alternative splicing of the APP transcript results in 8 different isoforms of the protein, 3 of which are the most highly expressed: the 695, 751 and 770 forms (O'Brien and Wong, 2011). APP is largely expressed in the brain, particularly in neurons where it is recruited to the presynaptic membrane (Wilquet and De Strooper, 2004; Zheng and Koo, 2006). Unexpectedly, the physiological role of APP is not yet known, although it has been reported to be involved in axonal growth, synaptic transmission, reactive oxygen species (ROS) detoxification and mitochondrial dysfunction. With respect to a role for APP in synaptic transmission, APP is recruited to the synapses, secreted APP levels correlate with synaptogenesis, and APP binding with Fe65 appears to be important for growth cone dynamics and cell motility. Another potential role for APP is in cell signalling, as APP is structurally similar to the receptor Notch. Like Notch, APP is also cleaved and produces an intracellular domain (AICD) and an extracellular fragment (Zheng and Koo, 2006).

1.1.2.2. Amyloid-β peptide formation

APP undergoes proteolytic cleavage following two pathways, the non-amyloidogenic pathway, which involves the α-secretase, and the amyloidogenic pathway, which involves the β-secretase (Figure 1.1). The first truncation by the α-secretase, a member of the ADAM metaloprotease family, cuts APP into the extracellular soluble sAPPα fragment, and the C83 fragment, which remains in

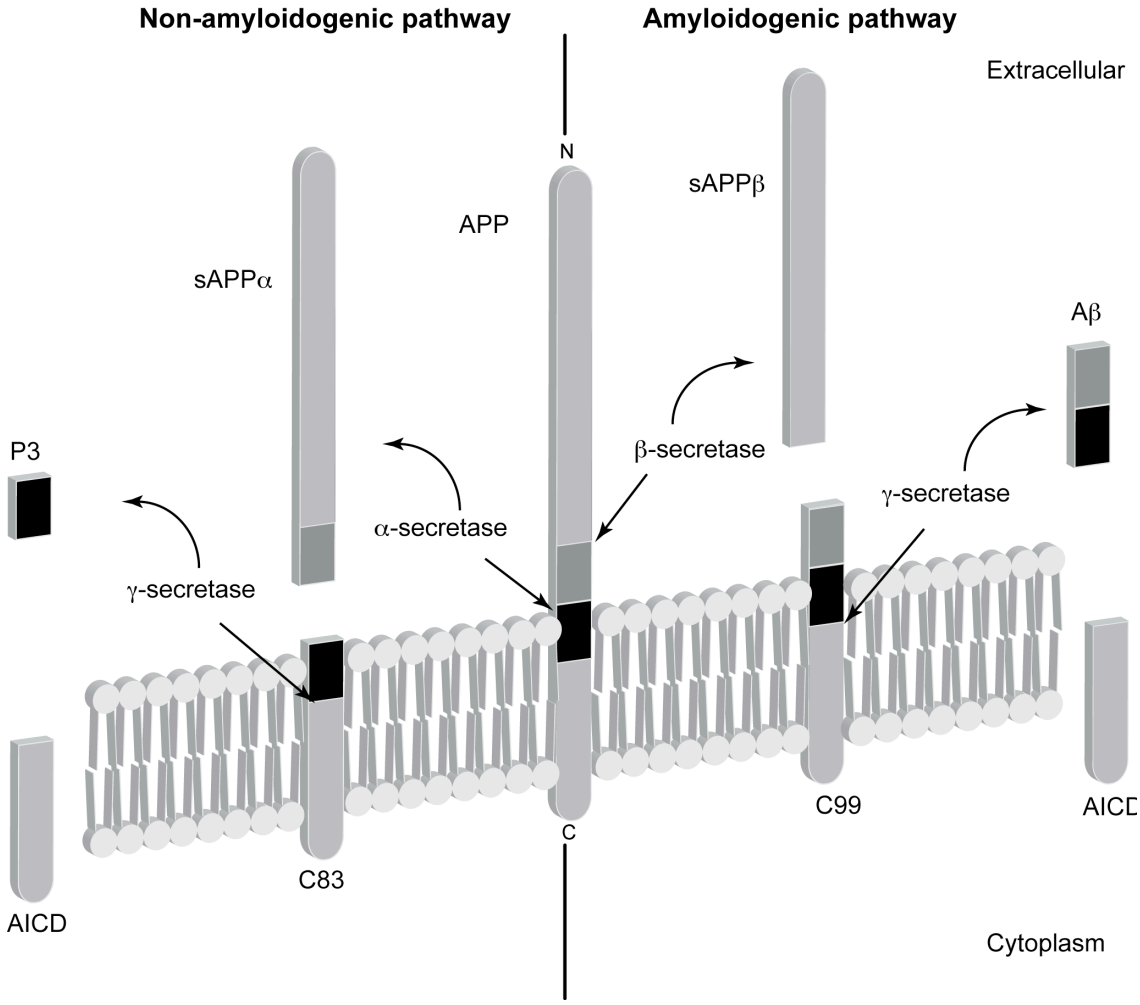

Figure 1.1. *APP processing*. APP is cleaved by α, β and γ secretases following two mechanisms: the non-amyloidogenic and amyloidogenic pathways. Only the amyloidogenic pathway, involving the β and γ secretases, produces Aβ.

the plasma membrane. The neuronal β-secretase is called BACE1 for β-site APP cleavage 1, and produces an extracellular fragment, sAPPβ, and an intramembrane fragment, C99. The γ-secretase, a complex of proteins that includes presenilin (PS) (Wilquet and De Strooper, 2004; Zheng and Koo, 2006; O'Brien and Wong, 2011), cleaves the C83 and C99 intramembrane fragments. PS mutation has been shown to be responsible for most of the familial forms of AD (Reitz *et al*., 2011). C83 cleavage produces an APP intracellular domain (AICD) and a short fragment called P3 (3 kDa), whereas C99 truncation produces the AICD and a range of Aβ, a peptide from 38 to 44 kDa. The $A\beta_{40}$ and $A\beta_{42}$ fragments are the most extensively studied, as both have been shown to accumulate in Aβ plaques. Although APP KO mice develop age-dependent cognitive impairment, they do not exhibit hippocampal neuron or synapse loss.

Thus, it implies that the increased neuronal death and synaptic dysfunction observed in the hippocampus of AD patients is probably a result of abnormal APP processing into Aβ rather than a loss of function of APP (Phinney *et al.,* 1999). Indeed, neurons exposed to Aβ die in 24h, with $A\beta_{42}$ as the most toxic form (LaFerla *et al.*, 2007). Aβ is normally degraded by enzymes, including the insulin degrading enzyme (IDE) and neprilysin (NEP). One hypothesis in Aβ accumulation is that NEP can be easily overwhelmed by Aβ production as it is rate-limiting in the brain (Wang YJ *et al.*, 2006).

1.1.2.3. Aβ accumulation

Aβ is the main component of senile plaques (Finder, 2010; Bugiani *et al.*, 1989). Aβ deposits can also occur with normal ageing in the absence of dementia, and in individuals with mild cognitive impairment (MCI) or with Down's syndrome. Normally undetectable in young adult brains, the production of Aβ appears to be the result of 2 imbalances: the increase of the amyloidogenic pathway over the non-amyloidogenic pathway, and the dysregulation of the production/clearance of the Aβ.

According to Braak staging, amyloid deposits are first found in the basal layers of the neocortex (stage A), then progress to the neocortex excluding the primary cortices (the hippocampus, for instance, is free of deposit) (stage B), and finally reach all parts of the neocortex (stage C) (Braak and Braak, 1991). Other Aβ progression schemes have been described which take into account other parts of the brain besides the cerebral cortex, for example the eventual deposition of Aβ in the cerebellum (Thal *et al.*,2002). Senile plaques are composed of a focal deposit of Aβ, surrounded by a corona, containing astrocytic and neuritic components. Aβ plaques can be decorated by lipids that include cholesterol and several proteins such as Apolipoprotein E, a ligand in receptor-mediated endocytosis of lipoprotein, of which the allele ε4 remains the principal genetic risk factor in the sporadic form of AD (Reitz *et al.*, 2011; Duyckaerts *et al.*, 2009; Selkoe 2001, Selkoe 2011). Although most Aβ deposits described are the senile plaques, diffuse and focal Aβ accumulations can also be observed.

1.1.3. Tau

In the middle of the 1970's, Weingarten *et al.* described a new protein that promotes microtubule assembly, which they called tau. It is the presence of the microtubule-binding domain (MBD) and a projection domain that defines tau as a microtubule-associated protein (MAP) (Dye *et al.*, 1993). Tau belongs to the MAP2/tau protein sub-family, the most abundant MAP family in the neuronal system (Kanai and Hirokawa, 1995; Dehmelt and Halpain, 2005).

1.1.3.1. Tau protein

Tau gene and protein isoforms. The single tau gene is located on chromosome 17 and is composed of 16 alternatively spliced exons generating six different isoforms of tau, which range from 352 to 441 amino acids (aa) (Goedert *et al.*, 1989; Hernandez *et al.*, 2008; Morris *et al.*, 2011; Buee *et al.*, 2000). The insertion of one or two 29 amino acid regions in the N-terminus occurs as a result of the alternative splicing of exon 2 and 3 (called N), whereas the presence of exon 10 produces an additional repeat region (called R) (Figure 1.2, A). Therefore, the tau isoforms are divided into two main groups, with 3 (3R) or 4 (4R) repeat regions respectively, which in turn possess 0 (0N3R/0N4R), 1 (1N3R/1N4R) or 2 (2N3R/2N4R) N-terminal insertions (Figure 1.2, A). All six isoforms are expressed in the adult brain, but only the 0N3R isoform is found at the foetal stage. Some particularly long and large axons in the spinal chord and retina possess an unusual splicing form of exon 4, called exon 4A (Georgieff *et al.*, 1993). Tau protein is composed of 4 main domains, the N-terminus, a proline rich domain, a microtubule-binding domain (MBD) also called the repeat domain region and a C-terminus (Figure 1.2, B).

Tau localisation. Tau is mainly expressed in neurons, (Trojanowski *et al.*, 1993; Kanai and Hirokawa, 1995; Dehmelt and Halpain, 2005), although it can be found in pancreatic cells (Vanier *et al*., 1998) and fibroblasts (Ingelson *et al*., 1996) in humans, in heart, skeletal muscle, lung and kidney in rats (Gu *et al*., 1996) and in oligodendrocytes in rats and mice (Muller *et al*., 1997; Klein *et al.,* 2002). In neurons, tau localisation is mostly axonal, whereas MAP2, another member of the MAP2/tau family is essentially found in the cell body and dendrites (Trojanowski *et al.*, 1993; Kanai and Hirokawa, 1995). However,

studies suggest that tau is also localised in the dendrites and synapses (Ittner *et al.,* 2010). Moreover, tau has been described to be recruited to organelles, the plasma membrane and in lipid-rich microdomains, important platforms for cell signalling (Brandt *et al.,*1995; Farah *et al.*, 2006; Rendon *et al*., 1990; Pooler and Hanger, 2010).

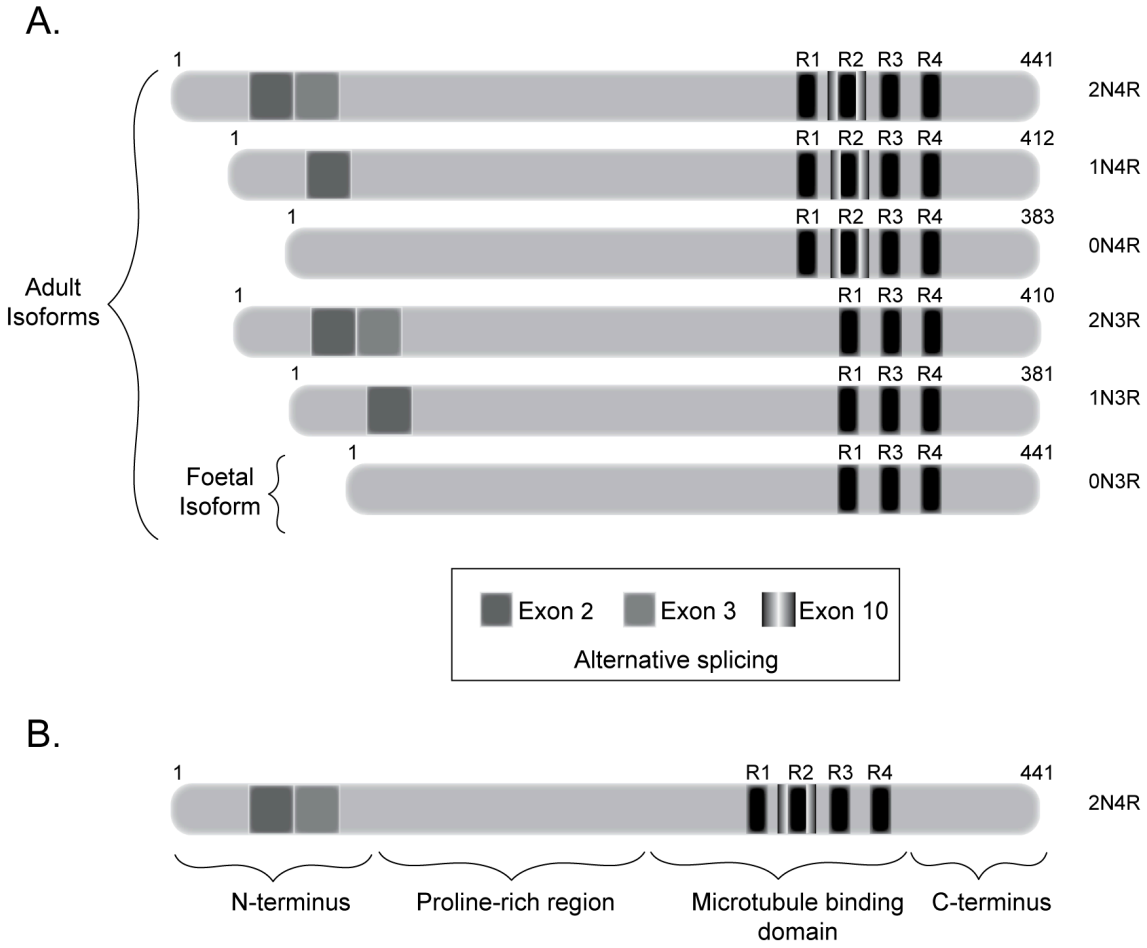

Figure 1.2. *Tau splicing and domain structure*. (A) The alternative splicing of exon 2 and 3 in the N-terminus and exon 10 in the C-terminus generates 6 different isoforms of tau, all expressed in adult brain. Exon 3 is always spliced with exon 2. The splicing of exon 10 produces an extra repeat region (R2), important for binding microtubules. (B) Tau protein is composed of 4 main domains, the N-terminus, the proline-rich region, the microtubule-binding domain (MBD) and the C-terminus. The N-terminus and the proline-rich region comprise the projection domain.

1.1.3.2. Tau domains and function

Microtubule-binding domain (MBD). Tau longitudinally decorates the microtubule protofilaments via its MBD domain, with its N-terminus projecting outward. In this arrangement, tau increases the rigidity of the microtubules by bridging the protofilaments (Hirokawa *et al.*, 1988; Al-Bassam *et al.*, 2002).

Interestingly, the MBD interacts directly with protein phosphatase 2A (PP2A), which is involved in tau regulation via its dephosphorylation. The repeat regions are also important for binding PS1 (Takashima *et al.*, 1998).

Projection domain. With the MBD attached to the microtubules, the rest of the N-terminus of the tau protein, including the proline-rich region, acts as a projection domain. The projection domain of tau regulates the spacing between microtubules and therefore, is an important modulator of axon diameter. The MAP projection domains, highly variable in length and rather small in the tau family, are thought to interact with proteins and other cell components (Feng and Walsh, 2001). The N-terminal region of tau interacts with the plasma membrane, organelles such as mitochondria and Golgi, and components of the cytoskeleton, including actin (Buee *et al.*, 2000; Morris *et al.*, 2011; Pooler and Hanger, 2010).

The proline-rich domain of tau is able to interact with phospholipase C-γ (PLC-γ) and with the SH3 domain Src-family non-receptor tyrosine kinase (SRK), in particular the SRK Fyn (Morris *et al.*, 2011, Lee G., 2005). In the dendrites, tau binds Fyn and is important for the recruitment of Fyn to the post-synaptic sites (Ittner *et al.,* 2010), and particularly to the NMDA-receptor, a substrate for the Fyn kinase. Therefore, the presence of the proline-rich domain suggests that tau is implicated in cell signalling.

Other tau functions. By regulating microtubule polymerisation and stabilisation, tau is involved in neurite formation. Tau is necessary for the correct formation of the growth cones in neurons, and might link the microtubules and microfilaments of actin to allow neuronal growth (DiTella *et al.*, 1994). Another potential role for tau and MAP is to regulate cell trafficking. Tau overexpression has been shown to inhibit the transport of organelles in cells and to block the anterograde transport in axons (Ebneth *et al.*, 1998; Dubey *et al.*, 2008). The MAP, via its interaction with the microtubules, reduces the availability for motor molecules such as kinesin to bind the tubulin heterodimers. Therefore, it blocks the plus-end directed transport and, consequently, the retrograde transport is increased (Stamer *et al.*, 2002).

1.1.3.3. Tau Regulation

Tau activity is regulated by several post-translational modifications. Glycosylation, glycation and nitration sites have been found in the tau sequence, and tau truncation by caspases and calpain has been detected in AD and tauopathies. However the most studied and important regulatory mechanism for tau remains phosphorylation/dephosphorylation (Martin *et al*., 2011).

Tau phosphorylation. Tau phosphorylation regulates its interaction with the microtubules, and therefore, influences microtubule polymerisation, the outgrowth of neuronal processes and axonal transport Johnson and Stoothoff, 2004; Cuchillo-Ibanez *et al*., 2008). A single phosphorylation of tau in the MBD, for instance on residues Ser262 and Ser356 alone, or on residue Thr231 in the proline-rich domain can inhibit tau interaction with microtubules (Biernat and Mandelkow, 1999; Fischer *et al*., 2009; Sengupta *et al*., 1998; Cho and Johnson, 2003). Dysregulation of tau phosphorylation is a common characteristic of tauopathies and tau associated diseases, and tau hyperphosphorylation promotes tau aggregation.

Forty-five serines (Ser), 35 threonines (Thr) and 5 tyrosines (Tyr) have been identified as putative phosphorylation sites on tau (on the longest splicing isoform). Among these 85 sites, 45 have been shown to be phosphorylated in control and patients affected with AD (Hanger *et al*., 2009; Martin *et al*., 2011). Interestingly, most of the phosphorylation sites are found in the proline-rich domain and the C-terminus (Hanger *et al*., 2009).

Tau kinases. Numerous kinases have been described to phosphorylate tau and can be divided into three classes: the proline-directed protein kinases (PDPK), the non-PDPKs and the tyrosine specific kinases (Hanger *et al*., 2009; Martin *et al*., 2011). Glycogen synthase kinase 3 (GSK3) and cyclin-dependent kinase 5 (cdk5) play a major role in the phosphorylation of tau and have therefore been studied extensively, and together with the mitogen-activated protein kinases (MAPKs), c-Jun N-terminal kinase (JNK) and p38, are members of the PDPK family implicated in tau phosphorylation. MAP/microtubule-affinity regulating kinase (MARK), cAMP-dependent protein kinase (PKA), protein kinase C (PKC), dual specificity tyrosine-phosphorylation-regulated kinase 1A (DYRK1A),

calcium/calmodulin-dependent protein kinase II (CaMKII) and casein kinase 1 (CK1) are examples of non-PDPKs involved in tau phosphorylation. The tyrosine specific kinases for tau belong to the SRC kinase family such as Src, Lck and Fyn. The specificity of each kinase and its importance in tau phosphorylation and regulation is not yet fully understood.

GSK3. GSK3 is expressed as two isoforms, α and β, that are not redundant. GSK3 is a Ser/Thr kinase first described to be involved in the glycogen synthase pathway, but has since been implicated in a wide range of mechanisms such as cell signalling, embryogenesis, metabolic control and cell death. The constitutively active GSK3 kinase is regulated through phosphorylation. Indeed, phosphorylation at Ser9 and Ser21 inhibits GSK3β and GSK3α respectively, while phosphorylation at Tyr216 and Tyr279 increases GSK3β and GSK3α activity respectively (Johnson and Stoothoff, 2004; Hanger *et al*., 2009). Its overexpression in cells and upregulation of expression in transgenic mice enhances tau phosphorylation (Cho and Johnson, 2003; Lucas *et al.*, 2001). On the contrary, lithium treatment, which inhibits GSK3 activity, reduces tau phosphorylation in cells and in mice (Lovestone *et al*., 1999; Caccamo *et al*., 2007).

GSK3 alone cannot phosphorylate all the putative tau phosphorylation sites, and some of the GSK3 target residues must first be primed by primary phosphorylation of the substrate by other kinases. It is thought that the kinases cdk5 and DYRK1A may prime tau in order for GSK3 to phosphorylate tau (Li *et al.*, 2006; Woods *et al*., 2001). Cdk5 activity is regulated by the activator p35 and its cleaved form p25. Interestingly, cdk5 overexpression seems to decrease GSK3β activity, whereas its inhibition enhances GSK3β activity (Wen *et al*., 2008). Almost all tau residues targeted by cdk5 are also phosphorylated by GSK3 and both have been reported to phosphorylate tau on Thr231, thus enhancing subsequent tau phosphorylation, reducing tau interaction with microtubules and promoting tau aggregation (Martin *et al*., 2011). It is interesting that a range of proteins are detected in NFTs. GSK3β and cdk5 antibodies label NFTs, which further confirm their role in tau aggregation and aggregate formation (Duyckaerts *et al.*, 2009).

Tau phosphatases. Tau is a substrate for protein phosphatases 1, 2A and 2B (PP1A, PP2A and B) and PP5, the expression of which are all decreased in AD thereby stabilising tau phosphorylation (Tian and Wang, 2002; Gong et al., 1995; Martin *et al*., 2011). PP2A can directly bind tau and is the most important phosphatase for tau regulation. Its inhibition by okadaic acid (OA) induces the hyperphosphorylation of tau and upregulates several tau kinases such as cdk5 or MAPK in neurons and rat brains (Tian and Wang, 2002).

1.1.3.4. Tau aggregation

Although the precise mechanism by which tau accumulates in NFTs remains unclear, its dephosphorylation/phosphorylation status is probably one of the first events. A precise balance between phosphorylation and dephosphorylation regulates tau activity and small changes in this equilibrium lead to tau hyperphosphorylation and aggregation. In AD, hyperphosphorylation of tau triggers its release from the microtubules. Following conformational changes, phosphorylated tau associates into anti-parallel stable dimers, which polymerise in β-sheet structures called protofilaments. Paired helical filaments (PHF) are composed of two twisted protofilaments, and in turn accumulate into NFT (Figure 1.3) (Martin *et al*., 2011). Tau accumulation in AD is limited to neurons. Besides the formation of NFTs, tau aggregates are found in dendrites as neuropil threads (NT), and decorate the corona of the Aβ neuritic plaques in structures called dystrophic neurites. The progression of NFT formation in AD patients' brains is closely related to cognitive decline, and defines the six main stages of AD, called Braak stages (Duyckaerts *et al.*, 2009).

1.1.3.5. Tauopathies and tau associated neurodegenerative diseases

Since the discovery of tau being the main component of NFTs in AD, several other diseases characterised by the neuropathological accumulation of tau have been described. Tau neuropathology has been secondarily implicated in AD, but is also a primary neuropathological feature for a group of diseases called "tauopathies". The "tauopathies" describe a group of diseases where tau aggregation is the principal feature and is linked to neuronal loss, such as corticobasal dementia (CBD), frontotemporal dementia and parkinsonism linked to chromosome 17 (FTDP-17), progressive supranuclear palsy (PSP) and

Pick's disease (PiD). Other neurodegenerative pathologies exhibit tau aggregation, yet always associated with other pathological features, as is the case in AD, Myotonic dystrophy, Postencephalitic parkinsonism, Prion disorder and Down's syndrome (Yancopoulou and Spillantini, 2003; Lee *et al*., 2001; Hernandez *et al*., 2008).

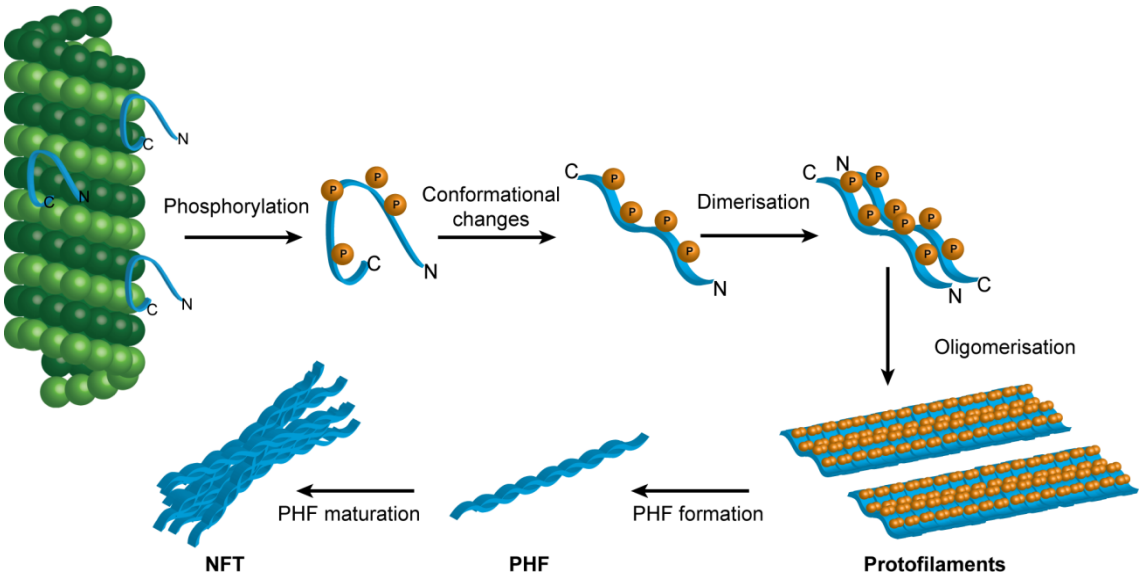

Figure 1.3. *Tau aggregation into NFTs*. Tau is normally attached to the microtubules, but is released when hyperphosphorylated and forms anti-parallel dimers. Dimers form β-sheet protofilaments, which aggregate in twisted structures called PHFs. PHFs accumulate in bigger aggregates called NFTs.

Frontotemporal dementia. Frontotemporal dementia (FTD), like AD, occurs in sporadic and familial forms. FTDP-17 is an inherited form of FTD, associated with tau mutations. Pathological features include severe neuronal loss, gliosis and atrophy of the frontal and temporal lobes. The discovery of mutations in tau in FTDP-17 demonstrated for the first time that tau alone could be a cause of neurodegeneration, and could thus induce neuron loss in other neurodegenerative diseases such as AD.

FTDP-17 is characterised by a wide range of tau mutations, more than 40 of which have been described so far in over 80 different families (Goedert, 2004; Rademarkers *et al*., 2012). Missense, deletion and silent mutations in the coding region, but also mutations in the intronic region that alter the splicing of exon 10, have been described. The intronic mutations do not alter the coding

sequence of tau but lead to an increase in the ratio of the 4R tau isoforms compared to the 3R isoforms (Lee *et al*., 2001). Therefore, a simple imbalance between the ratio of the 3R and 4R isoforms can cause tau aggregation, which emphasises the fact that dysregulation of normal tau, like in AD, can lead to neurodegeneration. Missense mutations usually reduce tau capacity to promote microtubule assembly, although some of them are also responsible for alternative splicing of exon 10. The mutated protein tau is then found to aggregate in straight filamentous structures or PHF (Buee *et al.*, 2000; Lee *et al*., 2001). The tau mutations P301L and P301S found in familial frontotemporal dementia are used in mice models for tau degeneration, as the characteristic feature of the 4R isoforms aggregated in filamentous structures associated with neuronal loss and gliosis are observed (Yancopoulou and Spillantini, 2003; Goedert, 2004, Schneider and Mandelkow, 2008).

Tau-positive frontotemporal lobar degeneration, "PiD, PSP and CBD". PiD, PSP and CBD are newly classified as tau-positive frontotemporal lobar degeneration (tau-positive FTLD) (Mackenzie *et al*., 2009). PiD is characterised by an atrophy of the frontotemporal lobe and limbic system associated with neuronal loss and gliosis, and like FTDP-17, is therefore also classified as causing FTD. Neurons are rounded, and exhibit tau-positive inclusions called Pick bodies. Interestingly, similarly to AD, tau aggregation occurs in the hippocampus, although in the granular cells rather than the pyramidal neurons (Lee *et al*., 2001). PSP and CBD seem to share common clinical and pathological features. PSP exhibits atrophy of the basal ganglia, subthalamus and brainstem, due to neuronal loss and gliosis. Similarly to AD, tau accumulates in NFTs and NT, yet filaments are straight and also occur in glial cells. Although PSP is not considered an inherited disease, a polymorphism in the splicing region between exon 9 and 10 of the tau gene might promote the occurrence of the disease, at least in the Caucasian population (Buee *et al*., 2000; Lee *et al*., 2001). CBD is a rare neurodegenerative disorder, affecting the cerebral cortex and substancia nigra, with severe neuronal loss and gliosis, and characterised by tau filamentous inclusions in neurons and glial cells. Glial pathology includes tau plaques in astrocytes and tau-positive inclusions in the white matter. Both straight filaments and PHF are detected in tau accumulations.

In conclusion, the common feature of filamentous hyperphosphorylated tau in numerous degenerative disorders supports the crucial role for tau in neurodegeneration.

1.1.4. Molecular mechanisms

The molecular mechanism by which tau and Aβ influence one another's toxicity, and the chronology of pathogenic events is beginning to emerge, as currently described by the Amyloid-β and GSK3 hypothesis.

The Aβ hypothesis. It is thought that the β-amyloid accumulation precedes NFT formation. This is supported by several findings. First, the familial form of AD is caused by mutation of the PS gene, which enhances the formation of Aβ peptides. Moreover, most of the genes considered as a risk factor for LOAD have been linked to Aβ formation and clearance. Second, patients with Down's syndrome develop an early form of AD, with amyloid deposits and NFTs. Down's syndrome is caused by trisomy of chromosome 21, where the APP gene is located. FAD and Down's syndrome patients develop tau pathology although the primary cause of the disease is directly related to APP processing (FAD) or APP expression levels (Down's syndrome), thus emphasising the potential upstream role of APP in Aβ and tau pathology. Finally yet importantly, severe dementias such as FTDP-17, caused by tau mutations and aggregation, do not exhibit any amyloid-β deposits (Hardy and Selkoe, 2002). Thus, tau aggregation as a primary cause of disease is never secondarily associated with Aβ accumulation. Recent findings have shown that while tau does not induce Aβ formation, the toxicity of Aβ in cultured cells and in animal models is mediated by tau and Fyn, a kinase involved in tau phosphorylation and recruitment to lipid rafts. Therefore, the amyloid and tau aggregation and neurotoxicity in AD would not be a linear event, but rather a deleterious cycle (Ittner and Götz, 2011).

The GSK3 hypothesis. One of the most promising links between Aβ and tau accumulation are the kinases, including GSK3, cdk5, Fyn and CK1 (Ittner and Götz, 2011; Wen *et al*., 2008; Flajolet *et al*., 2007). For instance, the interplay between insulin, GSK3 and the Wnt signalling pathway might bridge APP and

tau processing. Both the insulin and Wnt signalling pathways inhibit GSK3. Briefly, insulin activates PI3 kinase (PI3K), which in turn enhances Akt activity. Akt phosphorylates GSK3 on Ser9 and Ser21 (for the β and α isoforms respectively) thereby inhibiting its activity. Conversely, in the canonical Wnt signalling pathway, GSK3β activity is inhibited upon binding of the Wnt ligand to its receptor complex (composed of frizzled and the low-density lipoprotein receptor related protein) by a mechanism that does not involve the inhibitory phosphorylation on Ser9. Thus, β-catenin, the downstream effector of the canonical Wnt signalling pathway, escapes GSK3β-mediated phosphorylation and ubiquitination, and translocates to the nucleus to activate transcription (Hooper *et al*., 2008; Hernandez *et al*., 2010). It has been shown that in primary neurons, the Aβ peptide acts as an antagonist of insulin, thus inhibiting PI3K and Akt activity, which would enhance GSK3 activity and tau phosphorylation (Townsend *et al*., 2007). Similarly, in cell culture, the Aβ peptide blocks the canonical Wnt signalling pathway, which would result in increased levels of active GSK3 and phosphorylated tau (Magdesian *et al*., 2008).

Other mechanisms. The formation of NFTs and Aβ aggregations are not the only neuropathological features of AD. Mitochondrial deficiency, chronic neuroinflammation in the hippocampus, the activation of endoplasmic reticulum (ER) stress and the unfolded protein response (UPR), and defects in signalling pathways and cell cycle dysregulation have all been described (Crouch *et al*., 2008; Hernandez-Ortega *et al.,* 2011; Nijholt *et al*., 2011).
In addition, aggregation of Aβ and tau are symptomatic of a dysregulation of the quality control of proteins. Indeed, molecular chaperones, the ubiquitin-proteasome system (UPS) and autophagy are impaired or overwhelmed in AD and thus unable to reduce tau and Aβ accumulation.

1.2. Protein misfolding and aggregation

Protein homeostasis is exquisitely regulated in cells. Several steps are needed to ensure the correct folding of proteins from the native to the final folded conformation necessary for their function. A failure in this system can lead to misfolding, aggregation and eventually cell death. Newly synthesised proteins

are regulated by the housekeeping chaperones, which are also the first line of defence against misfolded proteins.

1.2.1. Molecular chaperones in Alzheimer's Disease

The correct 3-dimensional conformation of a protein is necessary for its function and stabilisation, as most of the hydrophobic residues which would otherwise be exposed to the hydrophilic cytoplasmic environment, are buried within the protein (Frydman, 2001). Although nascent proteins contain all the information to fold correctly *in vitro*, in the crowded intracellular milieu, they require the assistance of chaperones, the guardian of the proteome. Chaperones are constitutively expressed, but are upregulated in the case of stress. The chaperones are therefore also called stress proteins, or Heat shock proteins (HSP) (Hartl and Hayer-Hartl, 2002). Until recently, they were essentially classified according to their molecular weight, but a new nomenclature has emerged, and describes 6 classes of proteins based on their gene structure: HSPA (HSP70), HSPB (small HSPs), HSC (HSP90), HSPH (HSP110), DNAJ (HSP40) and chaperonins (HSP60 and CCT) (Kampinga et al., 2009).

Protein chaperones are responsible for the correct folding of proteins. Molecular chaperones are probably impaired or overwhelmed in neurodegenerative disorders, and their failure is the first step towards protein aggregation. Several inclusion bodies in neurodegenerative diseases are decorated with chaperones. Moreover, in cells, overexpression of chaperones often prevents aggregation, thus confirming that the HSPs and their co-factors play a crucial role in the regulation of misfolded proteins.

In AD, Aβ plaques are decorated by several chaperones, including HSP70, HSP27, GRP78 and HSP90, while NFTs are labelled with HSP90 and HSP27 (Muchowski and Wacker, 2005). In cells, both tau and Aβ are modulated by HSP70. HSP70 upregulation increases tau solubility and binding to the microtubules, and decreases its phosphorylation (Dou *et al*., 2003). HSP70 has been reported to reduce the toxicity of Aβ and its ability to aggregate (Luo *et al*., 2010). The co-chaperone carboxy terminus of HSC70-interacting protein (CHIP) has been found to be upregulated in AD patients, with the levels of CHIP

inversely proportional to the levels of tau. In mice, CHIP has been shown to attenuate tau aggregation (Sahara et al., 2005). In cells, CHIP and other HSPs are able to interact with APP and to influence Aβ formation (Kumar *et al*., 2007). Therefore, the upregulation of chaperones and co-chaperones is thought to be neuroprotective. On the other hand, inhibition of HSP90 by geldanamycin reduces insoluble and phosphorylated tau. Geldanamycin disrupts the interaction of HSP90 with the transcription factor HSF1, thus promoting the heat shock response and the increased expression of HS proteins.

1.2.2. Protein misfolding

Protein misfolding increases dramatically after exposure to stress, such as heat-shock or oxidative stress. When nothing can be done to repair or eliminate misfolded proteins, they tend to aggregate and cause numerous conformational protein diseases, including neurodegenerative diseases.

Misfolding and aggregation. In non-pathological situations, misfolding can occur as large proteins (more than 100 aa) form a partially folded intermediate state prone to misfolding and aggregation, before reaching their optimal conformation (Kopito, 2000; Hartl and Hayer-Hartl, 2009). However, it can also be a consequence of various defects, including mutations in the protein sequence, impairment of the chaperone system, abnormal post-translational modifications and structural modifications induced by environmental changes. The misfolding of the protein is driven mainly by hydrophobic forces and often leads to self-aggregation, in amorphous/globular or β-strand structures. The β-cross sheets are found in numerous diseases called amyloidosis, that includes AD and other neurodegenerative diseases. This type of association is extremely favourable for polymerisation and aggregation, and tends to form oligomers, protofibrils and fibrils. Oligomers are soluble, and often considered as the most toxic form of aggregation. Self-aggregation is exponential, and can also have dominant negative effects on the native protein, like the pathogenic form of prion protein, PrP^{sc}, that converts the normal protein PrP^{c} into misfolded aggregates (Moreno-Gonzalez and Soto, 2011).

Inclusions. Aggregates are considered an abnormal localisation (extra or intracellular) of poorly soluble non-native proteins. Inclusions describe any aberrant intracellular accumulation of protein, without distinction of secondary or tertiary structures. In contrast, inclusion bodies refer to the large, low number of foci where aggregated proteins are sequestered (Kopito, 2000; Ross and Poirier, 2005). In the seeding/nucleation model of protein aggregation and inclusion formation in cells, the soluble oligomers or aggregates are considered as “seeds”. The first phase of the model, called the lag phase, consists of a slow and low production of oligomers or aggregates in “nuclei”. These nuclei “seed” the formation of polymers, which elongate in a fast exponential manner. From the seeding/nucleation theory, inclusions are the fast-growing forms of polymer formation (Kopito, 2000; Moreno-Gonzalez and Soto, 2011).

Aggresomes. Microtubule-dependent inclusion bodies are called aggresomes. Aggresomes consist of the accumulation of aggregates at the microtubule organising centre (MTOC), located near the nucleus and the Golgi. Aggresomes are covered with vimentin or neurofilaments in neurons (Taylor *et al*., 2003). Depolymerisation of microtubules prevents the formation of aggresomes, but once formed, microtubule destabilisation does not disrupt the aggresome. Therefore, the aggresome is not a dynamic but a rather stable structure, thought to be protective by enhancing degradation (Kopito, 2000, Moreno-Gonzalez and Soto, 2011).

Quality control compartments. Juxtanuclear quality control (JUNQ) and insoluble protein deposit (IPOD) are two types of sequestration of misfolded proteins that differ by their intracellular localisation and association with protein clearance pathways. JUNQ refers to a compartment that interacts with the ER and preferably sequesters proteins that can be refolded or degraded by the UPS. Conversely, protein aggregated in the IPOD is not associated with either the UPS or chaperones, but with the autophagic protein Atg8. IPOD is thought to be the last of the two centres to form, when the insoluble protein is no longer able to be refolded or degraded by the UPS (Kaganovich *et al*., 2008).

Cells possess several mechanisms that respond to the toxicity of aggregated proteins. Nevertheless, the formation of aggregates is primarily a consequence

of the failure of chaperone systems to correctly fold proteins coupled with the failure of protein degradation pathways that try to eliminate the misconformed proteins.

1.2.3. Protein aggregation clearance

Homeostasis of the proteome is meticulously regulated by chaperones and degradation pathways (Figure 1.4). The best-known degradation system is the UPS, described in detail in chapter 1.3, that modulates the elimination of short-lived, misfolded or non-functional proteins. Misfolded proteins are first targeted by the UPS. However, due to its barrel-like shape, the proteasome needs the proteins to be partially or totally unfolded to enter the narrow cavity. Thus, in numerous pathologies associated with aggregate-prone proteins, once the protein starts to accumulate in a globular or β-sheet form, the UPS has been described to be impaired, overhelmed or unable to process them. Thus, aggregated proteins are targeted to the autophagy pathway. Lysosomal degradation is responsible for the degradation of long-lived proteins or organelles through autophagy, or exogenous elements through endocytosis and phagocytosis.

Three types of autophagy have been described: Macroautophagy (usually referred as “autophagy”), CMA and microphagy. Most of the conformational and neurodegenerative diseases are associated with impairment of CMA and macroautophagy.

Chaperone-mediated autophagy. Proteins than contain a lysine-phenylalanine-glutamic acid-arginine-glutamine (KFERQ) motif are specifically targeted by the chaperone HSC70/HSP70 to the lysosomes. The Lamp2a transmembrane protein of the lysosomes is a receptor for the CMA pathway. CMA is activated in normal conditions but is upregulated in conditions of stress, probably to recycle amino acids. CMA cannot degrade inclusions, and has therefore been described as “impaired” in several conformational diseases (Martinez-Vicente and Cuervo, 2007; Arias and Cuervo, 2011).

Autophagy. Autophagy is referred to as “in bulk” degradation as it engulfs the substrate without specificity. Autophagy occurs in response to stress, such as

starvation or heat-shock, and is necessary to promote the recycling of non-essential proteins and the degradation of misfolded proteins. Autophagy requires the formation of a double-membrane vesicular compartment called an autophagosome.

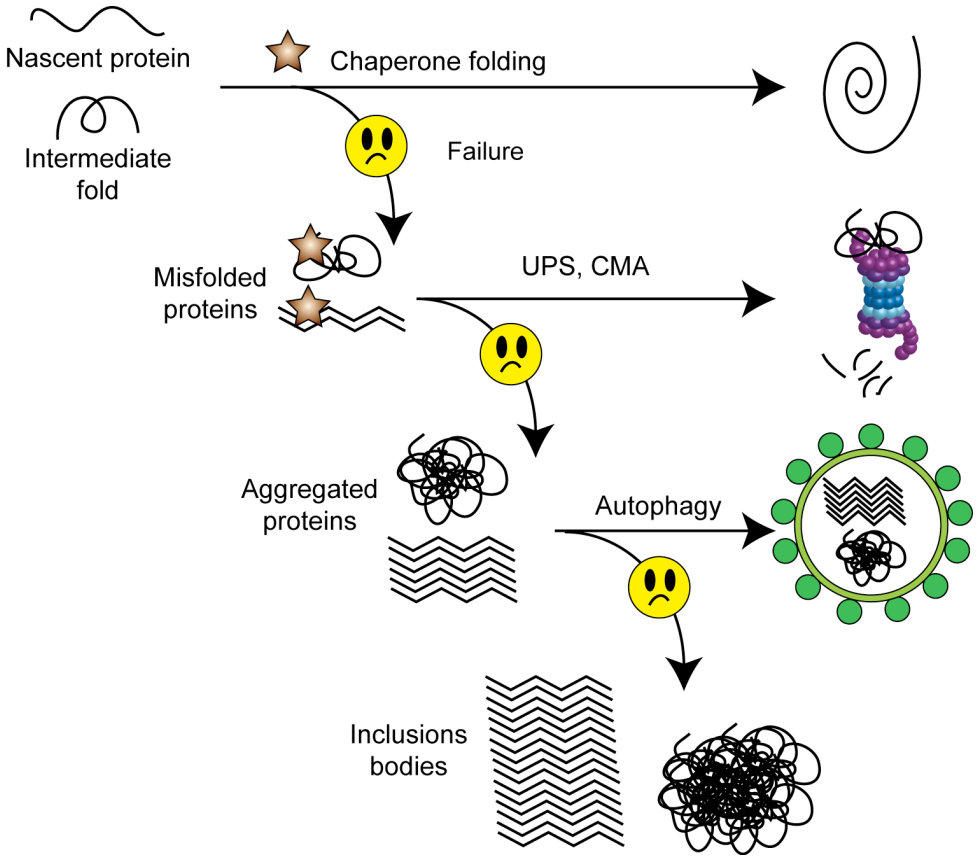

Figure 1.4. *Mechanisms of protein homeostasis*. Nascent proteins/folding intermediates are targeted by chaperones for correct folding. If this system fails, proteins are targeted to the proteasome or degraded by chaperone-mediated autophagy (CMA). Impairment of the CMA and UPS induce autophagy. If not degraded, aggregates accumulate and form inclusions.

The formation of autophagosomes involves the protein LC3/Atg8 and the complex Atg5/Atg12/Atg16, and requires a 3-step mechanism, similar to the E1, E2 and E3 cascade of ubiquitylation. Once formed, the autophagosome fuses with the lysosomes, allowing degradation of the substrate (Martinez-Vicente and Cuervo, 2007; Cheung and Ip, 2011).

Cross-talking. It is thought that the UPS, CMA and autophagy are complementary mechanisms in the clearance of aggregates. Thus, misfolded

proteins are preferentially refolded by chaperones, degraded by the UPS or CMA. However, if these systems fail, autophagy is enhanced. Indeed, inhibition of the UPS and CMA enhances autophagy mechanisms (Martinez-Vicente and Cuervo, 2007; Cheung and Ip, 2011). Impairment of this last degradation mechanism would exacerbate aggregation and lead to inclusion formation (Figure 1.4). Some hypotheses are beginning to emerge concerning the mechanism by which aggregates induce autophagy. P62, a protein that is detected in several inclusion bodies in neurodegenerative diseases, has been shown to target ubiquitylated aggregates and promote autophagy (Pankiv *et al*., 2007). The protein HDAC6, upon proteasome inhibition, co-localises with aggregated proteins and aggresomes and can trigger autophagy. Indeed, in a drosophila model of neurodegeneration, HDAC6 rescues neurodegeneration induced by UPS impairment via the activation of the autophagy pathway (Pandey *et al*., 2007).

1.3. The ubiquitin-proteasome system

In the 1970s, a new but highly conserved small protein was discovered that was involved in protein clearance: ubiquitin (Ub). Ub tags proteins for recognition by an efficient protein homeostasis regulator, the proteasome. Taken together, the UPS is, so far, the most important degradation system of the cell.

1.3.1. The 26S proteasome

The proteasome is an ATP-dependent machinery involved in protein degradation. The 26S proteasome is composed of a central core, the 20S subunit, and two 19S subunits at the top and bottom of the 20S core (Figure 1.5). The 19S subunit is the regulatory unit of the 26S proteasome which, with its ATPase activity, unfolds proteins before they enter the catalytic 20S unit (Herrmann *et al*., 2007). The 19S subunit consists of a base and a lid. The base is composed of six ATPase units that form an hexameric ring, three non-ATPase units and the proteasome subunit, non-ATPase, 4 (PSMD4, also called S5a) that recognises Ub and connects the base to the lid (Xie, 2010; Voges *et al*., 1999). The structure of the lid contains 13 regulatory non-ATPase subunits

(Lasker *et al.*, 2012; Xie, 2010, Deveraux *et al*., 1994) and 6 regulatory AAA-ATPases subunits (Lasker *et al.*, 2012). The barrel-shaped 20S subunit is composed of two symmetrical heptameric rings, α and β. The two outer α rings

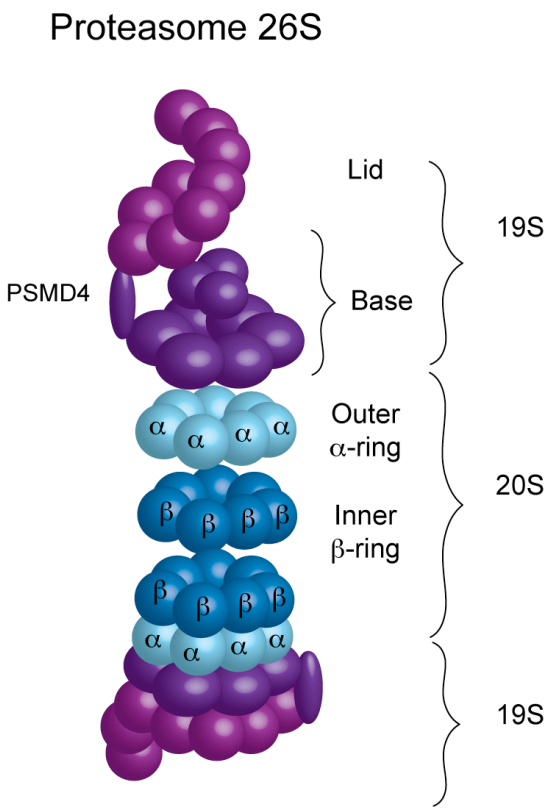

Figure 1.5. *Composition of the proteasome.* The two regulatory 19S units consist of a base and a lid, connected through the PSMD4 subunit. The catalytic 20S unit possesses 2 outer "gatekeeper" α rings, and 2 inner "core" β rings. The α and β rings are composed of heptamers of α and β subunits respectively. The heptameric β rings contain the chymotrypsin-like, trypsin-like and peptidyl-hydrolase catalytic units.

are composed of 7 α-subunits, and are called the "gatekeeper", opposed to the "catalytic core" made of the 2 inner heptameric β rings (Lasker *et al.*, 2012; Xie, 2010, Deveraux *et al*., 1994).

The β rings possess 7 β subunits including the β5, β2 and β1 subunits with chymotrypsin-like, trypsin-like and peptidyl-hydrolase catalytic activity respectively, which catalyse the cleavage of the protein substrate into small peptides (Voges *et al*., 1999).

1.3.2. Ubiquitin

Ub is a small polypeptide of 76 aa (8.5 kDa). Ub is highly conserved from protozoa to vertebrates, and is essential to all eukaryotic cells. Ub is known for its role in targeting proteins for their proteasomal degradation, but also for its role in conformational regulation and cell signalling. Ubiquitylation (or ubiquitination) of proteins involves a cascade of three enzymes that conjugate a monomer or a chain of polyubiquitin (polyUb, 4 to 7) to the protein target

(Hershko and Ciechanover, 1998; Herrmann *et al*., 2007). First, the ubiquitin-activating enzyme (E1) activates Ub for transfer to the ubiquitin-conjugating enzyme (E2) in an ATP-dependent manner. E2 transfers Ub to the ubiquitin-ligase (E3), which covalently conjugates Ub to its target (substrate) (Figure 1.6).

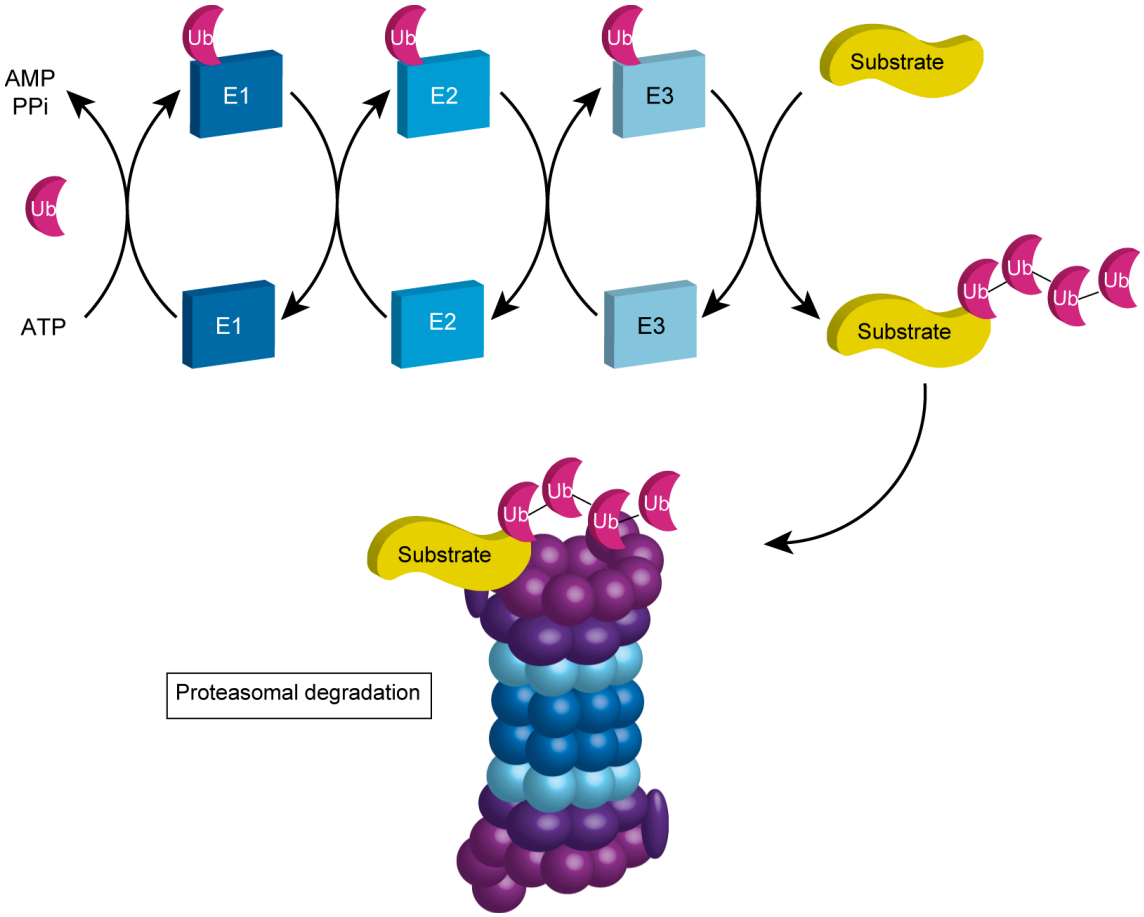

Figure 1.6. *Ub conjugation pathway*. Ub is bound to an E1 activating enzyme using ATP, then transferred to an E2 conjugating enzyme and finally to an E3 ubiquitin-ligase. The E3 ubiquitin-ligase binds Ub to its substrate. The substrate is polyubiquitinated before its degradation by the proteasome.

For the system to be efficient and specific, the number of different enzymes increases exponentially from E1 to E3. Indeed, only 2 isoforms of the E1 and 37 genes coding E2 enzymes have been found in human so far, while several hundred of E3 have been discovered (Herrmann *et al*., 2007, Shang and Taylor, 2011). E3 ligases are classified in two groups, based on their interaction with the substrate: the RING (really interesting new gene) domain and HECT (Homologous to E6-associated protein C terminus) type E3 ligases.

The number of Ub attached, but also the type of bond between the Ub monomers determines the pathway proteins are targeted for. Ub polymerises on its lysine residues. Ub possesses 7 lysine residues (K6, K11, K27, K29, K33, K48, K63), all thought to be involved in different mechanisms. For instance, if polyUb chains are linked by their lysine 48 (K48), the protein substrate will be targeted for proteasomal degradation. On the other hand, if polyUb are ligated via their lysine 63, the target protein will preferably be involved in regulatory functions such as signalling events (Shang and Taylor, 2011). Monoubiquitination can lead to a modification of the protein activity, but also to degradation (Herrmann *et al*., 2007). Therefore, Ub is now not only considered a crucial element of the protein degradation system, but also an active regulator of protein function and conformation. Mono or polyubiquitylation has been shown to be implicated in meiosis, DNA repair, translation, transcription, autophagy and endocytosis (Hicke, 2001).

Ubiquitylation is a reversible mechanism, which involves proteins called deubiquitinating enzymes (DUBs). So far, genes coding for nearly 100 DUBs have been discovered in the human genome. DUBs can remove polyUb chains or monoubiquitin (MonoUb) from the target protein, but also hydrolyse Ub from unanchored polyUb chains (Reyes-Turcu and Wilkinson, 2009).

1.3.3. Ubiquitin-proteasome system and neurodegeneration

As a regulator of protein homeostasis, the UPS plays an important role in neurodegenerative diseases. Indeed, Ub is found to decorate inclusions which suggests that although Ub targets the misconformed and aggregated protein, the UPS fails to degrade them. Indeed UPS impairment has been reported in numerous neurodegenerative disorders, such as AD, Parkinson's disease (PD), Huntington's disease (HD) and amyotrophic lateral sclerosis (ALS) (Ciechanover and Brundin, 2003; Dennissen *et al*., 2012). In such cases, the question remains whether the UPS both contributes to and is a consequence of neurodegeneration. Importantly, a reduction of UPS activity is a natural process of ageing, although it is not considered as pathological but rather as a consequence of decreased protein synthesis (Low, 2011). In pathological conditions, particularly late onset neurodegenerative diseases such as AD and

PD, there is already a functional decline in proteasome activity, which may increase the vulnerability of neurons to the pathological insult and contribute to neuron loss and dementia (Ciechanover and Brundin, 2003; Dennissen *et al*., 2012).

Huntington's disease (HD). HD is an autosomal dominant disorder, caused by abnormal repetition of the codon CAG at the N-terminus of the huntingtin gene. Therefore, the huntingtin protein (htt) exhibits a larger number of glutamine (polyQ) than usual, prone to aggregate. In patients with HD, the htt aggregates are decorated with ubiquitin, and in cells mutant htt has been reported to impair proteasome activity and exacerbate aggregation (Diaz-Hernandez *et al*., 2006; Ciechanover and Brundin, 2003).

Parkinson's disease (PD). PD is the second most common form of dementia after AD. A deficiency in the catalytic subunits of the 26S proteasome has been reported in the sporadic form of PD. Moreover, mutations in parkin, an E3 ubiquitin-ligase, cause autosomal recessive juvenile parkinsonism (AR-JP) (Ciechanover and Brundin, 2003; Chaugule *et al*., 2011). The ubiquitin-carboxy-terminal hydrolase (UCH-L1), a deubiquitinating enzyme, if mutated on its isoleucine 93 residue, causes parkinsonism (Ciechanover and Brundin, 2003; Andersson *et al*., 2011). Therefore, the UPS components parkin and UCH-L1 are directly implicated in neuropathogenesis in these cases, underlying the importance of the UPS in neurodegeneration.

Alzheimer's disease (AD). In the brains of patients with AD, an impairment of the UPS has been reported in areas related to dementia and the accumulation of senile plaques and NFTs, including the hippocampus (Keller *et al.*, 2000). Indeed, Aβ peptides and PHFs have been reported to inhibit proteasome activity (Oddo, 2008). NFTs and senile plaques are labelled by the UBB+1 mutant of Ub. UBB+1 is generated by molecular misreading of the *Ub* gene, which produces an aberrant frameshifted *Ub* mRNA due to dinucleotide deletions (Chadwick *et al.*, 2012). Thus, the UBB+1 mutant lacks the Gly 76 and possesses 19 aa more than Ub, and can form polyUb chains that cannot be depolymerised by DUBs and might inhibit proteasome activity (Chadwick *et al*., 2012; Upadhya and Hegde, 2007). Moreover, the deubiquitinating enzyme

UCH-L1 is downregulated in AD. UCH-L1 is abundantly expressed in neurons, and is involved in normal synaptic functions (Andersson *et al*., 2011). In double transgenic mice APP/PSEN (with APP and PS mutations), UCH-L1 rescues the decline of synaptic function and contextual memory (Riederer *et al*., 2011). An interesting new partner of the proteasome, ubiquilin-1, is also involved in AD. Ubiquilin-1 contains a ubiquitin-like (UBL) domain that binds the PSDM4 subunit of the 19S proteasome, and a ubiquitin-associated (UBA) domain that interacts directly with Ub and targets polyubiquitinated proteins. A single-nucleotide polymorphism downstream the exon 8 of the *UBLQN1* gene has been reported to be a risk factor for LOAD (Bertram et al., 2005). However, this remains controversial (Smemo *et al*., 2006). Moreover, ubiquilin-1 can interact with both APP and PS, and modulate APP trafficking to the plasma membrane (2010, Haapasalo *et al*., 2010). Finally, the levels of the co-chaperone and E3 ubiquitin-ligase CHIP have been shown to be inversely proportional to tau levels in AD brains (Sahara *et al*., 2005; Riederer *et al*., 2011). CHIP, an E3 Ub ligase for tau ubiquitination and degradation, interacts with tau phosphorylated by GSK3β.

In summary, defects in the UPS system have been implicated in neurodegenerative disorders at multiple and complex levels.

1.4. NUB1 and the ubiquitin-like modifiers

Besides Ub, new small proteins have been implicated in marking proteins for proteasomal degradation. The ubiquitin-like modifiers (ULM) share sequence homology with Ub, yet the biggest similarity is in the tertiary structure and mechanism of conjugation to target proteins. The ULM family includes various proteins such as SUMO, ISG15, FUB, Atg8/LC3, and Atg12, involved in a wide range of mechanisms from DNA transcription to autophagy (Herrmann *et al.*, 2007). Among the ULMs, NEDD8 and FAT10 target proteins for degradation and are shuttled to the proteasome by the NEDD8 ultimate buster 1, NUB1.

NEDD8 is a small molecule of 81 aa that is most similar to Ub, with 60% identity and 80% homology. One the other hand, the two UBL domains of FAT10 at the N-terminus and C-terminus share only 29% and 36% identity with Ub

respectively (Lim *et al.,* 2006). However, the tertiary structures of Ub, NEDD8 and the two UBL domains of FAT10 are very similar. They are all composed of 2 β-strands, a large α-helix and α-loop, and the characteristic β-strand-α-loop-β-strand motif (Figure 1.7).

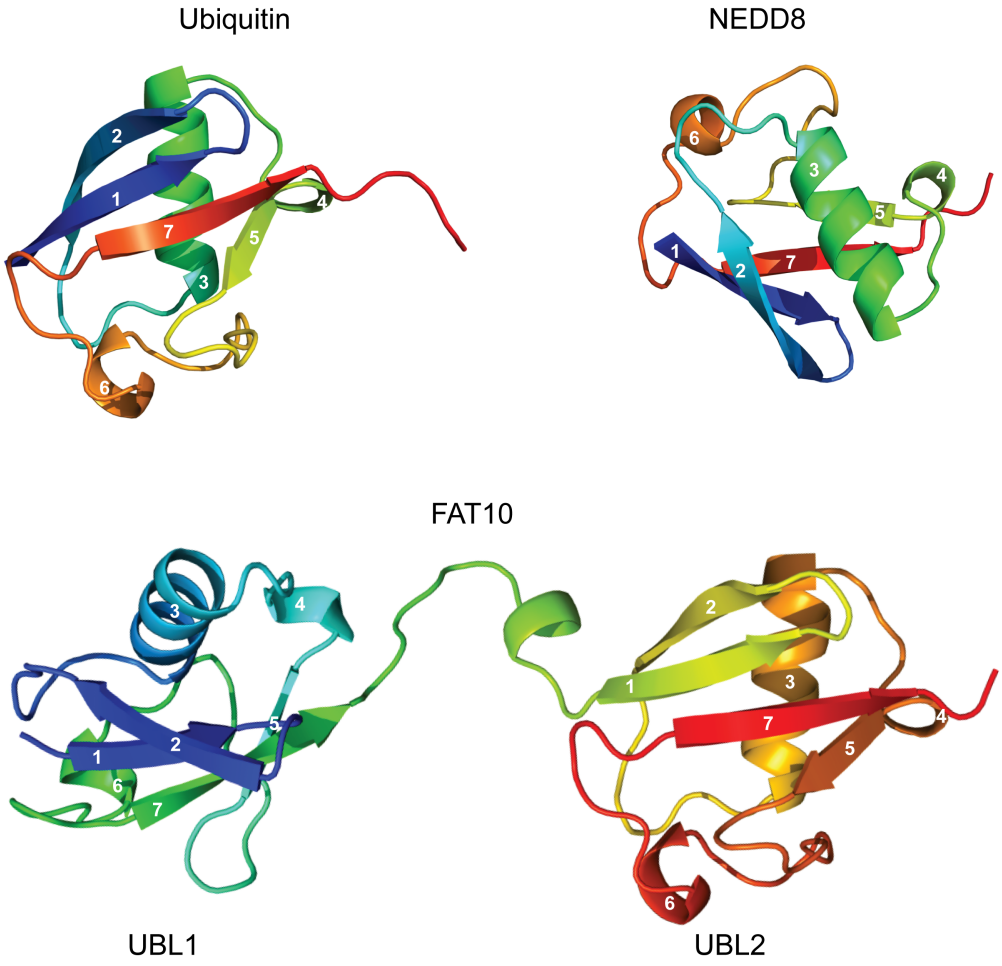

Figure 1.7. *Tertiary structure of Ub and the ULM NEDD8 and FAT10*. For each protein, the three dimensional (3D) structure is represented by a rainbow, from dark blue at the N-terminus to red at the C-terminus. Ub, NEDD8 and the two UBL of FAT10 are composed of (1) β-strand, (2) β-strand, (3) α-helix, (4) α-loop, (5) β-strand, (6) α-loop, (7) β-strand. The 3D structures were obtained from the aa sequence using the protein fold recognition server, PHYRE2, freely available on www.sbg.bio.ic.ac.uk/phyre2/ (Kelley and Sternberg, 2009).

1.4.1. The ubiquitin-like modifier NEDD8

1.4.1.1. NEDD8 conjugation

NEDD8 is a ULM first discovered as the neural precursor cell expressed developmentally downregulated 8 (NEDD8) (Kumar *et al*., 1992). Despite its significant homology to Ub, NEDD8 requires a specific set of E1, E2 and E3 enzymes to be conjugated to proteins (Figure 1.8).

NEDD8 is first processed by the E1-activating enzyme NAE (NEDD8 activating enzyme), composed of a heteromer of the amyloid precursor protein-binding protein 1 (APP-BP1) and Uba3. The second step is the transfer of NEDD8 to the E2 conjugating enzyme Ubc12. Several E3 ligases have been described for NEDD8, including Rbx1, Rbx2, Mdm2, SCF^{FBX011} and DCN1, all of which are RING finger domain E3 ligases with the exception of DCN1 (Watson *et al*., 2011). It is generally accepted that only one molecule of NEDD8 is covalently attached to its targets, yet NEDD8 is able to form chains on lysine 11, 22 and 48. Moreover, formation of mixed Ub and NEDD8 chains have been found, but their function is unknown (Jones *et al.,* 2008).

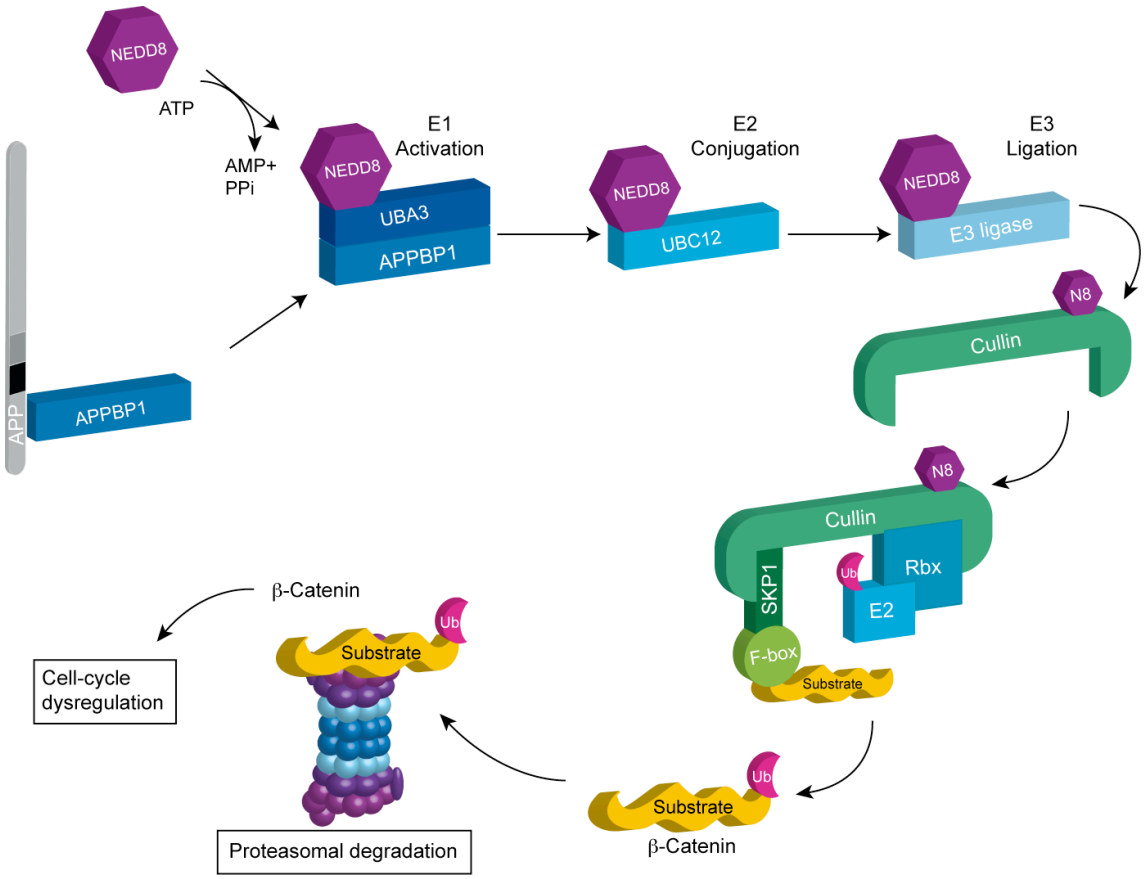

Figure 1.8. *NEDD8 conjugation pathway*. NEDD8 is conjugated to its substrates via the APP/BP1-UBA3 E1 activation enzyme, Ubc12 E2 conjugation enzyme and an E3 ligase. Its best characterized target is the CRLs, E3 ligases that ubiquitylate and target proteins for their proteasomal degradation. The cell-cycle regulator β-catenin is an example of protein targeted for ubiquitylation by the CRL.

The conjugation of NEDD8 to a protein is called neddylation and is reversible. The COP9 signalosome (CNS) is a protein of 8 subunits, highly similar to the lid

component of the 19S proteasome, which deneddylates proteins via a metalloproteinase activity (Wei and Deng, 2003). Moreover, as DUBs exist for Ub, deneddylating enzymes have been found, such as NEDP1 (Shen *et al.*, 2005). Furthermore, NEDD8 is regulated by NUB1, which targets NEDD8 and its conjugates for proteasomal degradation (Kamitani *et al.*, 2001)

1.4.1.2. NEDD8 targets

The primary function of NEDD8 is to regulate the activity and degradation of proteins. Through the regulation of cullins, Mdm2/p53 and BCA3/NF-κB, NEDD8 is directly or indirectly involved in numerous pathways, including modulation of the cell cycle, DNA repair, tumor progression and proteasomal degradation.

The cullin subunit. Contrary to Ub, the first role discovered for NEDD8 conjugation is to regulate protein function. The first and best characterised target protein for neddylation is the cullin subunit of the cullin-RING E3 ubiquitin-ligases (CRLs). The CRLs are the largest Ub E3 ligase family, involved in the regulation of numerous cellular processes, including gene transcription, cell signalling and cell cycle progression. The cullin proteins serve as a scaffold for different CRLs, for example cullin 1 (CUL1) in the SCF (Skp1-Cullin-F-box) complex. Neddylation of CUL1 induces the activation of the SCF, which, in turn, induces the degradation of numerous cell cycle activators. In the SCF, CUL1 binds a RING finger protein Rbx at its C-terminus, a docking site for E2 conjugating enzymes, while its N-terminus interacts with the Skp1/F-box complex, necessary for substrate recognition. It thereby brings the Ub on the Rbx E2 in close proximity to the substrate within the Ub CRL. Therefore, the Rbx plays a double role, it promotes the neddylation of cullins, but also binds the Ub E2 conjugating enzyme (Merlet *et al*., 2009). The SCF is a well known E3 ligase for the NF-κB inhibitor IκB, necessary for its ubiquitination and degradation. Therefore, by promoting the CUL1 activity, NEDD8 positively modulates NF-κB transcriptional activities. However, a new target for NEDD8 is the protein BCA3 (involved in breast cancer) which, upon neddylation, inhibits NF-κB transcriptional activities. Thus, NEDD8 could also downregulate NF-κB (Gao *et al*, 2006).

The other cullin family members are specific scaffold proteins of different E3 Ub ligase complexes (Merlet *et al*., 2009). Interestingly, NEDD8 conjugation is necessary for cullins to be fully functional and recognise E2 enzymes. Furthermore, neddylation can also prevent the inhibition of cullins by the cullin-associated and neddylation dissociated-1 (CAND-1). Indeed, CAND-1 normally disrupts the association between Skp1 and CUL1, thus preventing the formation of the SCF, but neddylation of the CUL1 inhibits CAND-1-mediated dissociation of CUL1 with Skp1 (Liu J *et al*., 2002).

Other targets. Another interesting target for neddylation is the Mdm2/p53 complex. Upon stress, p53 is activated resulting in the transcription/translation of several proteins involved in cell growth arrest and apoptosis. The oncogene Mdm2 is an E3 ligase that directly interacts with p53 and promotes its ubiquitylation and degradation. Recently, Mdm2 has been shown to induce neddylation of both p53 and itself, which stabilises Mdm2 and inhibits the transcriptional activity of p53 (Xirodimas *et al*., 2004; Xirodimas, 2008; Watson *et al*., 2011).
NEDD8 also targets both the C99 fragment and the AICD of APP. These findings directly implicate neddylation in APP processing and function.

NEDD8 in neurodegeneration. NEDD8 has been detected in numerous inclusions in neurodegenerative diseases, including NFTs and senile plaques in AD, Lewy bodies in PD, and Pick bodies in PiD (Dil Kuazi *et al.*, 2003). Neddylation of the C99 and AICD fragments of APP blocks AICD interaction with Fe65 and AICD transcriptional activity (Lee MR *et al.*, 2008). Although the role of AICD is not fully understood, AICD is thought to form a complex with Fe65 and TiP60 and to regulate gene expression, including p53, GSK3β and caspases 3 and 6. Thus, AICD has been shown to induce apoptosis in cells, and to be involved in synaptic plasticity and cytoskeleton dynamics (Muller *et al.*, 2008)
Neddylation is activated by the APP-BP1/Uba3 E1 enzyme. APP-BP1 interacts directly with the C-terminal domain of APP and downregulates $A\beta_{42}$ formation probably via promoting the degradation of the C-terminal fragment of the PS component of the APP γ-secretase (Chen *et al*., 2007). APP-BP1 is also

implicated in cell-cycle regulation. Indeed, APP-BP1 depletion in fetal neural cells blocks the cells in G1 phase, and in neurons mediates the S-M phase transition and promotes apoptosis (Joo *et al*, 2010; Chen *et al*., 2000). NEDD8, through regulation of the CRL, is also involved in cell-cycle regulation, downregulating several targets of the SCF. Indeed, homozygous mutation of Uba3, that lacks the catalytic subunit of the NEDD8 activating enzyme, was lethal in mice. Embryo analysis showed that cells could not enter the S-phase, exhibited upregulation of cyclin E and p57, and accumulation of β-catenin, a well known target of SCF (Tateishi *et al*., 2001). Notably, β-catenin is the downstream effector of GSK3β in the canonical Wnt signalling pathway, modulation of which is central to the GSK3β hypothesis that links Aβ and tau neurotoxicity. In summary, cell cycle dysregulation is a pathological feature of AD, and the NEDD8 pathway could be an integral part of this dysregulation.

1.4.2. The ubiquitin-like modifier FAT10

The F-adjacent transcript 10 (FAT10) is an 18 kDa ULM. It is a small protein of 165 aa, composed of 2 UBL domains joined in a head-to-tail fashion separated by a short linker, which originally gave it the name of Ubiquitin D or di-ubiquitin like protein. Unlike NEDD8 and other ULM, the FAT10 conjugates and enzymes are not fully known. The E1 activating enzyme for FAT10 is UBA6, followed by the UBA6-specific E2 enzyme (USE1) as an E2 conjugating enzyme. Interestingly, USE1 is auto-FAT10ylated (Aichem *et al.*, 2010). Another potential E1 activating enzyme for FAT10 is E1-L2, which is found to activate both Ub and FAT10 (Chiu *et al.*, 2007).

FAT10 expression and function. FAT10 is constitutively active in mature B cells and can be induced by interferon-γ or tumour necrosis factor-α (Liu YC *et al*., 1999). Interestingly, FAT10 can directly interact with the 26S proteasome, via its UBL domains (Schmidtke *et al*., 2006). Like NEDD8, NUB1 binds FAT10 and accelerates its degradation by the proteasome (Hipp *et al*., 2004). Moreover, NUB1 is necessary for FAT10 degradation by the proteasome (Schmidtke *et al*., 2009). Thus, along with NEDD8, FAT10 is a new marker of Ub-independent proteasomal degradation via the recruitment of NUB1.

Although its functions are not fully understood, FAT10 is upregulated in various

cancers and it can induce apoptosis. FAT10 interacts with MAD2, a spindle-assembly checkpoint protein, and the FAT10 levels are cell-cycle dependent. FAT10 is therefore probably involved in cell cycle regulation (Raasi *et al*., 2001; Lim *et al*., 2006). Moreover, FAT10 is downregulated by the tumor suppressor p53 (Zhang *et al*., 2006). However, its relationship with p53 is unclear, as a recent study by Li *et al*, 2011, showed that p53 is FAT10ylated, which modifies p53 transcriptional activity. Another potential target for FAT10 is NF-κB. Gong *et al*, 2010, suggests that FAT10 mediates the TNFα-dependent activation of NF-κB reducing its transcriptional activities.

Recently, FAT10 has been shown to interact with HDAC6, a protein involved in aggresome formation and activation of autophagy, following inhibition of the proteasome. Moreover, FAT10 co-localised with the aggresomes, thus suggesting that FAT10 is a regulator of protein aggregation/degradation (Kalveram *et al*., 2006). This correlates with a new study by Nagashima *et al*, 2011, who found that FAT10 deficiency in cells enhanced the aggregation of polyQ proteins. Therefore, accumulation of FAT10 in aggresomes upon proteasome inhibition and interactions with polyQ proteins reveals new regulatory functions for FAT10/NUB1.

1.4.3. NUB1

The NEDD8 ultimate buster 1 (NUB1) targets NEDD8 and FAT10 as well as neddylated and FAT10ylated proteins for proteasomal degradation.

NUB1 structure. The 601 aa protein has one UBL domain at the N-terminus, and two UBA domains at the C-terminus as an integral part of its structure. A naturally occurring longer splicing isoform, NUB1L, contains an insertion of 14 aa that completes the C-terminal half of a second UBA domain in NUB1L (Figure 1.9). Moreover, NUB1 has one PEST domain at the C-terminus, and a bipartite nuclear localisation signal (NLS) between residues 414-431 (Figure 1.9).

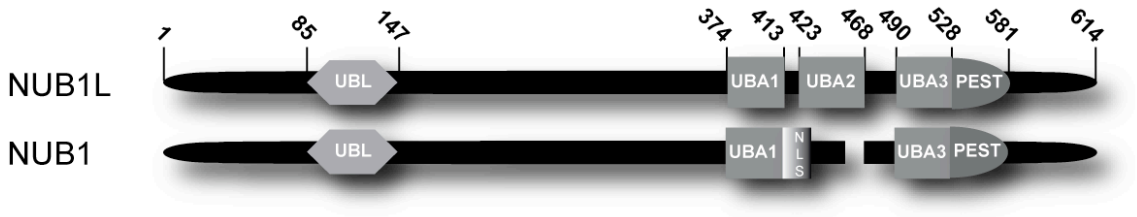

Figure 1.9. *NUB1 and NUB1L structure*. NUB1/NUB1L have a UBL domain at the N-terminus. With an insertion of 14 aa, NUB1L exhibits one extra UBA than NUB1 at the C-terminus. The predictive NLS (from aa 414 to 431) overlaps with the second UBA domain in NUB1L.

Although the UBA domains are necessary to bind FAT10, NUB1 interacts with NEDD8 via the PEST domain, between residues 536 and 584 (Schmidtke *et al.*, 2006; Kamitani *et al.*, 2001). No major functional differences between NUB1 and NUB1L have been detected, with the exception that NUB1L interacts more strongly with NEDD8 compared to NUB1 (Tanaka *et al.*, 2003). Interestingly, NUB1 and NUB1L have a greater affinity for FAT10 than NEDD8 (Hipp *et al.*, 2004).

NUB1 belongs to the UBL/UBA family proteins. Although not much is known about the UBL and UBA domains of NUB1, the UBA and UBL domains, by definition, are closely related to the UPS system, and more generally to the regulation of protein homeostasis.

1.4.3.1. The ubiquitin-associated domain

The ubiquitin-binding domains (UBD) encompass a vast number of interacting motifs for Ub, that occur in a large diversity of proteins, which are involved in a variety of processes including proteasomal degradation, deubiquitylation, endocytosis, signalling and DNA repair. The UBA domain was one of the first UBD to be discovered, using bioinformatic methods, in proteins that bind mono or polyUb (Hicke *et al.*, 2005). The UBA is a small domain of about 40 aa, formed by 3 α-helices. It is very similar to another UBD, the coupling of Ub conjugation to endoplasmic reticulum degradation domain (CUE) (Buchberger, 2002; Dikic *et al.*, 2009). Multiple UBA domains can be found within a protein, and the UBA domain often occurs in association with other UBDs or the UBL domain (Hicke *et al.*, 2005). The UBA domains are very variable in their interaction with Ub, and have led to a suggested classification of UBA domains: selective interaction with K48 (class I) or with K63 (class II) polyUb, no

interaction with Ub (class III) or interaction with polyUb with no linkage preference (class IV) (Raasi *et al*., 2005; Hurley *et al*., 2006).

UBA domain proteins and neurodegeneration. Several proteins with a UBA domain are important in neurodegenerative disorders. The protein E2-25K is a small E2 conjugating enzyme (25 kDa) that can interact with huntingtin (htt), and is therefore also called huntingtin interacting protein 2 (Wilson *et al*., 2009). In cells expressing the htt polyQ mutant, E2-25K enhances aggregate formation and cell death (de Pril *et al*., 2007). The function of the UBA domain is not fully understood, but probably contributes to the formation of the Ub binding surface (Wilson *et al*., 2009). E2-25K is highly expressed in the brain, and has been associated with AD. The UBA domain seems to be involved in E2-25K interaction with the UBB+1 Ub mutant, which accumulates in AD. Indeed, E2-25K triggers the capping of unanchored polyUb chains with the UBB+1 mutant, which inhibits the proteasome activity (Chadwick *et al*., 2012; Song and Jung, 2004). Moreover, E2-25K is upregulated in AD and in neurons exposed to Aβ peptide, where E2-25K would enhance Aβ toxicity (Song *et al*., 2003).

P62 or sequestosome 1 (SQSTM1) is a 440 aa protein that encompasses a UBA domain at its C-terminus and several other domains, including a PB1 and TBS domain that are implicated in signal transduction. P62 is involved in the regulation of protein homeostasis through proteasomal degradation and autophagy induction. P62 selectively binds K63 polyubiquitylated proteins via its UBA domain, and interacts with the proteasome via its N-terminus to target proteins for proteasomal degradation (Geetha and Wooten, 2002; Salminen et al., 2012). P62 decorates numerous inclusion bodies in neurodegenerative diseases, including PiD, PD, Frontotemporal lobar degeneration with TDP43 positives inclusions (FTDP-TDP43), spinocerebellar ataxias, AD and ALS (Kuusisto et al., 2001; Mizuno *et al*., 2006). In a mouse model of HD, p62 levels are increased and related to an early activation of autophagy (Heng *et al*., 2010). Interestingly, p62 KO mice exhibit accumulation of hyperphosphorylated tau and NFTs that lead to synaptic dysfunction, neuron loss and deficiency of working memory (Wooten *et al*., 2008). Moreover, p62 loss clearly increased the levels of GSK3β, Akt and MAPK. Indeed, p62 seems necessary for the proteasomal degradation of tau, and tau aggregates in p62 deficient mice are

K63 polyubiquitylated (Babu *et al*., 2005; Wooten *et al*., 2008).

1.4.3.2. The ubiquitin-like domain

Along with UBDs, another motif, the UBL domain, is commonly found in numerous proteins. Proteins with a UBL, called UBL-domain proteins (UDPs), are implicated in diverse cellular functions, including degradation, deubiquitination, transcription and dephosphorylation (Hartmann-Petersen and Gordon, 2004).

In contrast to the UBA domain, the UBL domain is less well characterised. The UDPs also often possess a UBD. One of the characteristics of the UBL domain is to directly bind the proteasome. A proteasome interacting motif (PIM) can be found in a group of UDPs (such as Parkin), but other UDPs that can bind the proteasome do not exhibit a PIM (including Rad23). UDP functions, however numerous, are mostly related to the proteasome and protein homeostasis (Hartmann-Petersen and Gordon, 2004). Thus, through their role in the regulation of protein levels, several UDPs have been implicated in neurodegenerative disorders, including Bag-1, Parkin and Sacsin.

UBL domain proteins and neurodegeneration: Bag1. The Bcl-2-associated athanogene 1 (Bag1) is an HSC70/HSP70 co-chaperone (Hartmann-Petersen and Gordon, 2004). Bag1 can bind the proteasome via a UBL domain at the N-terminus, and a BAG domain at the C-terminus is important for its interaction with HSC70/HSP70. Bag1 stimulates the release of substrate from HSC70/HSP70 and associates with the E3 ligase CHIP (Demand *et al*., 2001). Bag1 therefore links the protein folding chaperone system with the protein degradation system. Bag1 is involved in neuronal differentiation and neurodegenerative diseases including HD and AD (Kermer *et al*., 2002; Sroka *et al*., 2009, Elliott *et al*., 2009). In HD, Bag1 accumulates in inclusion bodies and is protective against htt toxicity *in vitro* (Jana and Nukina, 2005). In AD, Bag-1 co-localises and co-immunoprecipitates with tau and APP (Elliott *et al*., 2009). Moreover, the Bag1-M isoform is upregulated in AD patients compared to control patients. Interestingly, although Bag-1 has been shown to assist proteasomal degradation of misfolded proteins, in cells, Bag1 seems to inhibit tau proteasomal degradation via its association with HSC70/HSP70 (Elliott *et*

al., 2007).

Parkin. Parkin is a UDP protein mostly known for its role in PD. Mutation of Parkin causes AR-JP. Parkin exhibits a UBL at the N-terminus and a RING-finger box at the C-terminus. The UBL domain of Parkin binds the PSDM4 subunit of the proteasome and is important for auto-regulation of its own levels (Safadi *et al*., 2011; Sakata *et al*., 2003; Finney *et al.*, 2003). Interestingly, some mutations of Parkin that cause AR-JP are found in the UBL domain itself, and disrupt the interaction with the proteasome. As an E3 ligase, Parkin ubiquitinates several proteins, including a modified form of α-synuclein and itself (Shimura *et al*., 2001). Parkin is involved in synaptic function and mitochondrial regulation (Finsterer, 2011). Parkin targets the degradation of mitochondria by autophagy (mitophagy) via the recruitment of p62 and HDAC6 (Lee, JY *et al*., 2010; Plowey and Chu, 2011). Interestingly, in cells, Parkin has been shown to interact with Aβ, reduce its levels, reverse the inhibition of the proteasome and therefore promote cell survival (Burns *et al*., 2009; Rosen *et al.*, 2010).

Sacsin. Sacsin is a large protein of 4579 aa, containing a UBL domain at the N-terminus and a J-domain at the C-terminus. Sacsin mutations cause the neurodegenerative disorder autosomal recessive spastic ataxia of Charlevoix-Saguenay (ARSACS). The UBL domain of Sacsin binds the proteasome and Sacsin has been shown to reduce ataxin-1 aggregation (Parfitt *et al*., 2009).

1.4.3.3. UBL/UBA domain proteins and neurodegeneration

UBL/UBA proteins were first described in yeast, as proteasome substrate carriers. The yeast proteins Rad23 and Dsk2 interact with the 26S proteasome via their UBL domain, and more precisely with the Rpn10 (PSMD4 in human) subunit of the 19S proteasome (Hartmann-Petersen and Gordon, 2004). The equivalent human proteins hHR23A and B for Rad23 and Ubiquilin-2/PLIC-2 for Dsk2 also interact with the proteasome, and surprisingly with each other (Figure 1.10) (Kang *et al*., 2007).

hHR23A and B. The hHR23A/B proteins possess a UBL domain at the N-terminus, and two UBA domains at the C-terminus. The UBA domains interact with monoUb and polyUb with different affinity and preference. Besides protein

degradation, hHR23A/B has been implicated in DNA nucleotide excision repair (Chen and Madura, 2006). Recently, the proteins hHR23A/B have been shown to interact with the wild-type and mutant protein ataxin-3 (atx-3). Aggregation of atx-3 via an expanded polyQ tail causes the neurodegenerative disorder spinocerebellar ataxia type 3 (SCA-3).

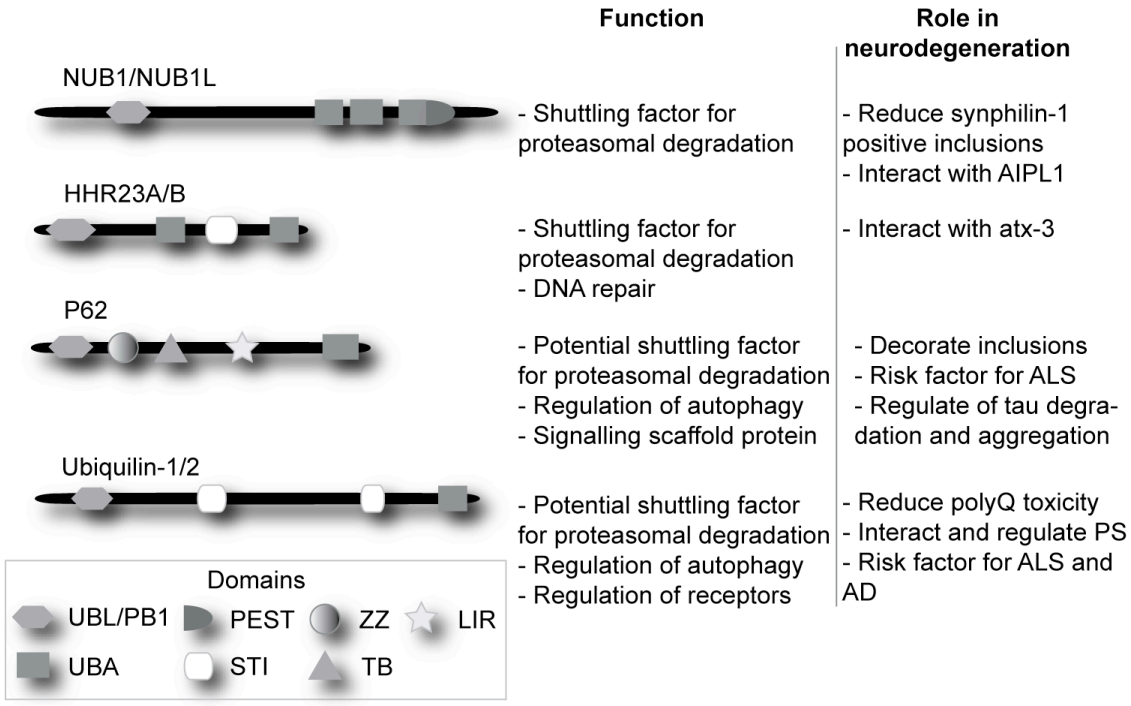

Figure 1.10. *UBL/UBA proteins*. The three proteins hHR23A/B, Ubiquilin-1/2 and NUB1/NUB1L possess a N-terminal UBL domain and one or several C-terminal UBA domains, that predict a role in proteasomal degradation. Ubiquilin-1/2 and hHR23A/B also exhibit one or two STI domains, characteristic of co-chaperone proteins, which interact with HSPs. PEST: regions rich in proline, glutamate, serine, and threonine; ZZ: zinc finger domain; TB: TRAF6 bindng domain; LIR: LC3 interacting region.

In cells, hHR23A/B both interact with atx-3 via their UBL domains, and hHR23A co-localises with aggregated atx-3 (Wang *et al*., 2000; Reina *et al*., 2010).

Ubiquilin protein family. The study of Ubiquilin-2 (PLIC-2 or UBQLN2) led to the discovery of another isoform, Ubiquilin-1 (also called PLIC-1 or UBQLN1), both of which are involved in neurodegeneration. A third isoform, Ubiquilin-3 (or UBQLN3), seems to be expressed only in the testis (Conklin *et al.,* 2000). The Ubiquilins have one N-terminal UBL domain and one C-terminal UBA domain. Both Ubiquilin-1 and -2 can interact with the proteasome via their UBL domain, and with Ub via their UBA domain. Therefore, a potential role for these proteins

is the shuttling of ubiquitylated proteins to the proteasome (Kleijnen *et al*., 2000; Ko *et al*., 2004).

Another role of Ubiquilins is to regulate autophagy. Upon starvation, cells with depletion of Ubiquilins are sensitized to cell death (N'Diaye *et al*., 2009). Both Ubiquilins have been shown to regulate receptors, but not in the same pathways. Ubiquilin-1, via its UBA domain, interacts with the $GABA_A$ receptor and regulates its trafficking through the ER (Saliba *et al*., 2008). On the other hand, Ubiquilin-2, via its UBL and UBA domains, downregulates the endocytosis of G-protein coupled receptors (N'Diaye *et al*., 2008). In addition, both Ubiquilin-1 and -2 are implicated in aggresome formation and neurodegeneration, although not always for the same disorders. For instance, they have both been shown to accumulate with polyQ inclusions in a cell model and mouse model of HD (Doi *et al*., 2004). However, if Ubiquilin-1 has been shown to be involved in AD, Ubiquilin-2 has mostly been implicated in ALS.

Several studies links Ubiquilin-1 and AD, via the regulation of both PS and APP. A yeast-two hybrid analysis demonstrated that Ubiquilin-1 interacts with both PS1 and PS2 (Mah *et al*., 2000). Interestingly, overexpression of Ubiquilin-1 in cells induces PS2 accumulation, probably by facilitating protein synthesis (Mah *et la*., 2000). Similarly, ectopic expression of Ubiquilin-1 has been shown to increase the high molecular weight form of PS1 and to trigger its accumulation in aggresomes, without altering the γ-secretases activity (Wiswanathan *et al*., 2011). In this study, they propose that Ubiquilin-1 targets ubiquitinated PS1 either for proteasomal degradation or aggresome accumulation. Moreover, Ubiquilin-1 downregulation in cells increased the maturation of APP, its trafficking to the plasma membrane, the secretion of sAPP (α and β) and the formation of $A\beta_{40}$ and $A\beta_{42}$. As the down-regulation of Ubiquilin-1 did not affect the activity of α, β and γ-secretases activity, they suggest that Ubiquilin-1 is a "gate-keeper," a trafficking factor which, in co-operation with PS for instance, might regulate the APP secretory pathway (Hiltunen *et al*., 2006). In addition, NFTs from AD patients and Lewy bodies from PD patients were both positive for Ubiquilin-1 (Mah *et al*., 2000). Following these results, a single nucleotide polymorphism (SNP) in the *UBQLN1* gene that resulted in an alternative splicing of the gene lacking the exon 8 was suggested to be a risk factor for late

onset AD (Bertram *et al*., 2005). However, this hypothesis remains controversial (Slifer *et al*., 2006). Apart from AD, Ubiquilin-1 may be implicated in ALS. The UBA domain of Ubiquilin-1 were suggested to be involved in recruitment of TDP-43 to aggresomes and activation of autophagy, while a mutant form of TDP-43 asociated with sporadic ALS was no longer able to bind Ubiquilin-1, which reduced their association in aggregates (Kim *et al*., 2009).

Besides its potential involvement in polyQ diseases, Ubiquilin-2 interacts with and recruits Eps15 to aggresomes via its UBL domain (Regan-Klapisz *et al*., 2005). However, Ubiquilin-2 is mostly known for its role in ALS. Indeed, recent studies have demonstrated that mutations in the Ubiquilin-2 gene cause ALS (Deng HX *et al*., 2011). A total of about 2% of cases of familial ALS (FALS) harbored a mutation in the C-terminus of Ubiquilin-2, but none were in the UBA or in the UBL domain. Ubiquilin-2 positive inclusions were found in the spinal cord of FALS patients but also in patients with sporadic ALS. Furthermore, Ubiquilin-2 positive inclusions were found in the hippocampus of ALS patients with dementia, but not in patients without dementia. Although further studies are necessary, Ubiquilin-2 is probably an important new factor in ALS and dementia (Deng HX *et al*., 2011; Daoud and Rouleau, 2011). Recently, inclusions from various neurodegenerative disorders were positive for Ubiquilin-2, including Lewy bodies in PD and dementia with Lewy bodies, and in six different polyQ-associated pathologies, which suggests a wider role for Ubiquilin-2 in neurodegeneration (Mori *et al*, 2012).

1.4.3.4. The UBL/UBA domain protein NUB1

NUB1/NUB1L is an interesting UBL/UBA protein. Indeed, the necessity for its UBL domain in proteasome binding is controversial, and its UBA domains are not always involved in target recognition (Tanji *et al.*, 2005; Rani *et al.*, 2012). For instance, the UBA domains are necessary for NUB1/NUB1L to bind FAT10 and UbC1, but NEDD8 interacts with NUB1 at its C-terminus near the PEST domain. However, the UBA2 domain of NUB1L can also interact with NEDD8 (Tanaka *et al*., 2003; Schmidtke *et al*., 2006). Nonetheless, NUB1 has been shown to promote proteasomal degradation of proteins, and to be involved in apoptosis, cell cycle regulation, cell signalling and neurodegeneration.

The primary function of NUB1/NUB1L is shuttling proteins for proteasomal degradation. Indeed, NUB1/NUB1L can directly bind the PSMD4 subunit of the 19S proteasome, although probably not via its UBL domain (Tanji *et al*., 2005). The best characterised targets for NUB1/NUB1L mediated proteasomal degradation are the ULM NEDD8 and FAT10 as well as their conjugates. NUB1 also interacts with the Ub precursor UbC1, and together with an Ub C-terminal hydrolase mediates the C-terminal hydrolysis of UbC1, thus resulting in the release of Ub monomers consequently available for the polyubiquitination of target proteins. Therefore, NUB1 may play a role in regulating the availability of Ub monomers for conjugation (Tanaka *et al*., 2004).

NUB1 may also directly modulate cell-cycle activity and cell proliferation. NUB1 interacts with p53 in a NEDD8-dependent manner, thereby increasing p53 ubiquitylation and translocation to the cytoplasm, and inhibiting p53 transcriptional activity (Liu and Xirodimas, 2010). NUB1 overexpression has recently been shown to be anti-proliferative in renal carcinoma cells. Indeed, NUB1 overexpression downregulated NEDD8 levels, and induced apoptosis and cell cycle arrest in the S-phase (Hosono *et al*., 2010).

NUB1 function has been implicated in neurodegeneration. NUB1 interacts with the aryl hydrocarbon receptor interacting protein-like 1 (AIPL1). Mutations in AIPL1 cause Leber congenital amaurosis (LCA) leading to the early and severe neurodegeneration of the retinal photoreceptors causing early-onset blindness. AIPL1 induces a cytoplasmic translocation of NUB1 from the nucleus, and consequently probably regulates NUB1 functions (van der Spuy *et al*., 2004). Indeed, wild-type AIPL1 inhibits the NUB1-dependent degradation of FAT10 and its conjugates, whereas AIPL1 mutants that cause LCA are unable to delay FAT10 degradation. Thus, NUB1-dependent degradation of FAT10 and FAT10 conjugated proteins might be an important underlying mechanism of AIPL1 associated retinal degeneration (Bett *et al*., 2012).

An intriguing role for NUB1 is its capacity to interact with synphilin-1, a protein that accumulates in Lewy bodies in various neurodegenerative diseases, including PD. NUB1 interacts directly with synphilin-1 via the same region that interacts with NEDD8, thereby promoting synphilin-1 proteasomal degradation

and reducing synphilin-1 positive inclusions (Tanji *et al*., 2006). Moreover, NUB1 is detected in Lewy bodies in PD and in dementia with Lewy bodies, and accumulates in presynaptic neurites along with protein kinase (PK)-resistant α-synuclein (Tanji *et al*., 2007; Tanji *et al*., 2011).

In conclusion, there is a lot of evidence to support a role for the ULM NEDD8 and the NEDD8 ultimate buster 1, NUB1, in neurodegeneration. In particular, NEDD8 appears to have an important role in AD, exemplified by its accumulation in NFTs and senile plaques. Furthermore, the downregulation of NEDD8 expression and direct targeting of synphilin-1 by NUB1 emphasizes the importance of NUB1 in protein homeostasis and in neurodegenerative disorders. Thus, the NUB1 pathway might play an important regulatory role in pathogenic mechanisms of AD.

1.5. Aims of this study

This study set out to test the hypothesis that NUB1 may have an important function in neurons and in neuropathogenic mechanisms in AD.

The first aim was to examine the expression and localisation of endogenous NUB1 and the ULM regulated by NUB1 in brain sections of AD patients. Moreover, the localisation of NUB1, tau and GSK3β was also explored in primary rat cortical neurons.

The second objective was to assess the role of NUB1 in the modulation of tau in neuroblastoma cells. Therefore, the formation of inclusions of wild type tau in the presence of GSK3β and proteasome inhibitors was assessed, and the influence of NUB1, NUB1L and NUB1L UBL/UBA mutants on tau aggregation was investigated.

The third aim was to analyse the potential interactions between NUB1, GSK3β and tau in neuroblastoma cells. Moreover, the effect of NUB1, NUB1L and NUB1L UBL/UBA mutants on the levels of total and phosphorylated tau and on the turnover of GSK3β was examined.

Finally, the fourth aim was to explore the functional implications of the findings for the endogenous complex. In particular, the affect of the downregulation of endogenous NUB1 by RNA interference on the turnover of endogenousGSK3β was investigated.

Chapter 2

Materials and Methods

2.1. Reagents

The source and catalogue number of all reagents are listed in appendix A. All the solution compositions are listed in appendix B.

2.2. Molecular techniques

2.2.1. Plasmids

All the plasmids used for this study are listed in table 2.1.

Table 2.1. *Plasmids.*

Vector	cDNA insert	Source	Tag	Tag location	Resistance
pEGFP-C1	Tau 0N4R isoform	Utton *et al., 2005*	GFP	N-terminus	Kanamycin (50 µg/ml)
	NUB1	van der Spuy *et al., 2004*			
	Empty				
pCMV-DsRed	Tau 0N4R isoform	Dr Diane Hanger	DsRed	N-terminus	Kanamycin (50 µg/ml)
pCMV-Tag3B	NUB1	Constructed in the laboratory	c-Myc	N-terminus	Kanamycin (50 µg/ml)
	Empty	Sigma			
pCMV14/3xFLAG	NUB1	Bett *et al.*, 2012	FLAG	C-terminus	Ampicillin (100 µg/ml)
pCDNA3.1	NUB1	Schmidtke *et al.,* 2006	HA	N-terminus	Ampicillin (100 µg/ml)
	NUB1L				
	NUB1LΔUBL				
	NUB1LΔUBA1-3				
pMT2	GSK3β	Lovestone *et al.*, 1994	HA	N-terminus	Ampicillin (100 µg/ml)

2.2.2. Amplification of plasmids

Plasmids were amplified by bacterial transformation. Briefly, 50 ng of plasmid was incubated with 25 µl of JM09 competent cells on ice for 10 min, followed by a heat-shock (42°C, 45 sec) and incubation on ice for 2 min. After adding 975 µl of warm (37°C) Luria-Bertani broth (LB), cells were left to grow for 1 h at 37°C with agitation (300 rpm). A volume of 50 µl of cells was plated on LB/agarose containing antibiotics (Table 2.1), and incubated at 37°C for 18 h. A single colony of bacteria was inoculated in 2 ml of LB with antibiotics for 7 h at 37°C with agitation. The starter culture was diluted at 1:1000 in 50 ml of LB with antibiotics and incubated overnight (O/N) at 37°C with agitation before plasmid extraction.

2.2.3. Plasmid extraction and purification

Plasmid DNA was extracted using the HISpeed Plasmid Midi kit according to the manufacturer's protocol. After precipitation with isopropanol, the DNA was washed with ethanol, eluted in 0.8 ml of water, and stored at -20°C. DNA concentration was measured using a ND-1000 Nanodrop spectrophotometer (Labtech international, East Sussex, UK).

2.2.4. NUB1 siRNA

The ON-TARGETplus Specificity-Enhanced small interfering RNA (siRNA) against NUB1 was obtained from Dharmacon. In addition, a non-targeting siRNA was used as a negative control. Sequences are shown in table 2.2.

Table 2.2. *SiRNA sequences.*

siRNA	Sequence	Reference
NUB1	5'-CGAUGGUGCUUGAACUAAAUU-3'	Tanji *et al*, 2006
Non-targeting	5'-UAGCGACUAAACACAUCAA-3'	Evans *et al*, 2010

2.2.5. NUB1 antibody

To generate the NUB1 antibody (AB), a rabbit polyclonal anti-serum was raised against a C-terminal polypeptide (LSYVENRKSATKKN, from residues 588 and 601 included) of human NUB1 protein, conjugated to keyhole limpet

hemocyanin (van der Spuy *et al*, 2003) (Genosys Biotechnology, Cambridge, UK).

2.3. Cell culture

2.3.1. Culture of adherent cells

The origin of all cells cultured is presented in table 2.3.

2.3.1.1. Immortalised neuroblastoma cells

Human SK-N-SH and SH-SY5Y neuroblastoma cells were grown at 37°C and 5% CO_2 in complete media, i.e. Dulbecco's Modified Eagle's Medium (DMEM), supplemented with 10% foetal bovine serum (FBS) and penicillin (100 U/ml), streptomycin (100 µg/ml) in a T75 flask. For propagation, every 2-3 days, cells were washed with Hank's Balanced Salt Solution (HBSS), trypsinised with trypsin-ethylenediaminetetraacetic acid (Trypsin-EDTA, 0.05%), and diluted in 15 ml of complete media at 1:5 for SK-N-SH and 1:4 for SH-SY5Y cells in a T75 flask to grow at 37°C.

2.3.1.2. Primary neurons

The extraction of primary cortical neurons was performed by authorised personnel in Dr. Diane Hanger's laboratory, at the Institute of Psychiatry, London, UK (Pooler *et al*., 2012). Primary cortical neurons were extracted from Sprague Dawley rat embryos (stage E18) and incubated at 37°C and 5% CO_2 in complete rich media, i.e. in Neurobasal medium, supplemented with 2% B27, penicillin (100 U/ml), streptomycin (100 µg/ml) and 0.5 mM L-glutamine.

Table 2.3. *Origin of cell lines.*

Cell line	Species	Tissue	Origin	Morphology	Reference
SK-N-SH	Human	Bone Marrow	Neurobla-stoma	Epithelial	Biedler *et al*, 1973
SH-SY5Y	Human	Bone Marrow	SK-N-SH cells	Epithelial	Biedler *et al*, 1978
Rat cortical neurons	Rat	Brain	Sprague Dawley ® strain	Primary neurons	Pooler *et al*, 2012

2.3.2. Transient transfection of neuroblastoma cells

2.3.2.1. Plating of cells

Cells were plated in preparation for transfection as described in table 2.4.

Table 2.4. *Number of cells plated for transfection.*

Cell line	Dish	Type of transfection	Number of cells/well	Volume of media/well	Time before transfection
SK-N-SH	6-well plate	Plasmid	$5x10^5$	2 ml	24 h
	8-well chamber slide	Plasmid	$5x10^4$	0.25 ml	24 h
SH-SY5Y	6-well plate	Plasmid	$6.5x10^5$	2 ml	24 h
		siRNA	$2x10^5$	2 ml	24 h
	8-well chamber slide	Plasmid	$6.5x10^4$	0.25 ml	24 h
Rat cortical neurons	6-well plate	Plasmid	$1x10^6$	2 ml	5 days
	12-well plate	Plasmid	$0.5x10^6$	1 ml	5 days

2.3.2.2. Transient transfection of plasmid DNA

SK-N-SH and SH-SY5Y cells were plated at the density described (Table 2.4) with complete media. Cells were transfected 24 h after plating, using lipofectamine and Plus reagent in DMEM free of serum and antibiotics (serum free media, SF) as described by the manufacturer (Invitrogen, Paisley, UK). The total quantity of DNA per transfection was equalised by the addition of an empty vector if necessary. Untransfected cells and mock transfected cells, which were treated with lipofectamine and Plus reagent in the absence of DNA, were used as controls.

In a 6-well plate. A total of 2.4 µg of DNA per well (amount of each plasmid detailed in table 2.5) diluted in 100 µl of SF was incubated with 8 µl of Plus reagent for 15 min at room temperature (RT). 4 µl of lipofectamine per well was diluted in 800 µl of SF. A final volume of 804 µl of SF/lipofectamine was added to the DNA/Plus mix and incubated for 15 min at RT. Cells were washed three times with SF, and incubated with 900 µl of the final DNA mix for 3 h at 37°C. Finally, 900 µl of DMEM supplemented with 20% FBS and 2% of antibiotics was added to each well, and cells were left to grow for at least 24 h.

In an 8-well Permanox chamber slide. A total of 0.3 µg of DNA (amount of each plasmid detailed in table 2.5) was mixed with 1 µl of Plus reagent and SF to a final volume of 12.5 µl, and incubated at RT for 15 min. 0.5 µl of lipofectamine was incubated with 100 µl of SF per well. The SF/lipofectamine mix was added to the DNA/Plus mix and incubated at RT for a further 15 min. A total volume of 112 µl of final mix per well was added to the cells for 3 h, before adding 112 µl of DMEM supplemented with 20% FBS and 2% antibiotics. Cells were left to grow for at least 24 h.

Table 2.5. *Amount of each plasmid transfected in 6-well plates and 8-well chamber slides*. N/A: non applicable**.**

Plasmid	Protein expressed	Amount of DNA per well	
		6-well plate	8-well chamber slide
pEGFP-0N4R	GFP-tau	0.4 µg	0.05 µg
pDsRed-tau	DsRed-tau	0.4 µg	N/A
pEGFP-NUB1	GFP-NUB1	0.8 µg	0.1 µg
pCMV-Tag3-NUB1	c-Myc-NUB1	0.8 µg	0.1 µg
pCMV14-NUB1	NUB1-FLAG	0.8 µg	0.1 µg
pCDNA3.1-NUB1	HA-NUB1	0.8 µg	0.1 µg
pCDNA3.1-NUB1L	HA-NUB1L	0.8 µg	0.1 µg
pCDNA3.1-NUB1LΔUBL	HA-NUB1LΔUBL	0.8 µg	0.1 µg
pCDNA3.1-NUB1L ΔUBA1-3	HA-NUB1LΔUBA1-3	0.8 µg	0.1 µg
pMT2-GSK3β	HA-GSK3β	1.2 µg	0.15 µg

Optimisation of relative amounts of plasmids. Cells were plated in 8-well chamber slides as described in table 2.4. Transient transfection was performed as described above with increasing amounts of pMT2-GSK3β while that of pEGFP-0N4R remained constant at either 25 ng, 50 ng or 100 ng (Table 2.6.) The total amount of DNA transfected was 0.2 µg, equalized by the addition of empty plasmid where necessary.

Table 2.6. *Quantity of plasmids transfected for the optimisation of tau inclusions in the presence of GSK3β.*

Plasmid	**Quantity of plasmid transfected (ng)**											
pEGFP-0N4R	25	25	25	25	50	50	50	50	100	100	100	100
pMT2-GSK3β	25	50	100	150	25	50	100	150	25	50	75	100
Ratio tau:GSK3β	1:1	1:2	1:4	1:6	1:0.5	1:1	1:2	1:3	1:0.25	1:0.5	1:0.75	1:1

Titration of NUB1 plasmids. Cells were plated in 8-well chamber slides as described in table 2.4. Transient transfection was performed as described above. A total amount of 0.3 µg plasmid DNA, equalized by the addition of empty vector where necessary, was transfected as listed in table 2.7.

Table 2.7. *Quantity of plasmid transfected for the effect of NUB1, NUB1L or NUB1L mutants on tau inclusions.*

Plasmid	**Quantity of plasmid transfected (ng)**							
pEGFP-0N4R	50	50	50	50	50	50	50	50
pMT2-GSK3β	N/A	N/A	N/A	N/A	150	150	150	150
pCDNA3.1 NUB1 or pCDNA3.1 NUB1L or pCDNA3.1 NUB1LΔUBL or pCDNA3.1 NUB1LΔUBA1-3	25	50	75	100	25	50	75	100
Ratio NUB1:tau	1:0.5	1:1	1:1.5	1.2	1:0.5	1:1	1:1.5	1.2

With the exception of the optimisation of relative amounts of plasmids and the titration of NUB1 plasmids described above, SK-N-SH cells were transfected as described as listed in table 2.5.

2.3.2.3. Transient transfection of siRNA

Cells were plated in a six well plate in preparation for transfection as described in table 2.4, in serum rich media without antibiotics (SR). All siRNA were transfected using DharmaFECT according to the manufacturer's protocol (Dharmacon, Thermo Scientific, Northumberland, UK). Briefly, 24 h after plating, 100 µl of 200 nM siRNA were mixed with 100 µl of SR and left to incubate for 5 min at RT. 2 µl of Dharmafect reagent 1 was mixed with 198 µl of SR. The siRNA/SR and Dharmafect/SR were mixed together and incubated for 15 min at

RT. 1.6 ml of SR was added to the final mix, and 2 ml of the solution was added to the cells for 72 h at 37°C if not said otherwise.

2.3.3. Transient transfection of rat primary cortical neurons

All biochemical analysis of proteins were performed in 6-well plates, and immunodetection of proteins in 12-well plates, with a glass coverslip added to the bottom of the well before plating cells at the density described in table 2.4.

Cells were transfected after 5 days *in vitro* (DIV) culture using lipofectamine 2000 in Opti-MEM according to manufacturer's instructions (Invitrogen, Paisley, UK). 3 µg of either pEGFP-C1 or pEGFP-C1-NUB1 was mixed with 200 µl of Opti-MEM and 7 µl of lipofectamine 2000 per well, and incubated for 20 min at RT. The media was removed from the cells and retained at 37°C, and replaced by the addition of 1 ml of Opti-MEM to the cells. 0.8 ml of Opti-MEM was added to the DNA/lipofectamine solution. The Opti-MEM was removed from the cells which were then incubated with 1 ml of the final DNA mix for 5 h at 37°C. After removing the transfection solution, 1 ml of the previously retained complete media and 1 ml of fresh complete media were added to the cells.

2.3.4. Treatment of cells with proteasome inhibitors

All drugs and vehicles were diluted in serum rich media, and treatments were performed at least 24 h after transfection (table 2.8).

Cells were transfected as described in chapter 2.3.2. Cells were treated with a vehicle (NT), epoxomicin (EPO), lactacystin (LAC), Z-Leu-Leu-Leu-al (MG132), or a combination of two (LAC+MG132, EPO+MG132 and LAC+EPO) for 2, 4 and 6 h (Table 2.8). In subsequent experiments, cells were treated with MG132 or a vehicle for 4 h, 30 h after transfection.

Table 2.8. *Drug treatments.* Ki: inhibition constant, obtained from the manufacturer's data sheet.

Drug	Concentration	Vehicle	Potency	Treatment
Lactacystin	10 µM	Water	K_i = 4 nM	2, 4 or 6 h
Epoxomicin	10 µM	Dimethyl Sulfoxide (DMSO)	IC_{50} = 4 nM	2, 4 or 6 h

MG132	50 µM	DMSO	K_i = 4 nM	2, 4 or 6 h

2.4. Protein localisation

2.4.1. Immunohistochemistry

Immunohistochemistry (IHC) of proteins in brain sections was performed with the LSAB Dakocytomation kit. All the paraformaldehyde (PFA) fixed, paraffin embedded brain sections (8 µm) were provided by the London Brain Bank. Sections were dewaxed in three changes of xylene for 10 min each with agitation. Sections were then rehydrated in two changes of 100% and one change of 95% industrial methylated spirit (IMS) for 5 min each.

Tau, Ub, FAT10 and NEDD8 detection. To block endogenous peroxidase activity, sections were incubated in 0.5% hydrogen peroxidase (H_2O_2)/methanol for 30 min, and washed in water for 10 min. Sections were treated with 0.01 M citric acid, pH6, and boiled in a microwave oven for 4x2.5 min for antigen retrieval. Twenty minutes after the antigen retrieval, sections were washed in water for 10 min and in phosphate buffered saline (PBS) for 3x5 min with agitation, and blocked in 10% normal swine serum/2% bovine serum albumin (BSA)/PBS for 1 h at RT. After washing 3x5 min in PBS, sections were incubated with primary antibodies (table 2.9) in 0.1% BSA/PBS at 4°C O/N with gentle agitation. Sections were washed 3x5 min in PBS, and incubated for 30 min with the swine multilink secondary antibody (LSAB Dakocytomation kit, table 2.10) for 30 min or with the swine anti-rabbit polyclonal antibody in 0.1% BSA/PBS for FAT10 staining for 45 min at RT. Sections were washed as described above and incubated with peroxidase solution (Dakocytomation kit) for 30 min at RT. Sections were washed 3x10 min in PBS, incubated with 3,3-diaminobenzidine tetrahydrochloride (DAB, from the LSAB Dakocytomation kit) for 30 sec to 1 min and immediately washed in water for 10 min with agitation. Sections were dehydrated with one change of 70% and 95% IMS and three changes of 100% IMS. Finally, sections were cleared with three changes of xylene for 10 minutes each and mounted with DPX mounting media.

Table 2.9. *Primary antibodies*.

Name	Specificity	Host species	WB	ICC	IHC	IP
Anti-tau	Total human tau protein	Rabbit	1:40 000	1:2000	N/A	1:1000
Anti-pS396	Tau phosphorylated on S396	Rabbit	1:5000	1:500	N/A	N/A
AT8	Tau phosphorylated on S199, S202 and T205	Mouse	1:1000	1:250	1:1500	N/A
Anti c-Myc	c-Myc tagged proteins	Mouse	1:5000	1:1000	N/A	1:500
Anti-GFP	GFP tagged proteins	Mouse	1:2000	N/A	N/A	N/A
Anti-GSK3β	GSK3β	Rabbit	1:2000	1:100	N/A	1:100
Anti-FLAG	FLAG tagged proteins	Mouse	1:5000	N/A	N/A	1:500
Anti-HA	HA tagged proteins	Mouse	1:5000	1:500	N/A	1:500
		Rabbit	1:2000	1:250	N/A	N/A
Anti-FAT10	FAT10 and FAT10 conjugates	Rabbit	N/A	N/A	1:500	N/A
Anti-NEDD8	NEDD8 and NEDD8 conjugates	Rabbit	N/A	N/A	1:500	N/A
Anti-NUB1	NUB1, NUB1L and NUB1L mutant proteins	Rabbit	1:20000	N/A	1:1500	N/A
Anti-Ub	Ub and Ub-conjugated proteins	Rabbit	N/A	N/A	1:500	N/A
Anti-GAPDH	Glyceraldehyde 3-phosphate dehydrogenase	Mouse	1:20000	N/A	N/A	N/A
Anti-Actin	Actin	Rabbit	1:2000	N/A	N/A	N/A
Anti-tubulin	β-tubulin subunit	Mouse	1:2000	1:150	N/A	N/A

Table 2.10. *Secondary antibodies.*

Name	Raised against	WB/IP	ICC	IHC	Colour emitted
GαM HRP	Mouse	1:30 000	N/A	N/A	N/A
GαR HRP	Rabbit	1:30 000	N/A	N/A	N/A
Swine multilink biotinylated	Rabbit, Mouse, goat	N/A	N/A	From LSAB Dakocytomation kit, few drops	N/A
Swine biotinylated	Rabbit	N/A	N/A	1:300	N/A
Alexa Fluor® 488 goat	Mouse	N/A	1:1000	N/A	Green
Alexa Fluor® 488 goat	Rabbit	N/A	1:1000	N/A	Green
Alexa Fluor® 594 goat	Mouse	N/A	1:1000	N/A	Red
Alexa Fluor® 594 goat	Rabbit	N/A	1:1000	N/A	Red
Alexa Fluor® 647 goat	Mouse	N/A	1:1000	N/A	Purple
Alexa Fluor® 647 goat	Rabbit	N/A	1:1000	N/A	Purple

NUB1 detection. NUB1 immunostaining followed the same steps as described above with a number of changes. To block endogenous peroxidase activity, sections are incubated in 3% H_2O_2/methanol for 30 min, and for antigen retrieval sections were boiled in Mc Ilvane's citrate buffer. Anti-NUB1 (table 2.9) and swine anti-rabbit were used as the primary and a secondary antibody respectively. To verify the NUB1 AB specificity, NUB1 AB was incubated for 1 h at RT with the polypeptide (30 µg/ml) against which it was raised (Chapter 2.2.5), before incubation with the brain sections.

Localisation of NUB1 and NEDD8. The subcellular localisation of NEDD8 and NUB1 in the CA1-2 and CA4 areas of the hippocampus was observed, and divided into three categories: strictly nuclear (N), nuclear and cytoplasmic (N/C) and strictly cytoplasmic (C). To calculate the percentage of cells with nuclear or cytoplasmic NUB1 and NEDD8 localisation, at least 100 cells were counted for each region. Statistical significances were determined using the unpaired Student's *t*-test.

2.4.2. Fixation and permeabilisation of cells

Fixation and permeabilisation of SK-N-SH and SH-SY5Y cells. To detect the localisation of proteins by immunofluorescent laser scanning confocal microscopy, cells were plated and transfected as described in chapter 2.3.2 in an 8-well Permanox chamber slide. After treatment with MG132 or a vehicle for 4 h, cells were rinsed once with warm (37°C) PBS and once with warm (37°C) Pipes/ Ethylene glycol-bis(2-aminoethylether)-N,N,N′,N′-tetraacetic acid (EGTA)/Magnesium chloride ($MgCl_2$) buffer (PEM), fixed and permeabilised with 0.3% glutaraldehyde/0.5% Nonidet P-40 for 10 min. All fixations were performed at 37°C to preserve microtubule structures and associated proteins. All the subsequent steps were done at RT. Cells were rinsed with PBS, and treated with sodium borohydride ($NaBH_4$) for 7 min. After a wash with PBS, cells were incubated with 0.1 M glycine for 20 min to reduce background. Alternatively, in order to count cell inclusions, cells were fixed with 100% methanol for 10 min at -20°C and permeabilised with 0.1% Triton X-100 for 5 min at RT. Protein immunocytochemistry (ICC) was performed as described in chapter 2.4.3.

Fixation of primary neurons. Cells were plated and transfected as described in chapter 2.3.1.2 and 2.3.3 in a 12-well plate with glass coverslips. Cells were treated with MG132 or a vehicle for 4 h. Coverslips were washed 3x with warm PBS (37°C) and fixed with 4% PFA for 10 min at 37°C. Cells were rinsed with PBS, and permeabilised with 0.1% Triton X-100 for 5 min at RT. Protein immunodetection was performed as described in chapter 2.4.3.

2.4.3. Immunocytochemistry

After fixation and permeabilisation of cells, all the subsequent steps were done at RT. Cells were rinsed with PBS (5 min) and blocked with block solution (3% BSA/goat normal serum) for 1 h. Cells were incubated with primary antibody (table 2.9) diluted in block solution for 1 h. After 3x5 min washes with PBS, cells were incubated with an AlexaFluor secondary antibody (table 2.10) diluted in block solution for 45 min at RT. Cells were washed 2x5 min with PBS, and incubated with 4',6-diamidino-2-phenylindole (DAPI) (2 mg/ml diluted 1:5000 in

PBS) for 5 min. Cells were washed 1x5 min with PBS and mounted with Dako mounting medium. All images were taken with a Carl Zeiss LSM700 confocal microscope (Carl Zeiss Ltd, Hertfordshire, UK).

2.4.4. Analysis of NUB1 localisation

NUB1 localisation. The localisation of NUB1 in at least 100 cells was analysed in cells transfected with GFP-NUB1 in the presence or absence of MG132. Total Fluorescence intensity in the nucleus and in whole cells was measured using the ImageJ software (Image Processing and Analyse in Java, http://rsbweb.nih.gov/ij/). The ratio of nuclear fluorescence intensity was calculated as a percentage of the whole cell fluorescence intensity:

Nuclear (N) (%) = (Nuclear intensity/Whole cell intensity) x 100

The cytoplasmic fluorescence intensity was deducted from there:

Cytoplasmic (C) (%) = 100 – (N)

The error bars were the standard error of the mean.

NUB1 recruitment to tau. Pearson's and Mander's coefficients were measured to determine the co-recruitment of GFP-NUB1 and DsRed-tau to microtubules and DsRed-tau inclusions. The Pearson's coefficient (PC) and Mander's coefficient (M) were calculated using the Just Another Colocalization plugin (JACoP, http://rsbweb.nih.gov/ij/plugins/track/jacop.html, Bolte and Cordelieres, 2006) in ImageJ. At least 3 different cells for DsRed-tau and GFP-NUB1 co-localisation were analysed and the PC and MC calculated. Pearson's coefficient (PC) indicates the degree of overlap and scores between (-)1 and (+)1, where (-)1 indicates total exclusion, (+)1 a perfect image registration and (0) a random localisation. The Pearson's coefficient takes into account the shape and the intensity, but is affected by the presence of non-overlapping data, i.e. a signal present only in one channel. On the other hand, the Mander's coefficient indicates when the Red and Green channel are overlapping, and will give a number between 0 and 1 which is calculated from the contribution of the Green (GFP-NUB, M1) or the Red (DsRed-tau, M2) to the co-localising area,

independently of the intensity. However, this coefficient is very sensitive to background, therefore a threshold was set before calculation.

The mean and standard error of the mean were calculated using Excel and statistical significances were determined using the unpaired Student's-*t* test.

2.4.5. Quantitation of tau inclusions

To calculate the percentage (%) of cells expressing GFP-tau, at least 4 fields of 100 cells were counted. To calculate the percentage (%) of GFP-tau inclusions in GFP-tau transfected cells, at least 4 fields of 100 cells transfected with GFP-tau were counted and scored for the presence of inclusions. The percentage of GFP-tau inclusions in GFP-tau transfected cells was counted blind to experimental status. Statistical analysis was performed using an unpaired Student's *t*-test.

2.5. Protein levels and interactions

All protein analyses were performed in 6-well plates.

2.5.1. Sample preparation for western blotting

SK-N-SH and SH-SY5Y cells. Cells were plated in 6-well plates and transiently transfected as described in chapter 2.3.1.1 and 2.3.2.2 respectively. Cells were lysed with 200 µl of RIPA buffer supplemented with 2% protease inhibitor cocktail (PIC) and 1% phosphatase inhibitor cocktail (PhIC) for 5 min on ice. Cells were dislodged from the wells using a sterile cell scraper, collected and sonicated for 10 sec on ice (continuous pulse, 22.5 kHz, Amplitude 5) using a Misonix Ultrasonic Liquid Processor XL-2000 (Misonix Incorporated, Farmingale, NY). 20 µl of the sample was removed for protein quantification as described in chapter 2.5.2. After adding 60 µl of 4x loading buffer, samples were boiled for 3 min, and centrifuged for a few seconds at 12 000 rpm before resolving the proteins by denaturing sodium dodecyl sulphate-polyacrylamide gel electrophoresis (SDS-PAGE) (Chapter 2.5.3). If not said otherwise, 10 µg of proteins were resolved on a 10% polyacrylamide gel and analysed by western blotting (WB) as described in chapter 2.5.3 and 2.5.4.

Rat cortical neurons. Cells were plated in 6-well plates and transiently transfected as described in chapter 2.3.1.2 and 2.3.3 respectively. Cells were lysed with 1xLaemli buffer without dye, supplemented with 2% PIC and 1% PhIC for 5 min on ice. Cells were scraped together and after adding the bromophenol blue dye, cells were boiled for 15 min and centrifuged for a few seconds at 12 000 rpm. A total of 25 µg of proteins were resolved on a 10% polyacrylamide gel and analysed by WB as described in chapter 2.5.3 and 2.5.4.

2.5.2. Quantification of proteins

Protein concentration from cell lysates was determined using the bicinchonitic acid (BCA) Protein Assay kit. The BCA reagents A and B were mixed at a ratio 50:1, and 200 µl of the A/B mix was added to 10 µl of cell lysates in duplicate. In parallel, a standard curve was determined by adding 200 µl of the A/B mix to 10 µl of known amounts of BSA diluted in the same buffer used to lyse the cells giving a standard concentration ranging from 200 ng/ml to 2 000 ng/ml The test and standard samples were prepared in duplicate. The samples were incubated for 30 min at 37°C. The absorbance was measured at 562 nm with a spectrophotometer (Safire, Tecan, Reading, UK). The concentration of proteins from cell lysates was calculated by interpolation from the BSA standard curve, which was plotted using Excel software.

2.5.3. SDS-PAGE

The SDS-PAGE gels were prepared and ran using the Bio-Rad Protean II system (Bio-Rad, Hertfordshire, UK). For all the assays using WB analysis, a 10% polyacrylamide resolving gel was poured, followed by a 3% polyacrylamide stacking gel. Protein samples and a protein ladder were applied to the wells in the stacking gel, proteins were resolved by electrophoresis at 150 V until the bromophenol blue dye left the stacking gel and at 200 V until the dye reached the bottom of the gel. Molecular weights were determined using the Compute pI/Mw tool from the ExPASy website (www.expasy.org).

2.5.4. Western blotting

Resolved proteins were transferred to a nitrocellulose membrane for 22 min at 0.4 Amp, 15 V using a Transblot semi-dry transfer cell (Bio-Rad, Hertfordshire, UK). Transferred proteins were detected with Ponceau red dye. Membranes were blocked O/N at 4°C in 5% non-fat dried milk in PBS-Tween 20 (PBS-T). Proteins were detected with a specific primary antibody (table 2.9) diluted in 1% non-fat dried milk in PBS-T for 1 h at RT, with agitation. Membranes were washed 3x5 min and 1x15 min with PBS-T before incubation with a specific secondary antibody conjugated to horseradish peroxidase (HRP) (table 2.10) diluted in 1% dried milk in PBS-T for 45 min at RT, with agitation. After 3x5 min and 1x15 min wash in PBS-T, membranes were incubated for 5 min with the ECL Plus reagent. The peroxidase activity was revealed by chemiluminescence and visualised by autoradiography on Super RX X-Ray Fuji film.

2.5.5. Quantitative protein assay

Cells were plated and transiently transfected as described in chapter 2.3.1.1 and 2.3.2.2 respectively. Cells were treated with MG132 or a vehicle 28 h after transfection as described in chapter 2.3.4. Cells were lysed with 200 µl of 0.1% SDS buffer supplemented with 2% PIC and 1% PhIC for 5 min on ice. A nitrocellulose membrane was pre-equilibrated with three washes of 0.1% SDS buffer on a dot-blot apparatus (Bio-Rad, Hertfordshire, UK). After 10 sec of sonication (as described in chapter 2.5.1), 20 µl of cell lysates were removed for protein quantification, as described in chapter 2.5.2. The remaining volume of cell lysate was appropriately diluted (final volume: 100 µl per sample) in 0.1% SDS buffer, loaded in quadruplicate onto the nitrocellulose membrane on the dot-blot apparatus and allowed to bind for 20 min. The nitrocellulose membrane was washed twice with 0.1% SDS buffer. Proteins were detected by immunoblotting as described in chapter 2.5.4. Each experiment was performed at least twice.

Standard curve. A standard curve for the anti-tau and anti-pS396 antibodies that detect the total and phosphorylated tau levels respectively was established. A serial dilution of samples from cells transfected with GFP-tau or with GFP-tau and HA-GSK3β for detection with anti-tau and anti-pS396-tau antibodies

respectively was performed. Each dilution, from 1:20 to 1:5000, was applied to a nitrocellulose membrane in quadruplicate as described above and total or phosphorylated tau levels were detected by immunoblotting using the anti-tau and anti-pS396 antibodies (Chapter 2.5.4).

Quantitation. In each experiment, WB with the same exposure time were scanned in black and white and protein levels were analysed using the ImageJ software. The mean grey value of each spot was measured. The average intensity of the quadruplicate spots from the same sample was calculated along with the standard error of the mean using Excel software, and normalised to protein concentration. Statistical significance was determined using an unpaired Student's *t*-test. All values were normalised to a reference intensity. For comparison of changes in total tau levels, values were normalised to that of total tau in the absence of GSK3β or proteasome inhibition. For comparison of changes in phosphorylated tau levels, values were normalised to that of tau phosphorylated in the presence of GSK3β and in the absence of proteasome inhibition.

2.5.6. Immunoprecipitation

All the immunoprecipitations (IP) and co-immunoprecipitations (co-IP) were performed using magnetic dynabeads on a magnetic rack (Invitrogen, Paisley, UK). Before immunoprecipitation, magnetic beads were washed three times with RIPA-T buffer and blocked overnight with BSA–T blocking buffer to avoid non-specific attachment of proteins to the beads. Cells were plated and transiently transfected as described in chapter 2.3.1.1 and 2.3.2.2 respectively. Cells were treated with MG132 or vehicle, 28 h post-transfection. Cells were lysed with 200 µl of RIPA buffer supplemented with 5% PIC and 1% PhIC for 5 min on ice. After 10 sec of sonication as described previously, 30 µl of cell lysates were removed, mixed with 10 µl of 4x loading buffer and kept at 4°C for the input fraction. The remaining supernatant was incubated with 25 µl of magnetic dynabeads pre-washed in RIPA-T buffer with specific primary antibodies (table 2.9), O/N at 4°C. Alternatively, as controls, samples were incubated with a non-specific primary antibody (but raised in the same species, IgG), or with the beads only (BO) (table 2.11). The supernatant was removed

and the dynabeads were washed three times with RIPA-T buffer. Proteins were eluted in 40 µl of 4x loading buffer, and boiled for 3 min. After a quick spin at 12 000 rpm, 5 µl of inputs, 5 µl of IP product and 10 µl of co-IP product were loaded on a polyacrylamide gel and analysed by WB as described in chapter 2.5.3 and chapter 2.5.4.

Table 2.11. *Antibodies used as controls in IP and co-IP.*

Protein IP	Protein co-IP	Primary Antibody	Non-specific primary antibody
GFP-tau	NUB1-FLAG	Rabbit anti-pan tau	Rabbit anti-HA
	HA-GSK3β		Rabbit anti-flag
HA-GSK3β	GFP-tau	Mouse anti-HA	Mouse anti-c-Myc
	NUB1-FLAG		
NUB1-FLAG	GFP-tau	Mouse anti-FLAG	Mouse anti-c-Myc
	HA-GSK3β		

In each experiment, WB with the same exposure time were scanned in black and white and protein levels were analysed using the ImageJ software.

The mean grey value of each band of protein co-immunoprecipitated was measured and compared to the same protein band in the input fraction. Twice as much co-IP product (10 µl) was resolved compared to the input and IP samples (5 µl), and the concentration in the final co-IP samples was 4x higher than in the inputs (undiluted). Therefore, the following equations were used to calculate the percentage of total protein immunoprecipitated and co-immunoprecipitated:

(%) of protein IP = 100 x (Intensity of co-IP / (Intensity of inputs x 4))

(%) of protein co-IP = 100 x (Intensity of co-IP / (Intensity of inputs x 8))

2.5.7. Cycloheximide assays

Cells were plated and transfected as described in chapter 2.3.1.1 and chapter 2.3.2.2 respectively. 28 h after transfection, cells were treated with cycloheximide (CHX) for 2 h, 4 h or 6 h. Four hours before the end of the CHX treatment, cells were also treated with MG132 or vehicle for 4 h. Preparation of

the samples for WB and quantification of proteins were described in chapter 2.5.1. and 2.5.2. Samples were loaded three times on the same polyacylamide gel (10%), and electrophoresis and WB were carried out as described in chapter 2.5.3 and 2.5.4. Each experiment was performed at least twice.

Quantitation. In each experiment, WB with the same exposure time were scanned in black and white and protein levels were analysed using the ImageJ software. Average values and standard errors of the mean were calculated using Excel software. Statistical significance was determined using an unpaired Student's *t*-test. For determination of changes in the overall levels of GSK3β, all values were normalised to GSK3β in the absence of NUB1, proteasome inhibition or CHX treatment. For determination of the degradation rate, GSK3β levels after 2, 4 and 6 h of CHX treatment were calculated as a percentage of the initial GSK3β levels (0 h CHX treatment). Similarly, NUB1 levels were measured and were calculated as a percentage of the initial NUB1 levels (0 h CHX treatment) in the absence of MG132.

Chapter 3
Localisation of NUB1

3.1. Introduction

The NFTs in AD are composed of PHF, twisted tangles of protofilaments of hyperphosphorylated tau (Martin *et al.*, 2011; Braak and Braak, 1991). NFTs are only seen in neurons, and are described as either flame shaped or rounded (globose). After the death of the neuron, NFTs remain as ghost tangles. The progressive accumulation of NFTs throughout the brain has led to the description of 6 main stages of AD called Braak stages (Figure 3.1). First, NFTs accumulate in the entorhinal cortex, an important memory centre (Braak stage I and II). Subsequently, NFTs spread to the pyramidal layer of the hippocampus (Braak stages III and IV), a part of the limbic system involved in long-term memory and spatial navigation. Finally, NFTs reach layers III and IV of the neocortex (Braak stages V and VI), a part of the cerebral cortex implicated in sensory perception, language and the generation of motor commands (Figure 3.1) (Braak and Braak, 1991; Duyckaerts *et al.*, 2009). Braak stages correlate with the seriousness of the disease. Tau fibrils also appear in dendrites as NT, in dystrophic neurites (either dendrites or axons), and in the corona of the senile plaques.

NFTs are argyrophilic, and can therefore be detected using silver-staining techniques. The fluorescent dye Thioflavin S can also label NFTs and Aβ deposits, as it binds to the β-sheet structures of fibrillar aggregates. Different antibodies for tau aggregation in AD are used to label NFTs. The Alz50 primary antibody, for example, requires tau to be misconformed as it recognises two discontinuous epitopes (Duyckaerts *et al.*, 2009). The PHF-1 antibody specifically detects tau phosphorylated on two residues, Ser396 and Ser404. The AT8 antibody has been found to be one of the most consistent over the years of tau studies to label NFTs and NTs. AT8 has been used extensively to

detect PHF-tau in NFTs in samples from AD patients. AT8 is cross-reactive for 3 epitopes, it specifically recognises PHF-tau doubly phosphorylated on Ser199 and Ser202, Ser202 and Thr205, and Thr205 and Ser208 (Porzig *et al*., 2007).

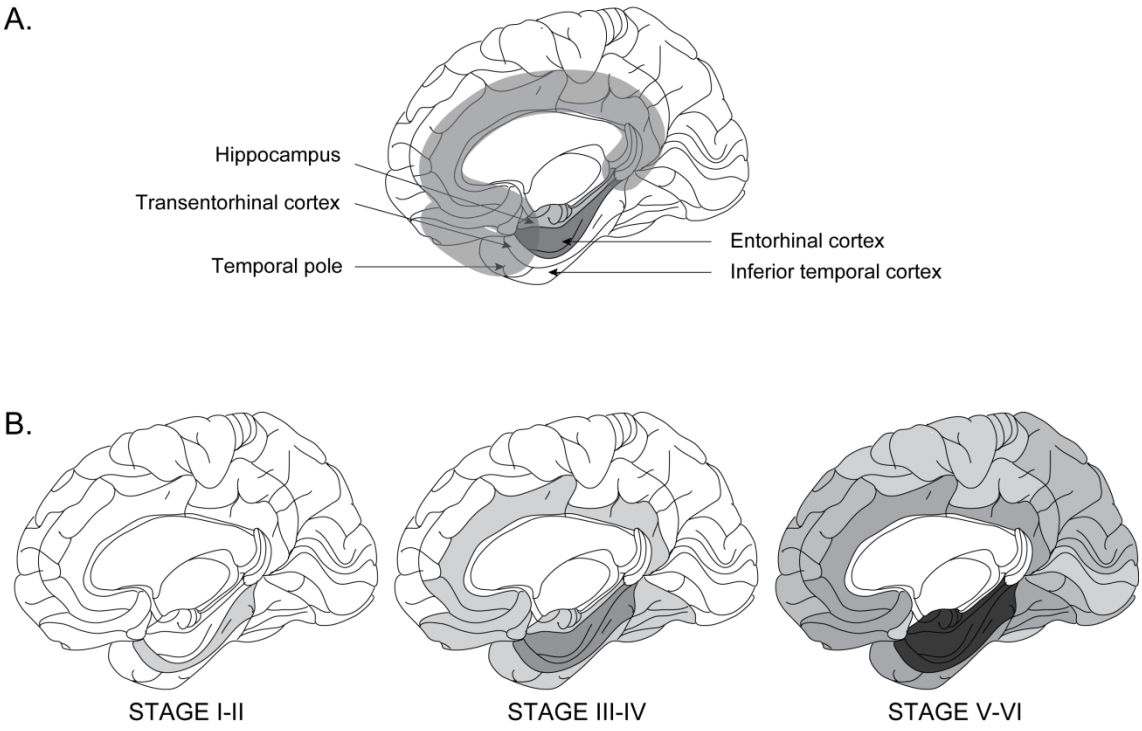

Figure 3.1. *Limbic system and NFT progression in AD*. (**A**) The limbic system is composed of the limbic lobe (grey shadow) and deep-lying structures such as the hippocampus and amygdala. (**B**) Braak stage I and II are characterised by lesions confined to the transentorhinal cortex. NFTs progress to the limbic system in stage II and IV, and finally spread to the isocortex in stage V to VI. The darker the colour, the greater the severity of NFT lesions.

A range of different proteins accumulate in NFTs. Often, but not always, Ub accumulates in NFTs and in the neuritic plaques. Ub accumulation in NFTs appears to correlate with the progression of AD, and is therefore considered a late event of NFT formation (He *et al*., 1993). A recent study by Garcia-Sierra *et al*. (2011) showed that 30% of NFTs are ubiquitinated, and that Ub labelling is associated with phosphorylated tau and tau truncated by caspase 3.

NFTs are also positive for the ULM NEDD8 (Chen *et al*., 2003; Mori *et al*., 2005). NEDD8 accumulates in different inclusions such as Lewy bodies in PD, and NFTs in AD. Interestingly, NEDD8 labelling appears to be related to Ub. Indeed, Mori *et al*., (2005) showed that Ub-negative inclusions, including NFTs

in corticobasal degeneration and progressive supranuclear palsy, and Pick bodies in PiD, are also NEDD8-negative. Interestingly, as a regulator of NEDD8, NUB1 localisation has been studied and shown to co-localise with Lewy bodies in PD, but not with NFTs (Tanji *et al*., 2007).

The accumulation of tau in PHFs and NFTs occurs only when tau is hyperphosphorylated by several kinases such as GSK3. In non-pathological conditions, tau localisation is mostly axonal in neurons, although tau can be found in the dendrites and the soma, but not in the nucleus (Dehmelt and Halpain, 2005). The tau kinase GSK3 is a cytosolic protein, however studies suggest that it is also activated in mitochondria and the nucleus (Bijur and Jope, 2003).

The aims of the following experiments were to determine the subcellular distribution of NUB1 and the ULM proteins *in vivo* in brain sections provided by the London Brain Bank, from AD patients and age-matched control patients, and to examine their correlation with the progression of tau aggregation and NFT formation.

Moreover, the localisation of GFP-NUB1 in rat cortical primary neurons was examined and compared to that of endogenous tau, microtubules and GSK3β.

3.2. Results

3.2.1. Tau accumulates in NTs and NFTs

Formalin fixed, paraffin embedded sections (8 µm) from the entorhinal cortex and hippocampus of a Braak stage VI AD patient were labelled with AT8, an antibody specific to hyperphosphorylated tau accumulated in PHFs and NFTs (Braak and Braak 1995; Duyckaerts *et al.*, 2009). Figure 3.2, A illustrates the accumulation of tau in the entorhinal cortex and from the CA1 to the CA4 areas of the hippocampus. As described by Braak and Braak (1991), tau first aggregates in the entorhinal cortex and then spreads to the neurons of the pyramidal layers (CA1 to CA4) of the hippocampus.

Tau localisation was analysed in detail in the entorhinal cortex, and in the CA2 and CA4 areas of the hippocampus of a Braak stage VI AD or age-matched control patient (Figure 3.2, B). Hyperphosphorylated tau (p-tau) accumulated in globose (long arrows) and flame-shaped (short arrows) NFTs in neurons, and in NT (small arrowheads) in dendrites. As tau aggregation is not cleared after cell death, p-tau was also detected in dystrophic neurites (large arrowheads).

A stronger AT8 background and greater number of globose NFTs and NTs were detected in the entorhinal cortex of the AD patient (Figure 3.2, B, a) compared to the control patient (Figure 3.2, B, d). In the CA2 (Figure 3.2, B, b and e) and CA4 (Figure 3.2, B, c and f) areas of the hippocampus, p-tau aggregation was detected in NFTs in the pyramidal neurons, and in NTs in both the AD (Figure 3.2, B, b and c) and control patient (Figure 3.2, B, e and f). However, a larger number of NFT and NTs were detected in the AD patient than the control patient in both the CA2 and CA4 areas. Moreover, dystrophic neurites were only detected in the AD patient. Overall, although p-tau could be detected in aggregates in age-matched control patients, a higher number of NTs, NFTs and dystrophic neurites were detected in the Braak stage VI AD patient. Moreover, the presence of NFTs in the control patient was sporadic in the entorhinal cortex and the CA4 area of the hippocampus, while they were widely spread in the AD patient and led to the detection of tau in dystrophic neurites.

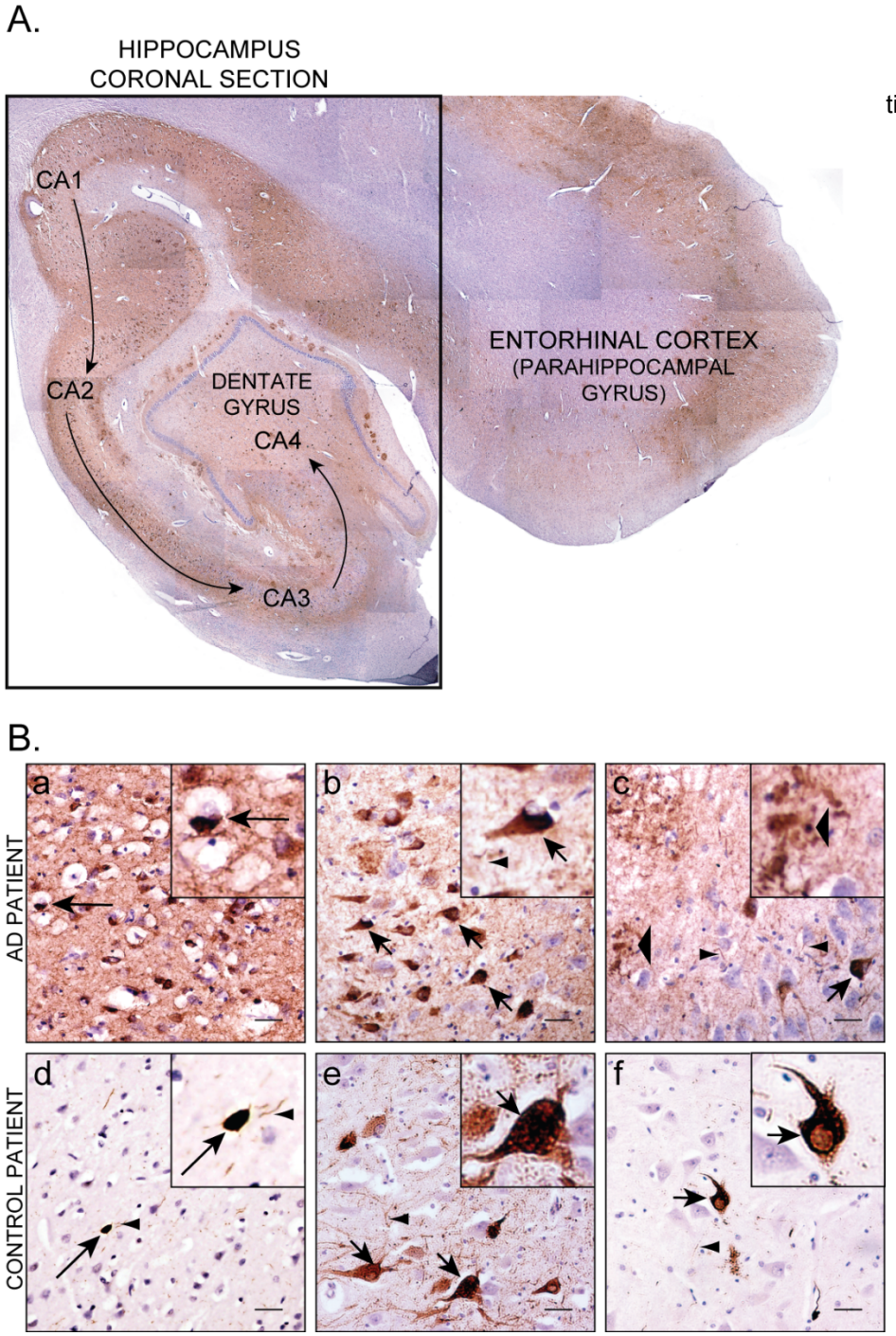

Figure 3.2. *Subcellular localisation of hyperphosphorylated tau in the entorhinal cortex and hippocampus of an AD patient and an age-matched control patient.* Hyperphosphorylated tau was detected by immunohistochemistry using the DAB/peroxidase method following the incubation of brain sections with the AT8 primary antibody. Nuclei were labeled with hematoxylin reagent (purple). (**A**) Composite of images taken from the entorhinal cortex and hippocampus from an AD patient. The arrows represent the dissemination of tau throughout the hippocampus, from the CA1 to the CA4 pyramidal layer of neurons. (**B**) The localisation of hyperphosphorylated tau was examined in the entorhinal cortex (a, d), CA2 (b, e) and CA4 (c, f) area of the hippocampus. Globose NFT (long arrows), flame-shaped NFT (short arrows), NTs (small arrowheads) and dystrophic neurites (large arrowheads) are demarcated. Scale bars = 25 μm.

3.2.2. Ubiquitin, FAT10, NEDD8 and NUB1 distribution in the entorhinal cortex and hippocampus of AD and control patients

The localisation of Ub, NEDD8, FAT10 and NUB1 was examined in a Braak stage VI AD patient and an age-matched control by immunohistochemical detection in brain sections.

Ub was detected in the entorhinal cortex and hippocampus in a non-affected and a Braak stage VI AD patient (Figure 3.3). Both in the control (Figure 3.3, D, E and F) and the AD patient (Figure 3.3, A, B and C), Ub accumulated in NFTs (arrows). However, Ub appeared to label NTs (small arrowheads) and extracellular structures, which could be either dystrophic neurites (large arrowheads) or senile plaques or both, only in the AD patient.

FAT10 localisation was analysed in an age-matched non-demented and a Braak stage VI AD patient (Figure 3.4). In both the entorhinal cortex and the hippocampus, FAT10 in the control appeared to be restricted to few cells (Figure 3.4, D, E and F, arrows), whereas it was more widespread in the AD patient. In the AD patient, FAT10 appeared to accumulate in extracellular structures similar to dystrophic neurites (Figure 3.4, A and B, arrowheads) and in individual cells (Figure 3.4, C, arrow). The subcellular localisation of FAT10 in cells in both the control and AD patient was mostly cytoplasmic.

NEDD8 was detected in the entorhinal cortex and hippocampus of a non-affected and a Braak stage VI AD patient (Figure 3.5). In these brain sections, NEDD8 was detected primarily in cells (Figure 3.5, arrows), and did not appear to accumulate in any extracellular structures. Noticeably, NEDD8 was detected in the majority of pyramidal neurons in the hippocampus (Figure 3.5, B, C, E, F, arrows), where NFTs accumulate, in both the control and the AD patient. NEDD8 subcellular localisation was mostly cytoplasmic in the CA2 and CA4 areas of the hippocampus whereas it was more nuclear in the entorhinal cortex (Figure 3.5, A and D, arrows).

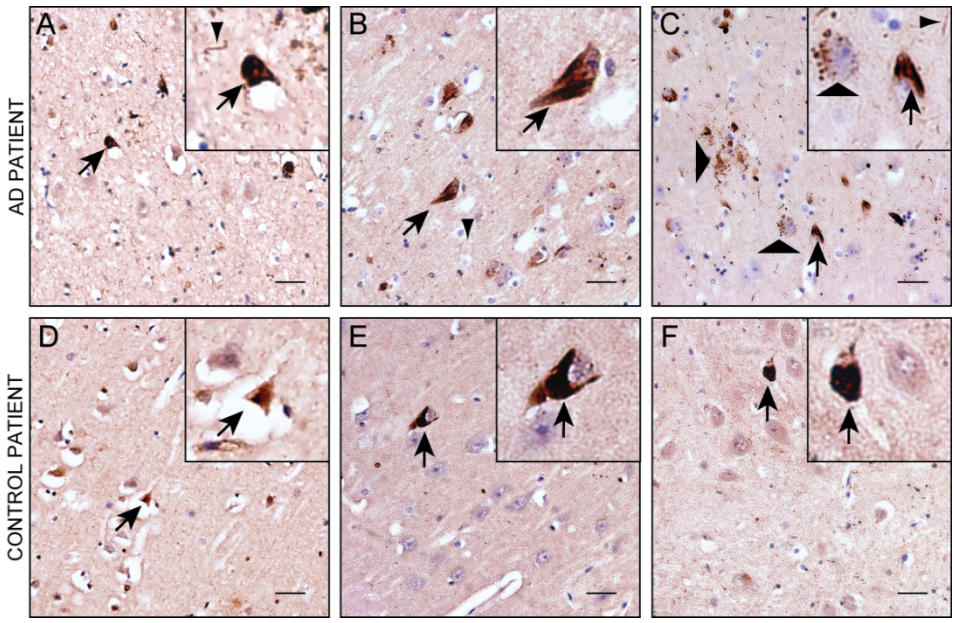

Figure 3.3. *Subcellular localisation of Ub in the entorhinal cortex and hippocampus of an AD patient and an age-matched control patient*. Ub was detected in brain sections by immunohistochemistry using the anti-Ub antibody and the DAB/peroxidase method. Nuclei were labeled with hematoxylin reagent (purple). Ub was detected in the entorhinal cortex (**A, D**), CA2 (**B, E**) and CA4 (**C, F**) area of the hippocampus of the AD patient (**A, B, C**) and the control (**D, E, F**). NTs (small arrowheads), NFTs (arrows) and dystrophic neurites (large arrowheads) are demarcated. Scale bars = 25 μm.

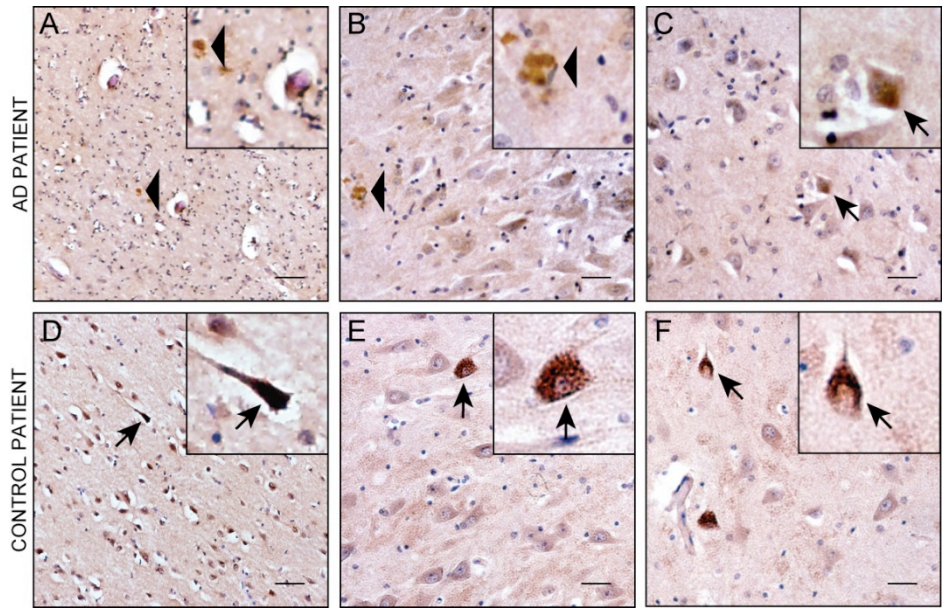

Figure 3.4. *Subcellular localisation of FAT10 in the entorhinal cortex and hippocampus of an AD patient and an age-matched control patient*. FAT10 localisation was detected in brain sections by immunohistochemistry using the anti-FAT10 antibody and the DAB/peroxidase method. Nuclei were labeled with hematoxylin reagent (purple). The FAT10 specific detection is depicted with arrowheads (extracellular localisation) and arrows (intracellular localisation) in the entorhinal cortex (**A, D**), CA2 (**B, E**) and CA4 (**C, F**) area of the hippocampus of the AD patient (**A, B, C**) and the control (**D, E, F**). Scale bars = 25 μm.

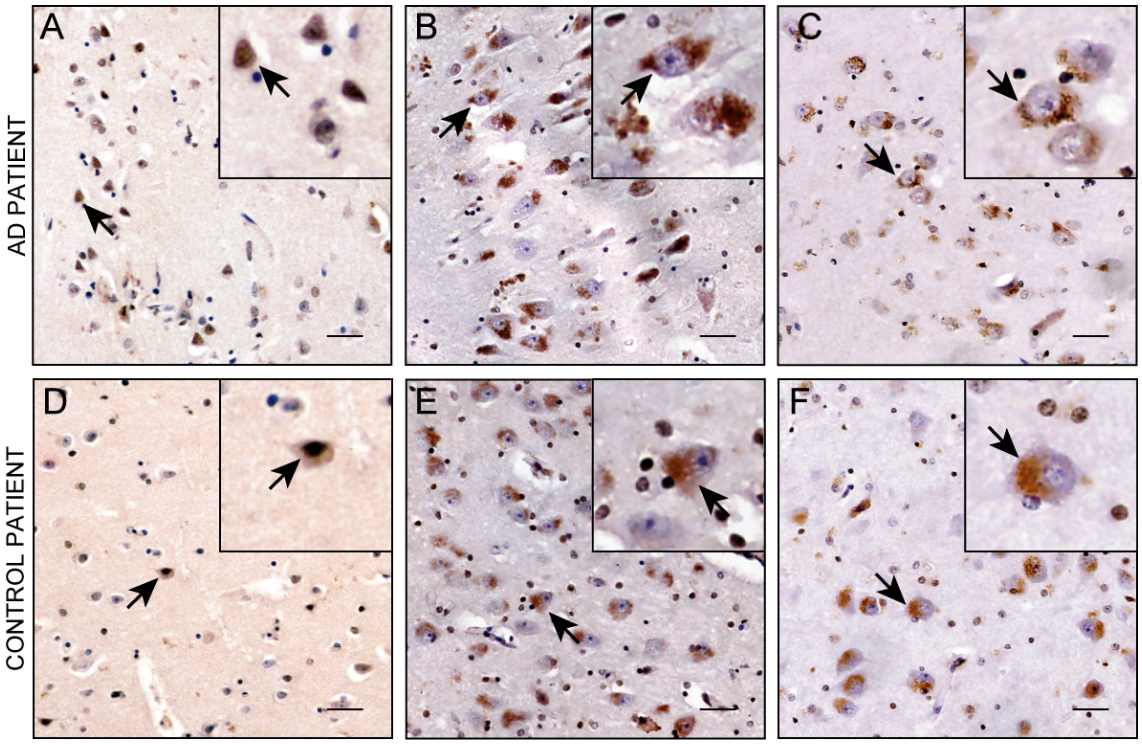

Figure 3.5. *Subcellular localisation of NEDD8 in the entorhinal cortex and hippocampus of an AD patient and an age-matched control patient*. NEDD8 localisation was examined by immunohistochemistry in brain sections using a primary antibody specific to NEDD8 and the DAB/peroxidase method. Nuclei were labelled with hematoxylin reagent (purple). The NEDD8 specific detection is shown with arrows in the AD patient (**A, B, C**) and in the control (**D, E, F**) in the entorhinal cortex (**A, D**), and the CA2 (**B, E**) and CA4 (**C, F**) areas of the hippocampus. Scale bars = 25 μm.

The NUB1 subcellular localisation was observed in a non-demented and a Braak stage VI AD patient. The NUB1 antibody is a peptide-directed antibody previously developed and characterised in our laboratory (van der Spuy *et al*., 2003), therefore the specificity of the NUB1 immunodetection in the brain sections was first assessed by peptide competition and by comparison with the pre-immune serum in a Braak stage VI AD patient (Figure 3.6). Pre-incubation of the primary antiserum with the NUB1 peptide (30 µg/ml) against which the antibody was raised significantly reduced the immunodetection of NUB1 in brain sections (Figure 3.6, D, E and F), and no specific NUB1 immunostaining was detected with the pre-immune serum (not shown). Therefore, the NUB1 detection was specific, and the localisation of NUB1 was compared in the entorhinal cortex and hippocampus of an age-matched non-demented and Braak stage VI AD patient (Figure 3.7). Noticeably, the NUB1 localisation was similar to that of NEDD8 (Figure 3.5). In both the AD patient and the control, NUB1 distribution was mostly cytoplasmic throughout the neurons in the entorhinal cortex and hippocampus, and did not appear to label extracellular structures. However, NUB1 was also detected in the nucleus in some cells of the entorhinal cortex, but only in the control patient. Interestingly, similar to NEDD8, NUB1 was detected in the pyramidal neurons of the hippocampus, in both the CA2 and CA4 areas of the AD patient and control, where NFTs are known to accumulate.

In conclusion, as previously described by Braak and Braak (1991), hyperphosphorylated tau accumulated in NTs, NFTs and dystrophic neurites in the entorhinal cortex and hippocampus of AD patients. Although tau aggregation was detected in a non-demented control, the NFTs in the control were only found sporadically in the entorhinal cortex and CA2 area of the hippocampus. The accumulation of tau in the NFTs has been shown to be co-labelled with Ub and NEDD8 and in the dystrophic neurites with Ub (Mori *et al*., 2005, Duyckaerts *et al.*, 2009).

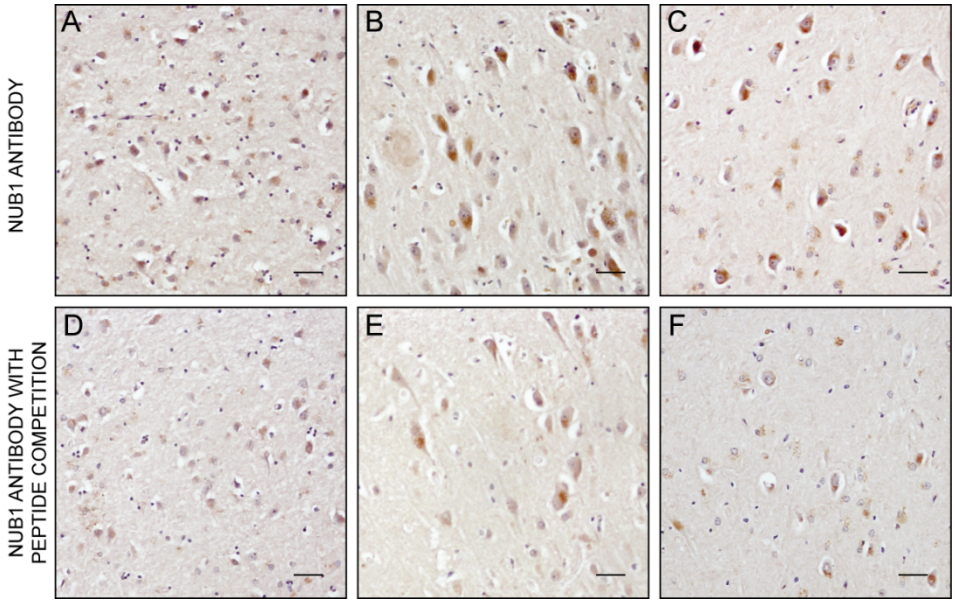

Figure 3.6. *Analysis of NUB1 detection in the entorhinal cortex and hippocampus of an AD patient*. NUB1 was detected in the entorhinal cortex (**A, D**), CA2 (**B, E**) and CA4 (**C, F**) areas of the hippocampus by immunohistochemistry using a primary antibody specific to NUB1 and the DAB/peroxidase method. The NUB1 antibody was pre-incubated for 1 h at RT either without peptide (**A, B, C**) or with peptide (30 µg/ml) (**D, E, F**) prior to labelling the brain sections. Nuclei were labelled with hematoxylin reagent (purple). Scale bars = 25 µm.

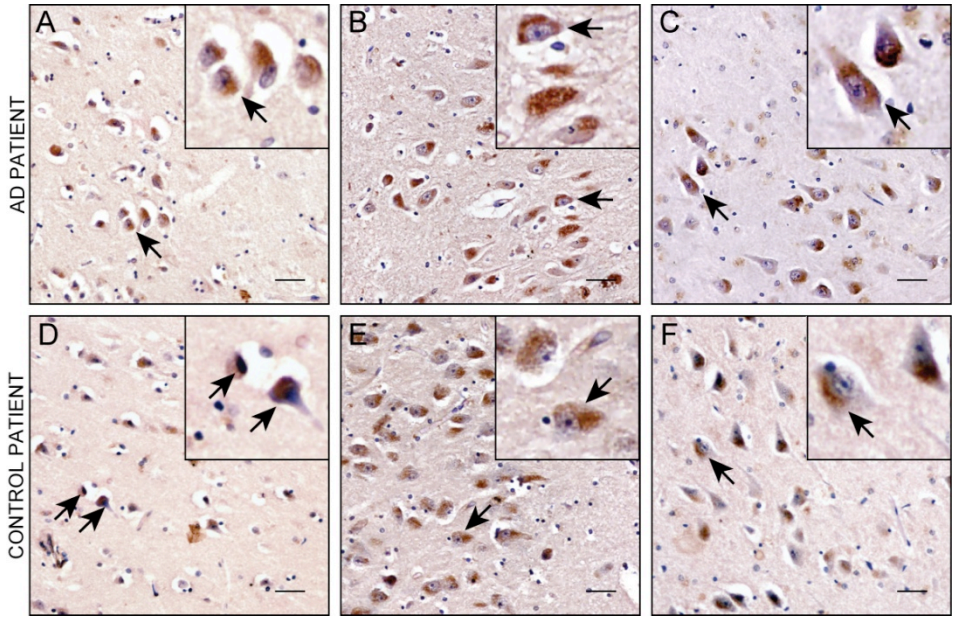

Figure 3.7. *Subcellular localisation of NUB1 in the entorhinal cortex and hippocampus of an AD patient and an age-matched control patient*. The localisation of NUB1 in brain sections was detected by immunohistochemistry using a primary antibody specific to NUB1 and the DAB/peroxidase method. Nuclei were labelled with hematoxylin reagent (purple). The NUB1 specific detection (arrows) is shown in the entorhinal cortex (**A, D**), and CA2 (**B, E**) and CA4 (**C, F**) areas of the hippocampus in the AD patient (**A, B, C**) and in the control (**D, E, F**). Scale bars = 25 µm.

Ub was detected in both control and AD patients, but was detected in extracellular dystrophic structures only in the AD patients. NEDD8 was also detected in control and demented patients, and was localised in the pyramidal layer neurons of the hippocampus, where NFT aggregation is most prominent in the late stages of AD. Interestingly, another ULM, FAT10, was expressed in the pyramidal neurons of the hippocampus, and appeared to localise in dystrophic neurites. Finally, NUB1, which specifically downregulates both the NEDD8 and FAT10 ULM, was specifically detected in the hippocampus and the entorhinal cortex of both control and AD patients, with a distribution very similar to that of NEDD8. Thus, NUB1 might regulate the degradation of neddylated and FAT10ylated proteins in neurons.

3.2.3. Comparison of NEDD8 and NUB1 distribution in the entorhinal cortex and hippocampus of AD and control patients

Chen *et al*. (2003) immunostained the hippocampus in five cases of AD and five age-matched controls with rabbit anti-NEDD8. In four out of five AD cases examined, NEDD8 was located primarily in the cytoplasm in hippocampal neurons. In contrast, in four out of five control cases, NEDD8 was located primarily in the nucleus in hippocampal neurons, showing a shift from a neuronal to a cytoplasmic localisation in affected regions of AD brain. However, we did not detect a similar shift in NEDD8 subcellular distribution (Table 3.1 and 3.2). Indeed, the subcellular distribution of NEDD8 in the AD patient and control was similar; NEDD8 was more nuclear in the entorhinal cortex, and more cytoplasmic in CA2 and CA4 areas of the hippocampus (Figure 3.5). Moreover, the localisation of NUB1 was similar to that of NEDD8 (Figure 3.7). Therefore, the localisation of NEDD8 and NUB1 was compared in 5 different control (Table 3.1) and 6 different AD patients (Table 3.2). The subcellular localisation of NEDD8 and NUB1 in the CA1-2 and CA4 areas of the hippocampus was observed, and divided into three categories: strictly nuclear (N), nuclear and cytoplasmic (N/C) and strictly cytoplasmic (C).

In the CA1-2 area of the non-demented controls (Table 3.1), only patient III showed any strictly nuclear (N) localisation of NEDD8 in 20% of cells counted. If this control is excluded, NEDD8 localisation was strictly cytoplasmic (C) in 63±2.4% of cells and both nuclear and cytoplasmic (N/C) in 37±2.4% of cells counted. Similarly, NUB1 distribution in the CA1-2 area was cytoplasmic (C) in 60±4.1% and both nuclear and cytoplasmic in 40±4.1% of cells counted. In the CA4 area of the hippocampus, NEDD8 localisation was cytoplasmic (C) in 68±4.0% and both nuclear and cytoplasmic (N/C) in 33±4.0% of cells counted. NUB1 distribution in the CA4 area was mostly cytoplasmic (C) (63±3.2%). In conclusion, in the hippocampus of the controls, the distribution of both NEDD8 and NUB1 was similar, and in most cells was localised predominantly in the cytoplasm.

In the AD patients (Table 3.2), only patient X showed a strictly nuclear localisation (N) for NEDD8 in both the CA1-2 and CA4 areas for 46% and 11% of cells counted respectively. With the exclusion of patient X, NEDD8 was on average predominantly localised in the cytoplasm (C) in 59.75±4.66% of hippocampal cells/neurons in the CA1-2 area, which was not significantly different from the percentage of strictly cytoplasmic localisation in the group of controls (63±2.4%, *p-value* = 0.401 using an unpaired Student's *t*-test).

In the CA4 area, NEDD8 was again mostly distributed in the cytoplasm (69±4.5%), which was not significantly different from that in the controls (68±4.1%, *p-value* = 0.478 using an unpaired Student's *t*-test). Similarly, NUB1 distribution in AD patients was predominantly cytoplasmic (C) in both the CA1-2 and the CA4 areas of the hippocampus (55±1.5% and 62±3.9% respectively), and was not significantly different from the cytoplasmic localisation in controls (60±4.1%, *p-value* = 0.056 and 63±3.2%, *p-value* = 0.769 using an unpaired Student's *t*-test in CA1-2 and CA4 respectively). However, NEDD8 had a significantly higher strictly cytoplasmic localisation (C) in the CA4 area compared to the CA1-2 area (69.29±4.51% and 59.75±4.66% respectively, *p-value* = 0.026) in the AD patients. Similarly, NUB1 distribution was significantly more strictly cytoplasmic (C) in the CA4 area than in the CA1-2 area (62.08±3.94 and 54.81±1.48 respectively, *p-value* = 0.005) in the AD patients.

Table 3.1. *Subcellular distribution of NEDD8 and NUB1 in the hippocampus of non-demented controls.* NEDD8 and NUB1 localisation was categorised as cytoplasmic (C), nuclear (N), or both nuclear and cytoplasmic (N/C) in hippocampal neurons.

Patient	Age (y)	Sex	PM delay (h)	Pathology	Localisation (%)						Area
					NEDD8			NUB1			
					N	C	N/C	N	C	N/C	
I	86	M	6	Normal adult brain		64	36		61	39	**CA1-2**
						67	33		65	35	**CA4**
II	81	M	18	Control- old cerebral infarct (BraakI)		69	31		65	35	**CA1-2**
						72	28		59	41	**CA4**
III	80	M	11	Normal adult brain	20	47	33		55	45	**CA1-2**
						65	35		66	34	**CA4**
IV	82	F	43	Normal adult brain		57	43	N/A	N/A	N/A	**CA1-2**
						63	37	N/A	N/A	N/A	**CA4**
V	92	F	17	Normal adult brain	N/A	N/A	N/A		58	42	**CA1-2**
					N/A	N/A	N/A		62	38	**CA4**

Table 3.2. *Subcellular distribution of NEDD8 and NUB1 in the hippocampus of AD patients.* NEDD8 and NUB1 localisation was categorised as cytoplasmic (C), nuclear (N), or both (N/C) in hippocampal neurons.

Patients	Age (y)	Sex	PM Delay (h)	Pathology	Localisation (%)						Area
					NEDD8			NUB1			
					N	C	N/C	N	C	N/C	
VI	88	M	22	AD braak stage V/VI		63	37		56	44	**CA1-2**
						69	31		66	34	**CA4**
VII	103	F	12	AD modified Braak stage V/VI with mild focal amyloid angiopathy		59	41		54	46	**CA1-2**
						65	35		56	44	**CA4**
VIII	80	M	15	AD Braak stage VI		64	36		57	43	**CA1-2**
						75	25		65	35	**CA4**
IX	71	F	21	AD		53	47		54	46	**CA1-2**
						68	32		62	38	**CA4**
X	67	F	56	AD Braak stage VI	46	1	53	N/A	N/A	N/A	**CA1-2**
					11	45	44	N/A	N/A	N/A	**CA4**
XI	88	M	5	AD Braak stage VI with amyloid angiopathy	N/A	N/A	N/A		53	47	**CA1-2**
					N/A	N/A	N/A		64	36	**CA4**

In conclusion, in the controls, both NEDD8 and NUB1 were predominantly cytoplasmic in both the CA1-2 and CA4 areas. In the AD patients, NEDD8 and NUB1 distributions were similar, with a predominant cytoplasmic localisation in the CA1-2 and CA4 areas. However, in AD patients, the NUB1 and NEDD8 distributions were more evenly distributed in the nucleus and cytoplasm in the CA1-2 areas, whereas it was more strictly cytoplasmic in the CA4 area.

3.2.4. Expression of endogenous NUB1 in rat cortical primary neurons.

NUB1 was detected in neurons of the hippocampus, where tau is known to accumulate in AD. Thus, to investigate the influence of NUB1 on endogenous tau, the localisation and expression of GFP-NUB1, endogenous NUB1, tau and GSK3β were explored in rat cortical primary neurons.

Primary cortical neurons were isolated from Sprague Dawley rat embryos on day 18 of gestation (E18). Between 5 to 7 days *in vitro* (DIV) culture, cells were transfected with GFP or GFP-NUB1 and treated with vehicle (PBS), or the pharmacological inhibitor of GSK3 activity, lithium chloride (LiCl) (10 mM, 2 h) (Ryves and Harwood, 2001; Tajes *et al.*, 2008). The expression of GFP, GFP-NUB1, tau and GSK3β was analysed by WB analysis (Figure 3.8).

Although six different isoforms of tau are expressed in the adult brain, only the 0N3R isoform is expressed in foetal brain (Buee *et al*., 2000). Therefore, in embryonic rat primary cortical neurons, endogenous tau was detected as a prominent band of ~50kDa (Figure 3.8, A). The inhibition of GSK3β activity and consequent reduced phosphorylation of tau in the presence of LiCl, resulted in an increased mobility of tau to a lower molecular weight. Moreover, tau expression appeared unchanged in the presence of GFP or GFP-NUB1.

Endogenous GSK3β (Figure 3.8, B) was detected as a single band of ~47kDa, and the LiCl treatment reduced GSK3β levels. Similar to tau, GSK3β levels were similar in the presence of GFP-NUB1 compared to GFP alone.

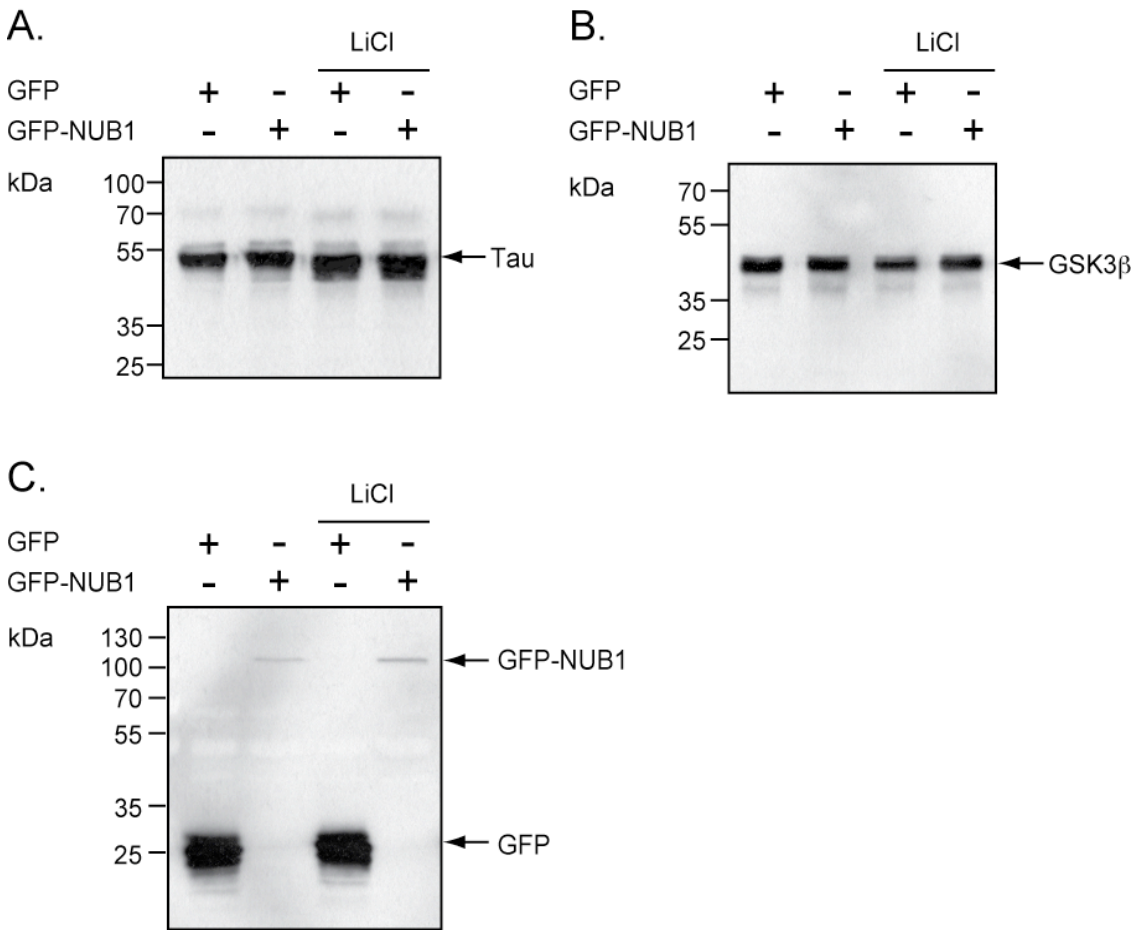

Figure 3.8. *Expression of tau, GSK3β and GFP-NUB1 in primary neurons*. Rat primary neurons were transfected with GFP or GFP-NUB1 plasmids. Twenty-four hours after transfection, cells were treated with vehicle (PBS) or LiCl (10 mM, 2 h). Samples were resolved on a polyacrylamide gel (10%) and proteins were detected by WB, using anti-tau (**A**), anti-GSK3β (**B**) or anti-GFP(**C**).

The detection of GFP and GFP-NUB1 in primary neurons with the anti-GFP antibody is shown in Figure 3.8, C. GFP was detected at ~27kDa, while GFP-NUB1 was detected at ~100kDa, similar to the predicted molecular weight (96kDa). GFP-NUB1 levels were reduced compared to GFP, possibly due to differences in transfection efficiency or protein expression in the neuronal cells, or both. Neither GFP nor GFP-NUB1 levels were affected by treatment with LiCl.

The expression of GFP-NUB1 was also detected with an antibody specific to NUB1 (Figure 3.9). This antibody is a peptide-directed antibody raised against a sequence derived from the C-terminus of human NUB1 (van der Spuy *et al*., 2003). GFP-NUB1 was detected by the NUB1 antibody (Figure 3.9, A). Surprisingly, a second band of ~66kDa, the putative molecular weight of endogenous rat NUB1, was also detected. In order to assess if the ~66kDa band was indeed endogenous rat NUB1, the NUB1 antibody was pre-incubated with the NUB1 peptide against which it was raised and which competes with NUB1 antibody antigen recognition. The immunodetection of both the ~66 kDa band and the GFP-NUB1 was lost when the NUB1 antibody was first pre-incubated with the NUB1 peptide (30 µg/ml, 1 h). Thus, the NUB1 antibody can specifically detect endogenous NUB1 in rat primary neurons. The levels of endogenous NUB1 and GFP-NUB1 were similar. LiCl treatment did not significantly alter the levels of endogenous NUB1.

In conclusion, the exogenous expression of GFP-NUB1 or GFP did not alter the expression of either tau or GSK3β. However, the low relative expression levels of exogenous GFP-NUB1, similar to that of endogenous NUB1, and the poor transfection efficiency of exogenous NUB1 (less than 6%) might explain the absence of any effect on endogenous tau and GSK3β levels. Indeed, the levels of endogenous tau and GSK3β in the cells that are not transfected with exogenous NUB1 could mask the influence of GFP-NUB1 in transfected cells. Endogenous NUB1 is expressed in rat primary neurons and was specifically detected with the human peptide-directed NUB1 antibody.

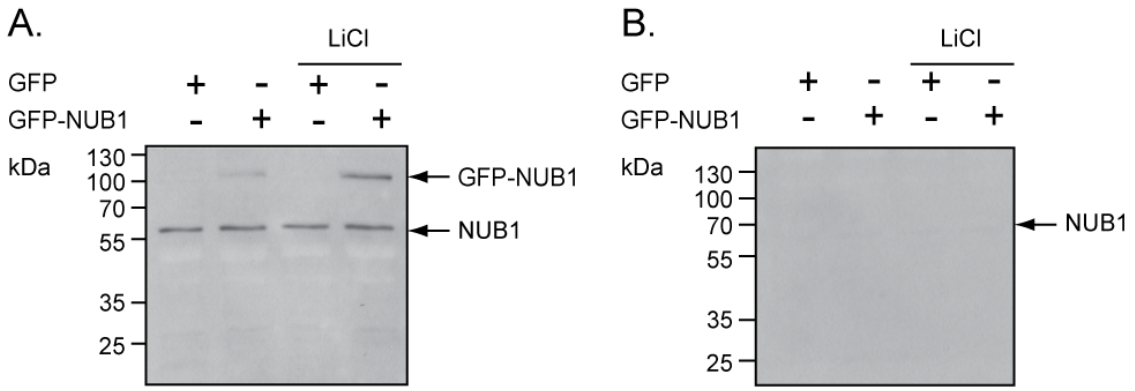

Figure 3.9. *Expression of GFP-NUB1 and endogenous NUB1*. Rat primary neurons were transfected with GFP or GFP-NUB1 plasmids. Twenty-four hours after transfection, cells were treated with vehicle (PBS) or LiCl (10 mM, 2 h). Samples were resolved on a polyacrylamide gel (10%) and endogenous NUB1 and GFP-NUB1 were detected using a rabbit anti-NUB1 primary antibody (**A**), or following the pre-incubation of the anti-NUB1 antibody with the NUB1 peptide (30 µg/ml) for 1 h (**B**).

3.2.5. Localisation of GFP-NUB1 in rat primary cortical neurons

The NUB1 peptide-directed antibody detected the expression of endogenous NUB1 in rat primary cortical neurons by WB analysis. However, it has been established in our laboratory that the NUB1 peptide-directed antibody is not suitable for immunocytochemical localisation. Therefore, primary cortical neurons were transfected with GFP-NUB1 in order to assess the subcellular localisation of GFP-NUB1 in these cells.

Rat primary cortical neurons were collected at embryonic day 18 (E18) and cultured *in vitro* for 5 days (5 DIV) prior to transfection. GFP-NUB1 and GFP plasmids were transfected by lipofection, and cells were fixed with paraformaldehyde (4%) 24 h after transfection. The percentage of total cells expressing GFP-NUB1 was ~5.6±0.7% while the GFP transfection efficiency was ~13.5±1.1%. The subcellular localisation of GFP-NUB1 and GFP alone is shown in Figure 3.10. GFP-NUB1 distribution (Figure 3.10, top row) was prominently nuclear, in accordance with the presence of a NLS in the C-terminal domain of the NUB1 sequence between residues 414 and 431. GFP-NUB1 was also observed in the neurites (axons and dendrites), and appeared prominently in the axonal varicosities (Figure 3.10, top row, white arrows). GFP, on the other hand, was expressed ubiquitously throughout the neurons, including the cell body, axons and dendrites.

3.2.6. GFP-NUB1 co-localisation with endogenous tau, GSK3β and β-tubulin in rat primary cortical neurons

In order to analyse the distribution of GFP-NUB1 compared to that of endogenous tau, microtubules and GSK3β, rat primary cortical neurons were transfected with GFP-NUB1 and labelled for tau, β-tubulin and GSK3β.

Endogenous tau (Figure 3.11, red) was detected prominently in the axons and dendrites, in accordance with the role of tau as a microtubule associated protein implicated in neuron growth (Buee *et al*., 2000; Gendron and Petrucelli, 2009). GFP-NUB1 (Figure 3.11, green) was detected in the nucleus, cell body and primary neurites. In the magnified image of the cell body, low levels of tau were

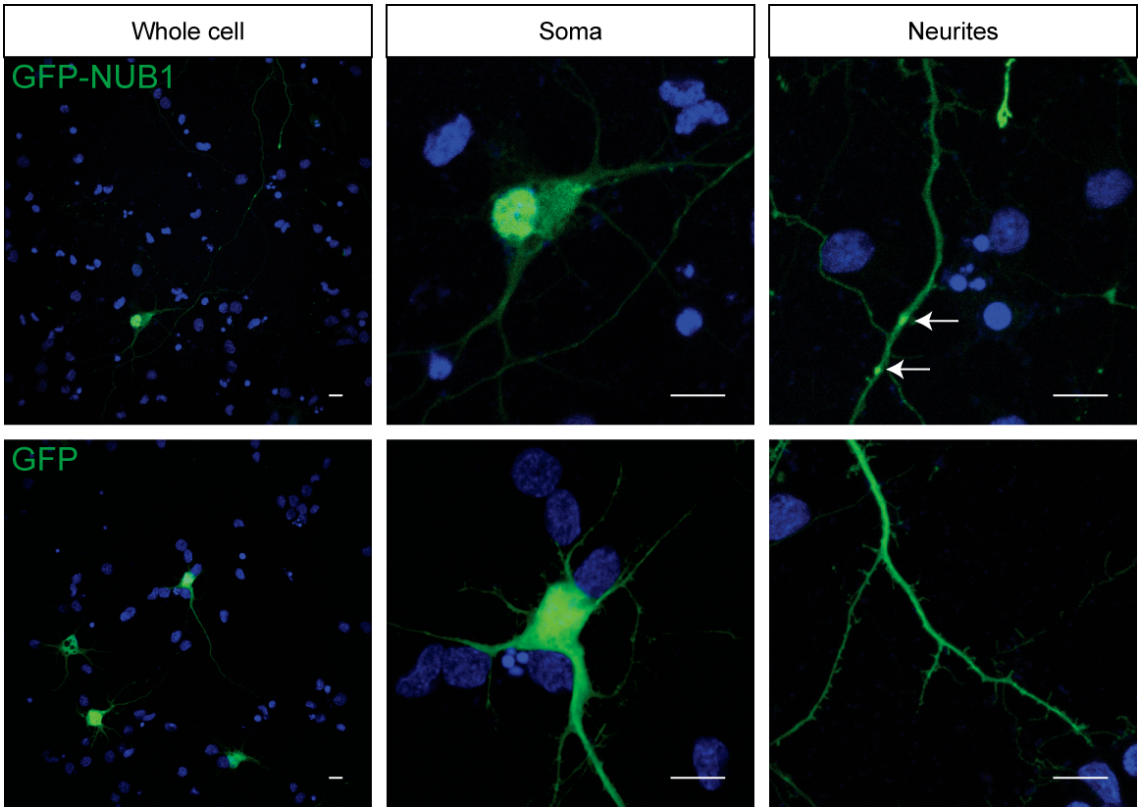

Figure 3.10. *Localisation of GFP-NUB1 and GFP in rat primary neurons*. Rat primary cortical neurons were transfected with GFP or GFP-NUB1 plasmids. Twenty-four hours after transfection, cells were fixed with paraformaldehyde (4%, 10 min, 37°C), and treated with DAPI to detect nuclei (blue). Images were acquired with a laser scanning confocal microscope (Zeiss LSM 700). White arrows show the varicosities. Scale bars = 10 µm.

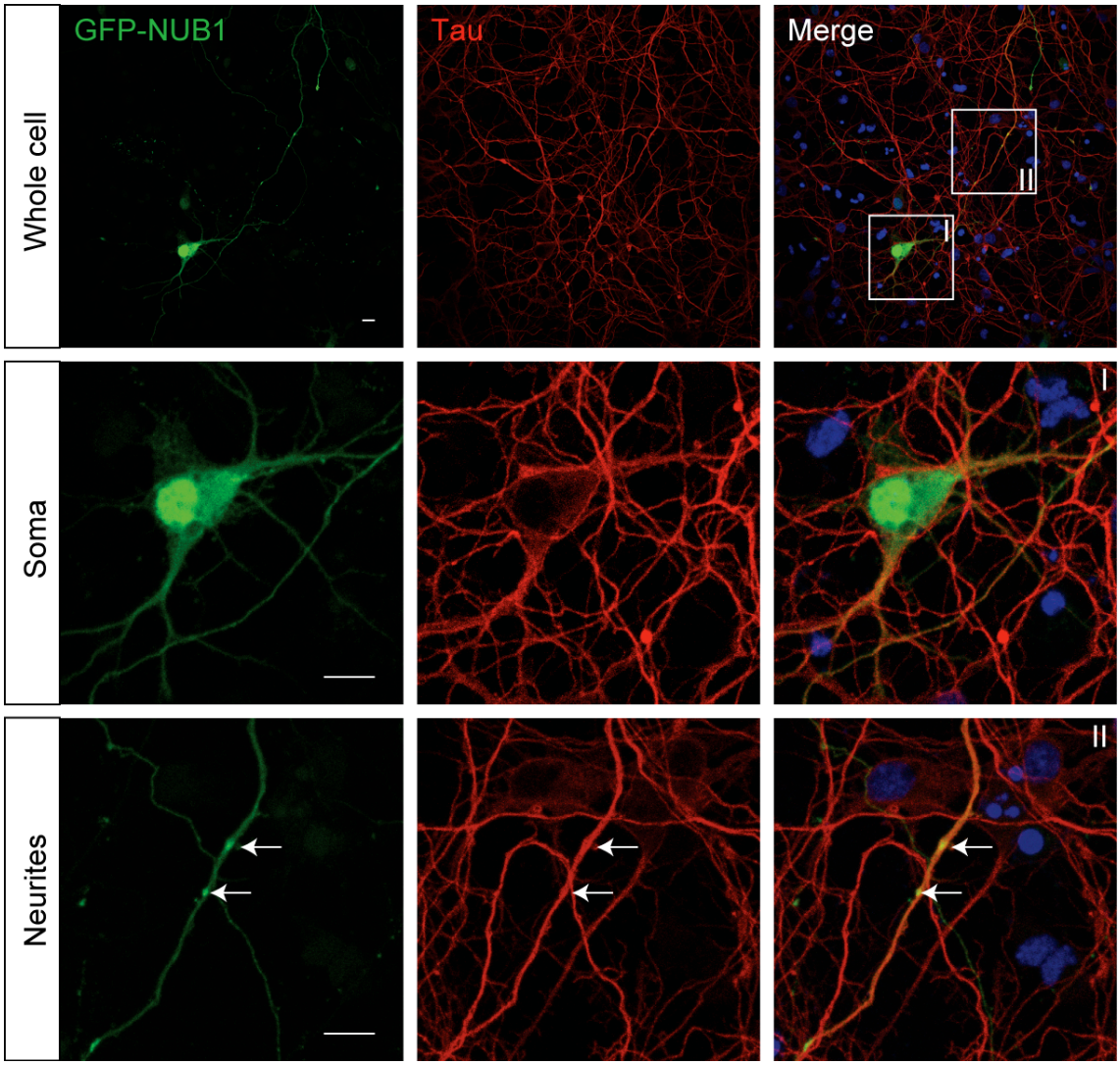

Figure 3.11. *Distribution of GFP-NUB1 and endogenous tau in rat primary neurons.* Rat primary cortical neurons were transfected with GFP-NUB1 plasmid. Twenty-four hours after transfection, cells were fixed with paraformaldehyde (4%, 10 min at 37°C). Cells were labelled with the anti-tau primary antibody in conjunction with the AlexaFluor 594 secondary antibody and treated with DAPI to detect nuclei (blue). Images were acquired with a laser scanning confocal microscope (Zeiss LSM 700). The white squares I and II demarcate the magnification of the cell body (soma, I) and neurites (II). The varicosities are highlighted by white arrows. Scale bars = 10 µm.

detected in the soma and no tau expression was detected in the nucleus (Figure 3.11, I, red). In contrast, GFP-NUB1 was predominantly detected in the nucleus with comparatively lower levels detected in the cell soma (Figure 3.11, I, green). Therefore, GFP-NUB1 and endogenous tau did not co-localise in the nucleus but both were detected in the soma. Moreover, GFP-NUB1 co-localised with tau in the primary neurites (Figure 3.11, II, merge) and in the varicosities (Figure 3.11, II, merge, arrowheads).

The microtubules, labelled with an antibody specific to β-tubulin, were detected in the dendrites and axons (Figure 3.12, red) similar to the distribution of tau. In the magnified image of the cell body, the microtubules (Figure 3.12, I, red) appeared to surround the cell body and were not detected in the nucleus. GFP-NUB1 (Figure 3.12, I, green) was detected prominently in the nucleus and also in the cytoplasm. Both GFP-NUB1 and β-tubulin were detected in the primary neurites (Figure 3.12, I and II). However a partial co-localisation of their distribution in these structures was evident, with the microtubules appearing to surround the GFP-NUB1 in the axon more than to co-localise with it (Figure 3.12, I). Interestingly, in the magnified image of the neurites (Figure 3.12, II, merge), it can be seen that GFP-NUB1 and β-tubulin seemed to inter-digitise with one another, with the microtubules surrounding the GFP-NUB1 in the varicosities (white arrows).

GSK3β localisation in rat primary neurons (Figure 3.13, red) was mostly detected in the cytoplasm of the cell body and in the primary neurites, although very low levels could be detected in the nucleus. In the magnified image of the soma (Figure 3.13, I, merge), the detection of GSK3β and GFP-NUB1 overlapped in the cytoplasm and the proximal part of the primary axon, resulting in a partial co-localisation with one another in the cytoplasm and axon. In the magnified image of the primary neurites (Figure 3.13, II), both GSK3β and GFP-NUB1 were detected, but GSK3β did not accumulate in the varicosities (white arrow), as GFP-NUB1 did.

In conclusion, GFP-NUB1 co-localised with endogenous tau in the primary neurites and varicosities, and with endogenous GSK3β in the cytoplasm and primary axon of the cell soma.

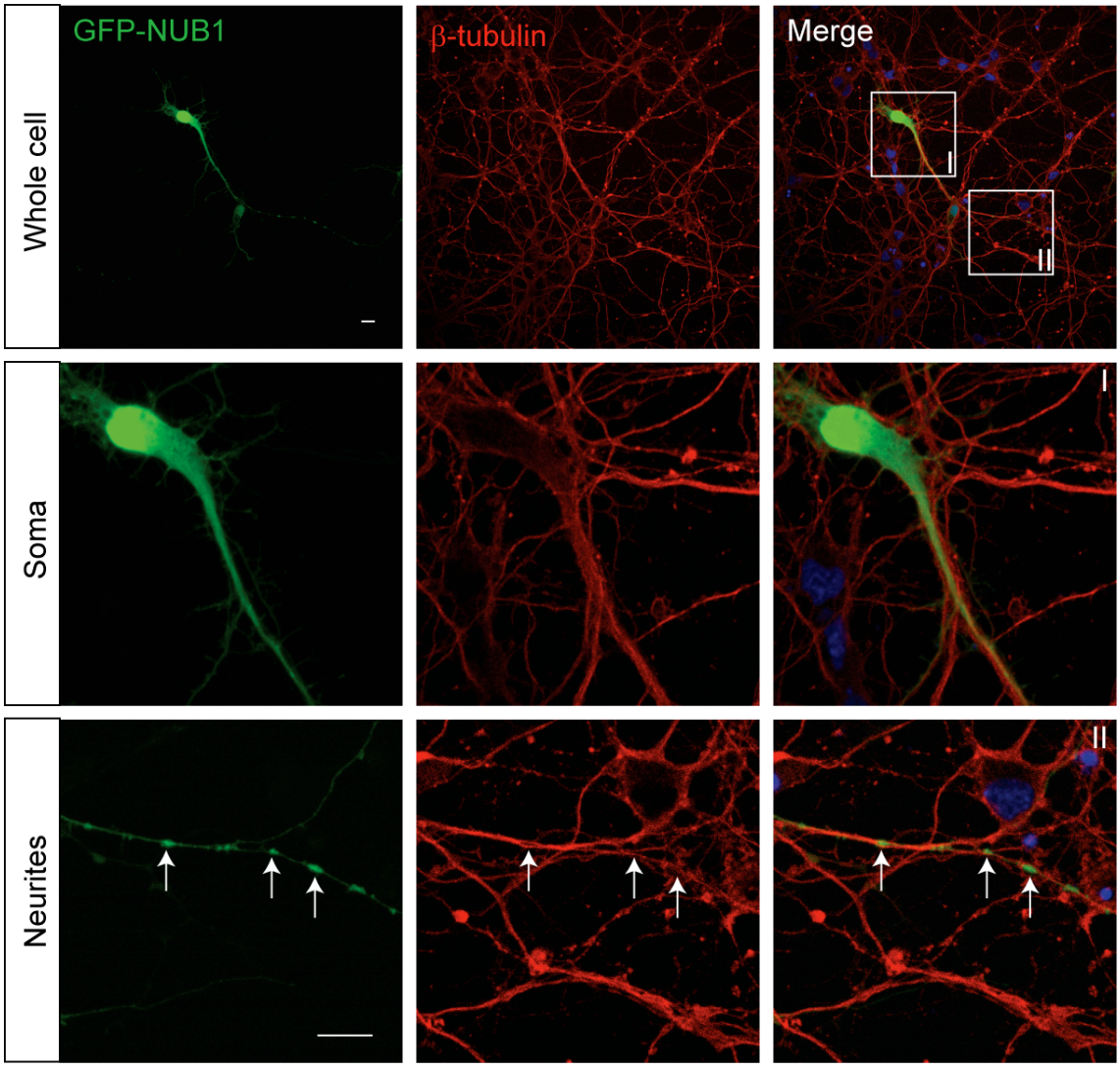

Figure 3.12. *Distribution of GFP-NUB1 and endogenous microtubules in rat primary neurons.* Rat primary cortical neurons were transfected with GFP-NUB1 plasmid. Twenty-four hours after transfection, cells were fixed with paraformaldehyde (4%, 10 min at 37°C). Cells were labelled with the anti-β-tub primary antibody in conjunction with the AlexaFluor 594 secondary antibody and treated with DAPI to detect nuclei (blue). Images were acquired with a laser scanning confocal microscope (Zeiss LSM 700). The white squares I and II demarcate the magnification of the cell body (soma, I) and neurites (II). The varicosities are highlighted by white arrows. Scale bars = 10 μm.

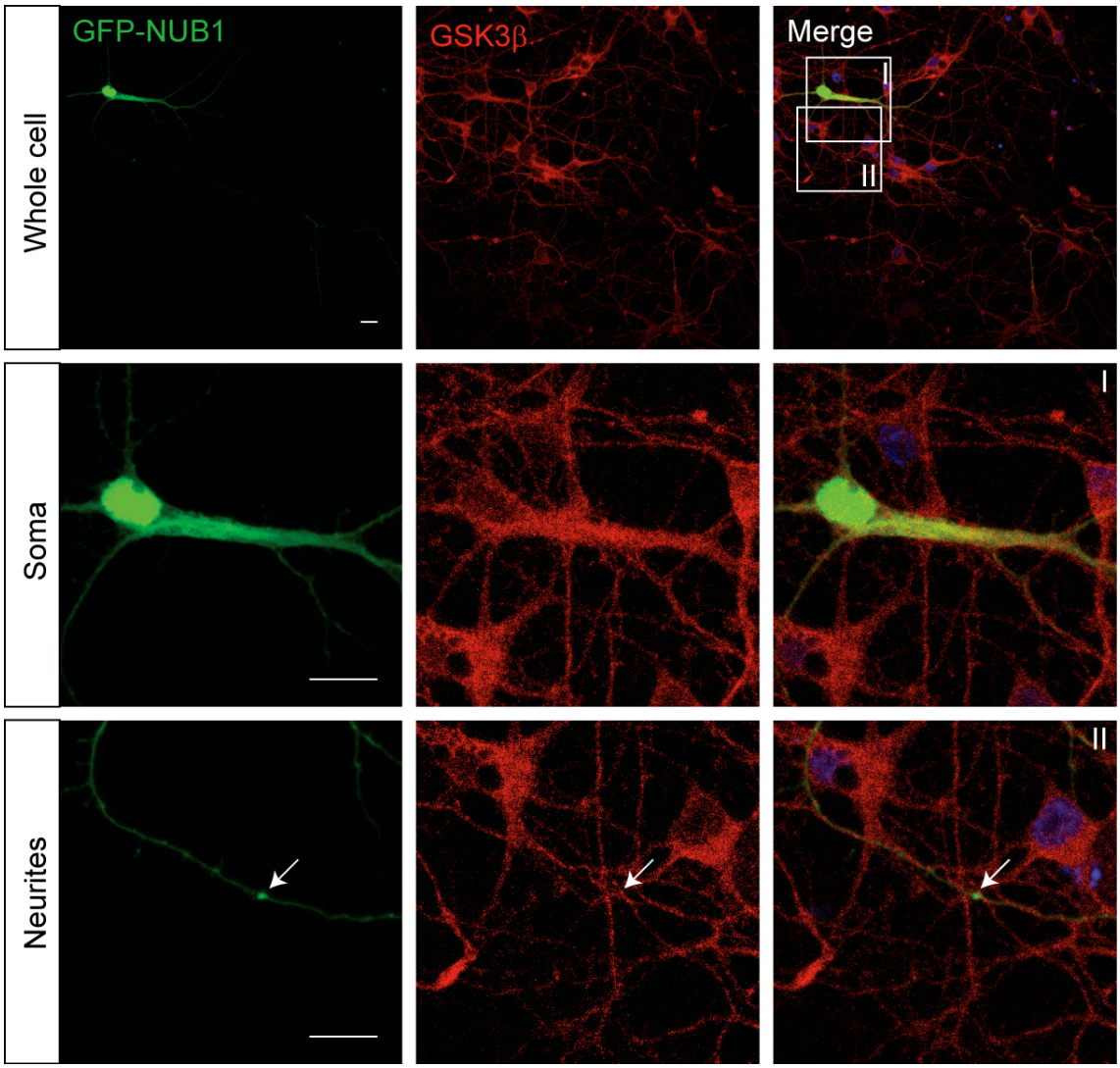

Figure 3.13. *Distribution of GFP-NUB1 and endogenous GSK3β in rat primary neurons.* Rat primary cortical neurons were transfected with GFP-NUB1 plasmid. Twenty-four hours after transfection, cells were fixed with paraformaldehyde (4%, 10 min at 37°C). Cells were labelled with the anti-GSK3β primary antibody in conjunction with the AlexaFluor 594 secondary antibody and treated with DAPI to detect nuclei (blue). Images were acquired with a laser scanning confocal microscope (Zeiss LSM 700). The white squares I and II demarcate the magnification of the cell body (soma, I) and neurites (II). The varicosities are highlighted by white arrows. Scale bars = 10 μm.

3.3. Discussion

As thoroughly described in previous studies, tau accumulates in NT, NFTs and the corona of neuritic plaques in AD patients. These inclusions are positive for hyperphosphorylated tau, and numerous other proteins including Ub and NEDD8.

In this chapter, detection of tau with the AT8 antibody, specific for hyperphosphorylated tau, in the entorhinal cortex and hippocampus of Braak stage V and VI patients validated the staging of the brain sections and the diagnosis. Although AT8 positive cells and tau aggregations could be detected in a control, the number of cells with NFTs and the quantity of NTs were far less abundant in the age-matched control compared to the AD patient. Moreover, no labelling of dystrophic neurites could be found in the control. The presence of NFTs and AT8 labelling in non-demented adults has been reported before. The difference with AD lies in the load and localisation of NFTs and NTs, twice less abundant in the hippocampus of controls than in demented adults (Shin et al., 1991). A recent study by Braak *et al*, (2011) on 2332 brain sections from patients aged from 1 to 100 years reported that AT8-positive neurons could be found in the brain of adults as young as 20 years old. The AT8 immunoreactivity was present in cells that contained pretangle tau, i.e. non-argyrophilic hyperphosphorylated tau that could not be detected using silver-staining techniques. Interestingly, they showed that the presence of hyperphosphorylated tau was inevitable after 40 years of age and that the vast majority of adults aged 70 or more had NFTs and NTs at least in the transentorhinal region. However, even in adults aged more than 90, the progression of NFTs was restricted to Braak stage I and II. Braak stage V and VI pathology was detected in 9.5 % of the total cases, and in 24.4% of people aged more than 80 years. Moreover, a marker of AD is brain shrinkage, particularly obvious in cortical regions, due to neuronal loss. The progression of NFTs is closely related to the seriousness of the disease, and the pattern and regions of NFT load matches the neuron loss. However, cell death within a region exceeds the number of NFTs. Furthermore, NFTs in cells can persist for decades before becoming ghost tangles, suggesting that tangle-bearing

neurons could still be functional and that the formation of NFTs is a neuroprotective mechanism. This might explain why not all patients with NFTs develop dementia. In fact, NFT formation could be a very slow process spread over decades, and the development of sporadic AD might occur only in individuals predisposed to pathogenic mechanisms because of environmental and genetic factors (Mattson and Magnus, 2006). The present study first confirmed the overload of AT8 positive inclusions in the hippocampus and entorhinal cortex of a Braak stage VI patient compared to a control patient, in order to correlate the subsequent findings with AD pathology.

One of the known pathogenic mechanisms in AD is the dysregulation of the UPS. NFTs and neuritic plaques are decorated with Ub, PHFs and Aβ peptides negatively influence the proteasome activity and impairment of the proteasome activity has been reported in AD (Oddo, 2008). In this study, Ub accumulated in pyramidal neurons of Braak stage VI patients, in structures similar to NFTs. Like AT8-specific tau labelling, Ub could be seen in NFT-shaped structures in AD patients and less frequently in age-matched control adults. Moreover, no extracellular structures (NTs and dystrophic neurites) exhibited strong Ub immunoreactivity in control patients compared to AD patients. Therefore the Braak stage VI AD patient had more Ub-positive depositions than the control patient. Normally, Ub is recycled after targeting a protein for proteasomal degradation. The accumulation of Ub in AD lesions suggests that UPS degradation mechanisms are impaired or overwhelmed and unable to trigger the clearance of aggregating polypeptides. Therefore Ub is sequestered to the aggregates.

The presence of both ULM FAT10 and NEDD8 in the hippocampus was revealed. Although NEDD8 has been reported to accumulate in NFTs in AD patients, it is the first time that FAT10 has been described in the hippocampus and entorhinal cortex of a control and AD patient. However, the detection of FAT10 and Ub in only one AD patient and one control cannot lead to thorough conclusions. Nonetheless, the fact that FAT10 immunoreactivity was more ubiquitously distributed in AD brain sections might be the result of increased neuroinflammation in AD, as inflammatory cytokines induce FAT10 expression (Lukasiak *et al*., 2008). Interestingly, FAT10, similarly to Ub, labelled

extracellular structures that were probably dystrophic neurites only in the AD patient. However, NFT-like structures were decorated with FAT10 in both AD patient and control. A role for FAT10 in proteasomal degradation has been described (Hipp *et al*., 2004). This suggests that FAT10 might target tau or a conformational population of tau for proteasomal degradation in a Ub-independent manner.

NEDD8 is thought to be a predominantly nuclear protein that is involved in proteasomal degradation and therefore the regulation of protein activity (Dil Kuazi *et al.*, 2003). Several studies have linked NEDD8 to Ub-positive inclusions in neurodegenerative disorders such as NFTs and senile plaques in AD (Chen *et al*., 2003; Dil Kuazi *et al.*, 2003; Mori *et al*., 2005). In this study, analysis of NEDD8 immunoreactivity in an AD Braak stage VI and control yielded interesting results. In fact, no major difference in NEDD8 immunoreactivity could be observed between the control and AD patient, while Chen *et al* (2003) showed than in the hippocampus of AD patients NEDD8 was shifted from a nuclear to a cytoplasmic localisation compared to control patients. This was suggested to occur as a consequence of cell cycle dysregulation in AD. In our study, NEDD8 staining was mostly nuclear in entorhinal cortical cells, and was predominantly cytoplasmic in the CA1 and CA4 areas of the hippocampus in both the control and AD patient. Contrary to the study by Mori *et al*., 2005, no typical AD inclusion bodies, such as NFTs or senile plaques, were found to be NEDD8 positive. However, NEDD8 was detected in most pyramidal neurons in the CA2 and CA4 areas of the hippocampus, where NFT formation occurs.

As NEDD8 and Ub have been shown to decorate NFTs in AD, double labelling with AT8 was performed to unequivocally determine the recruitment to NFT and other tau aggregations, but the autofluorescence of the brain sections could not be overcome despite the application of various techniques.

NUB1 can target NEDD8, FAT10 and their conjugated proteins for proteasomal degradation (Kamitani *et al.*, 2001; Hipp *et al*., 2004). Moreover, NUB1 reduces synphilin-1 positive inclusions in a model of PD (Tanji *et al*., 2006). Hence, the immunoreactivity of NUB1 was also explored in a Braak stage VI AD patient

compared to an age-matched control. However, a previous study from Tanji *et al*, 2007, found no NUB1 immunoreactivity in AD patients. Therefore, the specificity of NUB1 antibody was verified. The detection of NUB1 was strongly reduced when the NUB1 antibody was pre-incubated with the NUB1 peptide and no specific immunoreactivity was detected with the pre-immune serum, thus validating the specificity of this antibody. This major difference in our findings from those of Tanji *et al.*, (2007) could be explained in many ways, including the use of a different NUB1 antibody, variation in the methods used for antigen retrieval and antigen detection by immunohistochemistry, or characteristics of the brain sections themselves. Indeed, the post-mortem fixation delay and the type of embedment are factors that could influence the detection of proteins. Nonetheless, examination of NUB1 immunoreactivity was interestingly very similar to that of NEDD8. Notably, despite the presence of an NLS, NUB1 immunoreactivity was mostly cytoplasmic throughout the neurons in the entorhinal cortex and hippocampus of the AD patient and control, and in contrast to NEDD8 was also detected in the nucleus in some cells of the entorhinal cortex in the control patient only.

To verify these observations, the localisation of NEDD8 and NUB1 was directly compared in a panel of AD patients and controls. The localisation of NEDD8 and NUB1 in the pyramidal neurons of the CA1/2 and CA4 areas of the hippocampus was analysed. No major differences in NEDD8 and NUB1 immunoreactivity were observed between the control and AD patients, and the similarities between NUB1 and NEDD8 were confirmed with their localisation more cytoplasmic. This suggests that NUB1 and NEDD8 might cooperate in the cytoplasm of the cells in the hippocampus to modulate proteasomal degradation. The fact that both NEDD8 and NUB1 were more cytoplasmic in the CA4 area than in the CA1/2 area in the AD patient perhaps suggests a progressive redistribution of these proteins that correlates with the progression of disease severity. As NFTs spread from the entorhinal cortex, where NEDD8 and NUB1 were found to be more nuclear, to the dentate gyrus, NUB1 and NEDD8 relocate to the cytoplasm. It would therefore be interesting to analyse NUB1 and NEDD8 in other parts of the brain affected by AD, in order to assess if a similar shift could be observed.

The expression and localisation of NUB1 was compared to that of endogenous tau and GSK3β in rat primary cortical neurons. Lithium treatment clearly impaired GSK3β activity, both reducing the levels of endogenous GSK3β and decreasing the GSK3β-mediated phosphorylation of endogenous tau. However, LiCl had no effect on either GFP-NUB1 or GFP levels. Moreover, transiently overexpressed GFP-NUB1 did not have a significant effect on either endogenous tau or GSK3β levels. However, transiently expressed levels of GFP-NUB1 were dramatically inferior to those of GFP and similar to those of endogenous NUB1; therefore, GFP-NUB1 overexpression was probably not sufficient to have significantly affected endogenous tau and GSK3β.

An interesting discovery was that the NUB1 antibody could also specifically cross-react with endogenous rat NUB1 that shares 85.7% identity with human NUB1 (and 64,3% identity in the NUB1 epitope). Therefore, inhibiting endogenous expression of NUB1 by siRNA might be more informative than the overexpression of NUB1 in rat cortical neurons.

Analysis of GFP-NUB1 localisation with endogenous tau, GSK3β and microtubules showed interesting findings. As expected, NUB1 was mostly nuclear due to its C-terminal NLS. However, all cells expressing GFP-NUB1 also exhibited diffuse GFP-NUB1 in the cytoplasm and in the neurites. Therefore, although predominantly nuclear, NUB1 is also cytoplasmic and might participate in protein regulation, for example as a shuttle for proteasomal degradation as shown for synphilin-1 (Tanji *et al*., 2006). Neither β-tubulin, tau nor GSK3β were seen in the nucleus, even with GFP-NUB1 expression. In the cytoplasm of the cell body, GFP-NUB1 localisation overlapped with that of GSK3β. In the neurites, GFP-NUB1 localisation appeared to overlap with that of endogenous tau, yet to be enclosed by microtubules rather than to co-localise with them. Interestingly, GFP-NUB1 accumulated in what appeared to be varicosities. Endogenous tau, but not β-tubulin or GSK3β was also detected in these swellings. Indeed, β-tubulin and GFP-NUB1 expression in these swelling was mutually exclusive, as though the microtubules enclosed them. Varicosities, also called presynaptic boutons, are thought to be swellings of the axons rich in neurotransmitter substances and involved in intercellular signal transduction. This raises the interesting possibility that NUB1 and tau could

cooperate in either neurotransmitter trafficking, or regulation of signal transduction at synapses. Indeed, NFT bearing neurons in AD seem to have reduced synaptic proteins such as synaptophysin compared to NFT-free neurons (Callahan et al., 1995). Moreover, a study of AD synaptosomes showed that Aβ peptides were found to aggregate in the synaptosomes which were also decorated with phosphorylated tau (Sokolow et al., 2011). Thus, tau is probably involved in synaptic signalling through regulation of the cytoskeleton. Whether the GFP-NUB1 positive varicosities are synaptic structures could be tested by staining for specific synaptic markers, such as the glutamatergic presynaptic terminal marker, vesicular glutamate transporter 1 (Lin *et al*., 2010).

The analysis of NUB1 and the ULMs NEDD8 and FAT10 in Braak stage VI AD patients has shown that these proteins can be detected in areas of the brain that are vulnerable to degeneration in AD, where they may be involved in protein turnover. Moreover, NUB1 expression in rat cortical neurons revealed that NUB1 co-localised with endogenous tau in the neurites and varicosities, and with GSK3β in the cytoplasm of the cell body. Thus, NUB1 could interact functionally with them. Furthermore, the predominantly nuclear localisation of NUB1 implies that NUB1 might have an independent role in cell regulatory functions such as cell signalling. The localisation of NUB1 with tau in the neurites and varicosities, an important platform for signal transduction, suggests that NUB1 and tau might have a role in the regulation of neurotransmitter trafficking or release.

The next chapter will focus on the capacity of NUB1 to modulate the formation of tau inclusions in a cell model of tau phosphorylation and aggregation.

Chapter 4
NUB1 reduces tau aggregation

4.1. Introduction

The cytoskeletal microtubules are an essential support network for neuronal activity. Microtubules are composed of α and β dimers that polymerise in protofilaments. The flexibility and remodelling of microtubules are essential for the growth of neuronal processes. Wide and long microtubule filaments in the axon provide tracks for the dynamic transport of proteins. Therefore, the stability of microtubules, but not the rigidity, is crucial for the normal function of neurons. The MAP tau is involved in microtubule polymerisation and stability, and binds to the microtubules via its MBD domain composed of 3 or 4 repeat regions. The presence of 4 repeat regions in the MBD of the 4R isoforms enhances the strength of tau interaction with the microtubules and the ability of tau to promote microtubule assembly and stabilisation compared to the 3R isoforms. More precisely, it is a particular motif, KVQIINKK, located between the repeat regions R1 and R2 that confers the high affinity for microtubules to the 4R isoforms (Panda *et al*., 1995). Indeed, in mammalian cells, tau overexpression promotes microtubule bundling. Tau co-localises with microtubule bundles, the shapes of which vary from one cell type to another (Bruijn *et al*, 2004; Lovestone *et al*., 1996).

Tau phosphorylation regulates its binding to the microtubules and aggregation. Phosphorylation in the MBD (between residues 244-368) has the strongest influence on tau interaction with the microtubules. For instance, the residues Ser262 and Ser356 alone, if phosphorylated, inhibit tau interaction with the microtubules and are crucial for the outgrowth of neuronal processes (Biernat and Mandelkow, 1999; Fischer *et al.*, 2009). The phosphorylation of Thr231 and Ser214, in the proline-rich domain, also reduce the ability of tau to bind microtubules (Sengupta *et a*l., 1998; Cho and Johnson, 2003). Interestingly, in

cell models mimicking tau phosphorylation, the phosphorylation of tau at the N-terminus (before residue 208) inhibited tau aggregation, while phosphorylation at the C-terminus (from residue 396) induced tau aggregation (Abraha *et al*., 2000; Haase *et al*., 2004).

The formation of NFTs in AD is not linked to a mutation in the tau sequence but rather to post-translational modification such as its hyperphosphorylation. This would occur as a result of the combined upregulation of kinases (GSK3, cdk5, CK1) and downregulation of phosphatases (PP2A, PP5) (Hanger *et al*., 2009; Martin *et al*., 2011). *In vitro*, tau phosphorylated at specific sites (S396, S404, S422) is prone to aggregate (Liu F *et al*., 2007) and tau phosphorylated on Ser396 (pS396-tau) has been detected in PHF (Otvos *et al*., 1994). GSK3 is a major kinase for tau phosphorylation in AD as it can phosphorylate tau on many residues recognized by the antibodies Alz50, PHF-1, AT8, AT100 and AT180, antibodies specifically used to detect PHFs and NFTs in AD. Moreover, it has been shown that GSK3 activity is increased in AD brain, which is likely to be responsible for tau hyperphosphorylation (Hooper *et al*., 2008). The GSK3β isoform is highly expressed in the brain and neurons and co-localises with the microtubules (Johnson and Stoothoff, 2004; Hanger *et al*., 2009). Furthermore, *in vitro*, tau phosphorylation by GSK3β has been shown to trigger the formation of tangle-like structures (Rankin *et al*., 2008).

A consequence of the hyperphosphorylation of tau is a shift in its molecular weight detected on WB. Although the normal six isoforms of tau have a molecular weight distribution of between 50 kDa to 65 kDa, hyperphosphorylated tau in AD is seen as 3 prominent bands of 55, 64, and 69 kDa and a less prominent band of 74 kDa that represents the hyperphosphorylation of the 6 different tau isoforms. On the other hand, due to the overexpression of the 4R tau isoforms in PSP, CBD and FTDP-17 with mutations affecting tau splicing, only 2 prominent bands of 64 and 69 kDa and a smaller one at 74 kDa are detected (Lee *et al*., 2001; Buee *et al*., 2000).

As noted previously, NUB1 and NUB1L are UBL/UBA proteins that target the ULM NEDD8 and FAT10, and their conjugates, for proteasomal degradation. As seen in chapter 3, both NEDD8 and NUB1 are expressed in the pyramidal

neurons of the hippocampus in control and AD patients, suggesting that both NUB1 and NEDD8 have a functional role in this region of the brain.

NUB1 has been shown to reduce synphilin-1 positive inclusions in a cell model of PD (Tanji *et al*., 2006). Interestingly, the C-terminus of NUB1 was essential for direct interaction with synphilin-1, which might suggest that neddylation or FAT10ylation is not always necessary for NUB1 activity.

This chapter focused on the optimisation of a cell model for tau aggregation. Human neuroblastoma SK-N-SH cells, lacking detectable levels of endogenous tau protein, were transfected with the 0N4R isoform of tau fused with GFP at its N-terminus. In addition, GSK3β was overexpressed to induce the phosphorylation of tau, and the proteasome was inhibited to promote tau aggregation as proteasome failure is a feature of AD. The influence of NUB1 co-expression on tau aggregation was analysed. Furthermore, the effect of NUB1L and NUB1L mutants, lacking the UBL domain or the three UBA domains, on tau inclusion formation was assessed.

4.2. Results

4.2.1. Expression and localisation of GFP-tau

To analyse the expression and localisation of tau, GFP-tau was transiently overexpressed in SK-N-SH neuroblastoma cells (Figure 4.1)

Twenty-four hours after transfection, cells were harvested and 10 µg of total protein was resolved on a polyacrylamide gel (10%). Tau protein was detected by WB, using an antibody specific to total tau (anti-tau) or to the GFP tag (anti-GFP) (Figure 4.1, A). Although the six isoforms of tau are normally expressed in human adult brain (Buee *et al*., 2000), endogenous tau protein could not be detected in SK-N-SH cells (Figure 4.1, A), even with longer exposures and increased amounts of protein. However, GFP-tau was detected with both the anti-tau and the anti-GFP antibodies as a single band of ~91kDa. Because of the absence of detectable endogenous tau protein, the SK-N-SH neuroblastoma cell line was considered a very useful tool to control the expression and the aggregation of exogenous tau protein.

The subcellular distribution of GFP-tau was examined in SK-N-SH cells, following a 4 h treatment of cells with a vehicle (DMSO) or with MG132 (50 µM) 24 h after transfection. The inhibition of the proteasome has been shown to induce the formation of GFP-tau inclusions (Goldbaum *et al*., 2003), and impairment of the proteasome in AD has been reported to be an underlying pathogenic mechanism exacerbating the aggregation of tau and formation of NFTs (Keck *et al*, 2003). Subsequently, cells were fixed with 0.3% glutaraldehyde for 10 min at 37°C. The endogenous microtubule network was labelled using the anti-β-tubulin (anti-β-tub) primary antibody in conjunction with the AlexaFluor 594 secondary antibody. In Figure 4.1, B, GFP-tau (green) was detected in the cytoplasm, in a prominent microtubule network co-labelled by anti-β-tub (red). GFP-tau overexpression induced the formation of microtubule bundles (arrows), (Lewis *et al*., 1989; Bruijn *et al*., 2004). Following inhibition of the proteasome (Figure 4.1, B, bottom row), GFP-tau was detected in protein aggregates (arrowhead). However, these inclusions were not microtubule positive.

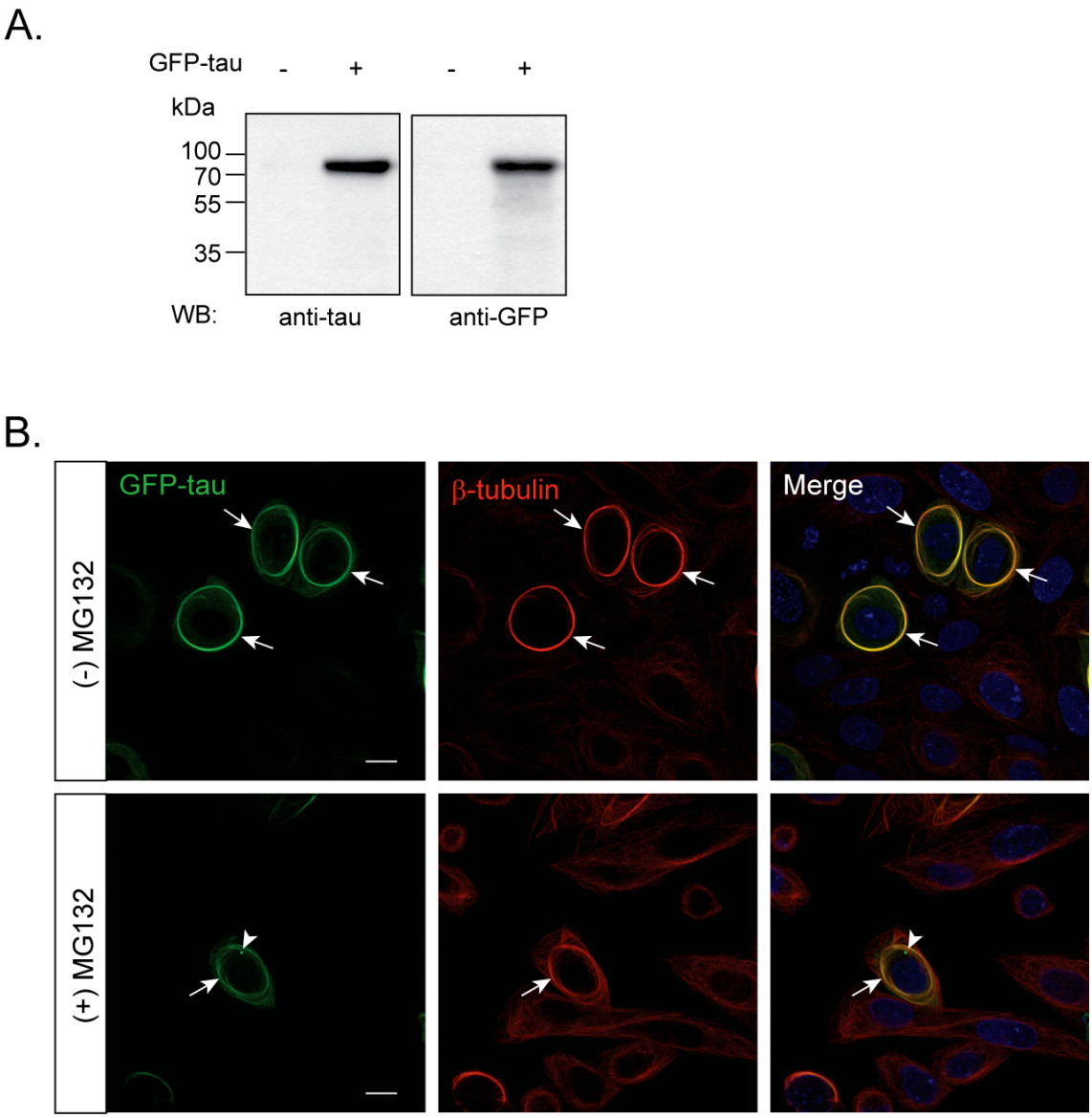

Figure 4.1. *Expression and localisation of GFP-tau in SK-N-SH cells*. (**A**) Cells were transfected with with 50 ng of GFP-tau plasmid. Twenty-four hours after transfection, cell lysates (10 µg of total cellular protein) were resolved on a polyacrylamide gel (10%) and proteins were detected by WB, using the anti-tau or anti-GFP antibody. (**B**) Cells were transfected with 50 ng of GFP-tau. Twenty-four hours after transfection, cells were treated with a vehicle (DMSO) or with MG132 (50 µM) for 4 h. Cells were fixed with 0.3% glutaraldehyde for 10 min at 37°C. The microtubules (red) were detected using the anti-β-tub antibody and the AlexaFluor 594 secondary antibody. Nuclei were detected with DAPI (blue). GFP-tau (green) was detected in microtubule bundles (arrows) and protein aggregates (arrowheads). Images were acquired with a laser scanning confocal microscope (Zeiss LSM 700). Scale bars = 10 µm.

Thus, GFP-tau was normally associated with the microtubules, but upon inhibition of the proteasome, detached from the microtubule network and formed inclusions.

4.2.2. Expression and localisation of HA-GSK3β

In AD, tau aggregation occurs following its hyperphosphorylation by several kinases such as GSK3β (Buee *et al*., 2000; Hanger *et al*., 2009). Therefore, the expression of endogenous GSK3β and transiently expressed HA-GSK3β was analysed in SK-N-SH cells (Figure 4.2).

Twenty-four hours after transfection, 10 µg of total cellular protein was resolved on a 10% polyacrylamide gel and proteins were detected by WB using the anti-GSK3β or the anti-HA antibody (Figure 4.2, A). The endogenous GSK3β was detected in SK-N-SH cells as a single band of ~47 kDa, but at very low levels compared to the exogenous HA-GSK3β, even with long exposures and significantly increased amounts of protein. The recombinant protein HA-GSK3β was specifically detected by both the anti-GSK3β and the anti-HA antibodies as a single band of ~50 kDa.

To analyse the subcellular localisation of GSK3β in SK-N-SH neuroblastoma cells, HA-GSK3β was detected with the anti-HA primary and the AlexaFluor 594 secondary antibody (Figure 4.2, B). HA-GSK3β was localised ubiquitously throughout the cytoplasm, both with and without proteasome inhibition. However, following proteasome inhibition, the appearance of HA-GSK3β was more particulate in the cytoplasm and HA-GSK3β was also detected in the nucleus.

4.2.3. HA-GSK3β induces GFP-tau inclusion formation

The anomalous hyperphosphorylation of tau by GSK3β is an important pathogenic mechanism of tau aggregation in AD (Balaraman *et al*, 2006; Giese, 2009). Moreover, the failure of the UPS system to clear tau inclusions has been described to enhance the formation of NFTs (Oddo, 2008). Therefore, both the co-transfection of HA-GSK3β with GFP-tau and the inhibition of the proteasome were optimised in SK-N-SH cells to induce GFP-tau aggregation.

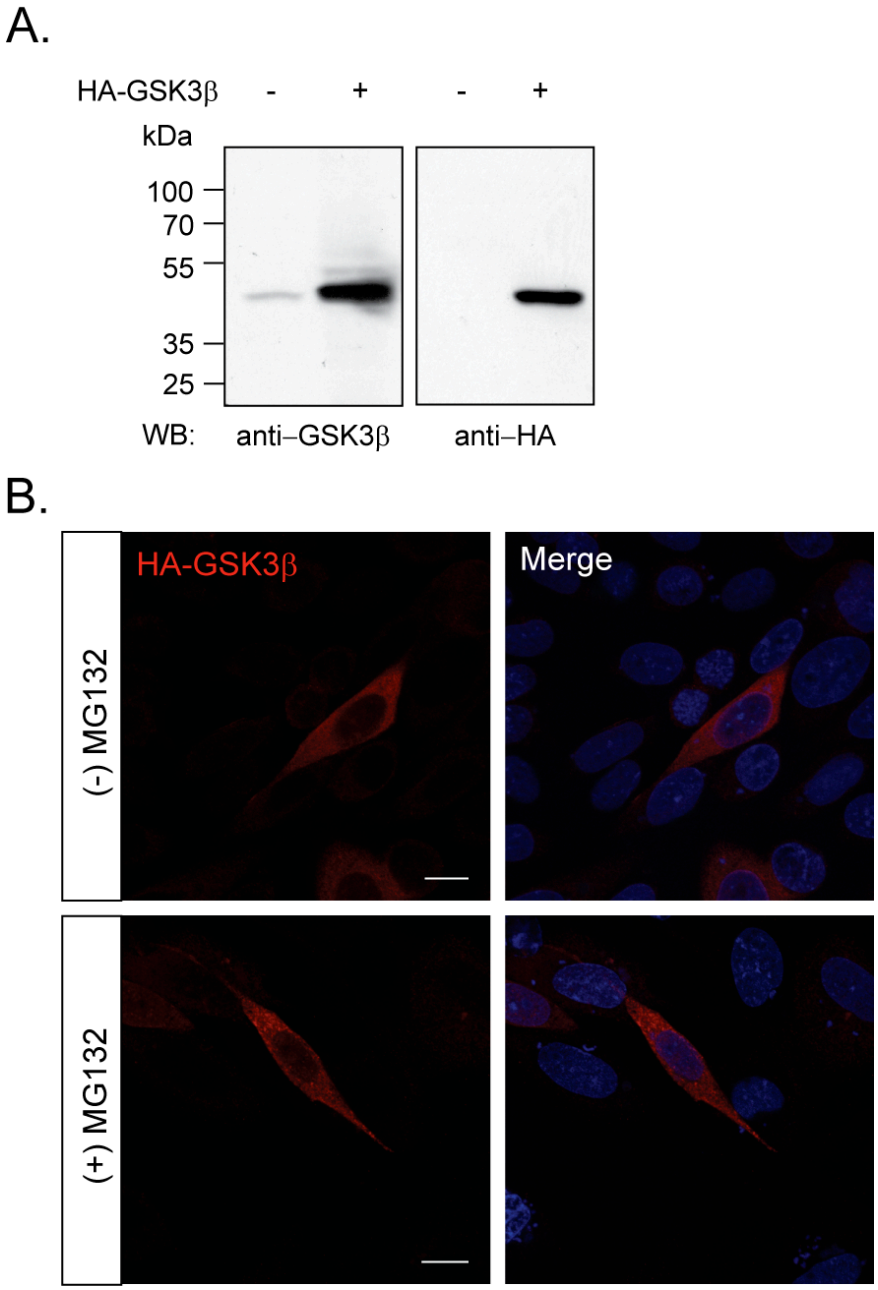

Figure 4.2. *Expression and localisation of HA-GSK3β in SK-N-SH cells*. (**A**) Cells were transfected with a control plasmid (-) or with 150 ng of HA-GSK3β (+).Twenty-four hours after transfection, cell lysates (10 µg total cellular protein) were resolved on a polyacrylamide gel (10%) and proteins were detected by WB, using the anti-GSK3β or anti-HA antibody. (**B**) Cells were transfected with 150 ng of HA-GSK3β plasmid. Twenty-four hours after transfection, cells were treated with a vehicle (DMSO) or with MG132 (50 µM) for 4 h. Cells were fixed with 0.3% glutaraldehyde for 10 min at 37°C. HA-GSK3β (red) was detected using the anti-HA antibody and the AlexaFluor 594 secondary antibody. Nuclei were detected with DAPI (blue). Images were acquired with a laser scanning confocal microscope (Zeiss LSM 700). Scale bars = 10 µm.

To confirm that HA-GSK3β could phosphorylate exogenous GFP-tau, cells were transfected with GFP-tau alone or with HA-GSK3β, and the detection of two phosphorylable epitopes of tau, Ser396 and AT8 epitopes, was analysed by WB (Figure 4.3, A).

Tau residue S396 and the AT8 epitopes are two targets for GSK3β-dependent phosphorylation (Plattner *et al*., 2006, Hanger *et al*., 2009; Qian *et al.*, 2010). In the absence of HA-GSK3β, a basal level of tau phosphorylated on S396 could be detected in SK-N-SH cells, whereas phosphorylation of tau on the AT8 epitopes could not be observed. Phosphorylation of tau on the AT8 epitopes was only detected in the presence of HA-GSK3β. An increase in phosphorylation of GFP-tau S396 was seen with HA-GSK3β co-expression, as well as a shift in GFP-tau molecular weight. Indeed, with the two antibodies anti-tau and anti-pS396, a second higher molecular weight band was observed as a result of hyperphosphorylation of GFP-tau in the presence of exogenous GSK3β.

To detect and define GFP-tau inclusions, cells were transfected with GFP-tau and HA-GSK3β. Twenty-four hours after transfection, cells were treated with a vehicle (DMSO) or with MG132 (50 μM) for 4 h. Subsequently, cells were fixed with 0.3% glutaraldehyde for 10 min at 37°C, and GFP-tau inclusions were labelled with the AT8 antibody. The AT8 antibody does not normally detect tau unless it is abnormally phosphorylated (Figure 4.3, A) (Braak and Braak, 1995). Figure 4.3, B, shows that, in addition to the microtubule bundles, GFP-tau (green) was also diffusely localised in the cytoplasm both in the absence (top row) and the presence (bottom row) of proteasome inhibition with HA-GSK3β co-transfection compared to GFP-tau alone (Figure 4.1). Moreover, GFP-tau inclusions that were AT8 positive were detected (arrows). In the presence of MG132 (Figure 4.3, B, bottom row), GFP-tau was noticeably detected diffusely in the cytoplasm and AT8 also detected some of the GFP-tau labelled microtubule bundles. Therefore, AT8 co-labelling confirmed the formation of GSK3β-dependent GFP-tau inclusions in SK-N-SH cells.

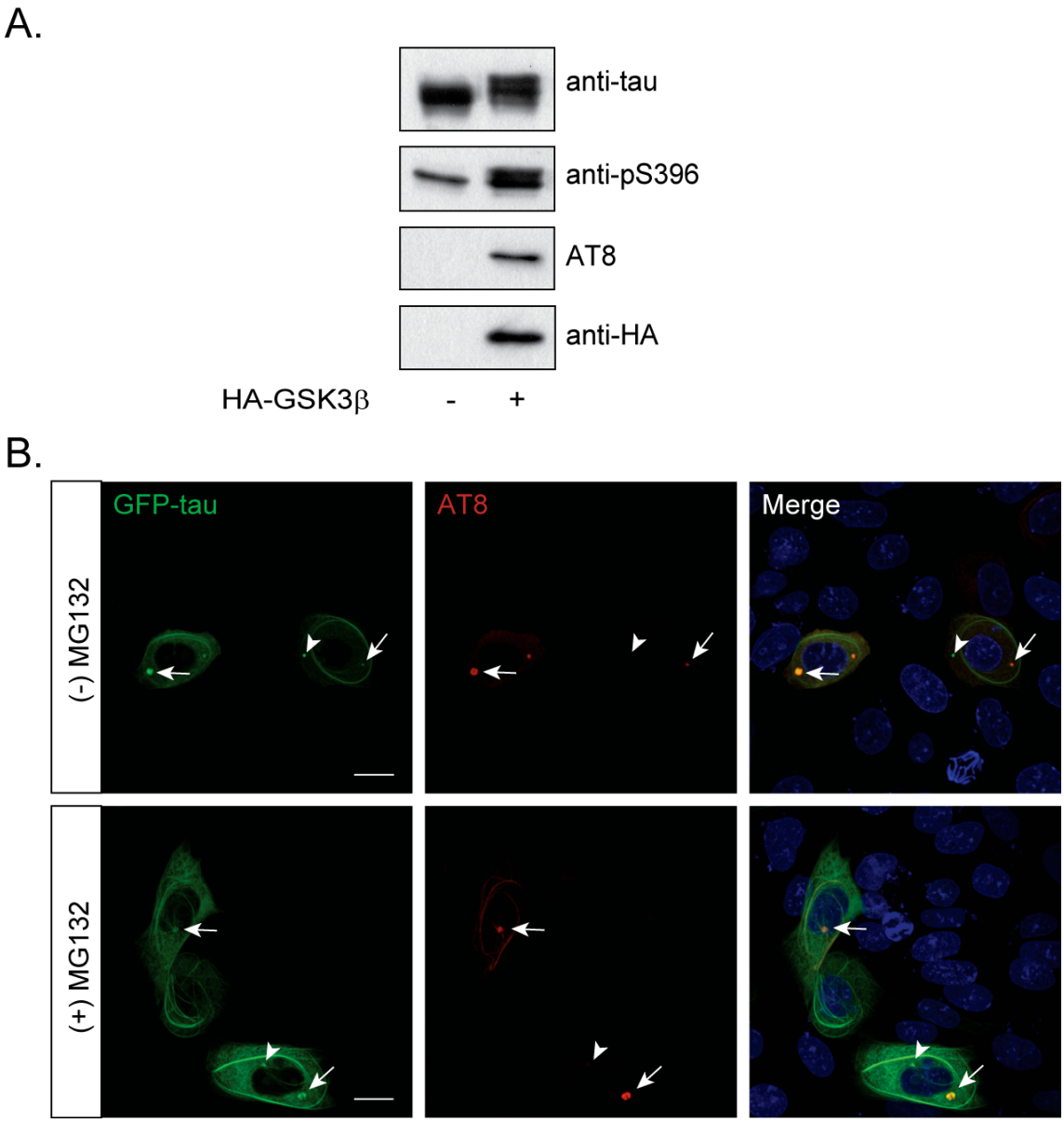

Figure 4.3. *GSK3β-dependent GFP-tau phosphorylation and inclusion formation.* (**A**) Cells were transfected with GFP-tau alone or in combination with HA-GSK3β plasmids. Twenty-four hours later, cells were lysed with RIPA buffer and samples (10 µg) were resolved on a polyacrylamide gel (10%). Proteins were detected by WB using the anti-tau, anti-pS396, AT8 and anti-HA primary antibodies. (**B**) Cells were transfected with 50 ng of GFP-tau and with 150 ng of HA-GSK3β plasmids. Twenty-four hours after transfection, cells were treated with a vehicle (DMSO) or with MG132 (50 µM) for 4 h. Cells were fixed with 0.3% glutaraldehyde for 10 min at 37°C, and immunocytochemistry performed with the AT8 primary antibody and AlexaFluor 594 secondary antibody. GFP-tau inclusions (green) were AT8 positive (red) (arrows) or AT8 negative (arrowhead). Images were acquired with a laser scanning confocal microscope (Zeiss LSM 700). Scale bars = 10 µm.

HA-GSK3β was able to phosphorylate tau and induce tau inclusion formation. The optimal ratio between GFP-tau and HA-GSK3β that would induce tau aggregation was explored in SK-N-SH cells. Cells were co-transfected with increasing amounts of GFP-tau and HA-GSK3β (Figure 4.4).

Twenty-four hours after transfection, cells were treated with MG132 (50 μM) for 4 h, and GFP-tau inclusions were detected using the AT8 antibody in conjunction with the AlexaFluor 594 secondary antibody (Figure 4.4). The data showed that with any given amount of GFP-tau, there was generally a proportionate increase in the number of cells with AT8 positive inclusions with increasing amounts of GSK3β. However, the same ratio from different relative amounts of GFP-tau and HA-GSK3β co-transfected gave different percentages of GFP-tau inclusions. For instance, the ratio GFP-tau:GSK3β = 1:1 with 25 ng, 50 ng and 100 ng of each produced 13.3±0.3%, 8±1.9% and 15.5±2.3% of GFP-tau transfected cells with inclusions respectively. Therefore, the percentage of GFP-tau inclusions was dependent on both the absolute amounts of each and their relative ratio. The co-transfection of 50 ng of GFP-tau and 150 ng of HA-GSK3β (GFP-tau:GSK3β = 1:3) yielded the greatest percentage (22.7±1.7%) of GFP-tau inclusions and was used in all further experiments.

4.2.4. Proteasome inhibition enhances GFP-tau inclusion formation

In AD, impairment of the UPS has been implicated in the failure to clear tau aggregates (Upadhya and Hegde, 2007; Riederer *et al*., 2011). Moreover, the inhibition of the proteasome in cells has been shown to stabilise the formation of tau inclusions (Goldbaum *et al.*, 2003). Therefore, the effect of proteasome inhibition on GFP-tau inclusion formation was examined in SK-N-SH cells. Cells were transiently transfected with 50 ng of GFP-tau and 24 h later treated with vehicle (DMSO) (NT) or five different combinations of proteasome inhibitors: 50 μM MG132 (MG132), 10 μM lactacystin (LAC), 10 μM epoxomicin (EPO), 50 μM MG132 + 10 μM lactacystin (MG132+LAC), 50 μM MG132 + 10 μM epoxomicin (MG132+EPO), or 10 μM lactacystin + 10 μM epoxomicin (LAC+EPO).

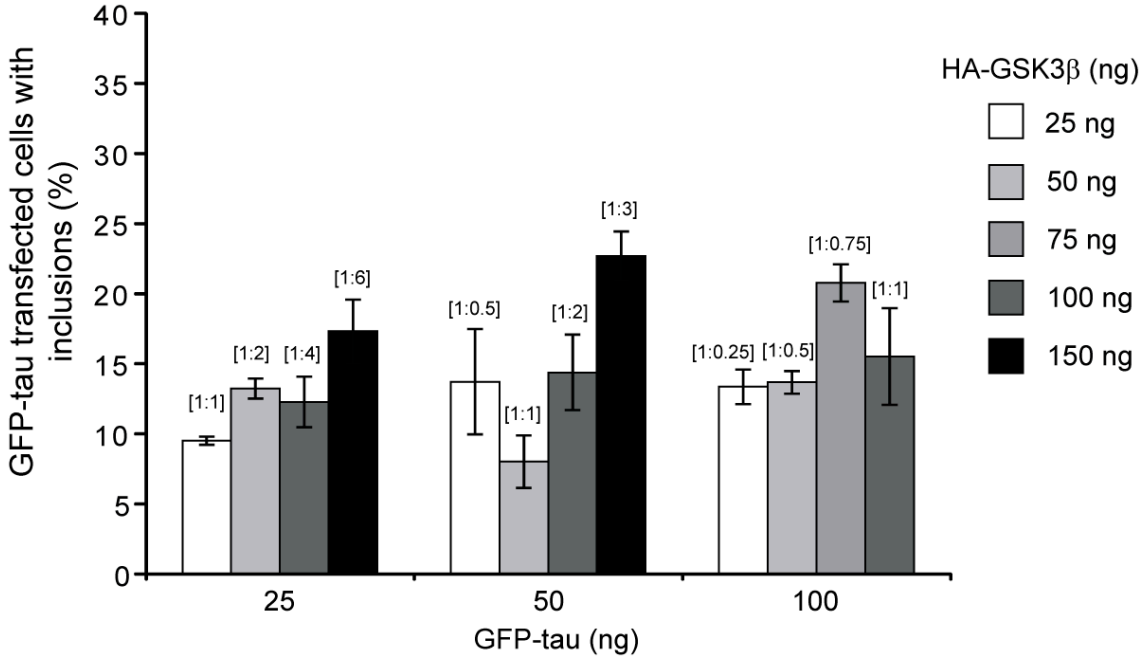

Figure 4.4. *Optimisation of GSK3β-dependent GFP-tau inclusion formation.* Cells were transfected with increasing amounts of GFP-tau and HA-GSK3β plasmids. Twenty-four hours after transfection, cells were treated with MG132 (50 μM) for 4 h, fixed with 100% methanol for 5 min at -20°C, and immunocytochemistry performed with AT8. At least 4 groups of 100 GFP-tau transfected cells (total, either with or without inclusions) for each of the two replicate experiments were counted using the Nikon Eclipse80i epifluorescent microscope, and the percentage of GFP-tau transfected cells with inclusions calculated. The GFP-tau:GSK3β ratio is shown in brackets. Error bars represent the standard error of the mean (SEM).

Cells were fixed and the percentage of cells transfected (Figure 4.5, A) as well as the percentage of cells transfected with inclusions (Figure 4.5, B) was counted.

With any given proteasome inhibition treatment, the percentage of transfected cells remained unchanged and was 34.3±0.8% (Figure 4.5, A). In the absence of proteasome inhibition, few GFP-tau inclusions were counted over time (Figure 4.5, B).

However, in the presence of proteasome inhibition, irrespective of the proteasome inhibitor used or combination thereof, the percentage of GFP-tau transfected cells with inclusions increased over time, even without GSK3β co-transfection. Therefore inhibition of the proteasome alone was sufficient to induce the formation of GFP-tau inclusions in SK-N-SH cells. After 4 h of treatment, lactacystin alone was the least effective proteasome inhibitor and did not induce more than ~11% of GFP-tau transfected cells with inclusions (Figure 4.5, B). In comparison, after 4 h of treatment, the percentage of cells with GFP-tau inclusions did not differ significantly (*p-value* > 0.8) following treatment with MG132 alone (18.3±0.3%), MG132+lactacystin (MG132+LAC, 18.7±5%) or MG132+epoxomicin (MG132+EPO, 18.15±3.3%). A 4 h treatment with MG132 alone was therefore suitable for the induction of inclusions. After 6 h of treatment, non-specific effects on cell survival were noted, and this duration of treatment was deemed too long.

Subsequently, cells were transfected with both GFP-tau and HA-GSK3β and the percentage of GFP-tau transfected cells (Figure 4.6, A) and percentage of GFP-tau transfected cells with inclusions (Figure 4.6, B) counted following proteasome inhibition over time. Similarly to the transfection of GFP-tau alone (Figure 4.5, A), proteasome inhibition did not affect the percentage of GFP-tau transfected cells (33.2±0.6%) in the presence of HA-GSK3β (Figure 4.6, A). Moreover, in the absence of proteasome inhibition, GFP-tau phosphorylation due to GSK3β co-transfection alone enhanced GFP-tau inclusion formation (6.8±3%, 0 h), but the percentage of inclusions did not significantly increase over time (8.3±2.4%, 6 h; *p-value* = 0.533, using an unpaired Student's *t*-test) (Figure 4.6, B).

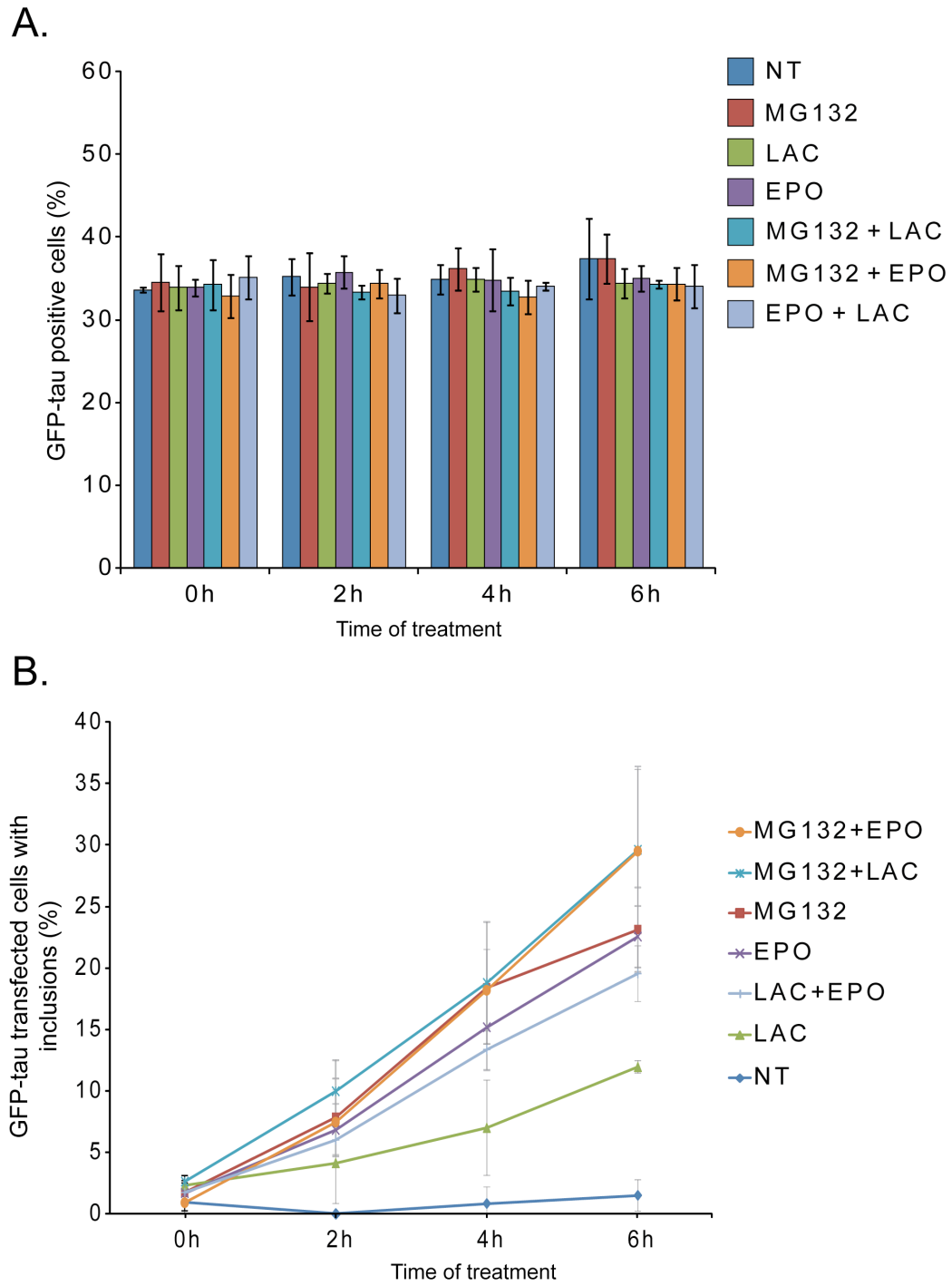

Figure 4.5. *Effect of Proteasome inhibition on GFP-tau aggregation.* SK-N-SH cells were transfected with 50 ng of GFP-tau plasmid, and 24 h post-transfection treated with a vehicle (NT), 50 μM MG132 (MG132), 10 μM lactacystin (LAC), 10 μM epoxomicin (EPO), 50 μM MG132 + 10 μM lactacystin (MG132+LAC), 50 μM MG132 + 10 μM epoxomicin (MG132+EPO), or 10 μM lactacystin + 10 μM epoxomicin (LAC+EPO) for 0, 2, 4 or 6 h. Cells were fixed with 100% methanol for 5 min at –20°C. The expression of GFP-tau (**A**) and the percentage of GFP-tau transfected cells with inclusions (**B**) were counted blind to experimental status in at least four groups of more than 100 cells for each condition in two separate experiments using the Nikon Eclipse80i epifluorescent microscope. Error bars represent the SEM.

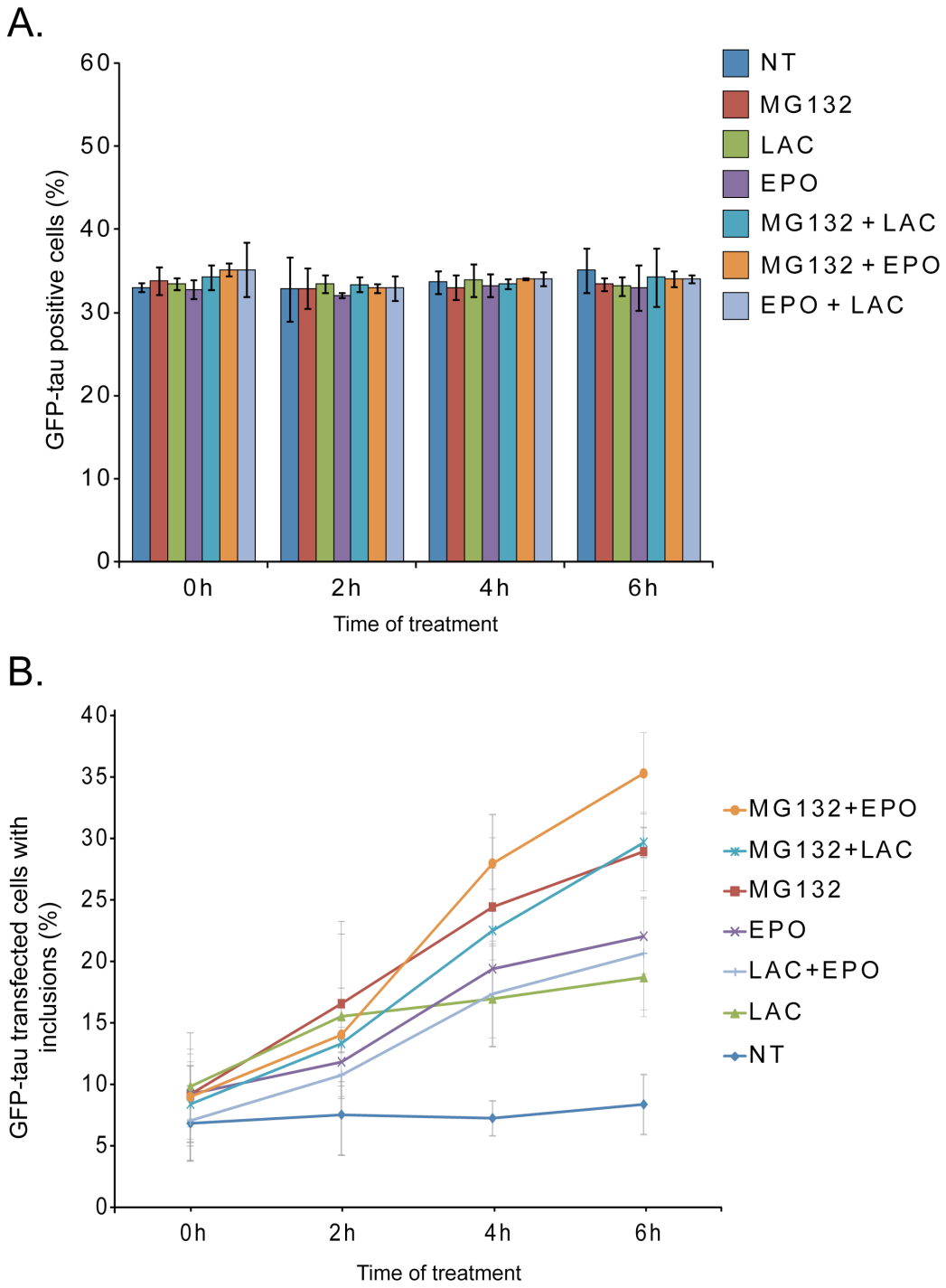

Figure 4.6. Effect of *Proteasome inhibition on GFP-tau aggregation with HA-GSK3β co-expression.* SK-N-SH cells were transfected with 50 ng of GFP-tau and 150 ng of GSK3β plasmids and 24 h post-transfection treated with a vehicle (NT), 50 μM MG132 (MG132), 10 μM lactacystin (LAC), 10 μM epoxomicin (EPO), 50 μM MG132 + 10 μM lactacystin (MG132+LAC), 50 μM MG132 + 10 μM epoxomicin (MG132+EPO), or 10 μM lactacystin + 10 μM epoxomicin (LAC+EPO) for 0, 2, 4 or 6 h. Cells were fixed with 100% methanol for 5 min at –20°C. The expression of GFP-tau (**A**) and the percentage of GFP-tau transfected cells with inclusions (**B**) were counted blind to experimental status in at least four groups of more than 100 cells for each condition in two separate experiments using the Nikon Eclipse80i epifluorescent microscope. Error bars represent the SEM.

Therefore, GSK3β-mediated phosphorylation of GFP-tau alone in the absence of proteasome inhibition was sufficient to induce the formation of GFP-tau inclusions.

The percentage of inclusions after 4 h of MG132 treatment was 18.3±0.3% in GFP-tau transfected cells and 24.3±1.3% in GFP-tau + HA-GSK3β transfected cells. MG132 treatment for 4 h after GFP-tau + HA-GSK3β transfection was therefore sufficient to observe GFP-tau inclusion formation. However, after a prolonged treatment of 6 h, proteasome inhibition may induce cell death, as many cells appeared abnormal with cell shrinkage and plasma membrane blebs, although the percentage of GFP-tau transfected cells remained unchanged. Therefore, all subsequent experiments were conducted following MG132 treatment for 4 h.

In conclusion, the combination of MG132 proteasome inhibition and HA-GKS3β co-expression enhanced the percentage of GFP-tau inclusions in SK-N-SH neuroblastoma cells.

4.2.5. HA-GSK3β is recruited to GFP-tau inclusions

The subcellular distribution of HA-GSK3β and GFP-tau phosphorylated on S396 was examined by immunocytochemistry (Figure 4.7). SK-N-SH cells were transfected with GFP-tau and HA-GSK3β, and 24 h post-transfection were treated with vehicle (DMSO) or MG132 (50 μM) for 4 h. Cells were fixed with 0.3% glutaraldehyde and the distribution of HA-GSK3β (Figure 4.7, A) and GFP-tau phosphorylated on S396 (Figure 4.7, B) was examined using the anti-HA or anti-pS396 antibody respectively.

In the presence of GFP-tau, HA-GSK3β (red) was detected in the cytoplasm, both in the absence (Figure 4.7, A, top row) and in the presence of MG132 (Figure 4.7, A, bottom row). Moreover, GSK3β was recruited to the GFP-tau inclusions (arrows) in both the absence and presence of MG132, and the

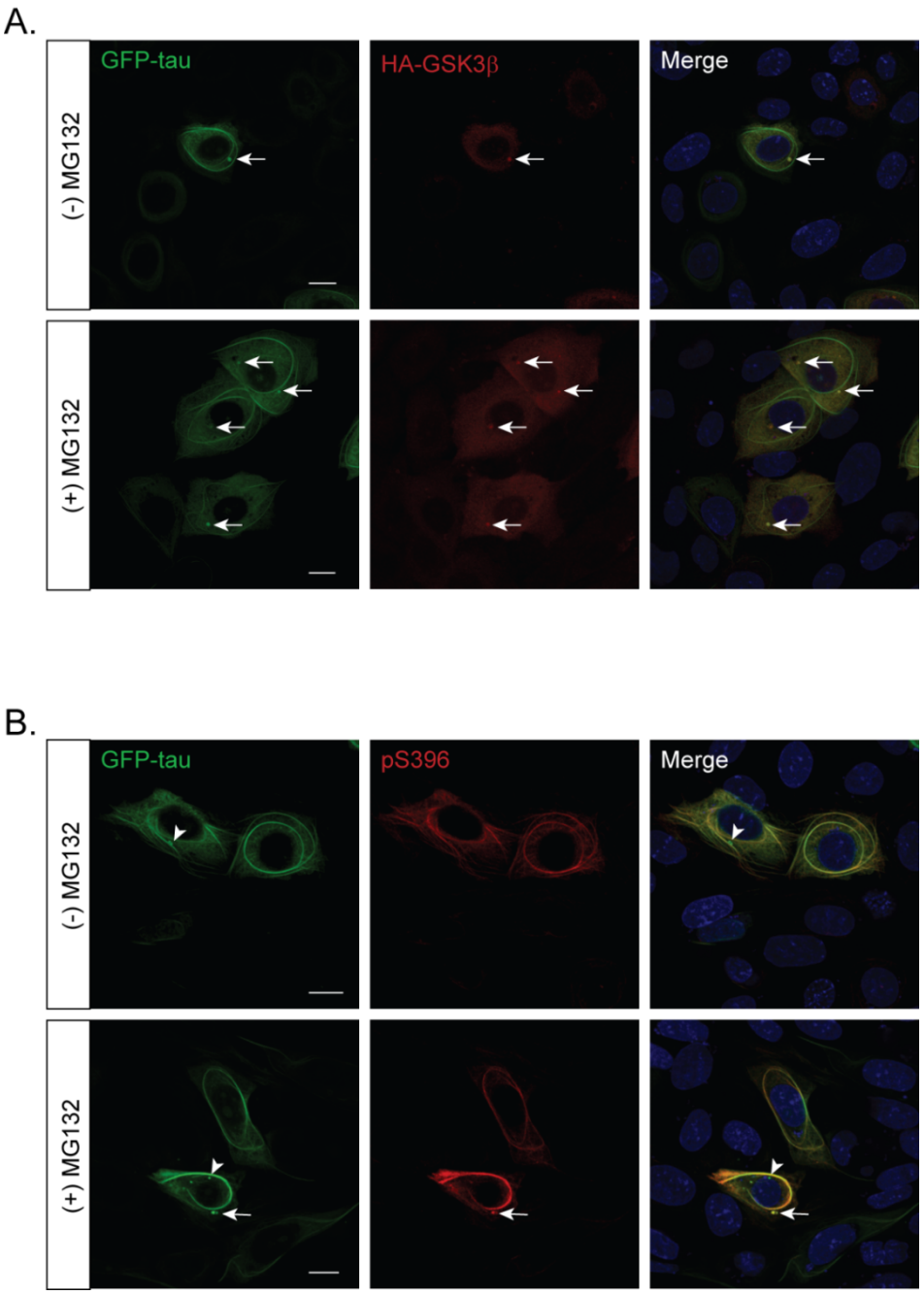

Figure 4.7. *GFP-tau inclusions are GSK3β and pS396-tau positive.* SK-N-SH cells were transfected with 50 ng of GFP-tau and 150 ng of HA-GSK3β plasmids, and 24 h post-transfection were treated with vehicle (DMSO) or 50 μM MG132. Cells were fixed with 0.3% glutaraldehyde for 10 min at 37°C. Subsequently, HA-GSK3β and pS396 GFP-tau were detected by immunocytochemistry with anti-HA (**A**) or anti-pS396 (**B**) in conjunction with the secondary antibody AlexaFluor 594. GFP-tau inclusions co-labelled with anti-HA or anti-pS396 are indicated by arrows, and GFP-tau inclusions negative for the anti-pS396 co-label are indicated by arrowheads. Images were acquired with a laser scanning confocal microscope (Zeiss LSM 700). Scale bars = 10 μm.

number of aggregates increased in the presence of MG132. In the presence of HA-GSK3β and MG132 (Figure 4.7, A, bottom row), in addition to the microtubule bundles, GFP-tau (green) was also diffusely co-localised with HA-GSK3β (red) in the cytoplasm.

In the presence of HA-GSK3β, GFP-tau (green) phosphorylated on Ser396 (pS396-tau, red) was detected both in the absence (Figure 4.7, B, top row) and in the presence (Figure 4.7, B, bottom row) of MG132. In contrast to AT8 which was mostly restricted to GFP-tau inclusions (Figure 4.3), pS396-tau co-localised with GFP-tau in the microtubule network. Moreover, the MG132 treatment increased the number of GFP-tau transfected cells with inclusions. However, some of the GFP-tau inclusions were pS396 positive (arrows), and some were not (arrowheads).

Therefore, AT8 positive phosphorylated GFP-tau was specifically detected in the inclusions, while GFP-tau phosphorylated on S396 was detected in the microtubule network and inclusions.

4.2.6. GFP-tau inclusion formation as a function of time

To assess the impact of GFP-tau inclusion formation on cells, the percentage of GFP-tau transfected cells and the percentage of cells with inclusions were compared to the percentage of GFP transfected cells over time. Cells were transfected with GFP or with GFP-tau and with HA-GSK3β. Cells were fixed at 3, 6, 12, 18, 24, 36, 48 and 72 h after transfection (Figure 4.8). The number of cells expressing GFP or GFP-tau (Figure 4.8, A) and the percentage of GFP-tau transfected cells with inclusions (Figure 4.8, B) was counted. Three hours after the beginning of transfection, less than 1% of cells were either GFP or GFP-tau positive.

Figure 4.8, A shows that the number of cells expressing GFP and GFP-tau increased over time to reach a maximum of 42.9±4.3% 36 h and 35±1.6% 24 h after the beginning of transfection respectively.

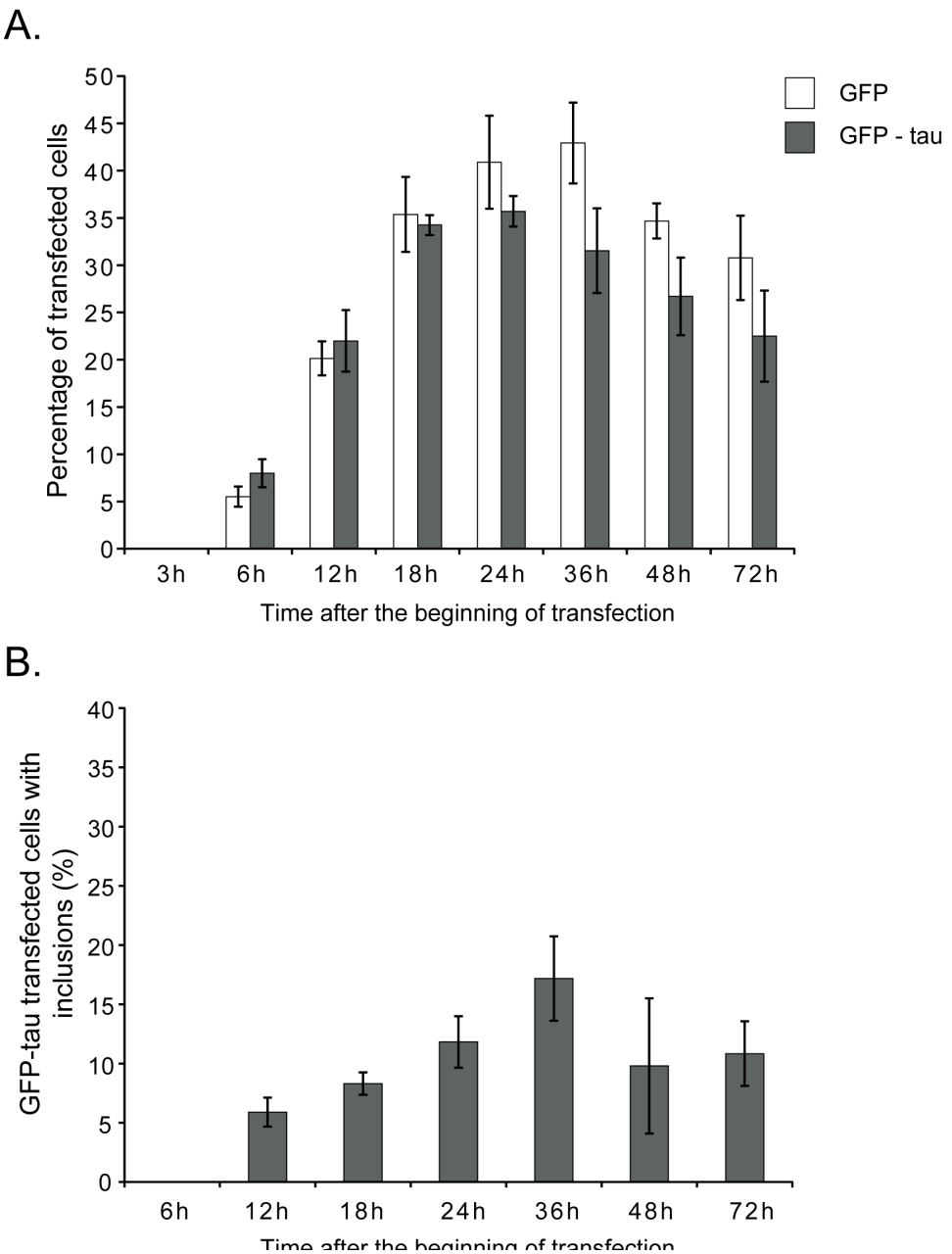

Figure 4.8. *GFP-tau expression and inclusion formation over time*. Cells were transfected with 50 ng of GFP or GFP-tau and 150 ng of HA-GSK3β plasmids. Cells were fixed with 100% methanol for 5 min at -20°C after 3, 6, 12, 18, 24, 36, 48 and 72 h after the beginning of transfection. Subsequently, cells were labelled with the AT8 antibody in conjunction with the AlexaFluor 594 secondary antibody. At least four groups of more than 100 GFP-tau or GFP transfected cells were counted for each condition, using the Nikon Eclipse80i epifluorescent microscope. (**A**) Percentage of GFP and GFP-tau transfected cells over time. (**B**) Percentage of GFP-tau transfected cells with inclusions. Error bars are the SEM.

The percentage of cells expressing GFP or GFP-tau was similar for the first 24 h (40.9±4.9% and 35.7±1.6% respectively, *p-value* > 0.05, using an unpaired Student's *t*-test), but was significantly different 36 h after the beginning of transfection (42.9±4.3% and 31.54±4.5% respectively, *p-value* = 0.01, using an unpaired Student's *t*-test). No inclusions could be detected in GFP transfected cells. The number of cells with GFP-tau inclusions increased over time with inclusions detected in 17.2±3.6% of GFP-tau transfected cells 36 h after transfection (Figure 4.8, B). Taken together, these results showed that a small significant change on the percentage of cells expressing GFP-tau compared to cells expressing GFP occurred with increased inclusion formation. Therefore, all experiments were conducted between 24 h and 36 h after the beginning of transfection.

4.2.7. Expression and localisation of NUB1 in SK-N-SH cells

NUB1 reduces synphilin-1 positive inclusions in an *in vitro* model of Parkinson's disease (Tanji *et al*., 2006). NUB1 also downregulates the expression of NEDD8, a ULM that co-labels NFTs in AD (Mori *et al*., 2005). Therefore, the subcellular distribution of NUB1 in SK-N-SH cells and effect on GFP-tau aggregation were analysed.

In order to examine the expression of NUB1 in SK-N-SH cells, the detection of endogenous NUB1 was compared to that of transiently transfected NUB1 protein fused with the GFP (GFP-NUB1), the Myc (Myc-NUB1) and the HA (HA-NUB1) tags at the N-terminus or with the FLAG tag (NUB1-FLAG) at the C-terminus. Twenty-four hours after transfection, cells were harvested and 10 µg of the total protein fraction was resolved on a 10% polyacrylamide gel. The expression of endogenous NUB1, GFP-NUB1, HA-NUB1, NUB1-FLAG and Myc-NUB1 was analysed by WB, using the anti-NUB1 antibody (Figure 4.9, A) or the tag-specific antibodies respectively (Figure 4.9, B). Endogenous NUB1 could not be detected with the anti-NUB1 antibody, although anti-NUB1 detected the four recombinant NUB1 proteins, GFP-NUB1, HA-NUB1, NUB1-FLAG and Myc-NUB1 as a single band of ~96.6, ~70.5, ~71.6 and ~70.8 kDa respectively.

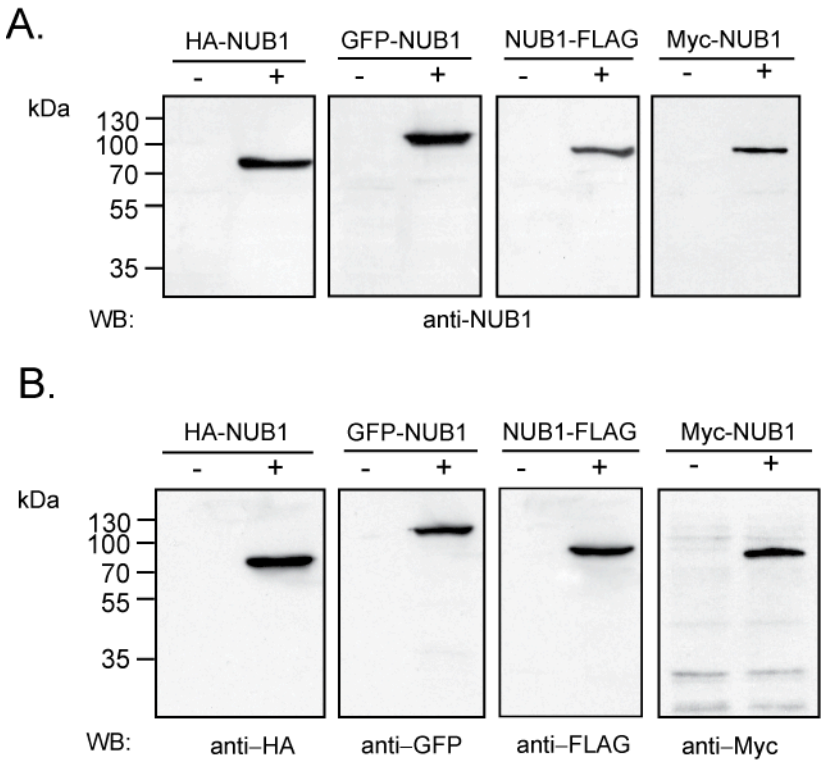

Figure 4.9. *Detection of recombinant NUB1*. SK-N-SH cells were transfected with a control plasmid (-) or with HA-NUB1, GFP-NUB1, NUB1-FLAG or Myc-NUB1 (+). Twenty-four hours after transfection, cells were harvested and 10 µg of proteins were resolved on a polyacrylamide gel (10%). Proteins were detected by WB using the anti-NUB1 antibody (**A**), or the antibody specific to the respective NUB1 tags (**B**).

The NUB1 antibody specifically detects endogenous NUB1 in tissues by immunohistochemistry and different cell lines by WB, and the absence of detection of endogenous NUB1 in SK-N-SH neuroblastoma cells is due to the low levels of NUB1 expressed and detected in this cell line (van der Spuy *et al*., 2003). In Figure 4.9 B, the anti-HA, anti-GFP, anti-FLAG and anti-Myc antibodies specifically detected the recombinant proteins HA-NUB1, GFP-NUB1, NUB1-FLAG and Myc-NUB1 respectively at the correct predicted molecular weights as for the anti-NUB1 antibody.

It has been established in our laboratory that the NUB1 peptide-directed antibody is not suitable for immunocytochemical localisation. Therefore, the localisation of exogenous GFP-NUB1 was analysed in SK-N-SH neuroblastoma cells. Twenty-four hours after transfection, cells were treated with a vehicle (DMSO) or the proteasome inhibitor MG132 (50 μM) for 4 h at 37°C. Subsequently, cells were fixed with 0.3% glutaraldehyde for 10 min at 37°C (Figure 4.10). GFP-NUB1 was predominantly detected in the nucleus, in accordance with its NLS, and its distribution in rat primary cortical neurons (Chapter 3.2.5) and in ocular tissues (van der Spuy *et al*., 2003). The distribution of GFP-NUB1 shifted from nuclear to cytoplasmic after MG132 proteasome inhibition. To quantify this shift, the intensity of fluorescence of GFP-NUB1 in the nucleus versus the cytoplasm was measured in a hundred cells using ImageJ (Figure 4.10, B). Without proteasome inhibition, the nuclear fluorescence of GFP-NUB1 was 73±10% of the total intensity of GFP-NUB1 fluorescence. However, with MG132 treatment, there was a decrease in the nuclear fluorescence intensity (from 73±10% to 52±12.5%) and a concomitant increase in the cytoplasmic fluorescence intensity (from 27±10% to 48±12.5%). Whether this mechanism involves a change in active translocation mechanisms or a relative proteasomal stabilisation of cytoplasmic NUB1 remains unclear.

4.2.8. Myc-NUB1 reduces GFP-tau aggregation

The formation of GFP-tau aggregates in SK-N-SH cells was exacerbated by GSK3β hyperphosphorylation and the inhibition of the proteasome. The effect of NUB1 co-expression on GFP-tau inclusions was subsequently examined in SK-N-SH neuroblastoma cells.

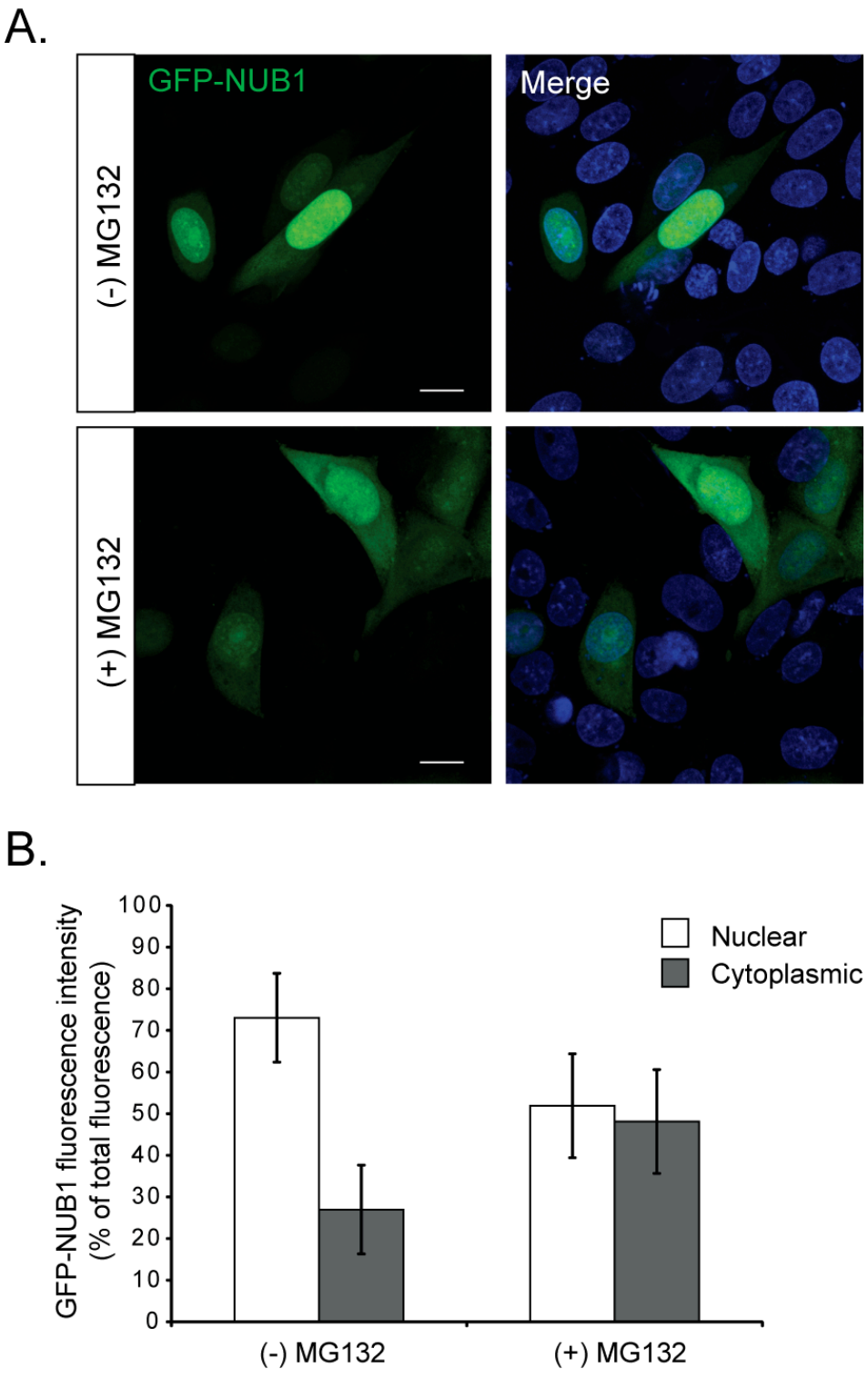

Figure 4.10. *Distribution of GFP-NUB1 in SK-N-SH cells.* Cells were transfected with the GFP-NUB1 plasmid. Twenty-four hours after transfection, cells were treated with a vehicle (DMSO) or with MG132 (50 μM) for 4 h. Subsequently, cells were fixed with 0.3% glutaraldehyde for 10 min at 37°C. (**A**) GFP-NUB1 localisation. Images were acquired with a laser scanning confocal microscope (Zeiss LSM 700). Nuclei were detected using DAPI. Scale bars = 10 μm. (**B**) GFP-NUB1 fluorescence intensity. Fluorescence intensity was measured in 100 cells blind to experimental status using ImageJ.

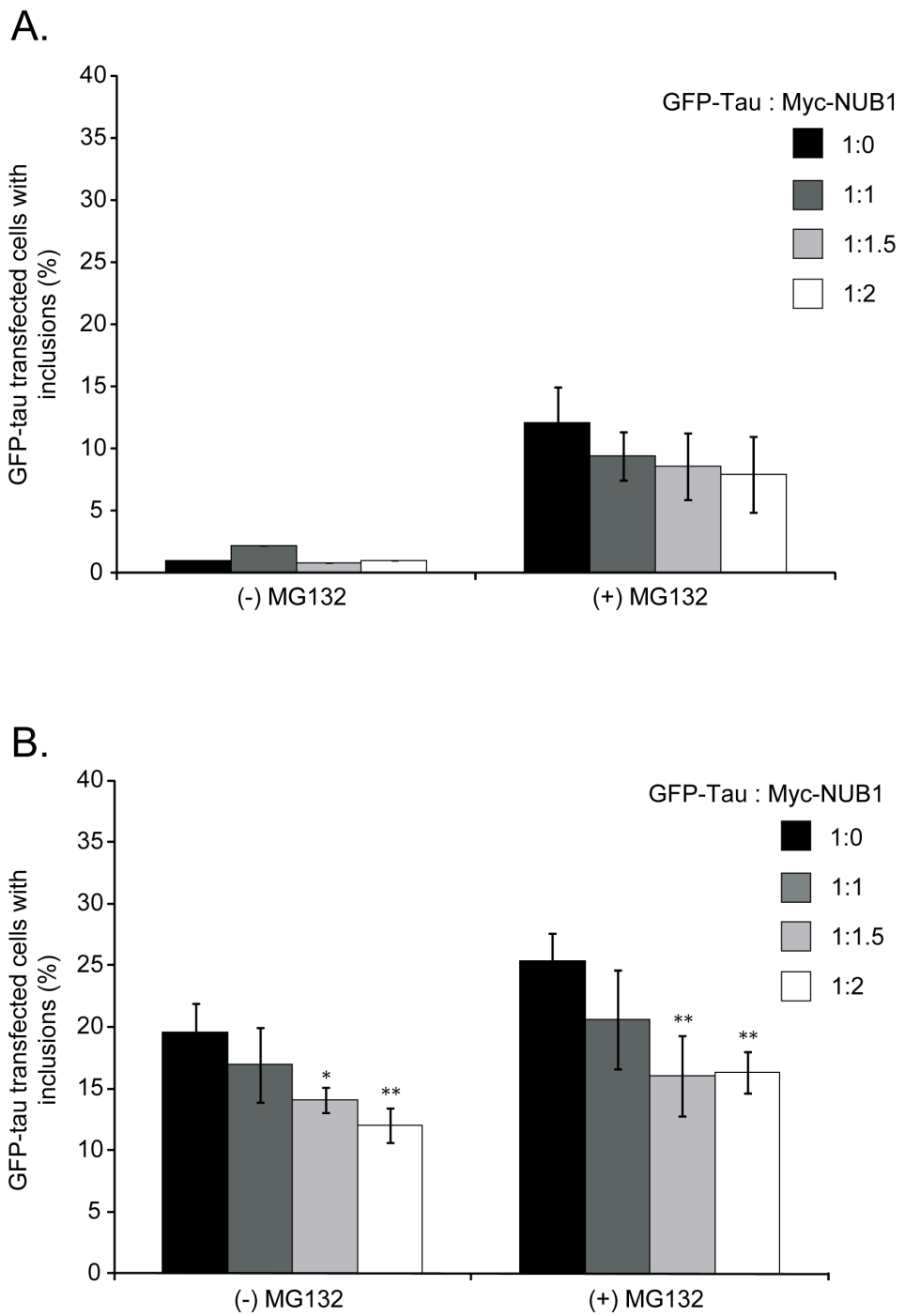

Figure 4.11. *Effect of Myc-NUB1 on tau aggregation.* SK-N-SH cells were transfected with 50 ng of GFP-tau and with 0 ng (1:0), 50 ng (1:1), 75 ng (1:1.5) and 100 ng (1:2) Myc-NUB1 plasmids, in the absence (**A**) or presence (**B**) of 150 ng of HA-GSK3β. Thirty hours after transfection, cells were treated with a vehicle (DMSO) or with MG132 (50 μM) for 4 h. Subsequently, cells were fixed with methanol for 10 min at -20°C, and the number of GFP-transfected cells with inclusions was counted. At least four groups of more than 100 GFP-tau transfected cells were counted for each condition using the Nikon Eclipse80i epifluorescent microscope. Statistical significance compared to the 1:0 for each condition was determined using an unpaired Student's *t*-test. **p-value*<0.05, ***p-value<0.01*. Error bars represent the SEM.

Cells were transfected with 50 ng of GFP-tau alone and with 0 (1:0), 50 (1:1), 75 (1:1.5) or 100 ng (1:2) of Myc-NUB1 (Figure 4.11, A). Thirty hours after transfection, cells were treated with the proteasome inhibitor MG132 (50 μM) or a vehicle (DMSO) for 4 h, and fixed with 100% methanol. At least four groups of 100 cells were counted blind to experimental status for each condition. The percentage of GFP-tau transfected cells did not change significantly, and was ~33.2±1.4%. Without HA-GSK3β co-expression (Figure 4.11, A), few inclusions were detected in GFP-tau transfected cells in the absence of proteasome inhibition. MG132 induced the formation of inclusions, and 12.1±2.8% of GFP-tau transfected cells with inclusions was detected in the absence of NUB1 (GFP-tau:NUB1 = 1:0). Although increasing amounts of Myc-NUB1 reduced the number of cells with inclusions, none of the ratios assessed reached significance.

Cells were transfected with 50 ng of GFP-tau and with 0 (1:0), 50 (1:1), 75 (1:1.5) or 100 ng (1:2) of Myc-NUB1, in the presence of 150 ng of HA-GSK3β (Figure 4.11, B). The percentage of GFP-tau transfected cells did not vary and was 35±2%. In the absence of MG132 and Myc-NUB1, the percentage of GFP-tau transfected cells with inclusions increased to 19.6±2.3%.

In the presence of Myc-NUB1 (50 ng; GFP-tau:NUB1 = 1:1), the percentage of GFP-tau transfected cells remained unchanged but the percentage of GFP-tau transfected cells with inclusions declined to 16.9±3%, although it did not reach significance. The presence of 75 ng (GFP-tau:Myc-NUB1 = 1:1.5) and 100 ng (GFP-tau:Myc-NUB1 = 1:2) of Myc-NUB1 significantly reduced the percentage of GFP-tau transfected cells with inclusions to 14.1±1% (*p-value* = 0.019) and 12±1.4% (*p-value* = 0.008) respectively.

In the presence of MG132 (Figure 4.11, B, right hand side), the percentage of GFP-tau transfected cells with inclusions increased to 25.3±2.2% in the absence of Myc-NUB1. Myc-NUB1 did not alter the percentage of GFP-tau transfected cells, but reduced the percentage of GFP-tau transfected cells with inclusions in a concentration-dependent manner. With a ratio of 1:1.5 and 1:2 between GFP-tau and Myc-NUB1, the percentage of GFP-tau transfected cells

with inclusions was significantly reduced to 16.1±3.2% (*p-value* = 0.003) and 16.3±1.7% (*p-value* = 0.001) respectively.

Taken together, these results showed that the overexpression of Myc-NUB1 reduced the number of GFP-transfected cells with inclusions.

4.2.9. GFP-NUB1 is recruited to DsRed-tau inclusions

Myc-NUB1 reduced the number of GFP-transfected cells with inclusions. The localisation of GFP-NUB1 and DsRed-tau was analysed in SK-N-SH cells (Figure 4.12).

Cells were transfected with GFP-NUB1 and DsRed-tau, and 28 h post-transfection were treated with a vehicle (DMSO) or MG132 (50 μM) for 4 h. Cells were fixed with glutaraldehyde (0.3%, 10 min) and the distribution of GFP-NUB1 and DsRed-tau was examined (Figure 4.12, A). In the presence of DsRed-tau and without proteasome inhibition, GFP-NUB1 localisation was predominantly nuclear (Figure 4.12, A, top row, green) similar to the distribution of GFP-NUB1 on its own (Figure 4.10). However, unlike GFP-NUB1 on its own, in the presence of DsRed-tau GFP-NUB1 appeared to co-label the microtubule-associated DsRed-tau (white arrows). No difference in DsRed-tau distribution could be detected in the presence or absence of GFP-NUB1. MG132 treatment (Figure 4.12, A, bottom row) enhanced the formation of DsRed-tau inclusions (white arrowheads) and induced a shift of GFP-NUB1 distribution from nuclear to cytoplasmic as before (Figure 4.10). GFP-NUB1 co-localised with both DsRed-tau inclusions and microtubule-associated DsRed-tau.

The co-localisation of GFP-NUB1 and DsRed-tau in the microtubule bundles and inclusions was further examined using the JAcOP software to measure the Pearson's and Mander's coefficients (Chapter 2.4.4) (Figure 4.12, B).

The Pearson's coefficient in the microtubule bundles was 0.67±0.18 and 0.60±0.02 in the absence or presence of MG132 respectively (Figure 4.12, B). This data indicated, therefore, that although GFP-NUB1 was localised diffusely throughout the cytoplasm, it co-localised with DsRed-tau in the cytoplasmic microtubule bundles, if only partially.

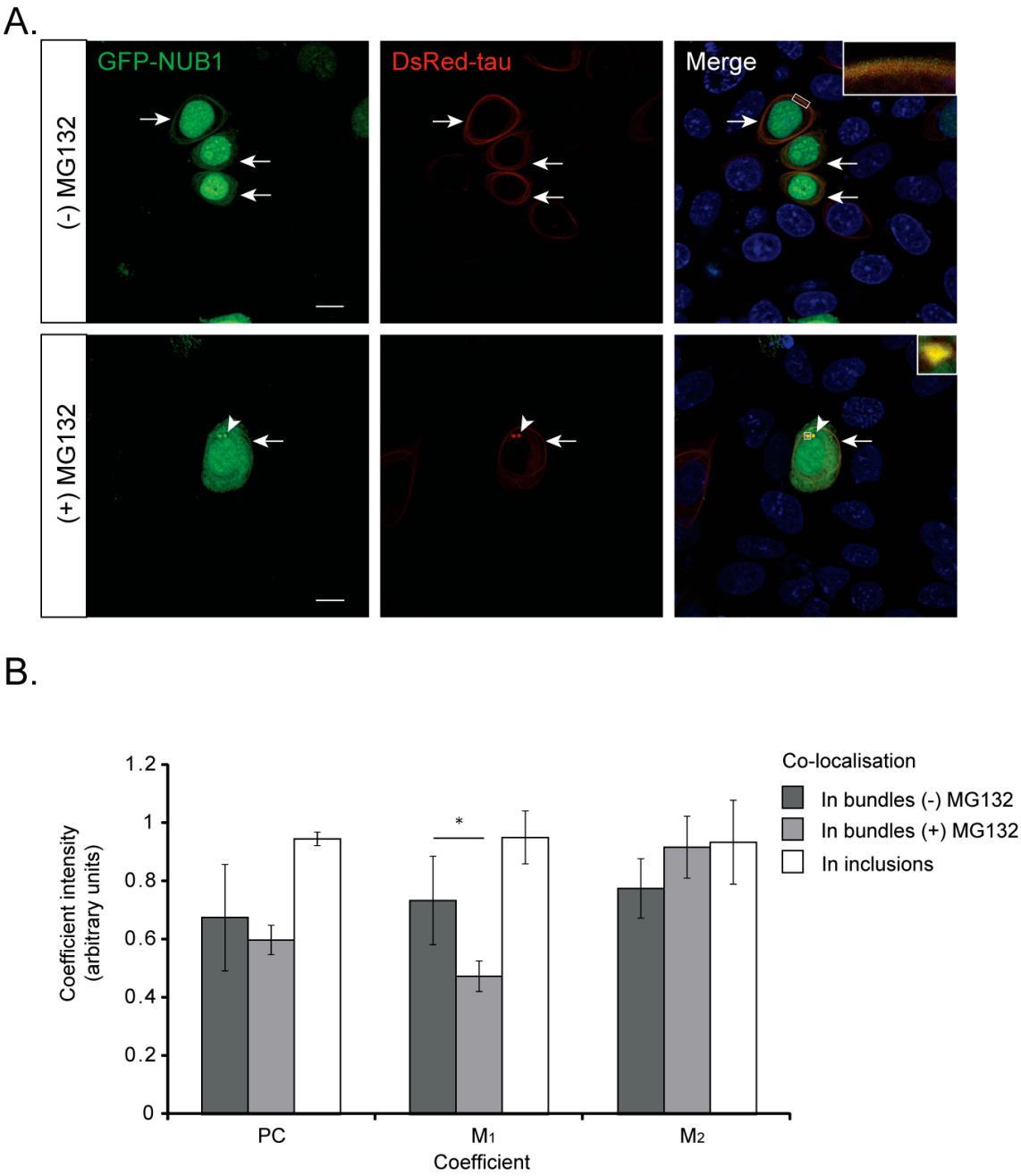

Figure 4.12. *Localisation of GFP-NUB1 and DsRed-tau in SK-N-SH cells*. Cells were transfected with 100 ng of GFP-NUB1 and 50 ng of DsRed-tau plasmids. Twenty-eight hours after transfection, cells were treated with a vehicle (DMSO) or with MG132 (50 μM) for 4 h. Cells were fixed with 0.3% glutaraldehyde for 10 min at 37°C, nuclei (blue) were labeled with DAPI. (**A**) Images were acquired with a laser scanning confocal microscope (Zeiss LSM 700). Microtubule bundles and inclusions are indicated by the white arrows and arrowheads respectively. The magnified images in the top right hand corner are a 10 x magnification of the white rectangle or square. Scale bars = 10 μm. (**B**) The Pearson's (PC) and Mander's (M1 and M2) coefficients were calculated in the microtubule bundles (white rectangle) and in the inclusions (white square) of at least three different cells. M1 = Green over Red, M2 = Red over Green. Statistical significance was determined using an unpaired Student's *t*-test. **p-value* <0.05. Error bars represent the SEM.

The Mander's coefficient measured the contribution of the green channel (GFP-NUB1, M1) and the red channel (DsRed-tau, M2) in the demarcated area of co-localisation over their total respective intensities (Figure 4.12, B). In the absence of MG132, the M1 and M2 coefficient were 0.73±0.15 and 0.77±0.1 respectively in the microtubule bundles, indicating that a large proportion but not all of the GFP-NUB1 and the DsRed-tau overlapped in microtubule bundles. In the presence of MG132, the M1 coefficient in the bundles was significantly lower (0.472±0.09, *p-value* = 0.04), indicating that the GFP-NUB1 was not only located in the bundles, but also in the surroundings. This might reflect the MG132-dependent increased fluorescence intensity of GFP-NUB1 in the cytoplasm and therefore a decrease in the proportion of the green signal coincident with a signal in the red channel over its total intensity in the Mander's calculation.

The M2 coefficient was higher in the microtubule bundles in the presence of MG132 (0.93±0.1) compared to in the absence of MG132 (0.77±0.1), but the difference was not significant. Overall, these data indicate that a portion of the cytoplasmic GFP-NUB1 was co-localised with DsRed-tau in the microtubule bundles.

MG132 induced the formation of DsRed-tau inclusions. Pearson's and Mander's coefficients were used to measure the co-localisation of GFP-NUB1 and DsRed-tau in the inclusions (Figure 4.12, B). Both the PC, M1 and M2 coefficients were very high (0.94±0.05, 0.95±0.05 and 0.91±0.14 respectively), indicating that GFP-NUB1 was recruited to DsRed-tau inclusions.

4.2.10. GFP-NUB1 and HA-GSK3β co-localise

Myc-NUB1 reduced the percentage of GFP-tau inclusions in GFP-tau transfected cells (Chapter 4.2.8) and GFP-NUB1 co-localised with DsRed-tau inclusions in SK-N-SH cells. HA-GSK3β was also recruited to tau aggregates (Chapter 4.2.5), therefore the localisations of NUB1 and GSK3β were examined (Figure 4.13).

SK-N-SH cells were transfected with GFP-NUB1 and HA-GSKβ, and 28 h post-transfection were treated with a vehicle (DMSO) or MG132 (50 μM) for 4 h.

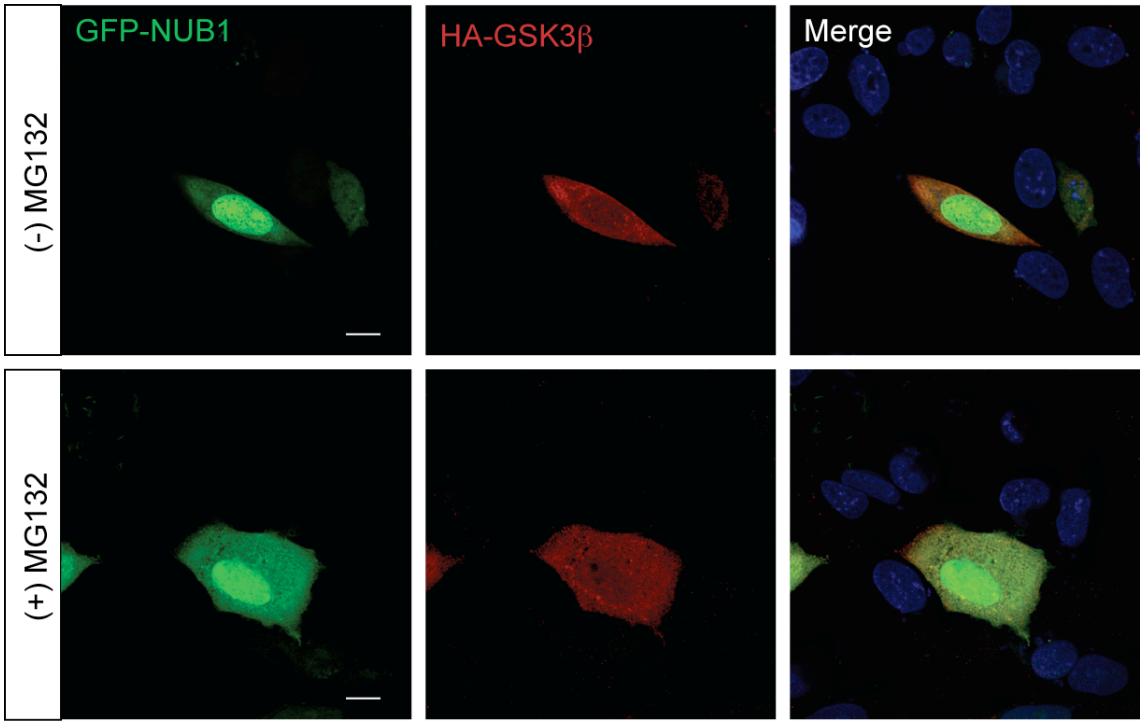

Figure 4.13. *Localisation of GFP-NUB1 and HA-GSK3β*. SK-N-SH cells were transfected with 100 ng of GFP-NUB1 and 150 ng of HA-GSK3β plasmids. Twenty-eight hours after transfection, cells were treated with a vehicle (DMSO) or with MG132 (50 μM) for 4 h. Cells were fixed with 0.3% glutaraldehyde for 10 min at 37°C, nuclei (blue) were detected using DAPI. Subsequently, HA-GSK3β was detected by immunocytochemistry with the anti-HA antibody in conjunction with the secondary antibody AlexaFluor 594. Images were acquired with a laser scanning confocal microscope (Zeiss LSM 700). Scale bars = 10 μm.

Cells were fixed with glutaraldehyde (0.3%, 10 min) and the HA-GSK3β and GFP-NUB1 distribution were examined (Figure 4,13). In the presence of GSK3β and without proteasome inhibition, GFP-NUB1 localisation was predominantly nuclear (Figure 4.13, top row, green) similar to the distribution of GFP-NUB1 on its own (Figure 4.10). Therefore, the subcellular distribution of GFP-NUB1 remained unchanged with HA-GSK3β co-expression. However, HA-GSK3β (Figure 4.13, top row, red) was more readily detected in the nucleus in the presence of GFP-NUB1 compared to when it was expressed on its own (Figure 4.2). With MG132 treatment (Figure 4.13, bottom row), GFP-NUB1 fluorescence intensity was increased in the cytoplasm and co-localised with HA-GSK3β in this cellular locale. In the presence of GFP-NUB1, no change in the HA-GSK3β distribution was detected in the absence and presence of MG132, although it appeared more particulate in the cytoplasm in the presence of MG132 as before (Figure 4.2). Moreover, in the presence of GFP-NUB1, HA-GSK3β appeared to be more nuclear than when it was expressed on its own, irrespective of proteasome inhibition.

These results suggest that the distribution of GFP-NUB1 and HA-GSK3β overlap in SK-N-SH cells.

4.2.11. HA-NUB1 reduces GFP-tau aggregation

In order to investigate the importance of the UBL and UBA domains of NUB1 and its longer splicing isoform NUB1L, the effect of NUB1L, NUB1LΔUBL and NUB1LΔUBA1-3 on tau aggregation was assessed in SK-N-SH cells.

SK-N-SH cells were transfected with NUB1, NUB1L, NUB1LΔUBL or NUB1LΔUBA1-3 fused with the HA tag at the N-terminus (Figure 4.14, A). Twenty-four hours after transfection, 10 µg of total cellular proteins were resolved on a polyacrylamide gel (10%) and proteins were detected by WB using the anti-NUB1 (Figure 4.14, B) or the anti-HA antibody (Figure 4.14, C).

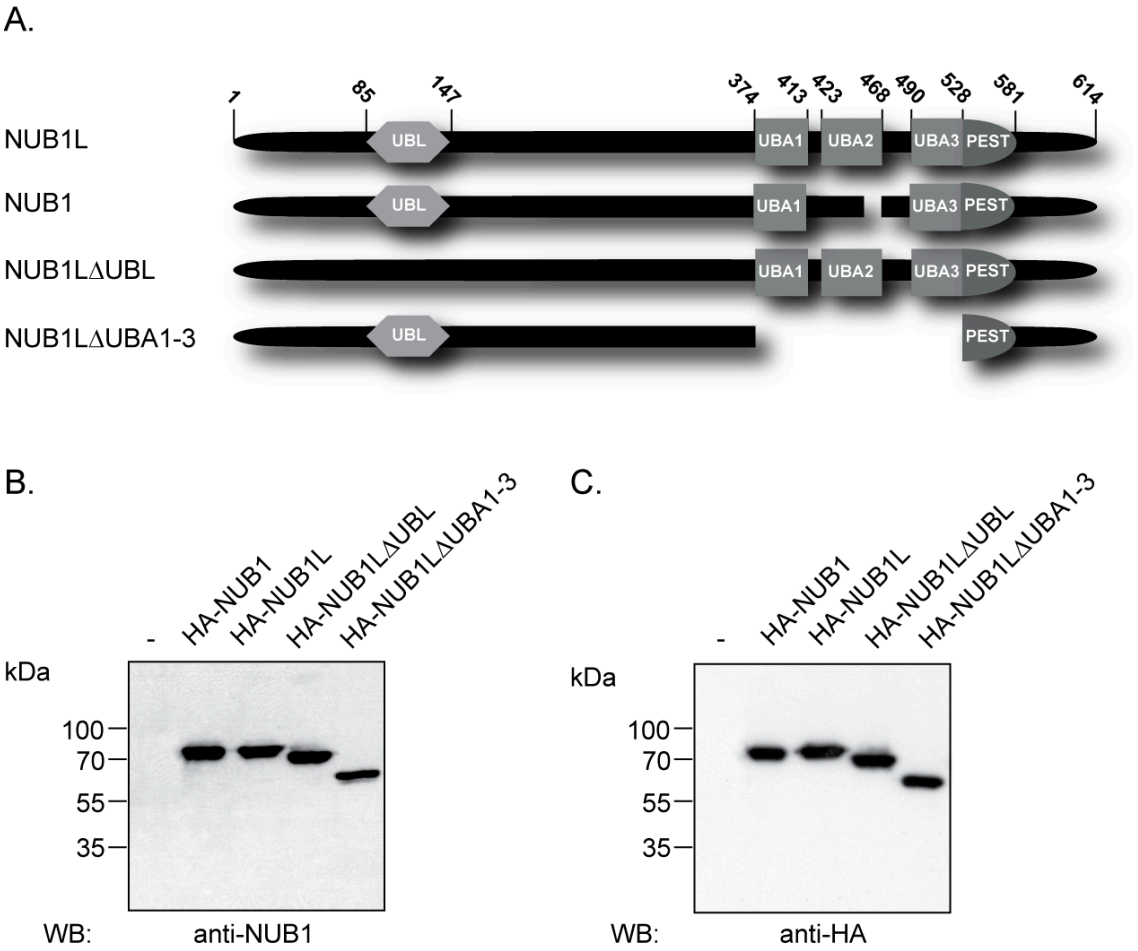

Figure 4.14. *Expression of HA-NUB1, HA-NUB1L and HA-NUB1L mutants in SK-N-SH cells*. (**A**) NUB1, NUB1L and NUB1L mutants. (**B**) and (**C**) Cells were transfected with 100 ng of a control plasmid (-), HA-NUB1, HA-NUB1L, HA-NUB1LΔUBL or HA-NUB1LΔUBA1-3. Twenty-four hours after transfection, cell lysates (10 µg of total cellular protein) were resolved on a polyacrylamide gel (10% acrylamide) and proteins were detected by WB, using the anti-NUB1 (**B**) or anti-HA antibody (**C**).

No endogenous NUB1 was detected in SK-N-SH cells, although anti-NUB1 specifically detected the four recombinant NUB1 proteins, HA-NUB1, HA-NUB1L, HA-NUB1LΔUBL and HA-NUB1LΔUBA1-3 as single bands of ~70.5, ~71.9, ~61.5 and ~54.5 kDa respectively (Figure 4.14, B). The anti-HA, antibody specifically detected HA-NUB1, HA-NUB1L, HA-NUB1LΔUBL and HA-NUB1LΔUBA1-3 at the correct predicted molecular weights as for the anti-NUB1 antibody (Figure 4.14, C).

The effect of HA-NUB1, HA-NUB1L, HA-NUB1LΔUBL and HA-NUB1LΔUBA1-3 on tau aggregation was investigated in SK-N-SH cells (Figure 4.15). Cells were transfected with 50 ng of GFP-tau, 150 ng of HA-GSK3β and with 0, 50, 75 or 100 ng of HA-NUB1 (Figure 4.15, A), HA-NUB1L (Figure 4.15, B), HA-NUB1LΔUBL (Figure 4.15, C) or HA-NUB1LΔUBA1-3 (Figure 4.15, D). Thirty hours after transfection, cells were treated with MG132 (50 μM) or a vehicle (DMSO) for 4 h, and fixed with 100% methanol. The percentage of GFP-tau transfected cells with inclusions was counted blind to experimental status, and HA-NUB1, HA-NUB1L, HA-NUB1LΔUBL and HA-NUB1LΔUBA1-3 were detected by WB using the anti-HA antibody.

In the presence of HA-NUB1, with or without proteasome inhibition, the percentage of GFP-tau transfected cells did not vary significantly and was 35.7±1.4%. The levels of HA-NUB1 increased with the amount of HA-NUB1 transfected and were stabilised in the presence of MG132 (Figure 4.15, A).

In the absence of MG132 and HA-NUB1, the percentage of GFP-tau transfected cells with inclusions was 15.1±1.2%. In the presence of increasing amounts of HA-NUB1, the percentage of GFP-tau transfected cells with inclusions decreased significantly to 10.7±1.2% at a ratio of GFP-tau to HA-NUB1 of 1:2 (*p-value* = 0.008) (Figure 4.15, A). Inhibition of the proteasome increased the percentage of GFP-tau transfected cells with inclusions. In the presence of MG132 the percentage of GFP-tau transfected cells with inclusions increased to 22.4±2% in the absence of HA-NUB1 (Figure 4.15, A). HA-NUB1 did not alter the percentage of GFP-tau transfected cells but reduced the percentage of GFP-tau transfected cells with inclusions in a concentration-dependent manner.

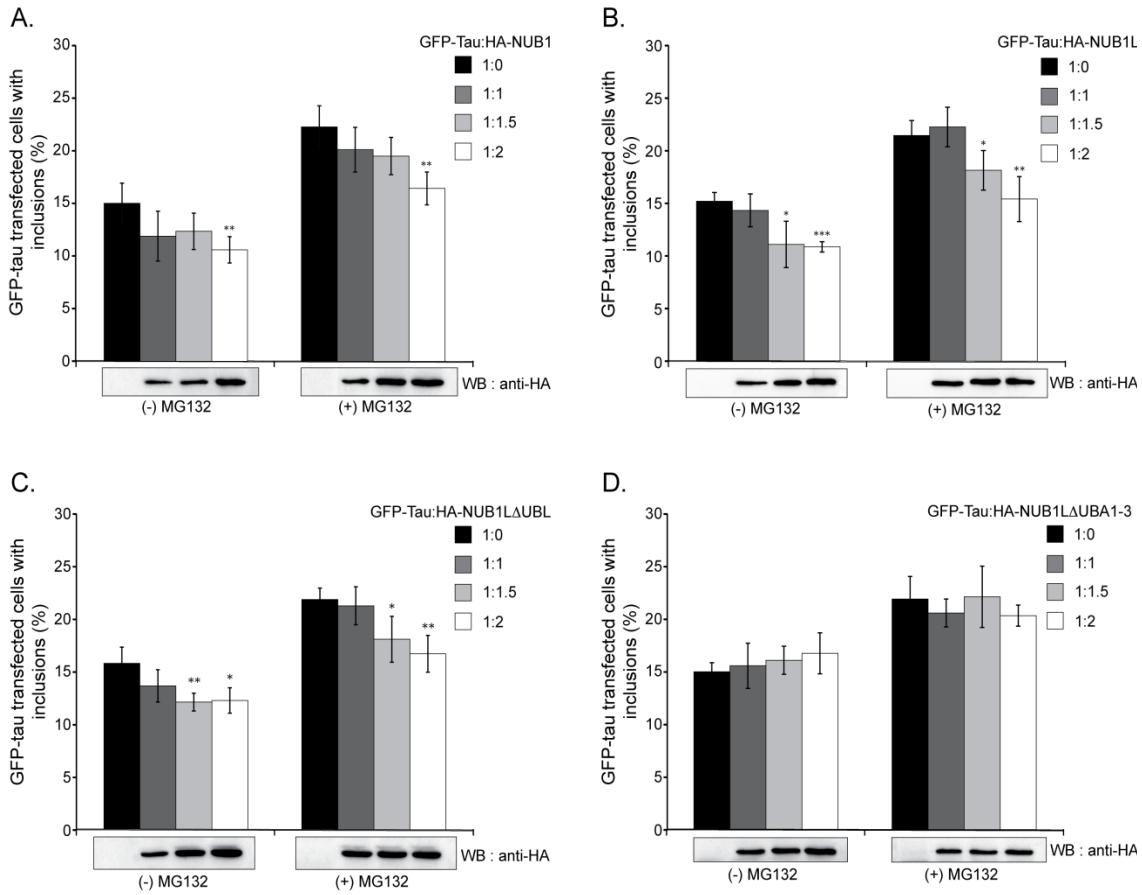

Figure 4.15. *Effect of HA-NUB1, HA-NUB1L and HA-NUB1L mutant on tau aggregation.* SK-N-SH cells were transfected with 50 ng of GFP-tau and 150 ng of HA-GSK3β and with 0 ng (1:0), 50 ng (1:1), 75 ng (1:1.5) and 100 ng (1:2) of HA-NUB1 (**A**), HA-NUB1L (**B**), HA-NUB1LΔUBL (**C**) or HA-NUB1LΔUBA1-3 plasmids (**D**). Thirty hours after transfection, cells were treated with a vehicle (DMSO) or with MG132 (50 μM) for 4 h. Subsequently, cells were fixed with methanol for 10 min at -20°C, and the number of GFP-transfected cells with inclusions was counted blind to experimental status. At least four groups of more than 100 GFP-tau transfected cells were counted for each condition using the Nikon Eclipse80i epifluorescent microscope. Statistical significance was determined using an unpaired Student's *t*-test. **p-value*<0.05, ***p-value<0.01,* ****p-value<0.001.* Error bars represent the SEM. Alternatively, cells were lysed and proteins (10 μg) were resolved on a 10% polyacrylamide gel. Proteins were detected by WB using the anti-HA antibody.

At a ratio of GFP-tau to HA-NUB1 of 1:2, the percentage of GFP-tau transfected cells with inclusions was significantly reduced to 16.5±1.6% (*p-value* = 0.004).

Similar results were obtained with HA-NUB1L (Figure 4.15, B). The percentage of GFP-tau transfected cells did not vary significantly and was 34.8±1.2%. The levels of HA-NUB1L increased with increasing amounts of HA-NUB1L transfected. In the absence of HA-NUB1L and MG132 treatment, the percentage of GFP-tau transfected cells with inclusions was 15.2±0.8%. HA-NUB1L decreased the percentage of GFP-tau transfected cells with inclusions in a concentration-dependent manner. At a ratio of GFP-tau to HA-NUB1L of 1:1.5 and 1:2, the percentage of GFP-tau transfected cells with inclusions significantly declined to 11.1±2.2% (*p-value* = 0.013) and 10.9±0.5% (*p-value* = 0.000) respectively (Figure 4.15, B). With proteasome inhibition, the percentage of GFP-tau transfected cells with inclusions increased to 21.5±1.4% in the absence of HA-NUB1L. A ratio of GFP-tau to HA-NUB1L of 1:1.5 and 1:2 significantly reduced the percentage of GFP-tau transfected cells with inclusions to 18.1±1.9% (*p-value* = 0.03) and 15.4±2.1% (*p-value* = 0.003) respectively.

Following the HA-NUB1L-mediated reduction of GFP-tau aggregation, the effect of HA-NUB1LΔUBL and HA-NUB1LΔUBA1-3 on GFP-tau inclusions was assessed.

The co-expression of HA-NUB1LΔUBL or inhibition of the proteasome did not significantly affect the percentage of GFP-tau transfected cells (35±1.4%). The levels of HA-NUB1LΔUBL increased with the amount of HA-NUB1LΔUBL transfected (Figure 4.15, C). In the absence of MG132, the percentage of GFP-tau transfected cells with inclusions was 15.9±1.5%. In the presence of increasing amounts of HA-NUB1LΔUBL, the percentage of GFP-tau transfected cells with inclusions decreased significantly to 12.2±0.8% (GFP-tau:HA-NUB1LΔUBL = 1:1.15) (*p-value*=0.006) and to 12.4±1.2% (GFP-tau:HA-NUB1LΔUBL = 1:2) (*p-value*=0.011). In the presence of MG132 the percentage of GFP-tau transfected cells with inclusions increased to 22±1% in the absence of HA-NUB1LΔUBL. HA-NUB1LΔUBL did not alter the percentage of GFP-tau transfected cells but reduced the percentage of GFP-tau transfected cells with

inclusions in a concentration-dependent manner. At a ratio of 1:1.5 and 1:2 (GFP-tau:HA-NUB1LΔUBL), the percentage of GFP-tau transfected cells with inclusions was significantly reduced to 18.2±2.1% (*p-value* = 0.021) and 16.8±1.8% (*p-value* = 0.002) respectively.

In comparison to HA-NUB1, HA-NUB1L and HA-NUB1LΔUBL, the HA-NUB1LΔUBA1-3 was unable to reduce the formation of inclusions. The percentage of GFP-tau transfected cells did not vary significantly (35.1±0.9%) in the presence of HA-NUB1LΔUBA1-3. The levels of HA-NUB1LΔUBA1-3 increased with increasing amounts of HA-NUB1L transfected (Figure 4.15, D). In the absence of MG132, the percentage of GFP-tau transfected cells with inclusions was 15.2±0.8%. HA-NUB1LΔUBA1-3 did not decrease the number of GFP-tau transfected cells with inclusions, irrespective of the ratio between GFP-tau and HA-NUB1LΔUBA1-3. The percentage of GFP-tau transfected cells with inclusions was 15.6±2.6, 16.1±1.3 and 16.7±19% at a ratio of 1:1, 1:1.5 and 1:2 (GFP-tau:HA-NUB1LΔUBA1-3) respectively. Proteasome inhibition increased the percentage of GFP-tau transfected cells with inclusions (21.9±2.1%), and HA-NUB1LΔUBA1-3 did not significantly decrease the percentage of cells with inclusions. The percentage of GFP-tau transfected cells with inclusions was 22.1±2.9% (*p-value* = 0.9) and 20.4±1% (*p-value* = 0.23) at a ratio of 1:1.5 and 1:2 (GFP-tau:HA-NUB1LΔUBA1-3) respectively.

In order to compare the effect of HA-NUB1, HA-NUB1L, HA-NUB1LΔUBL and HA-NUB1LΔUBA1-3 on GFP-tau aggregation to the same control, cells were transfected with 150 ng GSK3β, 50 ng GFP-tau and 100 ng HA-NUB1, HA-NUB1L, HA-NUB1LΔUBL or HA-NUB1LΔUBA1-3 (Figure 4.16). The percentage of GFP-tau transfected cells did not vary significantly and was 34.5±1.2%. Without proteasome inhibition, the percentage of GFP-transfected cells with inclusions was 16.1±2.3% (Figure 4.16, control).

This percentage declined significantly to 10.8±1.4% (*p-value* = 0.008), 11.7±1.3% (*p-value* = 0.017) and 11.4±1.4% (*p-value* = 0.013) with HA-NUB1, HA-NUB1L, and HA-NUB1LΔUBL respectively. In the presence of HA-NUB1LΔUBA1-3, the percentage of GFP-tau transfected cells with inclusions (15.6±1.3%) did not decrease significantly compared to the control.

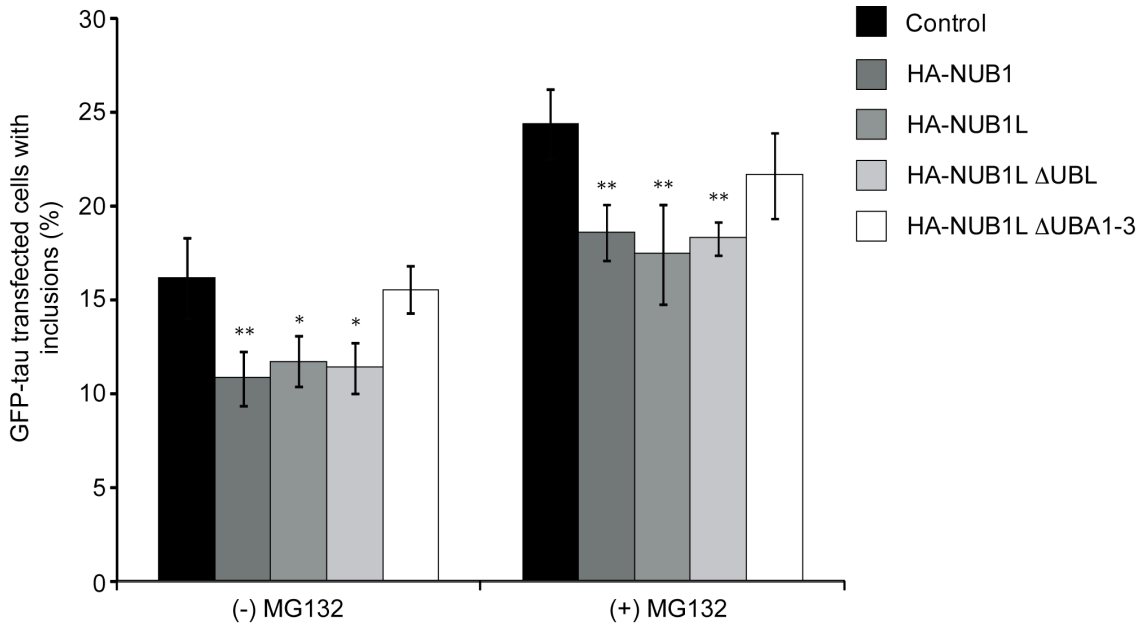

Figure 4.16. *Comparative effect of HA-NUB1, HA-NUB1L and HA-NUBL1 mutants on tau aggregation.* SK-N-SH cells were transfected with 50 ng of GFP-tau and 150 ng of HA-GSK3β (control) and with 100 ng of HA-NUB1, HA-NUB1L, HA-NUB1LΔUBL or HA-NUB1LΔUBA1-3 plasmids. Thirty hours after transfection, cells were treated with a vehicle (DMSO) or with MG132 (50 μM) for 4 h. Subsequently, cells were fixed with methanol for 10 min at -20°C, and the number of GFP-transfected cells with inclusions was counted. At least 4 groups of 100 GFP-tau transfected cells (total, either with or without inclusions) was counted using the Nikon Eclipse80i epifluorescent microscope, and the percentage of GFP-tau transfected cells with inclusions calculated. Statistical significance was determined using an unpaired Student's *t*-test. **p-value*<0.05, ***p-value<0.01.* Error bars represent the SEM.

With proteasome inhibition, the percentage of GFP-transfected cells with inclusions increased to 24.4±1.9% (Figure 4.16, control). This percentage was significantly decreased to 18.7±1.5% (*p-value* = 0.003), 17.5±2.7% (*p-value* = 0.005) and 18.3±0.9% (*p-value* = 0.001) with HA-NUB1, HA-NUB1L, and HA-NUB1LΔUBL. However, HA-NUB1LΔUBA1-3 failed to significantly decrease the percentage of GFP-tau transfected cells with inclusions (21.7±2.3%, *p-value* = 0.11).

Taken together, these results indicate that, irrespective of the tag (Myc or HA), NUB1 was able to reduce tau aggregation in SK-N-SH cells. Moreover, tau inclusions also declined in the presence of NUB1L and NUB1LΔUBL. However, NUB1LΔUBA1-3 failed to decrease tau aggregation.

4.3. Discussion

This chapter focused on the optimisation of tau aggregation in neuroblastoma cells as a model for the aggregation of tau in AD. Therefore, the aggregation of wild type tau without sequence changes upon phosphorylation and consequent release from the microtubules was modelled in cells. Furthermore, the effect of a potential proteasome shuttle, NUB1, on tau aggregation was assessed.

In mammalian cells, the ectopic expression of tau results in the formation of various types of microtubule bundles. The shapes and structures of microtubules differ in accordance with the type and role of the cells (Bruijn *et al*, 2004). In neurons, tau is important for the formation of neuronal processes (Lovestone *et al*., 1996, Lee and Rook, 1992). Endogenous tau as well as overexpressed tau are recruited to the microtubules and influence their stabilisation. In SK-N-SH cells expressing GFP-tau, the microtubules were bundled in rounded circles, similar to what has been observed upon tau overexpression in CHO cells (Bruijn *et al*, 2004). Bundles were not present in the absence of ectopic tau, as SK-N-SH neuroblastoma cells do not express detectable levels of wild type tau. Moreover, these microtubule bundles were co-labelled with GFP-tau, suggesting that GFP-tau influences the microtubule organisation via a direct interaction. It would be interesting to measure what proportion of the GFP-tau population was recruited to the microtubule bundles and inclusions upon phosphorylation and proteasome inhibition. Weissman *et al.* (2009) used photoactivatable GFP-tau to measure the mobility of tau in the neurites of living primary cortical neurons. They demonstrated that experimentally induced inhibition of GSK3β-mediated hyperphosphorylation of tau increased the effective diffusion constant indicating a decreased binding to microtubules. Therefore, we used fluorescence recovery after photobleaching (FRAP) and live imaging to measure the mobility of GFP-tau in microtubule bundles in the presence and absence of HA-GSK3β. A decrease in GFP-tau bound to the microtubules could be observed in the presence of HA-GSK3β as well as an increase in GFP-tau sequestered to inclusions (Appendix C, Supplementary Figure 1). However, these observations did not correlate with

changes in the FRAP measurements, most likely as tau mobility in the bundles in SK-N-SH cells was too rapid to detect measurable differences using this technique. The co-expression of HA-GSK3β induced GFP-tau phosphorylation on AT8 and Ser396. In SK-N-SH cells, about 70±1.5% of GFP-tau transfected cells were AT8 positive. Importantly, no cells that were transfected with GFP-tau alone in the absence of GSK3β exhibited AT8 labelling, whereas a basal level of GFP-tau was phosphorylated on ser396 probably via the endogenous kinases. This was confirmed by WB analysis where detection of the AT8 epitope was only possible in cells co-transfected with both GFP-tau and GSK3β. Several studies have demonstrated that phosphorylated tau has less affinity for the microtubules, and detaches from the protofilaments. It has been described before that GSK3β reduces tau binding with the microtubules in mammalian cells (Lovestone *et al*., 1996). Similarly, in our cell model, the overexpression of GSK3β reduced the recruitment of GFP-tau to the microtubule bundles and resulted in a diffuse distribution of GFP-tau in the cytoplasm, as shown in figure 4.7. Moreover, GFP-tau positive inclusions were not labelled with β-tubulin, suggesting that aggregated tau did not bind the microtubules. Hyperphosphorylation has been shown to be an important step in tau aggregation. It is interesting that wild-type tau itself can form inclusions, if hyperphosphorylated. Indeed, upregulation of tau kinases has been described in AD. In SK-N-SH cells, with GSK3β co-expression, GFP-tau formed inclusions that were detected using the AT8 antibody, which recognises tau phosphorylated on several epitopes found in the NFTs. AT8 labelled GFP-tau inclusions, and sometimes also GFP-tau in microtubule bundles. The increase of GFP-tau phosphorylated on Ser396 might participate in the formation of inclusions, as reported before (Liu *et al*., 2007). However, the S396 antibody labelled some but not all the GFP-tau inclusions, GFP-tau inclusions were mostly small, and restricted to one or two per cell. Interestingly, GFP-tau inclusions were labelled with GSK3β. This was consistent with the fact that NFTs in AD are also GSK3β positive (Duyckaerts *et al*., 2009). Inclusions could be found near the nucleus, therefore suggesting the formation of an aggresome. However, co-labelling with a marker specific for the centrosome (e.g. pericentrin) or aggresomes (e.g. p62) would be necessary to confirm this possibility.

In the absence of proteasome inhibition, the formation of GFP-tau inclusions required the presence of GSK3β. The optimal ratio between GFP-tau and GSK3β was assessed. Surprisingly, the relationship between GFP-tau and GSK3β was far from linear. The same ratio between the two proteins gave different percentages of cells with inclusions. Therefore, inclusion formation was also dependent on the relative amount of GFP-tau and GSK3β. This could be explained by a balance between phosphorylation/dephosphorylation and protein degradation. For example, at low levels of GSK3β expressed relative to GFP-tau, endogenous phosphatases could counteract GSK3β activity. The highest percentage of cells with inclusions was observed with 50 ng of GFP-tau and 150 ng of GSK3β co-transfected, where GFP-tau is most likely not yet deleterious and GSK3β activity can no longer be counter-balanced by endogenous phosphatases. Indeed, these absolute relative amounts of GFP-tau and GSK3β transfected also showed one of the highest percentages of GFP-tau transfected cells that was AT8 positive (77±3%).

An impairment of the UPS has been reported in AD and is thought to participate in Aβ and tau aggregation. More precisely, although the quantity of proteasomes remains similar in demented and non-demented patients, the chymotrypsin-like activity is significantly reduced in AD patients (Cecarini *et al*., 2007). Formation of GFP-tau inclusions in SK-N-SH cells was enhanced by proteasome inhibition. In fact, all proteasome inhibitors were able to induce the formation of GFP-tau inclusions, although at a low level for lactacystin. Lactacystin, MG132 and epoxomicin principally inhibit the chymotrypsin-like activity of the proteasome. The trypsin-like activity is also inhibited by lactacystin and epoxomicin, but to a lesser extent (Lee and Goldberg, 1998; Meng et al., 1999). Lactacystin and epoxomicin are considered more specific inhibitors of the proteasome than MG132. However, MG132 alone was able to maximally induce the aggregation of GFP-tau into inclusions before any cytotoxic effects became evident. The presence of exogenous GSK3β exacerbated the formation of inclusions upon proteasome inhibition.

The formation of inclusions is a dynamic process. This chapter demonstrated that GFP-tau inclusion formation was time-dependent, and that although inclusions could be seen as soon as 12 h after transfection their number was

the greatest 36 h after transfection. This was correlated with the number of GFP-tau positive cells, which increased until 24 h after transfection. The decrease of both GFP-tau inclusions and the number of cells transfected with GFP-tau at 48 h after transfection is most likely related to the fact that the adherent cells begin to die, due to contact inhibition as they reached confluence. Interestingly, cells expressing GFP-tau started to drop off at a similar rate as cells expressing GFP, suggesting that GFP-tau expression and inclusion formation did not appear to be significantly more cytotoxic to the cells than GFP alone. It is thought that the insoluble oligomers rather than the inclusions are not the most toxic species of aggregation-prone proteins. Therefore, GFP-tau toxicity could be balanced by sequestering GFP-tau oligomers/small aggregates into bigger inclusions. Nonetheless, the number of cells expressing GFP-tau and the percentage of GFP-tau expressing cells with inclusions was greatest between 24 h and 36 h after transfection.

Proteasome inhibition together with the co-transfection of both GFP-tau and GSK3β induced the highest percentage of GFP-tau expressing cells with inclusions (~25%). Attempts were made to chemically increase tau phosphorylation by treating cells with okadaic acid (OA) or calyculin A, which inhibit PP2A/B and both PP1 and PP2A respectively. OA had little effect on tau phosphorylation, probably because OA has been shown to increase the levels of the inactive form of GSK3β, phosphorylated on Ser9. On the other hand, calyculin A efficiently increased the phosphorylation of tau on Ser396 and the AT8 epitope, but was highly toxic for the cells, even at a low concentration.

Nevertheless, the co-expression of a wild-type isoform of tau and GSK3β, combined with proteasome inhibition, induced the formation of inclusions that were AT8 positive and validated the use of SK-N-SH neuroblastoma cells as a good model to study tau aggregation.

To assess the effect of NUB1 on tau aggregation, the localisation and expression of NUB1 were first investigated. The expression of endogenous NUB1 in SK-N-SH cells could not be detected. Indeed, the levels of NUB1 protein detected in different cell lines have been shown to be highly variable. The localisation GFP-NUB1 was investigated in SK-N-SH neuroblastoma cells,

and was predominantly nuclear. However, proteasome inhibition induced a shift of GFP-NUB1 from mostly nuclear to nuclear and cytoplasmic. This was also observed when cells were transfected with c-Myc-NUB1 and HA-NUB1 (data not shown). Proteasome inhibition may have resulted in the stabilisation of NUB1 levels. The increased detection of NUB1 in the cytoplasm with proteasome inhibition reflects the fact that NUB1 localisation may be dynamic and that NUB1 is able to translocate from the nucleus to the cytoplasm. However, the underlying mechanisms of this redistribution with proteasome inhibition were not investigated further. Proteins cross the nuclear membrane through the nuclear-pore complex (NPC). Although small molecules less than about 60 kDa can passively translocate through the NPC, protein trafficking generally involves receptor-mediated transport pathways via the karyopherins (importin and exportin). Importins recognise proteins that possess a NLS, and exportins bind the nuclear export sequence (NES) of cargoes. Importins/exportins interact with the NPC and permit the translocation of targeted proteins, with the consumption of GTP. NUB1, with a C-terminal NLS, may be actively transported to the nucleus (Grunwald *et al.*, 2011), since the molecular weight of NUB1, ~61 kDa, is at the limit of the cut-off size for passive transport. Leptomycin B inhibits the signal-mediated (via NES) nuclear export of proteins, and could be used to assess if NUB1 is passively or actively translocated to the cytoplasm (Kudo *et al*., 1998).

Analysis of GFP-NUB1 localisation with DsRed-tau or HA-GSK3β yielded interesting results. Indeed, GFP-NUB1 was recruited to both DsRed-tau labelled microtubule bundles and to DsRed-tau inclusions. Both the Pearson's and Mander's coefficients were high for NUB1 and tau localisation in inclusions, indicating that both proteins were co-localised rather than and merely non-specifically overlapping. Recruitment of NUB1 to tau inclusions suggests that tau may be a target for NUB1, and that the reduction of inclusions occurred as a result of a direct effect of NUB1 on tau. GFP-NUB1 localisation in the microtubule bundles was less obvious. Although GFP-NUB1 remained mostly nuclear, most of the cytoplasmic population of GFP-NUB1 appeared to co-localise with tau in microtubule bundles. With proteasome inhibition, some, but not all, of the cytoplasmic GFP-NUB1 was localised in the bundles.

Interestingly, whereas HA-GSK3β was mostly cytoplasmic when expressed alone or with GFP-tau, GFP-NUB1 co-expression promoted a slightly increased detection of HA-GSK3β in the nucleus. Both proteins overlapped in the cytoplasm and the nucleus. Therefore, NUB1 might influence GSK3β activity in addition to tau.

The ectopic expression of NUB1 reduced the number of GFP-tau transfected cells with inclusions both in the absence and presence of proteasome inhibition. Importantly, the number of cells expressing GFP-tau was unchanged. When the incidence of GFP-tau inclusions was maximally increased by the co-expression of both GFP-tau and GSK3β, NUB1 significantly reduced tau aggregation in a concentration-dependent manner. Interestingly, treatment with MG132 did not abolish the effect of NUB1 on tau aggregation in the presence of GSK3β. This does not exclude a proteasome dependent effect of NUB1, but rather that the affect of NUB1 on GFP-tau was initiated before the treatment with MG132. Indeed, the number of cells with inclusions increased with proteasome inhibition, in the presence or absence of NUB1.

To investigate which NUB1 domains might be important for the NUB1-mediated reduction in tau inclusions, the affect of the longer isoform, NUB1L, and the NUB1L mutants, NUB1LΔUBL and NUB1LΔUBA1-3, on tau aggregation in the presence of GSK3β was assessed. The fact that HA-NUB1 could reduce the number of cells with GFP-tau inclusions in concentration-dependent manner confirmed that the effect of NUB1 was independent of the tag used. NUB1L has been reported to have the same effect on FAT10 and NEDD8 as NUB1, and even to be more efficient. As expected, HA-NUB1L was also able to reduce the number of cells with inclusions in a concentration-dependent manner. So was the mutant lacking the UBL domain, HA-NUB1LΔUBL. These findings suggest that if NUB1 regulation of tau is dependent on its ability to bind the proteasome, it is not via its UBL domain. Indeed, although most of the UBL/UBA proteins interact with the proteasome via their UBL domain, NUB1 has been reported to bind the proteasome via its C-terminus (Tanji *et al.*, 2005). This is controversial, as Schmidtke et al, (2006) showed that NUB1LΔUBL mutant was no longer able to bind the proteasome and accelerate FAT10 degradation. Nonetheless, the UBL domain was not necessary for NUB1 to reduce tau inclusions. On the other

hand, the HA-NUB1LΔUBA1-3 mutant failed to show any effect on tau aggregation. Indeed, no decrease, and even a slight increase of the number of cells with inclusions was seen with increasing amounts of HA-NUB1LΔUBA1-3 expressed. This suggests that the UBA domains of NUB1/NUB1L are necessary for the effect on tau inclusions. Whether the UBA domains are important for binding tau or GSK3β, either directly or following modification with a ULM, or the proteasome remains unclear. For instance, the UBA domains of NUB1L are essential for binding FAT10, but not for accelerating FAT10 degradation. FAT10 itself can bind the proteasome, thus Schmidtke et al., (2006) propose that NUB1L interaction with the proteasome would induce a conformational change of the proteasome and facilitate FAT10 and FAT10ylated protein degradation independently of NUB1L interaction with FAT10 via its UBA domains. It could also simply be a conformational issue, in that the deletion of all the UBA domains might be too disruptive for the protein NUB1/NUB1L to fold correctly, and thus to be active.

Chapter 5
NUB1 interacts with tau and GSK3β

5.1. Introduction

GSK3 is a ubiquitous Ser/Thr kinase highly expressed in the hippocampus and cerebral cortex. Separate genes encode the two isoforms of GSK3, GSK3α and GSK3β, which share an overall 85% homology. The two isoforms, although they are able to target a shared group of substrates, are not redundant. Thus KO of GSK3β in mice embryos is lethal and is not compensated by GSK3α (Hur and Zhou, 2010; Lei *et al*, 2011). Indeed, studies on GSK3β expression levels in human tissue showed that GSK3β is expressed, on average, at higher levels than GSK3α (Lau *et al*., 1999). GSK3 can phosphorylate primed and non-primed residues, although priming enhances GSK3 efficiency. The consensus sequence for GSK3 phosphorylation is Ser/Thr (target residue)-X-X-X-(primed residue) Ser/Thr, where X is any amino acid residue (Jope and Johnson, 2004). GSK3 is thought to be a stable protein with a half-life of 48 h, and to be degraded by the proteasome (Hongisto *et al*, 2008). A recent study has demonstrated that GSK3β is also recruited to multi-vesicular bodies, an upstream event of lysosomal degradation, upon Wnt signalling (Taelman *et al.*, 2010).

Both isoforms of GSK3 have been shown to phosphorylate tau and be overexpressed in AD. Indeed, mice with conditional overexpression of GSK3β showed a reduction of β-catenin levels and an increase of both tau phosphorylation and neuron loss in brains that led to spatial learning deficits (Lucas *et al*., 2001; Avila *et al*., 2010). Although tau is a well-characterised substrate for GSK3β, little is known about their interaction. PS1 has been shown to bind both GSK3β and tau, and might be an intermediate protein in tau phosphorylation (Takashima *et al.*, 1998). Another study has shown that GSK3β is in a complex with tau in microtubules from bovine brains and interacts directly

with tau (Sun *et al*., 2002). Nonetheless, the phosphorylation of tau by GSK3β and its consequences in tau aggregation are well established.

In the previous chapter, we demonstrated that GSK3β overexpression phosphorylated ectopic tau, and participated in tau inclusion formation. Moreover, GSK3β was recruited to tau inclusions. NUB1 co-expression significantly reduced the formation of tau inclusions in SK-N-SH neuroblastoma cells. Furthermore, NUB1L and NUB1LΔUBL but not NUB1LΔUBA1-3 were able to reduce tau inclusions. NUB1 was recruited to both tau inclusions and microtubule bundles, and co-localised with GSK3β in the cytoplasm.

In this chapter, the interactions between and co-localisation of exogenous NUB1, tau and GSK3β were explored. Moreover, the functional impact of their association in SK-N-SH neuroblastoma cells was investigated. The effect of NUB1, NUB1L and the NUB1L mutants on the levels of total and phosphorylated tau was quantitated, and their role in the turnover of GSK3β investigated.

5.2. Results

5.2.1. GFP-tau and HA-GSK3β are in a binary complex

GSK3β induces tau phosphorylation *in vivo* and *in vitro* (Johnson and Stoothoff, 2004), and was recruited to GFP-tau aggregates in SK-N-SH neuroblastoma cells (Figure 4.7). Therefore, co-immunoprecipitation experiments of HA-GSK3β and GFP-tau were performed to analyse their interaction in SK-N-SH cells (Figure 5.1).

Cells were transiently transfected with either HA-GSK3β or GFP-tau alone, or with both proteins and treated with MG132 (50 μM) 28 h post-transfection. Cells were lysed and proteins were immunoprecipitated with the anti-tau (Figure 5.1, A) or anti-HA antibody (Figure 5.1, B) with magnetic beads (Chapter 2.5.6). Cell lysates were resolved on a polyacrylamide gel (10%) and proteins were detected by WB using the anti-tau or anti-HA antibody. Both HA-GSK3β and GFP-tau were detected in the input fraction. The anti-tau antibody successfully immunoprecipitated GFP-tau, and 2.8% of the total levels of HA-GSK3β were specifically co-immunoprecipitated (Figure 5.1, A) only when GFP-tau was also present. Moreover, neither GFP-tau nor GSK3β were immunoprecipitated with a non-specific antibody (IgG) or with the beads only (BO). Reciprocally, HA-GSK3β was immunoprecipitated and GFP-tau co-immunoprecipitated (0.6% of the total levels) with the HA antibody (Figure 5.1, B). Less than 0.1% of total GFP-tau levels was non-specifcally immunoprecipitated with the HA antibody in the absence of HA-GSK3β, and with a non-specific antibody (IgG).

These results confirmed that GFP-tau and HA-GSK3β interact reciprocally in a binary complex .

5.2.2. NUB1-FLAG and GFP-tau are in a binary complex

NUB1 was recruited to tau on microtubules and to aggregated tau in inclusions (Figure 4.12). Moreover, NUB1 reduced the formation of tau inclusions in SK-N-SH cells (Figures 4.11 and 4.15). Therefore, the co-immunoprecipitation of GFP-tau and NUB1-FLAG was performed in SK-N-SH cells to investigate their interaction.

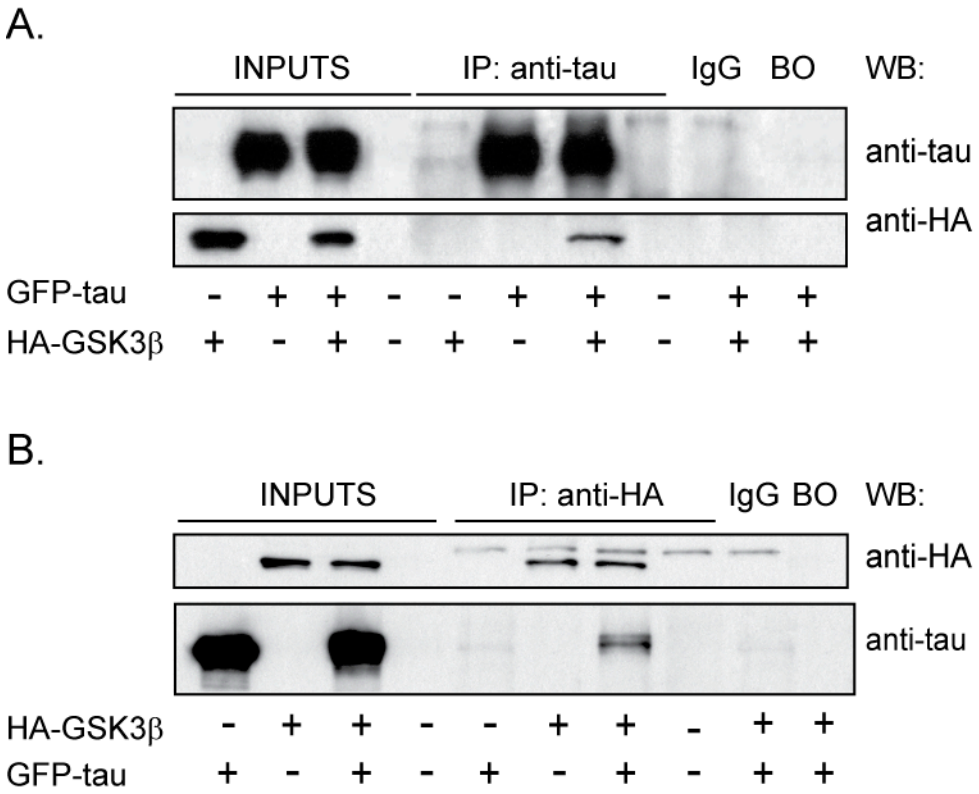

Figure 5.1. *Immunoprecipitation of GFP-tau and HA-GSK3β*. Cells were transfected with GFP-tau, HA-GSK3β or both plasmids, and 28 h post-transfection were treated with MG132 (50 μM) for 4h. Cells were lysed with RIPA buffer, and lysates were incubated with magnetic beads in the absence (BO, beads only) or presence of the anti-tau (1:1000, **A**), anti-HA (1:500, **B**), or a non-specific (IgG) antibody overnight at 4°C. Five μl (INPUTS) or 10 μl (IP) of samples were resolved on a polyacrylamide gel (10%) and proteins were detected using the anti-tau or anti-HA antibody.

Myc-NUB1 was non-specifically immunoprecipitated by the anti-tau antibody in the absence of GFP-tau (data not shown). Moreover, the anti-Myc antibody immunoprecipitated only a low level of Myc-NUB1 (1.3% of the total levels) and the specific co-immunoprecipitation of GFP-tau was consequently not detected (data not shown).

Therefore, as the anti-Myc antibody was not suitable for immunoprecipitation experiments, the interaction of GFP-tau and NUB1-FLAG was investigated in SK-N-SH cells. Cells were transiently transfected with GFP-tau and NUB1-FLAG and 28 h post-transfection were treated with MG132 (50 μM) for 4 h.

Cells were lysed and proteins were immunoprecipitated with the anti-tau (Figure 5.2, A) or anti-FLAG (Figure 5.2, B) antibody with magnetic beads (Chapter 2.5.6). Both GFP-tau and NUB1-FLAG were detected in the input fraction. The anti-tau antibody immunoprecipitated GFP-tau, and specifically co-immunoprecipitated NUB1-FLAG (Figure 5.2, A) in the presence of GFP-tau, with 0.44% of total NUB1-FLAG levels pulled-down. Moreover, neither GFP-tau nor NUB1-FLAG were immunoprecipitated with a non-specific antibody (IgG) or with the beads only (BO). Reciprocally, NUB1-FLAG was immunoprecipitated and 1.4% of the total GFP-tau levels was co-immunoprecipitated with the anti-FLAG antibody (Figure 5.2, B). However, a small percentage (0.25% of input) of GFP-tau was non-specifically immunoprecipitated with the FLAG antibody and with a non-specific antibody (IgG) in the absence of NUB1-FLAG.

These results therefore revealed that NUB1-FLAG and GFP-tau interact reciprocally in a binary complex .

5.2.3. NUB1-FLAG and HA-GSK3β are in a binary complex

HA-GSK3β and GFP-NUB1 co-localise in SK-N-SH cells (Figure 4.13), and both are recruited to GFP-tau inclusions (Figure 4.7 and 4.12), therefore the interaction between NUB1-FLAG and HA-GSK3β was asessed by co-immunoprecipitation in SK-N-SH cells (Figure 5.3).

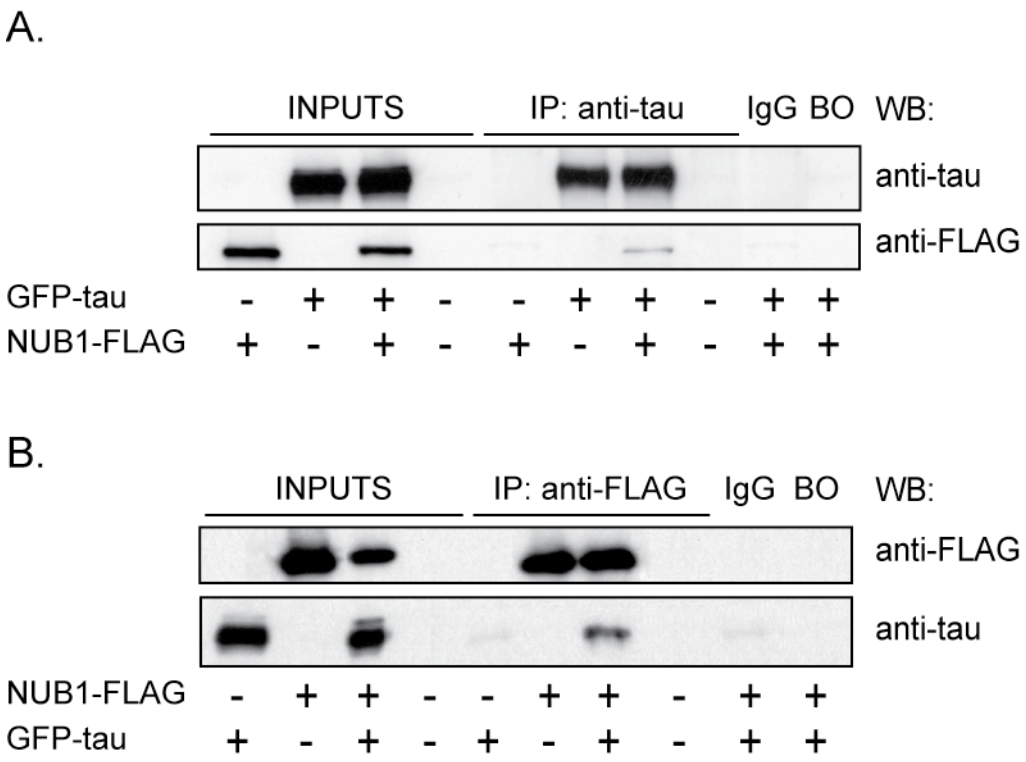

Figure 5.2. *Immunoprecipitation of GFP-tau and NUB1-FLAG*. Cells were transfected with GFP-tau, NUB1-FLAG or both plasmids, and 28 h post-transfection were treated with MG132 (50 μM) for 4 h. Cell were lysed with RIPA buffer, and lysates were incubated with magnetic beads in the absence (BO, beads only) or presence of the anti-tau (1:1000, **A**), anti-FLAG (1:500, **B**), or a non-specific (IgG) antibody overnight at 4°C. Five μl (INPUTS) or 10 μl (IP) of samples were resolved on a polyacrylamide gel (10%) and proteins were detected using the anti-tau or anti-FLAG antibody.

Cells were transiently transfected with HA-GSK3β and NUB1-FLAG and 28 h post-transfection were treated with MG132 (50 μM) for 4 h. Cells were lysed and proteins were immunoprecipitated with the anti-GSK3β (Figure 5.3, A) or anti-FLAG antibody (Figure 5.3, B) with magnetic beads (Chapter 2.5.6). Cell lysates were resolved on a polyacrylamide gel (10%) and proteins were detected using the anti-FLAG or the anti-HA antibody. Both HA-GSK3β and NUB1-FLAG were detected in the input fraction. The anti-GSK3β antibody immunoprecipitated HA-GSK3β, and specifically co-immunoprecipitated NUB1-FLAG (Figure 5.3, A) only in the presence of HA-GSK3β (0.44% of the total levels). Moreover, neither HA-GSK3β nor NUB1-FLAG were immunoprecipitated with a non-specific antibody (IgG) or with the beads only (BO). Reciprocally, NUB1-FLAG was immunoprecipitated and 7.4% of the total HA-GSK3β levels were specifically co-immunoprecipitated with the anti-FLAG antibody (Figure 5.4, B). No HA-GSK3β was non-specifcally co-immunoprecipitated with the anti-FLAG antibody in the absence of NUB1-FLAG, or with a non-specific antibody (IgG).

In conclusion, HA-GSK3β and NUB1-FLAG interact reciprocally in a binary complex.

5.2.4. Tau, GSK3β and NUB1 are in a ternary complex

Myc-NUB1 and HA-NUB1 reduced the percentage of GFP-tau inclusions in GFP-tau transfected cells (Figure 4.11 and Figure 4.15 respectively) and co-localised with DsRed-tau inclusions in SK-N-SH cells (Figure 4.12). HA-GSK3β was also recruited to GFP-tau aggregates (Figure 4.7). GFP-tau, NUB1-FLAG and HA-GSK3β were able to immunoprecipitate one another in binary complexes in a reciprocal manner. Therefore, the formation of a ternary complex between GFP-tau, HA-GSK3β and NUB1-FLAG was explored in SK-N-SH cells.

Cells were transfected with GFP-tau, HA-GSK3β or NUB1-FLAG alone, with the binary combinations of the three proteins, or with all three proteins together. Twenty-eight hours post-transfection, cells were treated with MG132 (50 μM) for 4 h.

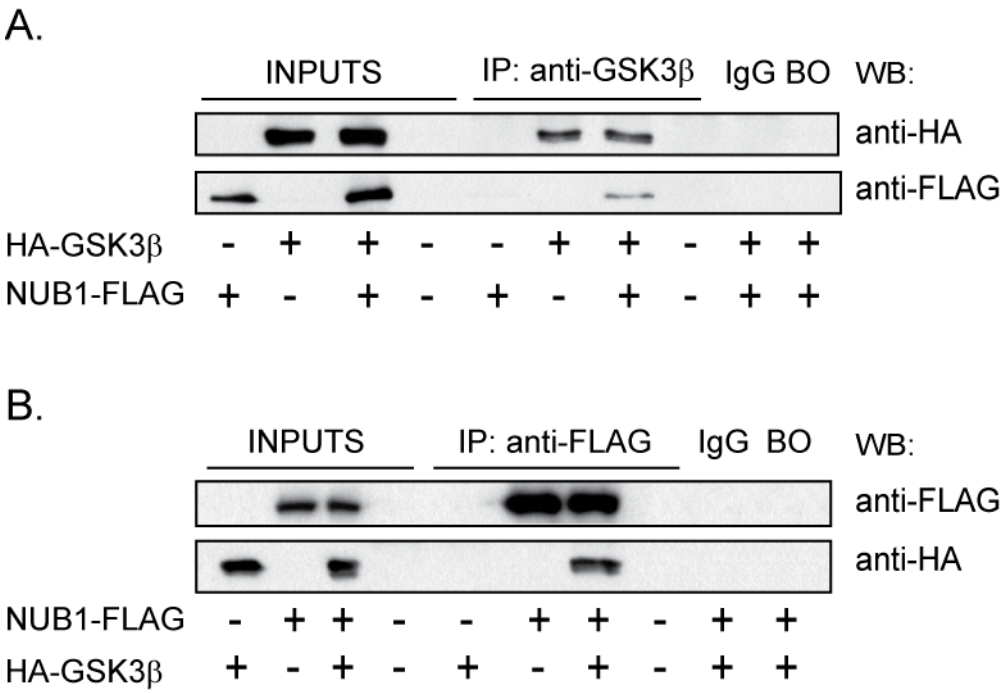

Figure 5.3. *Immunoprecipitation of NUB1-FLAG and HA-GSK3β*. Cells were transfected with NUB1-FLAG, HA-GSK3β or both plasmids, and 28h post-transfection were treated with MG132 (50 μM) for 4h. Cell were lysed with RIPA buffer, and lysates were incubated with magnetic beads in the absence (BO, beads only) or presence of the anti-GSK3β (1:100, **A**), anti-FLAG (1:500, **B**), or a non-specific (IgG) antibody overnight at 4°C. 5 μl (INPUTS) or 10 μl (IP) of samples were resolved on a polyacrylamide gel (10%) and proteins were detected using the anti-HA or anti-FLAG antibody.

Cells were lysed and proteins were immunoprecipitated with the anti-tau (Figure 5.4, A) or anti-FLAG antibody (Figure 5.4, B) with magnetic beads (Chapter 2.5.6).

Cell lysates were resolved on a polyacrylamide gel (10%) and proteins were detected using the anti-tau, anti-pS396, anti-FLAG or the anti-HA antibody. The three proteins, HA-GSK3β, NUB1-FLAG and GFP-tau could be detected in the input fractions (Figure 5.4, A and B, INPUTS). In the presence of HA-GSK3β, there was a small increase in the molecular weight of tau detected with anti-tau and anti-pS396, and increased levels of pS396-tau detected with anti-pS396, indicative of GSK3β-mediated phosphorylation of tau on serine 396. The anti-tau antibody immunoprecipitated GFP-tau, and specifically co-immunoprecipitated NUB1-FLAG and HA-GSK3β (Figure 5.4, A). NUB1-FLAG and HA-GSK3β were not co-immunoprecipitated in the absence of GFP-tau or with non-specific IgG, nor were they pulled down non-specifically by the beads only. When all three proteins were co-expressed in SK-N-SH cells (Figure 5.4, A, last lane), less HA-GSK3β (0.6% instead of 1.3% for the binary GFP-tau/HA-GSK3β co-IP) was co-immunoprecipitated with GFP-tau. The proportion of GFP-tau phosphorylated on Ser396 pulled down with the anti-tau antibody was similar when GFP-tau was co-transfected with NUB1-FLAG and HA-GSK3β or with HA-GSK3β alone.

The anti-FLAG antibody immunoprecipitated NUB1-FLAG and specifically co-immunoprecipitated GFP-tau and HA-GSK3β (Figure 5.4, B). GFP-tau and HA-GSK3β were co-immunoprecipitated specifically in the absence of NUB1-FLAG. In the presence of HA-GSK3β, the levels of pS396-tau were increased and both total tau and pS396-tau were shifted to a higher molecular weight, indicating the HA-GSK3β phosphorylation of GFP-tau. The NUB1-FLAG co-immunoprecipitated pS396-tau only when HA-GSK3β was present. When all three proteins were co-expressed, the proportion of HA-GSK3β and GFP-tau co-immunoprecipitated by the anti-FLAG antibody was reduced (0.6% instead of 11.2%, and 0.1% instead of 0.4% for HA-GSK3β and GFP-tau respectively). GFP-tau co-immunoprecipitated with NUB1-FLAG was also decreased when

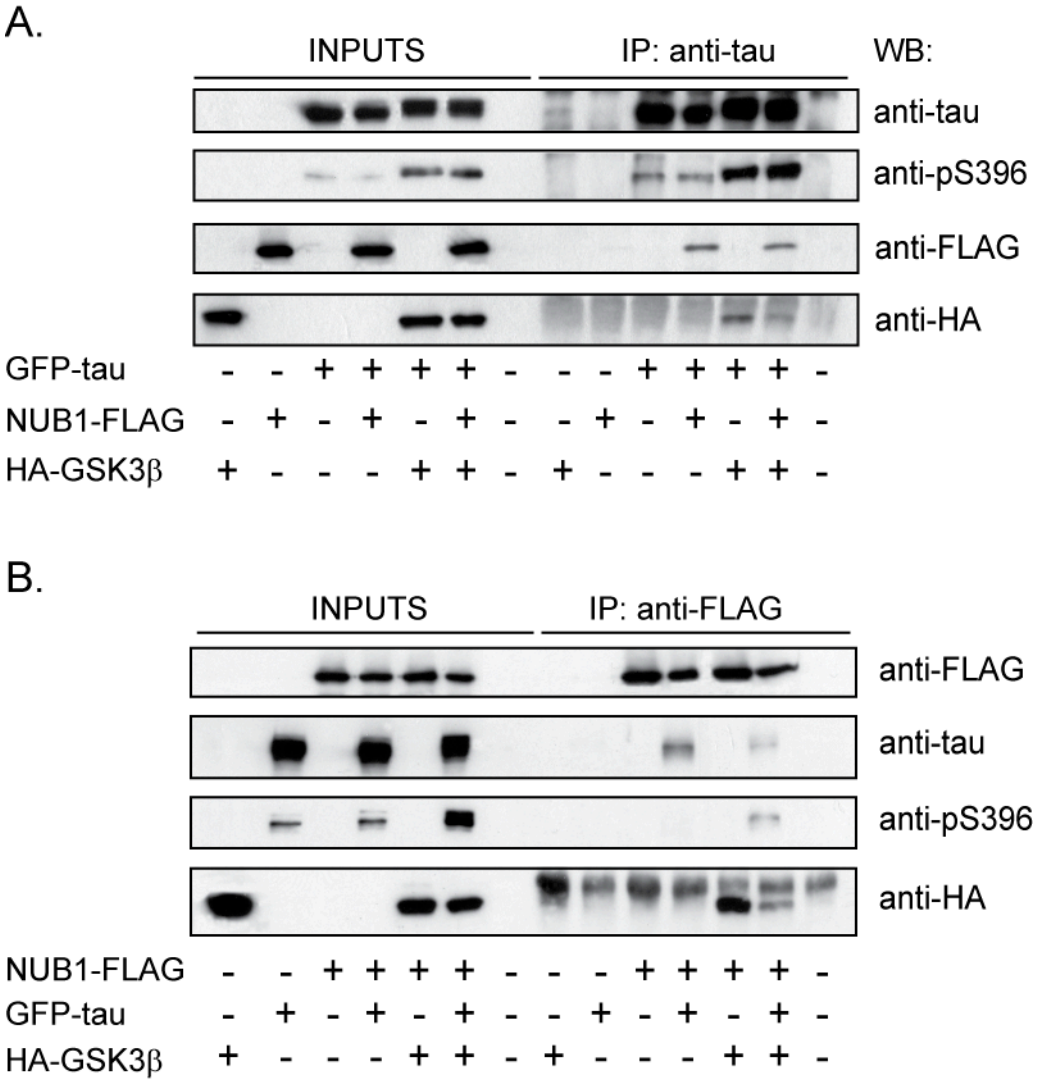

Figure 5.4. *Immunoprecipitation of GFP-tau, NUB1-FLAG and HA-GSK3β*. Cells were transfected with 50 ng of GFP-tau, 150 ng of GSK3β, or 100 ng of NUB1-FLAG plasmid alone, a combination of two plasmids or all three plasmids together. Twenty-eight hours post-transfection cells were treated with MG132 (50 μM) for 4 h. Cells were lysed with RIPA buffer, and lysates were incubated with magnetic beads in the presence of the anti-tau (1:1000, **A**) or anti-FLAG (1:500, **B**) antibody overnight at 4°C. Five μl (INPUTS) or 10 μl (IP) of samples were resolved on a polyacrylamide gel (10%) and proteins were detected using the anti-tau, anti-pS396, anti-HA or anti-FLAG antibody.

the all three proteins were co-expressed in cells, whereas the NUB1-FLAG immunoprecipitated remained unchanged.

GFP-tau and HA-GSK3β, GFP-tau and NUB1-FLAG, and HA-GSK3β and NUB1-FLAG interacted specifically and reciprocally with one another. Moreover, GFP-tau, HA-GSK3β and NUB1-FLAG associated with one another in a ternary complex, and GFP-tau was phosphorylated by HA-GSK3β when all three proteins were co-expressed in SK-N-SH cells. However, NUB1-FLAG reduced the co-immunoprecipitation of HA-GSK3β with GFP-tau, and the co-immunoprecipitation of both HA-GSK3β and GFP-tau with NUB1-FLAG in the ternary complex. Therefore, the three proteins may compete for an overlapping binding site on NUB1 within this complex. Furthermore, GFP-NUB1 was recruited to DsRed-tau microtubule bundles and inclusions, and co-localised with HA-GSK3β in the cytoplasm. Similarly, HA-GSK3β labelled GFP-tau inclusions. Thus, the localisation of each protein when the three are co-expressed in SK-N-SH was investigated.

Cells were transfected with GFP-NUB1, DsRed-tau, and HA-GSK3β, and 28 h post-transfection were treated with MG132 (50 μM) for 4 h. Cells were fixed with glutaraldehyde (0.3%, 10 min) and the distribution of GFP-NUB1, DsRed-tau and HA-GSK3β was examined (Figure 5.5).

GFP-NUB1 localisation (Figure 5.5, green), was predominantly nuclear but was also stabilised in the cytoplasm with proteasome inhibition, as noted before (Figure 4.10). GFP-NUB1 co-labelled the microtubule-associated DsRed-tau in the bundles and in the rest of the microtubule network, and the DsRed-tau in the inclusions (white arrows and arrowheads respectively). On the other hand, HA-GSK3β localisation (Figure 5.5, blue) was both cytoplasmic and nuclear, similar to its localisation in the presence of GFP-NUB1 alone as described previously (Figure 4.13). HA-GSK3β was detected in some of the DsRed-tau bundles, yet was excluded from the inclusions.This is contrary to what was described in chapter 4.2.5., where it was shown that in the absence of NUB1, GSK3β was recruited to the GFP-tau inclusions.

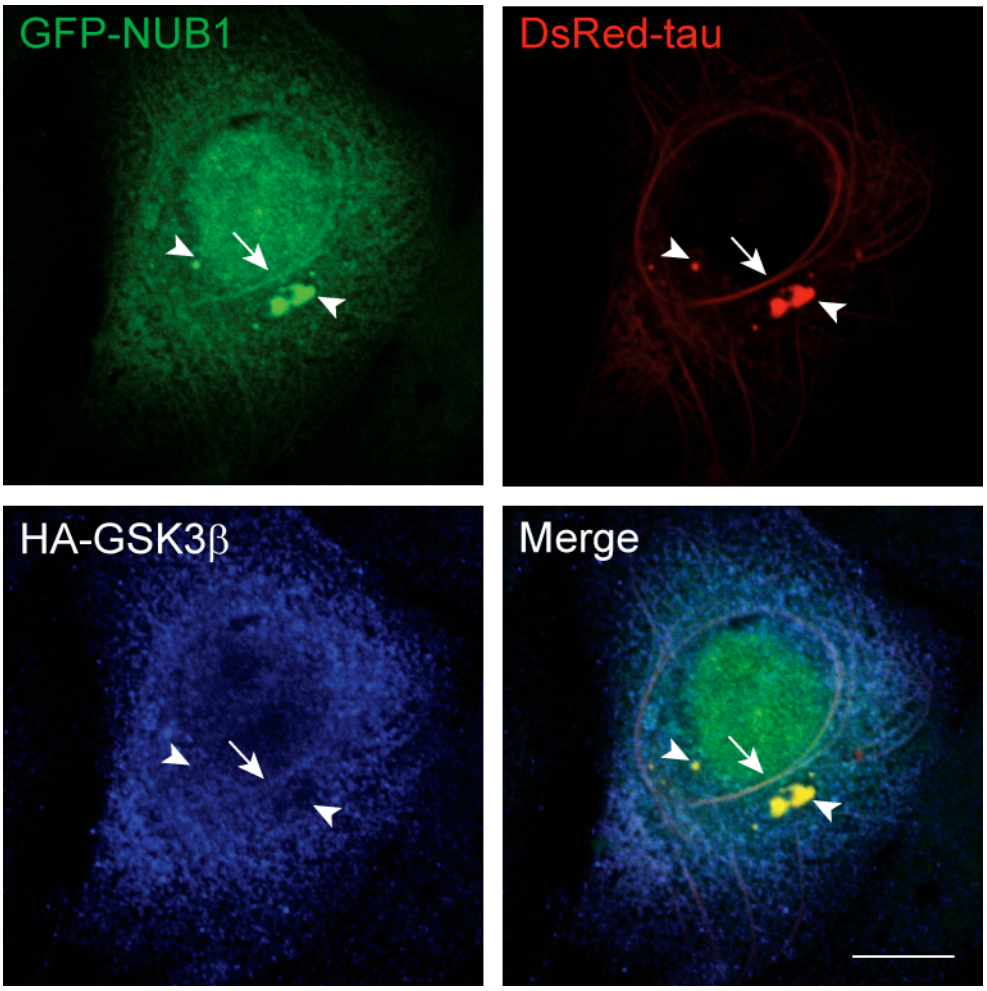

Figure 5.5. *Localisation of GFP-NUB1, DsRed-tau and HA-GSK3β in SK-N-SH cells*. Cells were transfected with 100 ng of GFP-NUB1, 50 ng of DsRed-tau and 150 ng of HA-GSK3β plasmids. Twenty-eight hours after transfection, cells were treated with MG132 (50 μM) for 4 h. Cells were fixed with 0.3% glutaraldehyde for 10 min at 37°C. Images were acquired with a laser scanning confocal microscope (Zeiss LSM 700). Microtubule bundles and inclusions are indicated by the white arrows and arrowheads respectively. Scale bars = 10 μm.

No difference in DsRed-tau distribution could be detected in the presence of both GFP-NUB1 and HA-GSK3β compared to tau localisation with either HA-GSK3β (Figure 4.7) or with GFP-NUB1 (Figure 4.12) alone.

In conclusion, when any binary combination of tau, NUB1 and GSK3β were co-expressed in SK-N-SH cells, the proteins specifically interacted with one another and were co-localised. However, when the three proteins were expressed together in cells, the interactions between them appeared to be reduced.

In fact, analysis of the localisation of the three proteins showed that GSK3β was no longer recruited to the tau inclusions in the presence of NUB1, whereas NUB1 and tau co-localised in both the microtubule bundles and inclusions. Therefore, NUB1 both reduced the interaction of tau and GSK3β and prevented the recruitment of GSK3β to tau inclusions.

5.2.5. The effect of HA-NUB1 on GFP-tau levels

Myc-NUB1, HA-NUB1, HA-NUB1L and HA-NUB1LΔUBL reduced the number of GFP-tau transfected cells with inclusions, while the mutant HA-NUB1LΔUBA1-3 did not have a significant effect on GFP-tau inclusions (Figure 4.15). Moreover, NUB1-FLAG interacted with both GFP-tau and HA-GSK3β (Figure 5.2 and 5.3 respectively) and reduced the association of HA-GSK3β with GFP-tau in the ternary complex (Figure 5.4). Therefore, the NUB1-mediated reduction of HA-GSK3β interaction with GFP-tau could reduce HA-GSK3β-dependent phosphorylation of GFP-tau and consequently GFP-tau inclusion formation. Moreover, NUB1 could directly reduce the levels of HA-GSK3β and GFP-tau as shown for synphilin-1 (Tanji *et al*., 2006). To test these proposals, the ability of NUB1 to reduce the levels of total tau and phosphorylated tau in cells was analysed by WB using a quantitative protein assay (QPA, Chapter 2.5.5).

In order to establish a standard curve for the detection of total GFP-tau levels, SK-N-SH cells were transfected with GFP-tau, and lysed 28 h post-transfection with SDS buffer. Serial dilutions of total cell lysates from 1:20 to 1:5000 were applied to a nitrocellulose membrane in triplicate on a dot-blot apparatus.

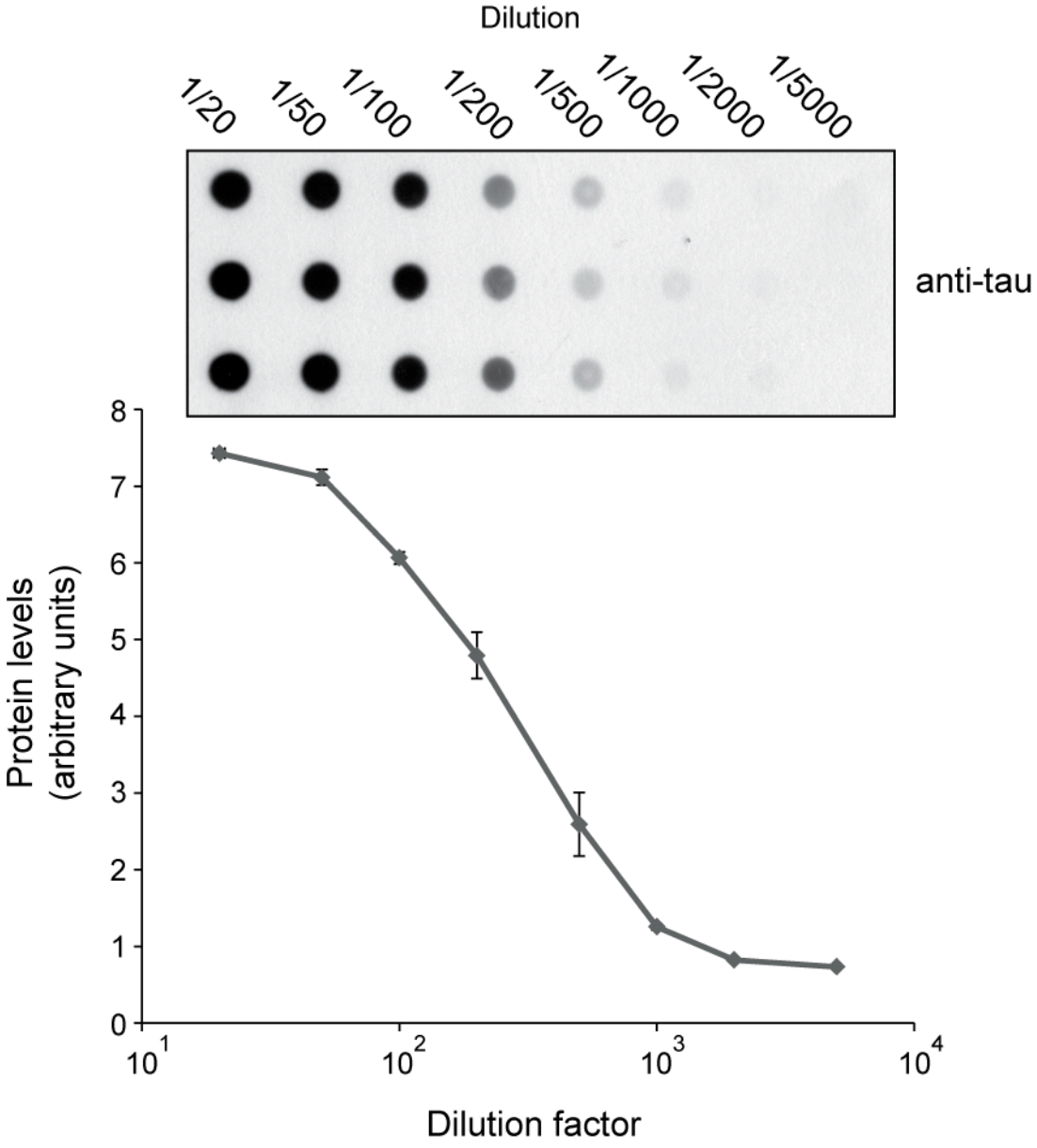

Figure 5.6. *Standard curve for the detection of GFP-tau levels using the anti-tau antibody*. Cells were transfected with 50 ng of GFP-tau plasmid. Twenty-eight hours post-transfection cells were lysed with 1% SDS buffer and a range of serial dilutions from 1:20 to 1:5000 of total cell lysates was applied to a nitrocellulose membrane on a dot-blot apparatus. Total levels of GFP-tau were detected with anti-tau (1:40 000). Spot intensities were measured using the ImageJ program. Error bars represent the SEM.

The total levels of GFP-tau were detected using the anti-tau antibody in the absence of proteasome inhibition (Figure 5.6). The titration curve of GFP-tau revealed that between the 1:10 and 1:100 dilutions, the detection of GFP-tau was saturated, while at the 1:1000 dilution and further the detection limits of available protein were reached. The linear range of the curve was between the 1:200 and 1:500 dilutions. A dilution of 1:400 was therefore selected based on the optimal detection of GFP-tau at this dilution within the linear range

To determine if HA-NUB1, HA-NUB1L and the HA-NUB1L mutants could influence the total levels of GFP-tau, SK-N-SH cells were transfected with GFP-tau alone or with both GFP-tau and HA-GSK3β, and with either HA-NUB1, HA-NUB1L, HA-NUB1LΔUBL or HA-NUB1LΔUBA1-3 (Figure 5.7).

Twenty-eight hours after transfection, cells were treated with a vehicle (DMSO) (Figure 5.8, A) or with MG132 (50 μM) for 4 h (Figure 5.7, B). Cells were lysed with SDS buffer and a 1:400 dilution of cell lysates was applied to a nitrocellulose membrane in quadruplicate on a dot-blot apparatus. GFP-tau was detected with the anti-tau antibody (non-phospho-specific) and the spot intensity measured using ImageJ. All spot intensities were normalised to protein concentration and to GFP-tau levels alone (levels = 1). In the absence of MG132 (Figure 5.7, A), the levels of GFP-tau did not change significantly when HA-NUB1, HA-NUBL1, HA-NUB1LΔUBL or HA-NUB1LΔUBA1-3 were co-expressed in cells. Similarly, none of the NUB1 constructs significantly altered the levels of GFP-tau when it was also co-expressed with HA-GSK3β (all *p-values* > 0.07) (Figure 5.7, A). Proteasome inhibition only slightly increased the GFP-tau levels (a 1.1 fold-increase) in the absence of HA-GSK3β (Figure 5.7, B), and more significantly in the presence of HA-GSK3β (1.7 fold-increase, *p-value* = 0.001). The co-expression of HA-NUB1, HA-NUB1L or HA-NUB1LΔUBL significantly reduced these levels by ~30%, ~41% and ~30% respectively (*p-value* = 0.003, 0.000, and 0.001 respectively). Unexpectedly, the HA-NUB1ΔUBA1-3 also significantly reduced the levels of GFP-tau by ~35% when it was co-expressed with HA-GSK3β in the presence of MG132 (*p-value* = 0.001).

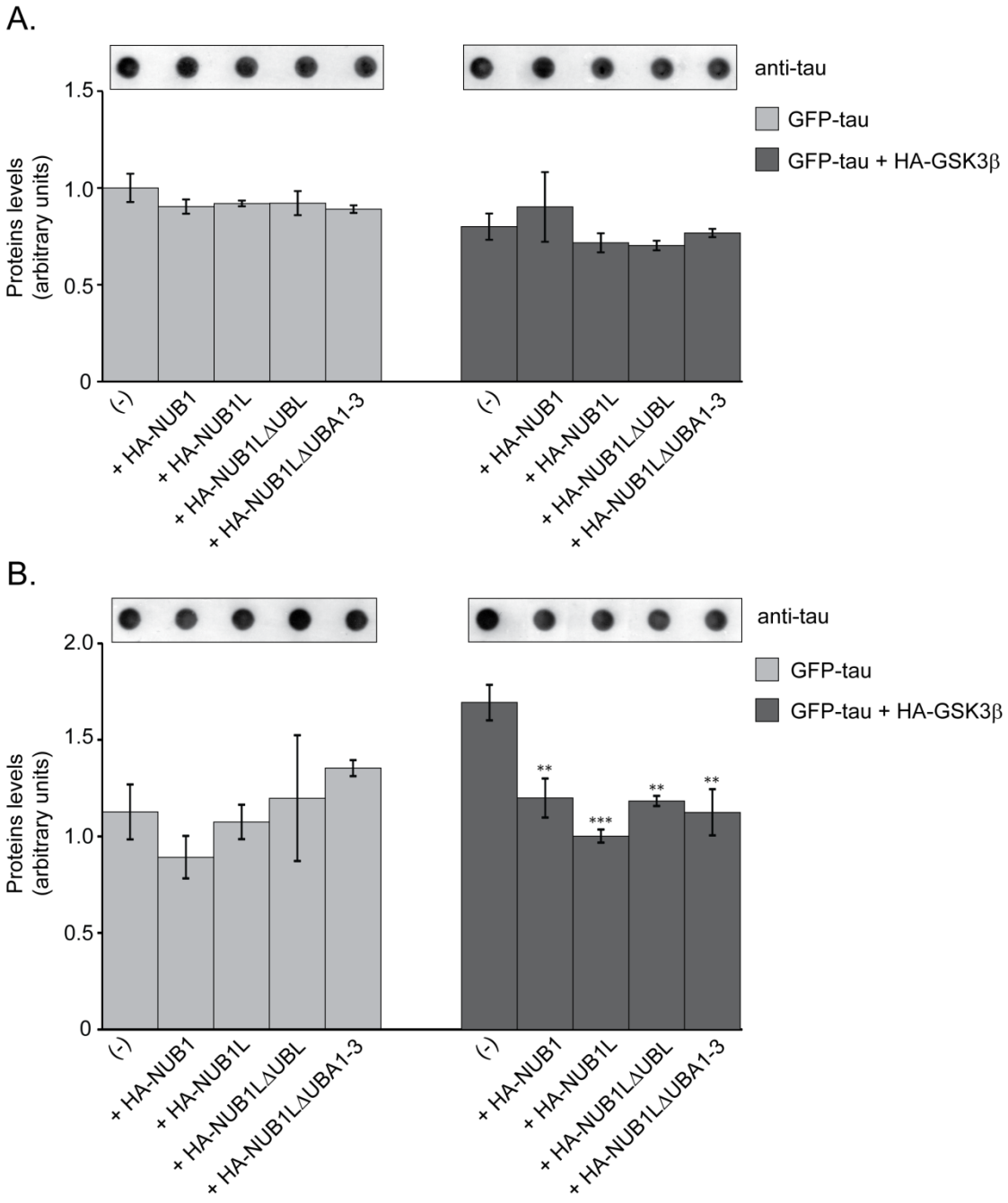

Figure 5.7. *GFP-tau levels are reduced by HA-NUB1, HA-NUB1L and the HA-NUB1L mutants when co-expressed with HA-GSK3β in the presence of MG132*. Cells were transfected with 50 ng of GFP-tau alone (GFP-tau), or with 50 ng of GFP-tau and 150 ng of HA-GSK3β (GFP-tau + GSK3β), either without (-) or with 100 ng of HA-NUB1, HA-NUB1L, HA-NUB1LΔUBL or HA-NUB1LΔUBA1-3 plasmids. Twenty-eight hours post-transfection cells were treated with a vehicle (DMSO), (A), or MG132 (50 μM), (B) for 4 h. Cells were lysed with SDS buffer and a 1:400 dilution of cell lysates was applied to a nitrocellulose membrane in quadruplicate on a dot-blot apparatus. Total levels of GFP-tau were detected with anti-tau (1:40 000). Spot intensities were measured using the ImageJ program, and normalised to levels of GFP-tau alone (= 1). The WB is a representation of one experiment out of three replicates. Statistical significance was determined using an unpaired Student's *t*-test. **p-value*<0.05, ***p-value<0.01,*****p-value<0.001.* Error bars represent the SEM.

5.2.6. The effect of HA-NUB1 on phosphorylated GFP-tau levels.

The effect of HA-NUB1, HA-NUB1L, HA-NUB1LΔUBL and HA-NUB1LΔUBA1-3 on phosphorylated GFP-tau was observed in SK-N-SH cells.

In order to derive a standard curve for the detection of pS396-tau, cells were transfected with both GFP-tau and HA-GSK3β, and lysed 28 h post-transfection with SDS buffer. Serial dilutions of cell lysates from 1:20 to 1:5000 were applied to a nitrocellulose membrane in triplicate on a dot-blot apparatus. The levels of GFP-tau phosphorylated on residue serine 396 (pS396-tau) were detected using the anti-pS396 antibody in the absence of proteasome inhibition (Figure 5.8). The titration curve of pS396-tau revealed that between the 1:20 and 1:50 dilutions, the membrane was saturated, while at the 1:500 dilution and further the detection limits of protein available were reached. A dilution factor of 1:100 was therefore selected based on the optimal detection of pS396-tau at this dilution within the linear range.

To determine if HA-NUB1, HA-NUB1L and the HA-NUB1L mutants could reduce the levels of tau phosphorylated on serine 396, SK-N-SH cells were transfected with GFP-tau alone or both GFP-tau and HA-GSK3β, either without (-) or with HA-NUB1, HA-NUB1L, HA-NUB1LΔUBL or HA-NUB1LΔUBA1-3 (Figure 5.9). Twenty-eight hours after transfection, cells were treated with a vehicle (Figure 5.9, A) or with MG132 (Figure 5.9, B). Cells were lysed with SDS buffer and a 1:100 dilution of total cell lysates was applied to a nitrocellulose membrane in quadruplicate on a dot-blot apparatus. The levels of pS396-tau were detected with the anti-pS396 antibody, and the intensity of the spots measured using ImageJ. The spot intensities were normalised to protein concentration and to GFP-tau + HA-GSK3β levels (levels = 1) (Figure 5.9). In the absence of HA-GSK3β, a basal level of pS396-tau was detected. pS396-tau was detected in the presence of HA-GSK3β, and the co-expression of HA-NUB1, HA-NUBL1, HA-NUB1LΔUBL or HA-NUB1LΔUBA1-3 significantly and efficiently reduced these levels by ~75%, ~80%, ~78% and ~81% respectively in the absence of MG132 (*p-value* = 0.005, 0.004, 0.004 and 0.004 respectively).

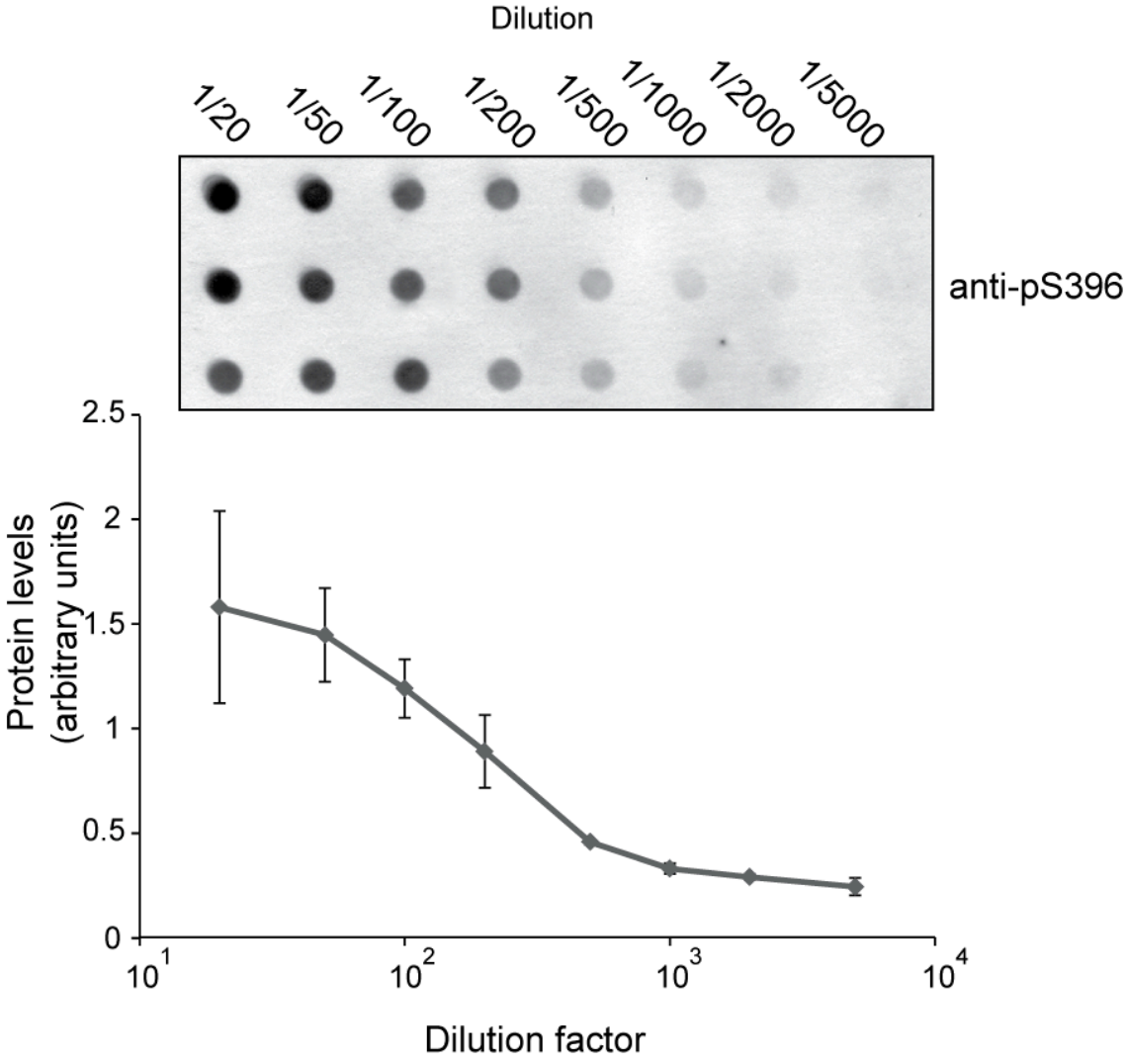

Figure 5.8. *Standard curve for the detection of GFP-tau phosphorylated on serine 396 using the anti-pS396 antibody*. SK-N-SH cells were transfected with 50 ng of GFP-tau and 150 ng of HA-GSK3β plasmids. Twenty-eight hours post-transfection cells were lysed with 1% SDS buffer and a range of serial dilutions from 1:20 to 1:5000 of cell lysates was applied to a nitrocellulose membrane in triplicate on a dot-blot apparatus. Levels of phosphorylated GFP-tau on Ser396 were detected with anti-pS396 (1:5000). Spot intensities were measured using the ImageJ program. Error bars represent the SEM.

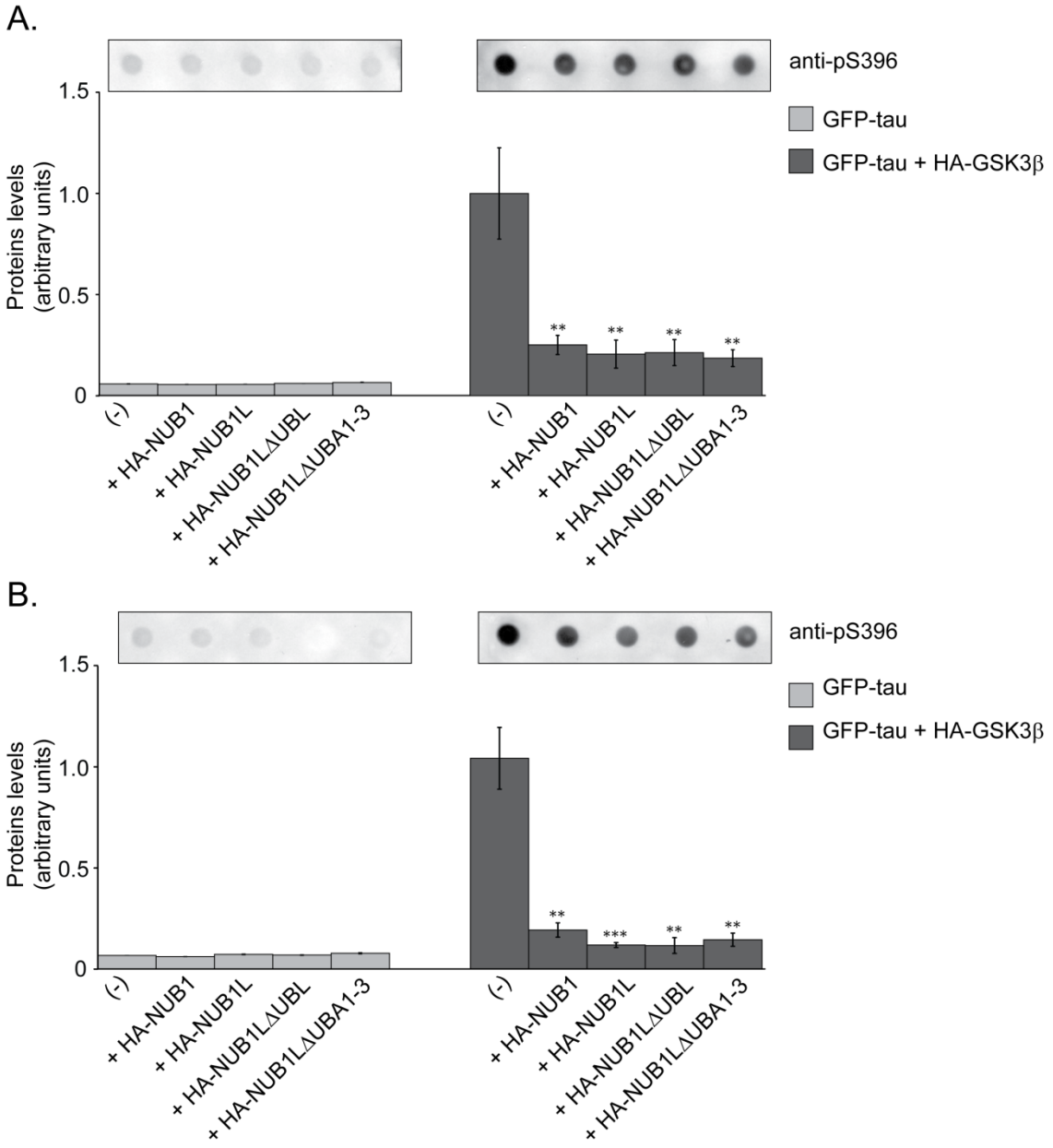

Figure 5.9. *pS396-tau levels are reduced by HA-NUB1, HA-NUB1L and the HA-NUB1L mutants*. SK-N-SH cells were transfected with 50 ng of GFP-tau alone (tau), or with 50 ng of GFP-tau and 150 ng of HA-GSK3β (tau + GSK3β), either without (-) or with 100 ng of HA-NUB1, HA-NUB1L, HA-NUB1LΔUBL or HA-NUB1LΔUBA1-3 plasmids. Twenty-eight hours post-transfection, cells were treated with a vehicle (DMSO), (A), or MG132 (50 μM) (B), for 4 h. Cells were lysed with SDS buffer and a 1:400 dilution of cell lysates was applied to a nitrocellulose membrane in quadruplicate on a dot-blot apparatus. Phosphorylated tau (pS396-tau) levels were detected with anti-pS396 (1:5000). Spot intensities were measured using the ImageJ program, and normalised to the levels of pS396-tau in the presence of HA-GSK3β (= 1). The WB is a representation of one experiment out of three replicates. Statistical significance was determined using an unpaired Student's *t*-test, **p-value*<0.05, ***p-value<0.01,* ****p-value<0.001* Error bars represent the SEM.

In the presence of MG132, the levels of HA-GSK3β phosphorylated pS396-tau were increased slightly by ~4%, and HA-NUB1, HA-NUBL1, HA-NUB1LΔUBL or HA-NUB1LΔUBA1-3 significantly and effectively reduced pS396-tau levels (~81% *p-value*= 0.001, 89% *p-value*=0.000, 89% *p-value* = 0.000 and ~85% *p-value* = 0.001 respectively).

In conclusion, HA-NUB1, HA-NUB1L, HA-NUB1LΔUBL and HA-NUB1LΔUBA1-3 were able to reduce the levels of pS396-tau.

5.2.7. HA-NUB1 alters HA-GSK3β levels.

NUB1 has been shown to be involved in protein regulation (Liu and Xirodimas, 2010; Tanaka *et al*., 2003). Indeed, it can target proteins, bind the proteasome and induce their proteasomal degradation (Tanji *et al*., 2006; Kamitani *et al.*, 2001). NUB1 reduced tau aggregation (Chapter 4.2.8 and 4.2.11), and significantly reduced the levels of phosphorylated tau (pS396-tau, Figure 5.9) compared to the total levels of tau (Figure 5.8). The pS396-tau levels detected were directly correlated with the levels and activity of GSK3β, as only basal levels of pS396-tau could be detected in the absence of GSK3β. Moreover, NUB1 co-localised (Figure 4.13) and interacted with GSK3β (Figure 5.3), and reduced the interaction of GSK3β and tau (Figure 5.4). Therefore, NUB1 might alter the levels or the activity of GSK3β. To assess this hypothesis, the influence of NUB1 on GSK3β turnover was investigated using a cycloheximide (CHX) assay in SK-N-SH cells.

Cells were transfected with HA-GSK3β alone, or with both HA-GSK3β and HA-NUB1. Twenty-eight hours after transfection, cells were treated with a vehicle (DMSO) or with MG132 (50 μM) for 4 h and with CHX for 0, 2, and 4 h. Cells were lysed with RIPA buffer and 10 μg of total protein was resolved on a polyacrylamide gel (10%). HA-NUB1, HA-GSK3β and GAPDH were detected by WB using the anti-HA and anti-GAPDH antibody respectively (Figure 5.10, A). GAPDH was used as a loading control, and the same results were obtained if protein levels were normalized to the loading control.

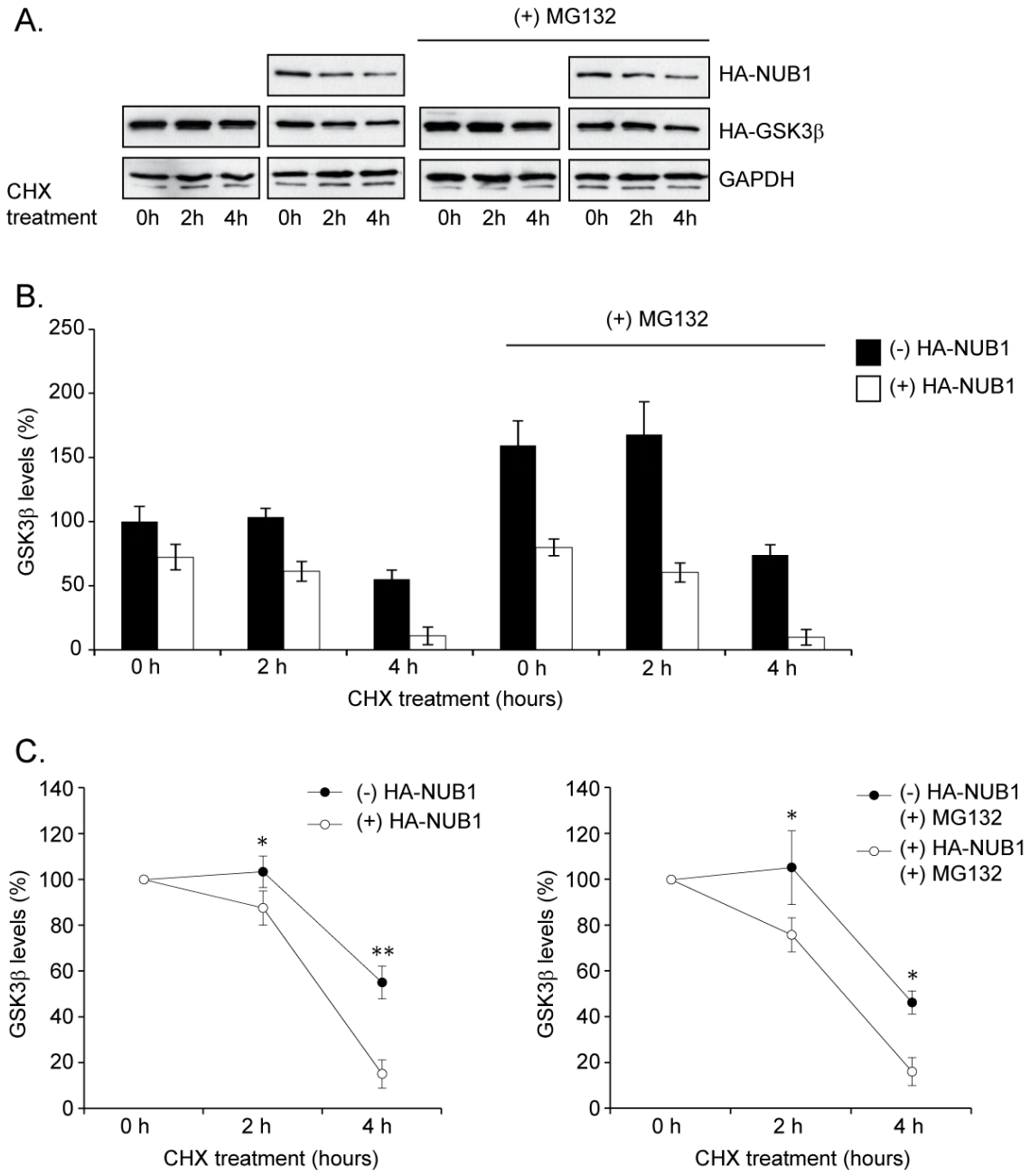

Figure 5.10. *HA-NUB1 effect on HA-GSK3β turnover.* Cells were transfected with HA-GSK3β either alone (150 ng) or with HA-NUB1 (100 ng) plasmids. Twenty-eight hours post-transfection, cells were treated with a vehicle (DMSO) or MG132 (50 μM) for 4 h and with CHX (50 μg/ml) for 0, 2, and 4 h, and lysed with RIPA buffer. Proteins (10 μg) were resolved on a polyacrylamide gel (10%) and were detected by WB using the anti-HA or anti-GAPDH antibody (**A**). The levels of GSK3β (band intensities) were measured using the ImageJ software (**B, C**). (**B**) Comparison of the GSK3β levels. (**C**) Rate of GSK3β degradation following CHX treatment for 0, 2 and 4 h. Statistical significance was determined using an unpaired Student's *t*-test. **p-value*<0.05, ***p-value<0.01.* Error bars are the SEM

HA-NUB1 expression decreased over time with CHX treatment in the absence of MG132, and after 4 h of CHX treatment, the levels of NUB1 were reduced to 26.1% compared to 0 h of CHX treatment. MG132 stabilised the levels of HA-NUB1, as they did not decrease as much after 4 h of CHX treatment (39.1%).

The levels of GSK3β (Figure 5.10, A) decreased temporally following the CHX treatment. However, in the cells co-transfected with HA-NUB1, HA-GSK3β levels decreased faster than in the cells transfected with HA-GSK3β alone. Moreover, HA-GSK3β levels were reduced in the cells co-transfected with HA-NUB1 in the absence of cycloheximide treatment. To quantitate this effect, the GSK3β levels were measured by densitometry using the ImageJ software (Figure 5.10, B and C).

Figure 5.10, B shows that in the cells transfected with HA-NUB1 and HA-GSK3β, without any CHX or MG132 treatment, the HA-GSK3β levels were significantly decreased to 72.3±7.2% (*p-value* = 0.041). The HA-GSK3β levels declined further to 61.3±11.5% and 11±0.7% with 2 h and 4 h of CHX treatment respectively in the presence of HA-NUB1, significantly lower than in the absence of HA-NUB1 (103±6.9% 2 h, 55±7.1% 4 h). Moreover, with MG132 treatment, HA-GSK3β levels increased to 159.3±19.2% in cells transfected with HA-GSK3β alone, whereas they were significantly lower in the cells co-transfected with HA-NUB1 (79.9±5.2%, *p-value* = 0.002). The levels of HA-GSK3β decreased further to 167.8±25.6% and 74±8% (2 h, 4 h CHX treatment respectively) in the absence of HA-NUB1, and to 60.3±5.9% and 9.8±3.8% (2 h, 4 h CHX treatment respectively) in the presence of HA-NUB1. The data indicate that the turnover of HA-GSK3β is in part mediated by the proteasome and that HA-NUB1 reduces the levels of HA-GSK3β. However, in the presence of HA-NUB1, HA-GSK3β levels did not seem to be stabilised by the proteasome inhibition. To directly compare the levels of GSK3β in the presence or absence of NUB1, the percentage of HA-GSK3β decrease from the levels measured in Figure 5.10, B was plotted in Figure 5.10, C. It shows that HA-NUB1 also accelerated the degradation of GSK3β. Indeed, the levels of HA-GSK3β were significantly lower in the cells co-transfected with HA-NUB1 compared to the cells transfected with HA-GSK3β alone when treated with CHX for 2 h

(87.6±7.7% and 103.4±6.9% respectively, *p-value* = 0.041) and for 4 h (15.2±7% and 55.1±7% respectively, *p-value* = 0.005). Interestingly, the MG132 treatment increased the overall levels of HA-GSK3β in the absence of HA-NUB1 (Figure 5.10, B), but it did not affect the rate of HA-GSK3β degradation. In the presence of HA-NUB1, the HA-GSK3β levels were significantly more rapidly degraded after 2 h (75.9±7.4% compared to 105.3±16%, *p-value* = 0.026) and 4 h (16.3±6.2% compared to 46.4±5%, p-value = 0.011) of treatment with CHX.

In conclusion, HA-NUB1 was able to significantly reduce HA-GSK3β levels and to accelerate its turnover.

5.2.8. HA-NUB1L alters HA-GSK3β levels

HA-NUB1 was able to accelerate GSK3β turnover (Chapter 5.2.7). Therefore, the influence of HA-NUB1L, HA-NUB1LΔUBL and HA-NUB1LΔUBA1-3 on HA-GSK3β levels was investigated.

Cells were transfected with 150 ng of HA-GSK3β alone or in combination with 100 ng of HA-NUB1L (Figure 5.11), HA-NUB1LΔUBL (Figure 5.12) or HA-NUB1LΔUBA1-3 (Figure 5.13). Twenty-eight hours after transfection, Cells were treated with a vehicle (DMSO) or with MG132 (50 μM) for 4 h and with CHX for 0, 2, and 4 h. Cells were lysed with RIPA buffer and 10 μg of total protein was resolved on a polyacrylamide gel (10%).

HA-NUB1L, HA-NUB1LΔUBL, HA-NUB1LΔUBA1-3, HA-GSK3β and actin were detected by WB using the anti-HA and anti-actin antibody respectively. Actin was used as a loading control, and the same results were obtained if protein levels were normalised to the loading control. As for HA-NUB1, the HA-NUB1L expression (Figure 5.11, A) was decreased over time with CHX treatment, with only 25.3% of protein levels remaining after 4 h of CHX treatment compared to non-treated cells. Interestingly, the HA-NUB1LΔUBL and HA-NUB1LΔUBA1-3 levels (Figure 5.12, A and 5.13, A respectively) did not decrease as much as the HA-NUB1 and HA-NUB1L levels, with 60,4% and 78,1% of levels remaining after 4 h of CHX treatment respectively.

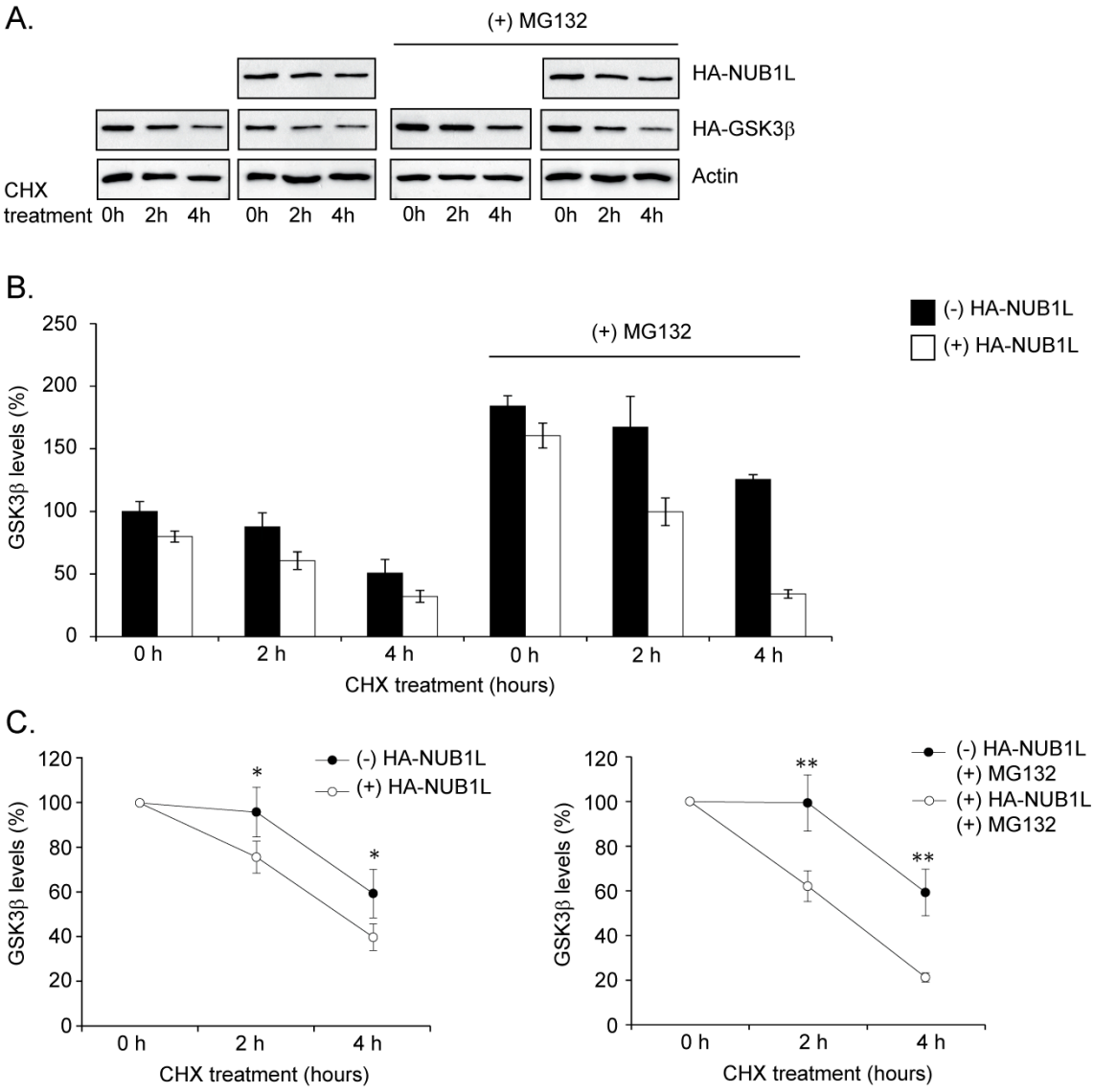

Figure 5.11. *HA-NUB1L effect on HA-GSK3β turnover.* Cells were transfected with HA-GSK3β alone (150 ng) or in combination with HA-NUB1L (100 ng) plasmids. Twenty-eight hours post-transfection, cells were treated with a vehicle (DMSO) or MG132 (50 μM) for 4 h and with CHX (50 μg/ml) for 0, 2, and 4 h, and lysed with RIPA buffer. Proteins (10 μg) were resolved on a polyacrylamide gel (10%) and were detected by WB using the anti-HA or anti-actin antibody (**A**). The levels of GSK3β (band intensities) were measured using the ImageJ software (**B, C**). (**B**) Comparison of the GSK3β levels. (**C**) Rate of GSK3β degradation following CHX treatment for 0, 2 and 4 h. Statistical significance was determined using an unpaired Student's *t*-test. *p-value<0.05, **p-value<0.01.* Error bars are the SEM.

Similar results were obtained with proteasome inhibition, with 28.9%, 65.3% and 75.2% of HA-NUB1L, HA-NUB1LΔUBL and HA-NUB1LΔUBA1-3 levels remaining after 4 h of CHX treatment. Figure 5.11, B, Figure 5.12, B and Figure 5.13, B show the levels of HA-GSK3β alone and in the presence of HA-NUB1L, HA-NUB1LΔUBL and HA-NUB1LΔUBA1-3 respectively, both in the absence and in the presence of MG132. In the absence of CHX and MG132 treatment both HA-NUB1L and HA-NUB1LΔUBL significantly reduced the overall levels of GSK3β, (80±4.5%, *p-value* = 0.019 and 79.3±4.4%, *p-value* = 0.02 respectively), whereas in cells co-transfected with HA-NUB1LΔUBA1-3, the HA-GSK3β levels were not significantly lower (88.5±12.8%) (0 h, CHX). Both HA-NUB1L and HA-NUB1LΔUBL significantly reduced the levels of HA-GSK3β over time compared to the levels of HA-GSK3β alone (after 4 h of CHX treatment, 32.1±4.7% vs. 50.7±10.8% and 38.6±3.4% vs. 61.3±3.2% respectively). However, HA-NUB1LΔUBA1-3 did not significantly reduce HA-GSK3β levels over time (after 4 h of CHX treatment, 62.8±15.5% compared to 59.6±6.6%). Therefore, in the absence of MG132, HA-NUB1LΔUBA1-3 was defective in its ability to significantly reduce GSK3β levels. With proteasome inhibition, the HA-GSK3β levels increased to 184±8.4%, 178.7±11.6% and 170.3±11.1% in the HA-NUB1, HA-NUB1LΔUBL and HA-NUB1LΔUBA1-3 experiments respectively, and were significantly decreased to 160.5±9.9% (*p-value* = 0.035), 89.8±13.8% (*p-value* = 0.002) and 114.1±24.5% (*p-value* = 0.02) in the presence of HA-NUB1L, HA-NUB1LΔUBL or HA-NUB1LΔUBA1-3 respectively (0 h, CHX). Surprisingly, in the presence of MG132, all three resulted in a significant decline in HA-GSK3β levels over time compared to HA-GSK3β alone. Indeed, at 4 h after CHX treatment, HA-NUB1LΔUBL and HA-NUB1LΔUBA1-3 decreased HA-GSK3β levels from 98.8±6.9% and 114.6±32% to 65.3±7.4% and 68.2±6.2% respectively, with HA-NUB1L more effective at reducing HA-GSK3β levels (from 125.6±3.7% to 34.1±3.4%). Interestingly, the overall levels of HA-GSK3β appeared to be stabilised upon proteasome inhibition with HA-NUB1L co-expression compared to HA-NUB1LΔUBL or HA-NUB1LΔUBA1-3, suggesting that the HA-NUB1L effect on HA-GSK3β is at least partially mediated by the proteasome.

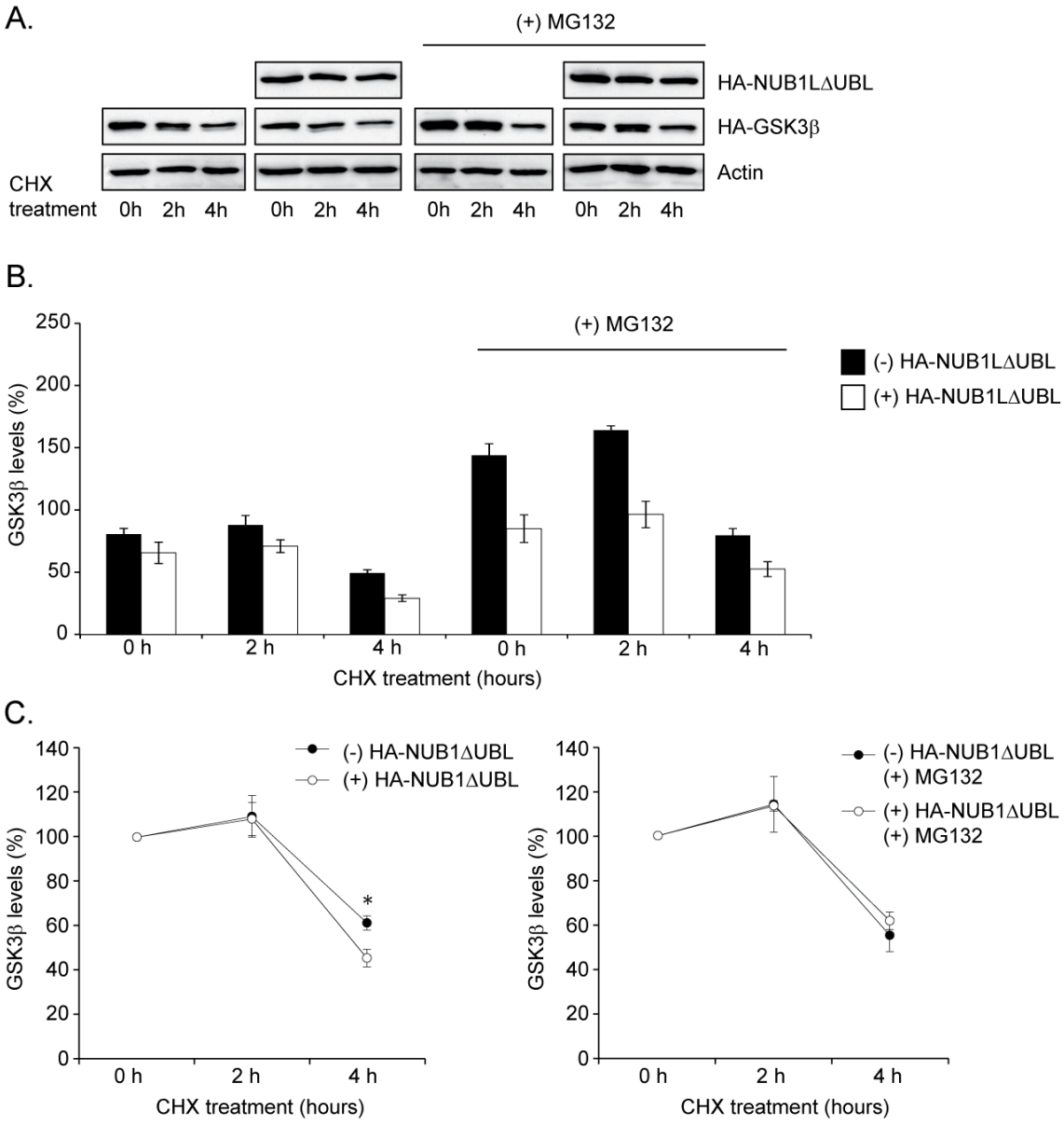

Figure 5.12. *HA-NUB1LΔUBL effect on HA-GSK3β turnover.* Cells were transfected with HA-GSK3β alone (150 ng) or in combination with HA-NUB1LΔUBL (100 ng) plasmids. Twenty-eight hours post-transfection, cells were treated with a vehicle (DMSO) or MG132 (50 μM) for 4 h and with CHX (50 μg/ml) for 0, 2, and 4 h, and lysed with RIPA buffer. Proteins (10 μg) were resolved on a polyacrylamide gel (10%) and were detected by WB using the anti-HA or anti-actin antibody (**A**). The levels of GSK3β (band intensities) were measured using the ImageJ software (**B, C**). (**B**) Comparison of the GSK3β levels. (**C**) Rate of GSK3β degradation following CHX treatment for 0, 2 and 4 h Statistical significance was determined using an unpaired Student's *t*-test. **p-value*<0.05, ***p-value<0.01.* Error bars are the SEM.

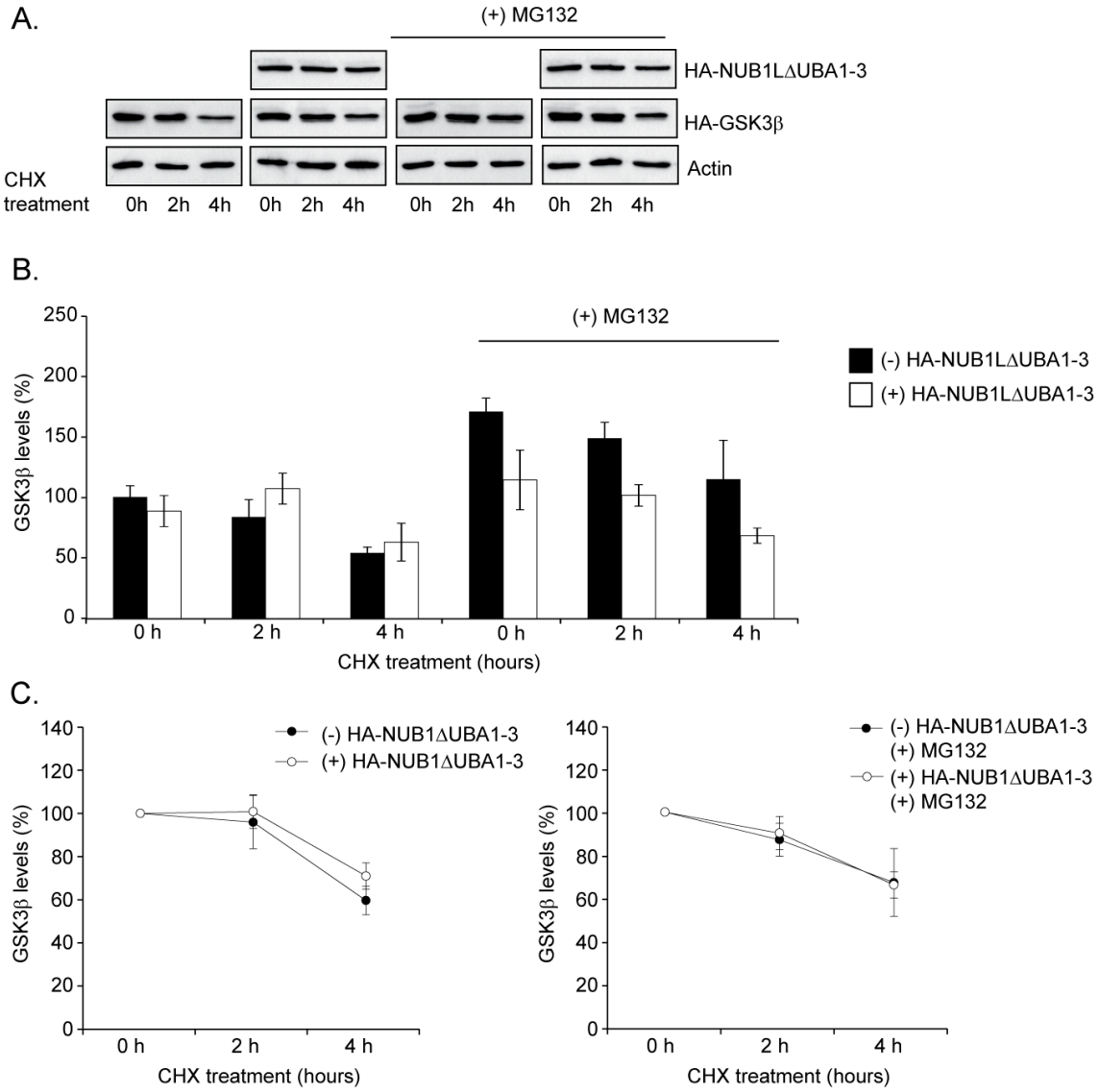

Figure 5.13. *HA-NUB1LΔUBA1-3 effect on HA-GSK3β turnover.* Cells were transfected with HA-GSK3β alone (150 ng) or in combination with HA-NUB1LΔUBA1-3 (100 ng) plasmids. Twenty-eight hours post-transfection, cells were treated with a vehicle (DMSO) or MG132 (50 μM) for 4 h and with CHX (50 μg/ml) for 0, 2, and 4 h, and lysed with RIPA buffer. Proteins (10 μg) were resolved on a polyacrylamide gel (10%) and were detected by WB using the anti-HA or anti-actin antibody (**A**). The levels of GSK3β (band intensities) were measured using the ImageJ software (**B, C**). (**B**) Comparison of the GSK3β levels. (**C**) Rate of GSK3β degradation following CHX treatment for 0, 2 and 4 h. Statistical significance was determined using an unpaired Student's *t*-test. **p-value*<0.05. Error bars are the SEM.

The percentage of HA-GSK3β decreased in the presence of HA-NUB1L (Figure 5.11, C), HA-NUB1LΔUBL (Figure 5.12, C) and HA-NUB1LΔUBA1-3 (Figure 5.13, C) were plotted respectively. Without MG132 treatment, the HA-GSK3β turnover was significantly accelerated by the presence of HA-NUB1L (Figure 5.11, C), after 2 h (75.9±7.1% compared to 95.9±12.3%, *p-value* = 0.037) and 4 h (40.2±5.9% compared to 59.6±5.6%, *p-value* = 0.006) of CHX treatment. On the other hand, the turnover of HA-GSK3β in the presence of HA-NUB1LΔUBL or HA-NUB1LΔUBA1-3 (Figure 5.12, C and 5.13, C) was similar to that of HA-GSK3β alone after 2 h of CHX treatment. After 4 h of CHX treatment, a small but significant reduction of HA-GSK3β levels occurred in the presence of HA-NUB1LΔUBL (45.4±4% compared to 61.3±3.2%, *p-value* = 0.032) but not HA-NUB1LΔUBA1-3 (71±9.3% compared to 59.6±6.6%). With proteasome inhibition, the presence of HA-NUB1L accelerated the degradation of GSK3β after 2 h (62.1±6.8% compared to 67.3±12.6%, *p-value* = 0.008) and 4 h (21.3±2.2% compared 59.3±10.4%, *p-value* = 0.001) of CHX treatment, whereas the presence of HA-NUB1LΔUBL or HA-NUB1LΔUBA1-3 did not alter the rate of HA-GSK3β turnover.

To conclude, similarly to HA-NUB1, HA-NUB1L was able to reduce GSK3β levels and accelerate its turnover. On the other hand, HA-NUB1LΔUBL reduced the overall levels of HA-GSK3β but did not alter its rate of turnover. HA-GSK3β levels did not decrease in the presence of HA-NUB1LΔUBA1-3 unless the proteasome was inhibited in cells, and HA-NUB1LΔUBA1-3 did not accelerate the rate of HA-GSK3β degradation irrespective of proteasome inhibition. Therefore, both HA-NUB1LΔUBL and HA-NUB1LΔUBA1-3 were defective compared to HA-NUB1L.

5.3. Discussion

Chapter 4 demonstrated that GSK3β and inhibition of the proteasome induced the formation of tau inclusions in cells. Moreover, NUB1 was able to reduce the formation of tau inclusions, and its UBA domains were necessary for the efficient reduction of tau aggregation. NUB1 was recruited to tau inclusions and co-localised with GSK3β, which suggested the formation of a complex between the three proteins.

Therefore, chapter 5 explored the possible interactions between NUB1, GSK3β and tau, and the consequences of this association on both total and phosphorylated levels of tau. Moreover, the effect of NUB1, as a potential shuttle for proteasomal degradation, on GSK3β stability was analysed.

GSK3β is known to target GFP-tau for phosphorylation. Here we showed that GFP-tau and HA-GSK3β co-immunoprecipitated reciprocally with each other. This interaction could be part of a complex, for instance, with PS1. Indeed, in cells, exogenous PS1 was able to bind both exogenous GSK3β and tau (Takashima *et al*., 1998). Moreover, a small population of endogenous tau and GSK3β were precipitated with PS1 in AD brain fractions. Another possibility would be a direct interaction between GSK3β and tau, or via the protein 14-3-3 (Sun *et al*., 2002; Agarwal-Mawal *et al*., 2003).

GFP-tau was also able to interact with NUB1-FLAG in a reciprocal manner. This was consistent with the recruitment of GFP-NUB1 to tau associated with microtubules and tau inclusions. However, neither the co-localisation analysis nor the co-immunoprecipitation experiments prove a direct interaction between NUB1 and tau. Therefore, NUB1 and tau are in a complex together, but might interact either directly or indirectly via a complex of proteins.

Similarly, HA-GSK3β and NUB1-FLAG co-immunoprecipitated reciprocally and their localisation overlapped in SK-N-SH cells. Therefore, the two proteins interact either directly or indirectly within in a complex, and suggest that GSK3β might be also modulated by NUB1. Conversely, it is possible that NUB1 might

be a substrate for phosphorylation-dependent regulation by GSK3β. Indeed, NUB1 possess several putative sites for GSK3 phosphorylation (10 sites, using the Group-based Prediction System (GPS), http://gps.biocuckoo.org/) although to date none of these have been confirmed experimentally, and a shift in NUB1 molecular weight was not seen in the presence of GSK3β. More experimental evidence would be required to unequivocally rule out the possibility of NUB1 as a substrate for GSK3β, however our data suggests that it is in fact NUB1 that is likely involved in the regulation of GSK3β.

As GFP-tau, HA-GSK3β and NUB1-FLAG interacted reciprocally in binary complexes, it was expected that when all three proteins were expressed in SK-N-SH cells, they would form a complex. Indeed, when the three proteins were co-expressed, GFP-tau immunoprecipitated both NUB1-FLAG and HA-GSK3β. However, whilst GFP-tau immunoprecipitated NUB1-FLAG with the same efficiency as in the binary immunoprecipitation, there was an obvious reduction in the interaction of HA-GSK3β with GFP-tau in the presence of NUB1-FLAG. This result could be explained by competition for a shared binding site on GFP-tau between NUB1-FLAG and HA-GSK3β. Another possibility is that HA-GSK3β might preferentially interact with NUB1-FLAG over GFP-tau, resulting in an increase in the HA-GSK3β/NUB1-FLAG complex over the GFP-tau/HA-GSK3β complex when the three proteins are expressed in SK-N-SH cells. However, NUB1-FLAG co-immunoprecipitation experiments revealed not only a reduction in the interaction of NUB1-FLAG with HA-GSK3β, but also with GFP-tau. These results suggest that NUB1-FLAG might disrupt the binding interface between HA-GSK3β and GFP-tau by sharing this interface in the ternary complex. Alternatively, epitope occlusion might occur when the three proteins are expressed and interact. In order to test these possibilities, experiments could be performed to map the binding interfaces of the proteins. Moreover, *in vitro* pull down experiments using heterologously expressed recombinant proteins could be performed to determine whether they are able to interact directly with one another.

The investigation of the localisation of GFP-NUB1, DsRed-tau and HA-GSK3β in SK-N-SH cells when the three proteins were co-expressed showed that

indeed, HA-GSK3β was no longer associated with tau inclusions. GFP-NUB1 remained recruited to inclusions, yet HA-GSK3β was completely excluded from them. However, both GFP-NUB1 and HA-GSK3β were found in structures similar to microtubule bundles formed in the presence of GFP-tau. Therefore, it is possible that NUB1 reduces the association of GSKβ with tau, thereby consequently reducing both the aggregation of tau and the recruitment of GSK3β to the aggregated tau. Alternatively, it is possible that a complex is formed between the three proteins which, when localised at inclusions of aggregated tau, prevents or occludes the detection of HA-GSK3β by the anti-HA antibody.

NUB1 can target proteins for proteasomal degradation. Hence, the ability of NUB1 to reduce tau inclusions could be via an increase in its proteasomal degradation. Thus, the effect of NUB1, NUB1L and the NUB1L mutants on the levels of total and phosphorylated tau was explored. Tau levels were not significantly decreased by HA-NUB1, HA-NUB1L or the HA-NUB1L mutants without proteasome inhibition in either the absence or presence of HA-GSK3β. With inhibition of the proteasome, GFP-tau levels were slightly increased in the absence of HA-GSK3β expression and were further enhanced when HA-GSK3β was co-expressed in cells. This data suggests that GFP-tau degradation is partially mediated by the proteasome, and that in the presence of HA-GSK3β, GFP-tau is more stable. A significant decline of GFP-tau levels was observed with the co-expression of HA-NUB1, HA-NUB1L or the HA-NUB1L mutants with proteasome inhibition and in the presence of HA-GSK3β. This suggests that HA-NUB1 might target a subpopulation of GFP-tau, probably a population that is also phosphorylated by GSK3β. Another possibility is that HA-NUB1, HA-NUB1L and the HA-NUB1L mutants target HA-GSK3β, thus reducing tau phosphorylation and stabilisation.

Indeed, the analysis of tau phosphorylated on S396 (pS396-tau) showed that HA-NUB1, HA-NUB1L and the HA-NUB1L mutants significantly and strongly reduced pS396-tau levels. It is therefore possible that NUB1 targets hyperphosphorylated tau for degradation. Noticeably, even the mutant HA-NUB1LΔUBA1-3 could reduce tau and pS396-tau levels, although this mutant could not reduce tau aggregation. Thus, the effect of NUB1 on tau aggregation

might not only be mediated by the reduction of total or phosphorylated tau levels. However, only one phospho-epitope of tau was analysed in this study. Therefore, HA-NUB1LΔUBA1-3 might be able to target pS396-tau but not tau phosphorylated on other residues, such as the epitopes recognised by the AT8 antibody that is mostly found in the inclusions. Thus, it would have been interesting to assess the levels of insoluble tau compared to soluble tau, and the resolution of tau phospho-epitopes in each of these fractions.

The reduction of phosphorylated tau levels on S396 could also be mediated by a reduction of GSK3β-dependent phosphorylation of tau. Indeed, the reduced interaction of GFP-tau and HA-GSK3β observed in the ternary complex might result from a NUB1-mediated decrease in HA-GSK3β levels. The hypothesis of a proteasomal degradation of GSK3β by NUB1 was tested using a cycloheximide (CHX) assay. CHX inhibits the transcription of proteins, and therefore the levels of a protein observed upon CHX treatment are directly related to its degradation or turnover rate. HA-GSK3β is thought to be a stable protein with a half-life of 48 h. However, in SK-N-SH cells, overexpressed HA-GSK3β levels started to decline after 4 h of CHX treatment. In the presence of HA-NUB1, the levels of HA-GSK3β were reduced even without CHX treatment and started to decline after only 2 h of CHX treatment. Moreover, the rate of HA-GSK3β degradation was accelerated, thus suggesting that HA-NUB1 modulates HA-GSK3β turnover. With proteasome inhibition, the levels of HA-GSK3β alone were stabilised although the rate of degradation was not significantly altered. This suggests that GSK3β degradation in the absence of NUB1 is partially mediated by the proteasome. HA-NUB1 accelerated the turnover of HA-GSK3β, however proteasome inhibition did not further stabilise or change the rate of degradation of HA-GSK3β, suggesting that the effect of HA-NUB1 on HA-GSK3β was not proteasome-dependent. A recent study proposes that HA-GSK3β is sequestered in MVBs and later degraded by lysosomes (Taelman *et al.*, 2010). In chapter 4, the presence of GFP-NUB1 induced a change of HA-GSK3β localisation, which was more particulate in nature than when it was expressed on its own and which was then also detected diffusely in the nucleus. The UBA domains of the human EPS15 and the yeast Ede1 proteins have been implicated in monoUb recognition and

endosomal sorting. Therefore, HA-NUB1 could mediate HA-GSK3β endosomal/lysosomal degradation via its UBA domains. It would be interesting to confirm this hypothesis with the use of markers for the endosomal pathway, such as Vps4.

The effect of HA-NUB1L and the HA-NUB1L mutants on HA-GSK3β turnover was also investigated. HA-NUB1L was able to significantly reduce the overall levels of HA-GSK3β and to accelerate its degradation rate. With proteasome inhibition, HA-NUB1L decreased the levels of HA-GSK3β although they were considerably stabilised in comparison to those in the absence of proteasome inhibition. Interestingly, although HA-NUB1L accelerated the turnover of GSK3β in both the absence and presence of MG132, the rate of degradation in each case was not significantly different, suggesting that the effect of HA-NUB1L on HA-GSK3β turnover was only partially mediated by the proteasome. Hence, both HA-NUB1 and HA-NUB1L significantly reduced the levels of GSK3β and accelerated the rate of degradation of GSK3β both in the presence and absence of proteasome inhibitor. MG132-dependent stabilization of GSK3β levels was significant only with HA-NUB1L, and the rate of turnover, although accelerated with both HA-NUB1 and HA-NUB1L, was the same irrespective of proteasome inhibition. Therefore, it is possible that the effect of NUB1 and NUB1L on GSK3β is only mediated in part by the proteasome.

On the other hand, HA-NUB1ΔUBL did not accelerate the degradation of HA-GSK3β, but did reduce the overall levels of HA-GSK3β. This suggests that the NUB1L mutant lacking the UBL domains is defective with respect to its proteasome-associated function and therefore did not accelerate HA-GSK3β degradation, but is consequently active in addressing HA-GSK3β to a degradation pathway other than proteasomal degradation. The mutant HA-NUB1ΔUBA1-3 reduced the overall HA-GSK3β levels only with proteasome inhibition. The mutant did not accelerate HA-GSK3β turnover, suggesting that like HA-NUB1LΔUBL, HA-NUB1LΔUBA1-3 is defective with respect to a proteasome-associated function. It is interesting in this regard that both NUB1LΔUBL and NUB1LΔUBA1-3 levels themselves appeared considerably stable following CHX treatment, suggesting their defective clearance. Unlike HA-NUB1 and HA-NUB1L, both HA-NUB1LΔUBL and HA-NUB1LΔUBA1-3

were unable to accelerate the turnover of GSK3β, irrespective of proteasome inhibition, but both significantly decreased the levels of GSK3β with proteasome inhibition. This might suggest that the targeting of GSK3β to the proteasome by these mutants is defective, and that following inhibition of the proteasome, GSK3β is consequently targeted to an alternative pathway by the mutants. Since the regulation of GSK3β by NUB1 appears to be mediated only in part by the proteasome, it is also possible that the mutants are defective in alternative clearance pathways for GSK3β and unable to accelerate the clearance via these pathways. Though the underlying mechanism of NUB1 regulation of GSK3β appears complex, these findings nevertheless highlight the importance of both the UBL and UBA domains in the NUB1-mediated regulation of GSK3β.

This chapter has demonstrated that NUB1 can interact with both tau and GSK3β, and is associated with these two proteins in a ternary complex. Moreover, NUB1 reduced the levels of phosphorylated tau in the presence of GSK3β, possibly as a result of an acceleration or increase in GSK3β degradation, via the proteasome and other degradation mechanisms.

Chapter 6
NUB1 targets GSK3β

6.1. Introduction

NUB1 targets FAT10 and NEDD8 and their conjugated proteins for proteasomal degradation. Indeed, NUB1 is able to bind the S5a subunit of the 19S proteasome. NUB1 is a UBL/UBA domain protein. However, NUB1 is an unconventional member of this family. Indeed, its UBA domains, although necessary to bind FAT10, are not always necessary to bind proteins targeted for proteasomal degradation, and its UBL domain does not appear to be involved in its interaction with the proteasome (Tanji *et al*., 2005; Schmidtke *et al.*, 2006). Indeed, NUB1 binds NEDD8, synphilin-1 and the proteasome via its C-terminus, near the PEST domain (Tanji *et al*., 2006). PEST domains are sequences of amino acids rich in proline (P), glutamic acid (E), serine (S) and threonine (T), thought to be characteristic of short-lived proteins and therefore involved in signalling that a protein be targeted for rapid proteasomal degradation. Thus, it is possible that the degradation of NUB1 itself or proteins associated with NUB1 is accelerated as the PEST domain acts as a degradation signal. Moreover, the UBA/UBL domains of NUB1 might be implicated in other regulatory mechanisms of protein degradation and turnover, such as autophagy and lysosomal degradation.

In previous chapters, NUB1 was shown to influence tau levels and GSK3β turnover. NUB1 co-localised with tau and GSK3β in rat cortical neurons and in SK-N-SH neuroblastoma cells. Moreover, NUB1 interacted with both exogenous tau and GSK3β, reduced phosphorylated tau levels and aggregation, and enhanced GSK3β turnover. However, although NUB1 is expressed endogenously in human hippocampal neurons, the physiological role of NUB1 in neurons is unknown. In this chapter, the expression of endogenous NUB1

was explored in SH-SY5Y neuroblastoma cells. Moreover, its interaction with endogenous GSK3β and its affect on the stability and turnover of endogenous GSK3β were investigated.

6.2. Results

6.2.1. Expression of tau, NUB1 and GSK3β in SH-SY5Y neuroblastoma cells

SK-N-SH neuroblastoma cells lack NUB1 and tau expression (Figure 4.1 and 4.7). Therefore, to investigate the effect of NUB1 on endogenous tau and GSK3β, their expression was analysed in another neuroblastoma cell line, SH-SY5Y.

SK-N-SH and SH-SY5Y cells were harvested and 5, 10, 20 and 40 µg of total protein was resolved on a polyacrylamide gel. Endogenous NUB1, tau and GSK3β were detected by WB using the anti-NUB1, anti-tau or anti-GSK3β antibody respectively (Figure 6.1). Tau and NUB1 could not be detected in SK-N-SH cells, even with 40 µg of total proteins resolved on the gel. In contrast, endogenous NUB1 was detected in SH-SY5Y cells at a molecular weight of ~66 kDa as expected from the predicted size. The NUB1 levels detected increased proportionally with the amount of protein resolved, however, a minimum of 10 µg of the total protein was necessary to detect endogenous NUB1. Several bands were detected by anti-tau in SH-SY5Y cells, with a prominent band detected at ~50 kDa corresponding to the smaller three isoforms of human tau, the molecular weight of which varies from 45 to 50 kDa. GSK3β was detected in both the SK-N-SH cells and SH-SY5Y cells as a single band of ~47 kDa. GSK3β levels increased proportionally with the amount of proteins resolved, and could be detected with only 5 µg of total protein.

6.2.2. Localisation of GFP-NUB1 with endogenous tau and microtubules in SH-SY5Y cells

It has been shown in Chapter 3 and 4 that NUB1 co-labelled GFP-tau. Therefore, the co-localisation of NUB1 with endogenous tau and microtubules was investigated in SH-SY5Y cells.

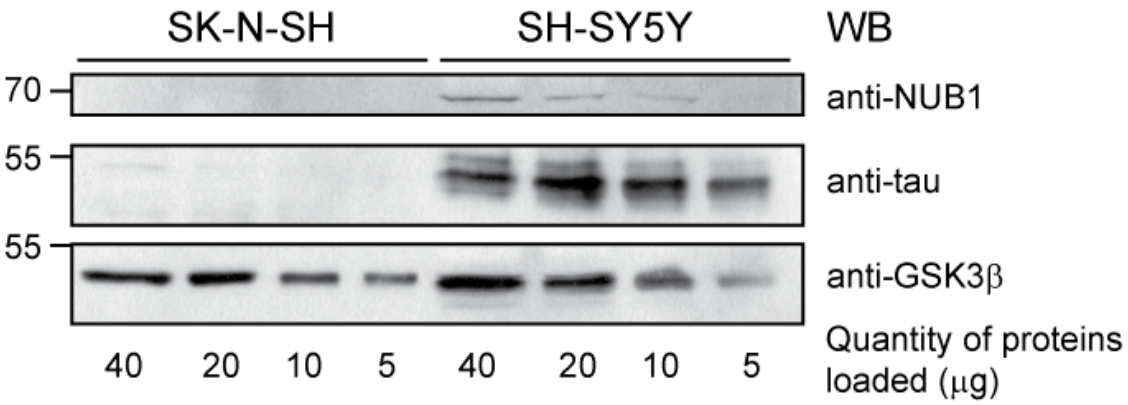

Figure 6.1. *Expression of NUB1, tau and GSK3β in SK-N-SH and SH-SY5Y cells*. Decreasing amounts (40, 20, 10, 5 μg) of SK-N-SH and SH-SY5Y cell lysates were resolved on a polyacrylamide gel (10%) and proteins were detected by WB using the anti-NUB1, anti-tau or anti-GSK3β antibody.

The NUB1 peptide-directed antibody is not suitable for immunocytochemical localisation. Therefore, the localisation of exogenous GFP-NUB1 was analysed in SH-SY5Y neuroblastoma cells. Cells were transfected with GFP-NUB1 and 24 h after transfection, cells were treated with a vehicle (DMSO) (Figure 6.2, A) or with MG132 (50 μM) (Figure 6.2, B), and fixed with glutaraldehyde (0.3%).

Tau was detected using the anti-tau antibody (Figure 6.2, A and B, red). Figure 6.2, A shows that GFP-NUB1 was, as expected, mostly nuclear. Similar to its localisation in primary neurons (Figure 3.10), it was also detected in the primary neurites. Tau was mostly localised in the cytoplasm and the neurites. With MG132 treatment (Figure 6.2, B), GFP-NUB1 distribution was enhanced in the cytoplasm. In the magnified images of the cell body and the neurites (Figure 6.2, A and B, I and II respectively), GFP-NUB1 partially co-localised with endogenous tau in both the absence and presence of proteasome inhibitor.

As tau is a microtubule associated protein, the distribution of GFP-NUB1 and microtubules was analysed in SH-SY5Y cells.

SH-SY5Y cells were transfected with GFP-NUB1. Twenty four hours post-transfection, cells were treated with a vehicle (DMSO) (Figure 6.3, A) or MG132 (50 μM) (Figure 6.3, B) and fixed with 0.3% glutaraldehyde. The microtubules were detected using the anti-β-tubulin antibody (Figure 6.3, red). As previously observed, GFP-NUB1 in SH-SY5Y cells was mostly nuclear but could also be detected in the cytoplasm and primary neurites, and its distribution in the cytoplasm was enhanced after proteasome inhibition (Figure 6.3, A and B). The microtubules (Figure 6.3, red) were detected as a filamentous network in the cytoplasm and the neurites but not in the nucleus. In the magnified images of the cell body and neurites, both in the absence and presence of MG132 (Figure 6.3, A and B, I and II), a partial overlap of GFP-NUB1 and β-tubulin could be observed. However, in the cell body (Figure 6.3, A and B, I), GFP-NUB1 generally did not co-localise with the microtubule network, and this was particularly evident at the cellular periphery (white arrows).

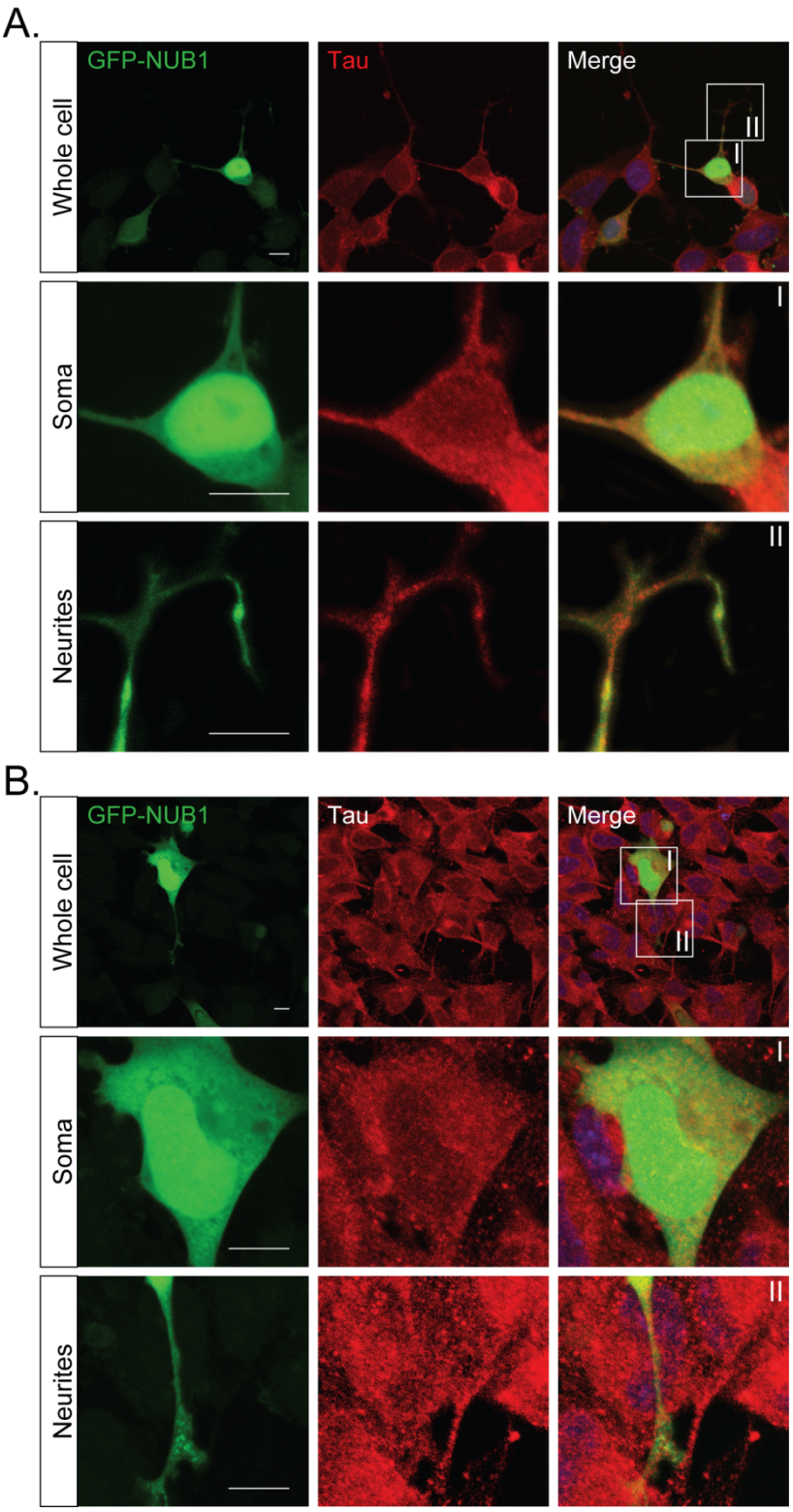

Figure 6.2. *Distribution of GFP-NUB1 and endogenous tau in SH-SY5Y cells.* Cells were transfected with GFP-NUB1. Twenty-four hours after transfection, cells were treated with a vehicle (**A**) or with MG132 (50 μM) (**B**) and fixed with glutaraldehyde (0.3%, 10 min at 37°C). Cells were labelled with the anti-tau primary antibody in conjunction with the AlexaFluor 594 secondary antibody and treated with DAPI to detect nuclei (blue). Images were acquired with a laser scanning confocal microscope (Zeiss LSM 700). The white squares highlight the magnified images of the cell body (soma, I) and neurites (II). Scale bars = 10 μm.

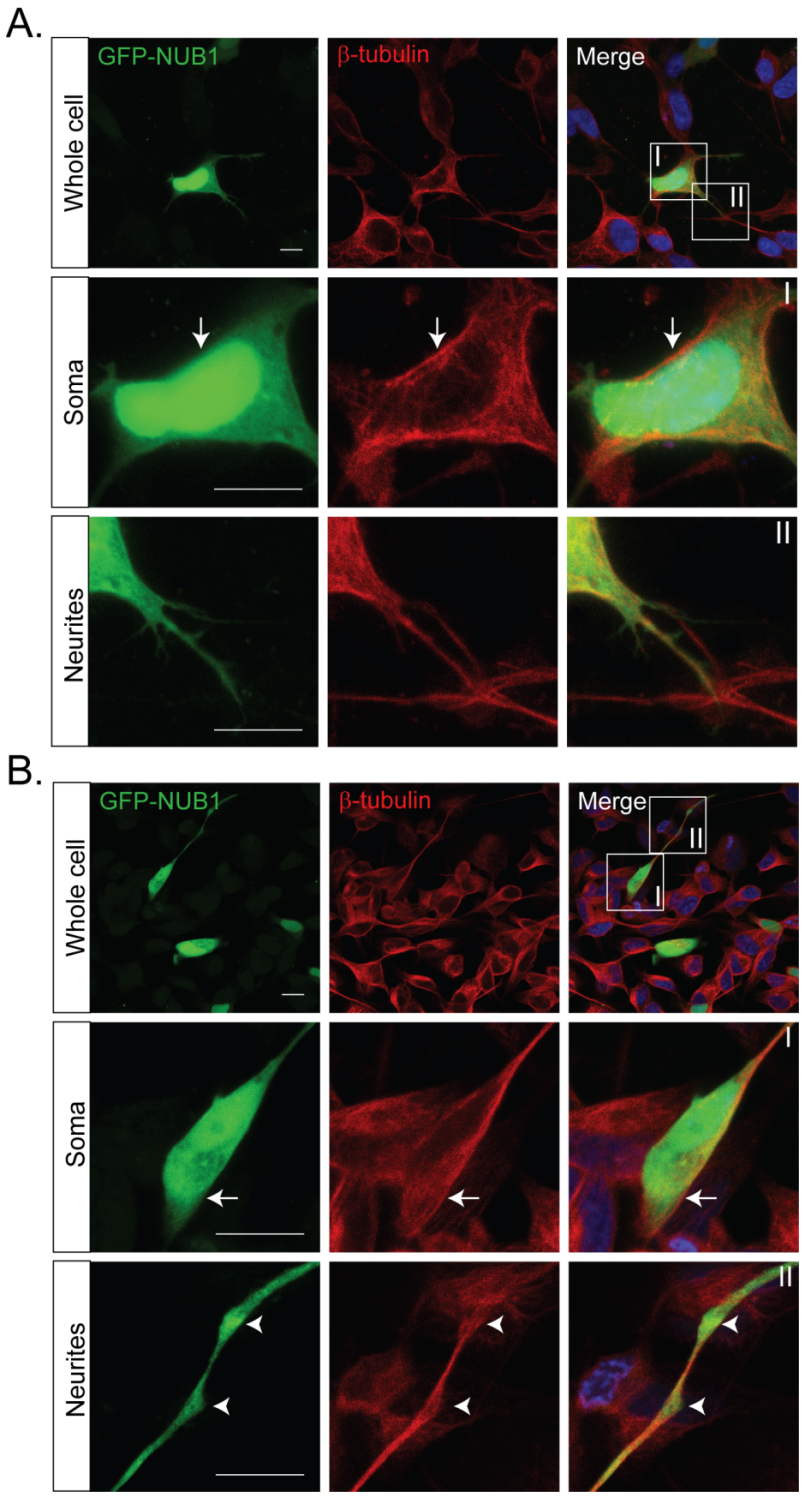

Figure 6.3. *Distribution of GFP-NUB1 and microtubules in SH-SY5Y cells.* Cells were transfected with GFP-NUB1. Twenty-four hours after transfection, cells were treated with a vehicle (A) or with MG132 (50 μM) (B) and fixed with glutaraldehyde (0.3%, 10min at 37°C). Cells were labelled with the anti-β-tubulin primary antibody in conjunction with the AlexaFluor 594 secondary antibody and treated with DAPI to detect nuclei (blue). Images were acquired with a laser scanning confocal microscope (Zeiss LSM 700). The white squares highlight the magnified images of the cell body (soma, I) and neurites (II). The arrows and arrowheads underline the non-overlapping staining. Scale bars =10μm.

In the neurites (Figure 6.3, A and B, II), although there was again some partial overlap, GFP-NUB1 generally did not co-localise with microtubules which could be seen to "surround" the GFP-NUB1 (white arrowheads). This was similar to what was observed in the rat primary cortical neurons (Figure 3.12).
The distribution of endogenous GSK3β was assessed, but although GSK3β was expressed in SH-SY5Y cells, the detection of the endogenous GSK3β with the anti-GSK3β antibody was unsuccessful.

6.2.3. NUB1-FLAG and endogenous GSK3β are in a binary complex in SH-SY5Y cells

NUB1-FLAG co-immunoprecipitated both GFP-tau and HA-GSK3β from SK-N-SH cells (Figure 5.2, 5.3 and 5.4). The anti-NUB1 antibody could not be used to successfully immunoprecipitate endogenous NUB1 from SH-SY5Y cells. Therefore, the interaction between NUB1-FLAG and endogenous tau and GSK3β was explored without proteasome inhibition. It could not be determined if the co-immunoprecipitation of endogenous tau with NUB1-FLAG was successful under the conditions used, as tau resolved to the same molecular weight as the immunoglobulin heavy chain (~ 50 kDa) (data not shown).

SH-SY5Y cells were transfected with NUB1-FLAG. Twenty-four hours after transfection, cells were lysed and proteins were immunoprecipitated with the anti-FLAG antibody (Figure 6.4, A) or anti-GSK3β antibody (Figure 6.4, B) using magnetic beads (Chapter 2.5.6). Cell lysates were resolved on a polyacrylamide gel (10%) and proteins were detected using the anti-FLAG or the anti-GSK3β antibody.

Both GSK3β and NUB1-FLAG were detected in the input fractions. NUB1-FLAG was immunoprecipitated and endogenous GSK3β specifically co-immunoprecipitated with the anti-FLAG antibody (Figure 6.4, A), although only 0.25% of the total levels of GSK3β were co-immunoprecipitated. No GSK3β was non-specifically co-immunoprecipitated with the anti-FLAG antibody in the absence of NUB1-FLAG, or with a non-specific antibody (IgG).

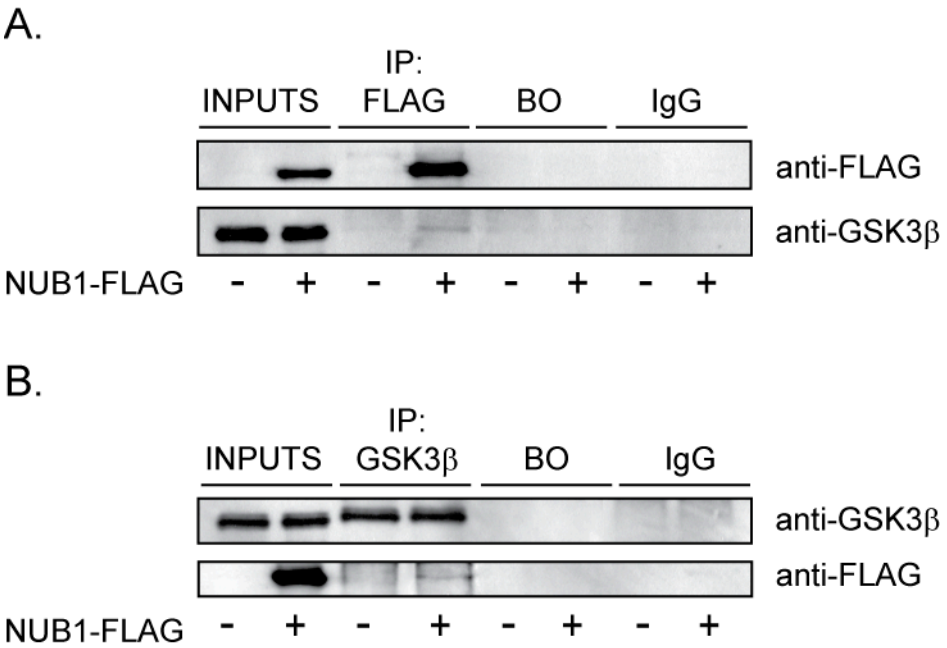

Figure 6.4. *Immunoprecipitation of NUB1-FLAG and GSK3β*. SH-SY5Y cells were transfected with 100 ng of NUB1-FLAG. Twenty-four hours after transfection, cells were lysed with RIPA buffer, and lysates were incubated with magnetic beads in the absence (BO) or presence of anti-FLAG (1:500, A), anti-GSK3β (1:100, B) or a non-specific (IgG) antibody overnight at 4°C. Five µl (INPUTS) or 10 µl (IP) of samples were resolved on a polyacrylamide gel (10%) and proteins were detected by WB using the anti-GSK3β or anti-FLAG antibody.

Reciprocally, the anti-GSK3β antibody immunoprecipitated endogenous GSK3β and specifically co-immunoprecipitated NUB1-FLAG (Figure 6.4, B), with 0.24% of total NUB1 co-immunoprecipitated with the anti-GSKβ antibody. Moreover, neither GSK3β nor NUB1-FLAG were immunoprecipitated with a non-specific antibody (IgG) or with the beads only (BO).

In conclusion, endogenous GSK3β and NUB1-FLAG interacted reciprocally in SH-SY5Y neuroblastoma cells.

6.2.4. NUB1 accelerates GSK3β degradation in SH-SY5Y cells

As shown in Chapter 5, HA-NUB1 reduced HA-GSK3β levels (Figure 5.10, A). Moreover, HA-NUB1 accelerated the degradation of HA-GSK3β after CHX treatment (Figure 5.10, B and C). Therefore, the effect of NUB1 on endogenous GSK3β levels was tested by silencing endogenous NUB1 with a small interfering RNA (siRNA) specific to NUB1 mRNA (Tanji *et al.*, 2006).

SH-SY5Y cells were transfected with a non-specific siRNA (NS siRNA) or NUB1-specific siRNA (NUB1 siRNA), or were mock transfected (Mock). Forty-eight, 72 and 96 h after transfection, cells were lysed and 20 µg of total protein was resolved on a polyacrylamide gel (10%). NUB1, GSK3β and actin were detected by WB using the anti-NUB1, anti-GSK3β or anti-actin antibody respectively (Figure 6.5). The detection of actin was used as a loading control for equal amounts of protein resolved on the polyacrylamide gel. NUB1 was detected in the NS siRNA and mock transfected samples, whereas a strong decrease of NUB1 expression was observed in cells transfected with the NUB1 siRNA at any given time after transfection. Interestingly, a corresponding increase in GSK3β levels was noted following the silencing of endogenous NUB1.

To investigate the role of NUB1 on GSK3β turnover, protein synthesis was inhibited by cycloheximide (CHX) following the silencing of endogenous NUB1 expression (Figure 6.6). Cells were transfected with non-specific siRNA (NS siRNA) or NUB1-specific siRNA (NUB1 siRNA) for 72 h, or were mock transfected (Mock).

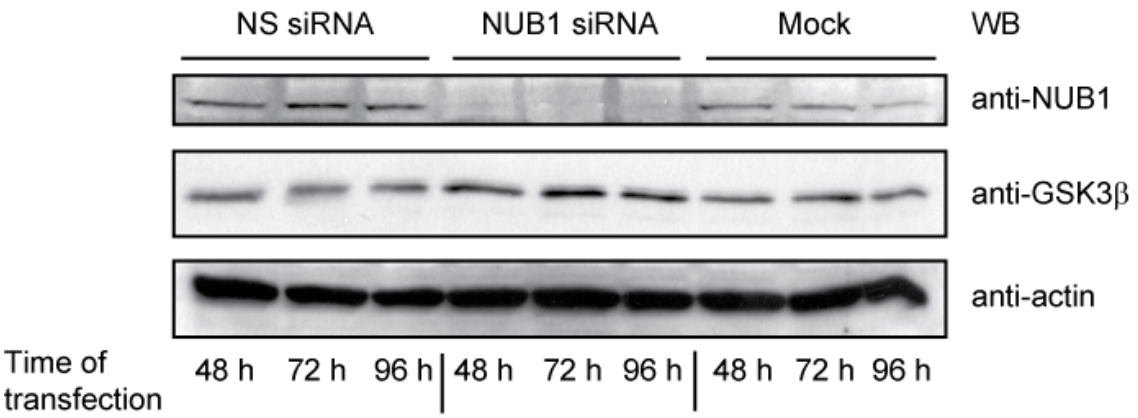

Figure 6.5. *NUB1 silencing in SH-SY5Y cells.* Cells were transfected with a non-specific siRNA (NS siRNA), siRNA specific to NUB1 mRNA (NUB1 siRNA), or were mock transfected (Mock). Cell were lysed with RIPA buffer 48, 72 or 96 h post-transfection and 20 μg of total protein was resolved on a polyacrylamide gel (10%). Proteins were detected by WB using the anti-NUB1, anti-GSK3β or anti-actin antibody.

Cells were treated with CHX for 0, 2, 4 and 6 h, lysed with RIPA buffer and 20 µg of total protein was resolved on a polyacrylamide gel (10%). NUB1, GSK3β and actin were detected by WB using the anti-NUB1, anti-GSK3β and anti-actin antibody respectively (Figure 6.6, A).

Actin, with a half-life of ~48 h (Antecol *et al*., 1986), was used as a loading control. NUB1 expression was detected in both the presence of non-specific siRNA (NS siRNA) and in mock transfected cells (Mock), and the levels of NUB1 decreased over time with CHX treatment (Figure 6.6, A). After 6 h of CHX treatment, the levels of endogenous NUB1 were 49.7±3.2% and 52.5±7% in cells transfected with non-specific siRNA and mock transfected cells respectively, compared to 0 h of CHX treatment.

The levels of NUB1 were specifically and effectively silenced by the NUB1-specific siRNA (Figure 6.6, A). The levels of endogenous GSK3β (Figure 6.6, A) decreased temporally following CHX treatment in the cells transfected with non-specific siRNA (NS siRNA) and in the mock transfected cells (Mock). However, in the cells transfected with the NUB1-specific siRNA, GSK3β levels did not decrease as much nor as rapidly as in the control cells (Figure 6.6, A). The GSK3β levels were measured by densitometry (Figure 6.6, B and C) using ImageJ software. Figure 6.6, B shows that in the mock or NS siRNA transfected cells without any CHX treatment, the GSK3β levels were significantly decreased to 61.7±9.5% and 75.3±11% respectively compared to those in the NUB1 siRNA transfected cells (*p-value* = 0.006 and *p-value* = 0.033 respectively). The GSK3β levels were significantly stabilised over time following the silencing of endogenous NUB1, after 2 h, 4 h and 6 h of CHX treatment (102.7±8.7%, 70.6±10.6% and 46.8±5.6% respectively) compared to GSK3β levels in mock (31.2±5.4%, 17.6±5.4 and 11.2±3.2% respectively; all *p-values* < 0.004) or NS siRNA transfected cells (46.5±8.4%, 29.5±8.5% and 15.4±3% respectively; all *p-values* < 0.009). Moreover, the analysis of the degradation rate of GSK3β (Figure 6.6, C) shows that the silencing of NUB1 expression delayed the degradation of GSK3β.

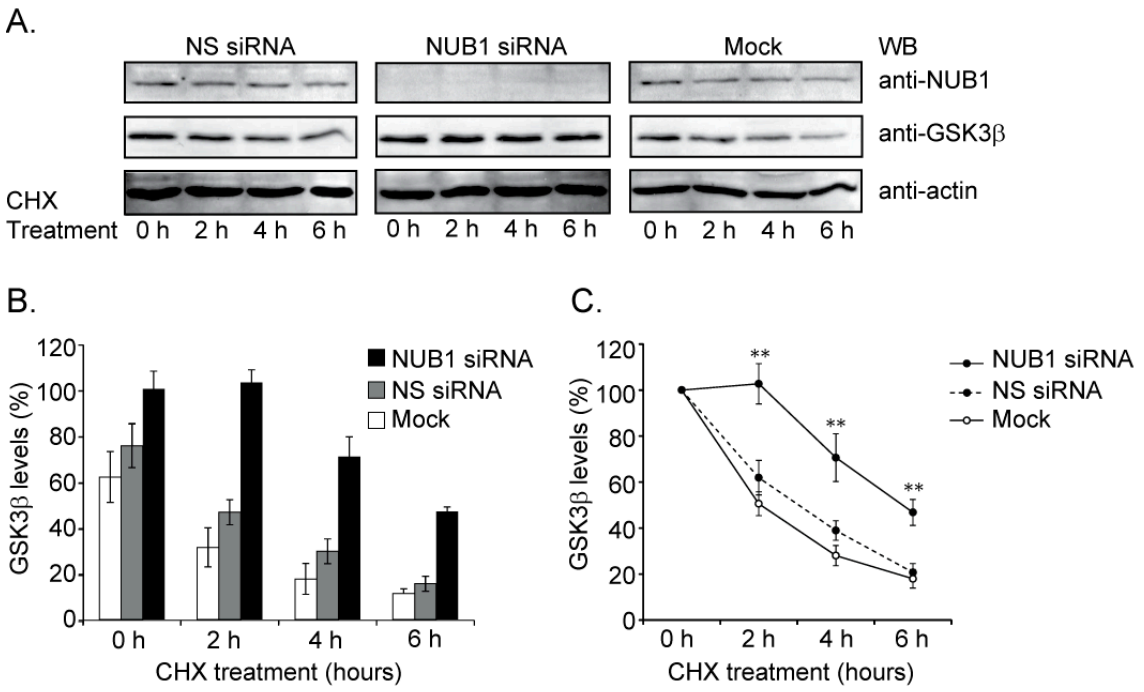

Figure 6.6. *NUB1 effect on GSK3β turnover.* Cells were transfected with a non-specific siRNA (NS siRNA), siRNA specific to NUB1 mRNA (NUB1 siRNA) or were mock transfected (Mock). Seventy-two h post-transfection, cells were treated with CHX (50 µg/ml) for 0, 2, 4, and 6 h, and lysed with RIPA buffer. Proteins (20 µg) were resolved on a polyacrylamide gel (10%) and were detected by WB using the anti-NUB1, anti-GSK3β or anti-actin antibody (**A**). The levels of GSK3β were measured using ImageJ software (**B, C**). (**B**) Comparison of the GSK3β levels. (**C**) Rate of GSK3β degradation following CHX treatment for 0, 2, 4 and 6 h. Statistical significance was determined using an unpaired Student's *t*-test. **p-value*<0.05, ***p-value<0.01.* Error bars are the SEM.

Indeed, after 2 h of CHX treatment in NUB1 siRNA transfected cells, the GSK3β levels were higher than at the 0 h time point (102.7±8.7%) and also significantly higher than the GSK3β levels in NS siRNA and mock transfected cells (61.9±7.5% and 50.6±5.1% respectively, *p-values* = 0.001). After 6 hours of CHX treatment, the levels of GSK3β were decreased to 18±4% and 20.7±3.8% in mock and NS siRNA transfected cells respectively, whereas they were significantly higher in NUB1 siRNA transfected cells (46.8±5.6%).

In conclusion, the increased levels and stability of endogenous GSK3β following the siRNA-mediated silencing of NUB1 expression suggest a role for NUB1 in GSK3β turnover and degradation.

6.3. Discussion

This chapter focused on the potential interactions between endogenous NUB1, tau and GSK3β. Previous chapters showed that NUB1 was a modulator of tau levels, phosphorylation state and aggregation. NUB1 could co-localise and interact with tau, but also with GSK3β. Indeed, chapter 5 demonstrated that NUB1 regulated GSK3β turnover and accelerated its degradation, probably via the proteasome and other pathways.

SK-N-SH neuroblastoma cells did not express detectable levels of either tau or NUB1 and very low levels of GSK3β were detected. Therefore, SK-N-SH cells were a useful tool to analyse the functional impact of the overexpression of the three proteins on one another. However, analysis of the endogenous proteins was thus not possible. Hence, another neuroblastoma cell line, SH-SY5Y, that endogenously expresses NUB1, tau and GSK3β, was used.

The NUB1 antibody raised in our laboratory was not suitable for immunocytochemistry. Thus, the localisation of NUB1 was investigated using GFP-NUB1. It is interesting that SH-SY5Y cells exhibited neurite-like processes, conversely to SK-N-SH cells. The distribution of GFP-NUB1 in SH-SY5Y cells was similar to its localisation in primary neurons and SK-N-SH cells, in that it was mostly nuclear but exhibited an increased cytoplasmic localisation with proteasome inhibition. Endogenous tau was expressed mainly in the cytoplasm, but surprisingly in the nucleus as well, although this could be a fixation/immunolabelling artefact. GFP-NUB1 co-labelled endogenous tau in the cytoplasm and the processes. Moreover, it was also localised with endogenous tau in swellings of the neurite-like processes similar to the varicosities in primary neurons, which were also co-labelled with endogenous tau. On the contrary, although the localisation of GFP-NUB1 appeared to overlap with that of β-tubulin, it is uncertain if this was a specific co-localisation between them. Indeed, similarly to rat primary cortical neurons, GFP-NUB1 appeared to be surrounded by microtubules at the cell periphery and in the swellings of the

neurite-like processes. These results suggest that NUB1 could interact with endogenous tau to modulate its levels and activity.

The anti-NUB1 antibody could not be used successfully in co-immunoprecipitation experiments. Indeed, the NUB1 antibody is a polyclonal antiserum and therefore, purification of the antibody by affinity chromatography using the peptide against which it was raised may have been necessary before its successful use in immunoprecipitation. Thus, co-immunoprecipitation was performed using NUB1-FLAG. The specificity of the co-immunoprecipitation of endogenous tau could not be determined as it resolved to the same molecular weight as the IgG heavy chain on WB. Nonetheless, NUB1-FLAG and endogenous GSK3β were co-immunoprecipitated in a reciprocal manner suggesting that the two proteins interact with each other.

To test the hypothesis that NUB1 could modulate the levels of endogenous GSK3β, GSK3β levels were measured in SH-SY5Y cells following the silencing of NUB1 expression by RNA interference, in the presence of CHX, that inhibits protein synthesis. Chapter 5 showed that overexpression of NUB1 in SK-N-SH cells decreased the stability and accelerated the degradation of GSK3β, therefore the silencing of endogenous NUB1 expression was expected to stabilise endogenous GSK3β levels. NUB1 siRNA successfully downregulated NUB1 levels as soon as 48 h after transfection. Moreover, the levels of GSK3β appeared to be increased in cells transfected with NUB1 siRNA compared to mock transfected cells or cells transfected with the non-specific siRNA. With CHX treatment, both GSK3β and NUB1 levels declined with time in mock transfected cells and cells transfected with the non-specific siRNA. However, in cells transfected with NUB1 siRNA, the levels of GSK3β remained the same after 2 h of treatment with CHX, after which it started to decline at a slower rate compared to the controls. Thus, knock-down of NUB1 delayed the degradation of GSK3β, suggesting that endogenous NUB1 is involved in regulating the turnover of GSK3β. Moreover, both NUB1 and GSK3β levels decline in control cells following treatment with CHX, suggesting that both proteins are degraded and that NUB1 is degraded at the same time as its target proteins. It would interesting to assess whether the effect is proteasome dependent.

To conclude, the analysis of endogenous NUB1, tau and GSK3β in SH-SY5Y neuroblastoma cells confirmed that NUB1 is involved in protein turnover. Indeed, it can co-localise with tau and interact with GSK3β. Moreover, it clearly influences GSK3β turnover, suggesting that NUB1 might be an important regulator of tau phosphorylation.

Chapter 7
Discussion

NUB1 alters tau aggregation and phosphorylated levels. Tau in SK-N-SH cells induced the formation of microtubule bundles, confirming the role of tau in microtubule binding and stabilisation. With the expression of GSK3β and inhibition of the proteasomal activity, a decrease in bundle formation and the formation of tau aggregates were observed. Moreover, the aggregation of tau correlated with an increase in the levels of phosphorylated tau, at least on the S396 and AT8 epitopes. Therefore, the accumulation of endogenous tau when hyperphosphorylated and with proteasome impairment was replicated in SK-N-SH neuroblastoma cells.

In this system, the expression of NUB1 clearly reduced the formation of tau inclusions. NUB1 co-localised with overexpressed tau in SK-N-SH cells, but also with endogenous tau in SH-SY5Y cells and rat primary cortical neurons. In SK-N-SH cells, NUB1 was clearly recruited to tau inclusions, and co-localised with tau in the microtubule bundles. Interestingly, although tau is a microtubule binding protein, NUB1 did not seem to co-localise with endogenous microtubules in rat cortical neurons and SH-SY5Y cells. Moreover, NUB1 and tau were reciprocally co-immunoprecipitated with one another, suggesting that the two proteins interact either directly or indirectly with each other in a complex. Taken together, these results suggest that NUB1 targets tau.

NUB1 reduced the levels of tau phosphorylated on S396, but not the total levels of tau, unless GSK3β was co-expressed and the proteasome activity inhibited. Furthermore, NUB1 co-localised with hyperphosphorylated tau in the inclusions, and with tau in the microtubules. Thus, it is possible that NUB1 targets phosphorylated tau disrupting its binding with the microtubules. Alternatively, NUB1 could indirectly influence tau phosphorylation and aggregation by modulating the tau kinase GSK3β.

NUB1 modulates GSK3β turnover. The levels of tau phosphorylated on S396 were greatly enhanced by the co-expression of GSK3β in SK-N-SH cells. The levels of tau phosphorylated on the AT8 epitope could not be detected without GSK3β co-expression, suggesting that the expression of endogenous kinases in SK-N-SH cells was not sufficient to induce tau hyperphosphorylation, or that their activity was compensated by the endogenous phosphatases. Furthermore, the exogenous expression of GSK3β greatly enhanced the formation of tau inclusions, suggesting that GSK3β, by phosphorylating tau, can promote wild-type tau aggregation. Indeed, GSK3β was found to interact with tau, either directly or indirectly, and to co-label tau inclusions.

The presence of NUB1 in SK-N-SH cells disrupted the interaction of tau and GSK3β, which correlated with the decreased levels of phosphorylated tau and with the fact that GSK3β could no longer be detected in tau inclusions. NUB1 and GSK3β interacted reciprocally in both SK-N-SH and SH-SY5Y cells. Moreover, NUB1 co-localised with GSK3β in the cytoplasm in SK-N-SH cells and rat primary cortical neurons, and increased the levels of GSK3β detected in the nucleus. Thus, NUB1 could target GSK3β and influence its interaction with tau. Indeed, inhibition of transcription by CHX in SK-N-SH cells expressing NUB1 accelerated the turnover of GSK3β, with GSK3β levels reducing faster in the presence of NUB1 than in its absence. This was confirmed by the downregulation of NUB1 in SH-SY5Y cells, which greatly stabilised the levels of endogenous GSK3β following CHX treatment. Interestingly, the levels of NUB1 were also decreased in the presence of CHX, suggesting that NUB1 was also degraded. Therefore, NUB1 might target GSK3β and be degraded along with its target.

NUB1 as a potential proteasome shuttle. Impairment of the UPS is an important factor in inclusion formation in cells, and has been reported in amyloidosis such as AD. Indeed, Ub and proteasomal components are recruited to NFTs in AD, as a result of the failure of the UPS to degrade tau. In human brain sections used in this study, Ub was seen to accumulate in NFTs and dystrophic neurites in AD patients, confirming the presence of Ub in tau and Aβ inclusions.

Interestingly, the ULM FAT10 was also observed to accumulate in brain sections from AD patients. Although the increased expression of FAT10 could result from an increase in the neuroinflammatory response, FAT10 could be upregulated in AD as a consequence of targeting tau or Aβ for NUB1-mediated regulation. FAT10 and its conjugates interact with NUB1, which induces their proteasomal degradation. A role for NUB1 in regulating protein levels in neurons was also emphasised by the similarity between the localisation of NUB1 and NEDD8, another ULM targeted by NUB1 for proteasomal degradation. In AD patients, the localisation of both NEDD8 and NUB1 was predominantly cytoplasmic in the surviving pyramidal neurons of the hippocampus, suggesting a specific function for both proteins in this subcellular location or a result of dysregulation of the cell cycle.

The proteasome independent influence of NUB1. NUB1 might also decrease GSK3β levels in a proteasome-independent manner. The fact that proteasome inhibition did not change the overall levels or the rate of degradation of GSK3β in the presence of NUB1 suggests that the increased rate of GSK3β turnover in the presence of NUB1 might be proteasome independent. GSK3β has been shown to be sequestered in MVBs upon Wnt signalling. It is therefore possible that NUB1 triggers GSK3β sequestration in MVBs or shuttles GSK3β to the endosomal pathway. Indeed, the expression of NUB1 induced a change in the GSK3β sub-localisation in cytoplasm, which was more particulate, perhaps as a result of sequestration to MVBs. Targeting of proteins into this degradative pathway is largely dependent on post-translation modification by Ub and proteins with UBA domains have been involved in ESCRT complex formation. FAT10 or NEDD8, similar to Ub, could be involved in substrate recognition and targeting to the MVBs.

Interestingly, NUB1 might influence Wnt signalling by sequestration of GSK3β to the MVB/endosomal pathway. Indeed, NUB1-dependent targeting of GSK3β to MVB and the endosomal pathway would free β-catenin from GSK3β-mediated phosphorylation and degradation. Therefore, β-catenin would be free to translocate into the nucleus and activate the transcription of its target genes, hence the canonical Wnt signalling pathway would be activated. On the other

hand, further regulation could occur at the level of the β-catenin CRL. NUB1, by targeting NEDD8 degradation, might inhibit β-catenin ubiquitination by the SCF, thus reducing β-catenin degradation. Therefore, the influence of NUB1 on Wnt signalling would be a double edged sword.

The localisation of NUB1 in SK-N-SH cells, SH-SY5Y cells, and even rat primary cortical neurons was predominantly nuclear but was stabilised in the cytoplasm following inhibition of the proteasome. Therefore, NUB1 localisation in cells may be highly dynamic and regulated by complex mechanisms (such as cell cycle or signalling pathways, e.g. Wnt signalling) to target specific substrates.

The UBA domains of NUB1 are necessary but not essential. The NUB1LΔUBA1-3 mutant was defective in mediating the accelerated turnover of GSK3β, suggesting that the UBA domains are required for the degradation of GSK3β. Notably, the proteasome binding site is thought to reside in the C-terminal domain of NUB1, and this may be lost in the NUB1LΔUBA1-3 mutant. However, the mutant may still effectively interact with GSK3β or tau or both within a complex, thereby disrupting the interaction between them and reducing the levels of tau phosphorylated on S396. The reason why the NUB1LΔUBA1-3 mutant was defective in reducing the aggregation of tau despite decreasing the levels of phosphorylated tau is still unclear. A potential explanation would be that even a small percentage of non-native oligomeric tau species would convert and sequester normal tau into an aggregation-prone conformation. NUB1 might be able to target tau as well as non-native oligomeric tau species and enhance their degradation before they form bigger aggregates of inclusions, which remains the end point of tau aggregation. Although the NUB1LΔUBA1-3 mutant might interfere with tau phosphorylation, its ability to induce tau degradation might also be impaired, thus the number of inclusions remain the same.

With proteasome inhibition, the levels of GSK3β were only slightly but not significantly stabilised in the presence of NUB1, although they were considerably stabilised and the rate of degradation of GSK3β was increased in the presence of NUB1L. This suggests that the presence of a third UBA domain

in NUB1L is responsible for the accelerated turnover of GSK3β levels, and is implicated in the proteasome-dependent influence of NUB1L. Taken together, the UBA domains are unable to reduce inclusions and GSK3β levels, but can still reduce tau phosphorylation. Thus, the mutant NUB1LΔUBA1-3 could still interact with GSK3β, preventing GSK3β-dependent tau phosphorylation. Therefore, the UBA domains might be necessary for the protein degradation role of NUB1 but not essential for protein targeting and interaction.

The mutant NUB1LΔUBL had a significant effect on tau aggregation and decreased the overall levels of GSK3β, although it did not accelerate the rate of GSK3β degradation. The UBL domain of NUB1L has been previously reported to be necessary for NUB1L acceleration of FAT10 proteasomal degradation (Schmidtke *et al*., 2006). Thus, it would seem that the UBL domain of NUB1 is not necessary for its effect on either tau aggregation or GSK3β degradation, but that the UBL domain might enhance the effect of NUB1 in terms of the accelerated turnover of substrates.

In conclusion, the following model has been proposed for the function of NUB1 in tau and GSK3β modulation. By interacting with both GSK3β and tau, NUB1 might disrupt the GSK3β-dependent phosphorylation of tau, thus preventing tau inclusion formation. NUB1 can reduce GSK3β levels by proteasomal degradation, or may induce GSK3β sequestration in MVBs and lysosomal degradation. On the other hand, NUB1 might also be able to target tau or altered tau species (e.g. hyperphosphorylated tau) for proteasomal degradation (Figure 7.1).

Therefore, this study has identified an important and novel role for NUB1 in the regulation of tau and GSK3β-dependent tau phosphorylation. Importantly, GSK3β has been found to be a novel target for NUB1-dependent degradation. The role of GSK3β in AD involves the anomalous phosphorylation of tau, but also anomalous cell-cycle regulation by targeting p53 and β-catenin, and might be a potential link between the Aβ and NFT pathologies in AD. On the other hand, NUB1 co-localises with and binds tau, and the duo NEDD8 and NUB1, both expressed in pyramidal neurons, might be implicated in targeting tau for

proteasomal degradation. Taken together, NUB1, by regulating tau and GSK3β may potentially be important in the neuropathogenesis of AD and other neurodegenerative disorders.

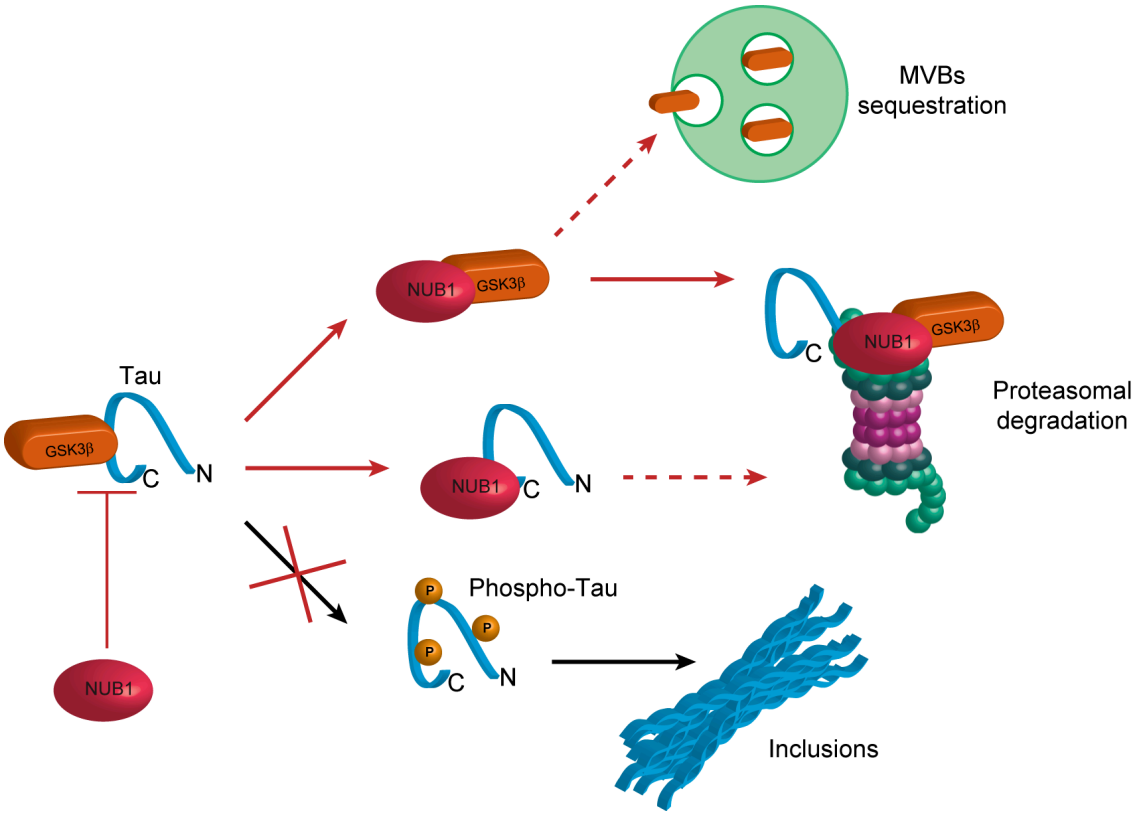

Figure 7.1. *Potential regulation of GSK3β and tau by NUB1*. NUB1 disrupts the interaction between GSK3β and tau, thus reducing tau phosphorylation and preventing tau inclusion formation. NUB1 targets GSK3β for proteasomal degradation and potentially lysosomal degradation via MVBs. NUB1 also interacts with tau and could target tau for proteasomal degradation. NUB1 interaction with either GSK3β or tau might be direct, or necessitate the primer neddylation of the proteins,

References

Abraha A, Ghoshal N, Gamblin TC, Cryns V, Berry RW, Kuret J, Binder LI, 2000. C-terminal inhibition of tau assembly in vitro and in Alzheimer's disease. J. Cell Sci. 113 Pt 21: 3737-3745.

Aichem A, Pelzer C, Lukasiak S, Kalveram B, Sheppard PW, Rani N, Schmidtke G, Groettrup M, 2010. USE1 is a bispecific conjugating enzyme for ubiquitin and FAT10, which FAT10ylates itself in cis. Nat. Commun. 1: 13.

Al-Bassam J, Ozer RS, Safer D, Halpain S, Milligan RA, 2002. MAP2 and tau bind longitudinally along the outer ridges of microtubule protofilaments. J. Cell Biol. 157: 1187-1196.

Andersson FI, Werrell EF, McMorran L, Crone WJ, Das C, Hsu ST, Jackson SE, 2011. The effect of Parkinson's-disease-associated mutations on the deubiquitinating enzyme UCH-L1. J. Mol. Biol. 407: 261-272.

Antecol MH, Darveau A, Sonenberg N, Mukherjee BB, 1986. Altered biochemical properties of actin in normal skin fibroblasts from individuals predisposed to dominantly inherited cancers. Cancer Res. 46: 1867-1873.

Arias E, Cuervo AM, 2011. Chaperone-mediated autophagy in protein quality control. Curr. Opin. Cell Biol. 23: 184-189.

Avila J, Gomez de BE, Engel T, Perez M, Martin-Maestro P, Fuster-Matanzo A, Goni-Oliver P, Lucas JJ, Hernandez F, 2010. Tau kinase I overexpression induces dentate gyrus degeneration. Neurodegener. Dis. 7: 13-15.

Babu JR, Geetha T, Wooten MW, 2005. Sequestosome 1/p62 shuttles polyubiquitinated tau for proteasomal degradation. J. Neurochem. 94: 192-203.

Balaraman Y, Limaye AR, Levey AI, Srinivasan S, 2006. Glycogen synthase kinase 3beta and Alzheimer's disease: pathophysiological and therapeutic significance. Cell Mol. Life Sci. 63: 1226-1235.

Ballard C, Gauthier S, Corbett A, Brayne C, Aarsland D, Jones E, 2011. Alzheimer's disease. Lancet 377: 1019-1031.

Ballatore C, Lee VM, Trojanowski JQ, 2007. Tau-mediated neurodegeneration in Alzheimer's disease and related disorders. Nat. Rev. Neurosci. 8: 663-672.

Bett JS, Kanuga N, Richet E, Schmidtke G, Groettrup M, Cheetham ME, van der SJ, 2012. The Inherited Blindness Protein AIPL1 Regulates the Ubiquitin-Like FAT10 Pathway. PLoS. One. 7: e30866.

Bertram L, Hiltunen M, Parkinson M, Ingelsson M, Lange C, Ramasamy K, Mullin K, Menon R, Sampson AJ, Hsiao MY, Elliott KJ, Velicelebi G, Moscarillo T, Hyman BT, Wagner SL, Becker KD, Blacker D, Tanzi RE, 2005. Family-based association between Alzheimer's disease and variants in UBQLN1. N. Engl. J. Med. 352: 884-894.

Biedler JL, Helson L, Spengler BA, 1973. Morphology and growth, tumorigenicity, and cytogenetics of human neuroblastoma cells in continuous culture. Cancer Res., 33, 2643-2652.

Biedler JL, Roffler-Tarlov S, Schachner M, Freedman LS, 1978. Multiple neurotransmitter synthesis by human neuroblastoma cell lines and clones. Cancer Res., 38, 3751-3757.

Biernat J, Mandelkow EM, 1999. The development of cell processes induced by tau protein requires phosphorylation of serine 262 and 356 in the repeat domain and is inhibited by phosphorylation in the proline-rich domains. Mol. Biol. Cell 10: 727-740.

Bijur GN, Jope RS, 2003. Glycogen synthase kinase-3 beta is highly activated in nuclei and mitochondria. Neuroreport 14: 2415-2419.

Bolte S, Cordelieres FP, 2006. A guided tour into subcellular colocalization analysis in light microscopy. J. Microsc. 224: 213-232.

Braak H, Braak E, 1991. Neuropathological stageing of Alzheimer-related changes. Acta Neuropathol. 82: 239-259.

Braak H, Braak E, 1995. Staging of Alzheimer's disease-related neurofibrillary changes. Neurobiol. Aging 16: 271-278.

Braak H, Thal DR, Ghebremedhin E, Del TK, 2011. Stages of the pathologic process in Alzheimer disease: age categories from 1 to 100 years. J. Neuropathol. Exp. Neurol. 70: 960-969.

Bramblett GT, Goedert M, Jakes R, Merrick SE, Trojanowski JQ, Lee VM, 1993. Abnormal tau phosphorylation at Ser396 in Alzheimer's disease recapitulates development and contributes to reduced microtubule binding. Neuron 10: 1089-1099.

Brandt R, Leger J, Lee G, 1995. Interaction of tau with the neural plasma membrane mediated by tau's amino-terminal projection domain. J. Cell Biol. 131: 1327-1340.

Bruijn LI, Krishnamurthy PK, Gallo JM, 2004. Distinct patterns of tau-dependent process formation in mammalian cell lines. Neuroreport 15: 2223-2226.

Buchberger A, 2002. From UBA to UBX: new words in the ubiquitin vocabulary. Trends Cell Biol. 12: 216-221.

Buee L, Bussiere T, Buee-Scherrer V, Delacourte A, Hof PR, 2000. Tau protein isoforms, phosphorylation and role in neurodegenerative disorders. Brain Res. Brain Res. Rev. 33: 95-130.

Bugiani O, Giaccone G, Frangione B, Ghetti B, Tagliavini F, 1989. Alzheimer patients: preamyloid deposits are more widely distributed than senile plaques throughout the central nervous system. Neurosci. Lett. 103: 263-268.

Bukau B, Weissman J, Horwich A, 2006. Molecular chaperones and protein quality control. Cell 125: 443-451.

Burns MP, Zhang L, Rebeck GW, Querfurth HW, Moussa CE, 2009. Parkin promotes intracellular Abeta1-42 clearance. Hum. Mol. Genet. 18: 3206-3216.

Caccamo A, Oddo S, Tran LX, LaFerla FM, 2007. Lithium reduces tau phosphorylation but not A beta or working memory deficits in a transgenic model with both plaques and tangles. Am. J. Pathol. 170: 1669-1675.

Calkins MJ, Manczak M, Mao P, Shirendeb U, Reddy PH, 2011. Impaired mitochondrial biogenesis, defective axonal transport of mitochondria, abnormal mitochondrial dynamics and synaptic degeneration in a mouse model of Alzheimer's disease. Hum. Mol. Genet. 20: 4515-4529.

Callahan LM, Coleman PD, 1995. Neurons bearing neurofibrillary tangles are responsible for selected synaptic deficits in Alzheimer's disease. Neurobiol. Aging 16: 311-314.

Cecarini V, Ding Q, Keller JN, 2007. Oxidative inactivation of the proteasome in Alzheimer's disease. Free Radic. Res. 41: 673-680.

Chadwick L, Gentle L, Strachan J, Layfield R, 2012. Unchained maladie - a reassessment of the role of Ubb(+1) -capped polyubiquitin chains in Alzheimer's disease. Neuropathol. Appl. Neurobiol. 38: 118-31.

Chaugule VK, Burchell L, Barber KR, Sidhu A, Leslie SJ, Shaw GS, Walden H. 2011. Autoregulation of Parkin activity through its ubiquitin-like domain. EMBO J. 30: 2853–2867.

Chen L, Madura K, 2006. Evidence for distinct functions for human DNA repair factors hHR23A and hHR23B. FEBS Lett. 580: 3401-3408.

Chen Y, Bodles AM, McPhie DL, Neve RL, Mrak RE, Griffin WS, 2007. APP-BP1 inhibits Abeta42 levels by interacting with Presenilin-1. Mol. Neurodegener. 2: 3.

Chen Y, Liu W, McPhie DL, Hassinger L, Neve RL, 2003. APP-BP1 mediates APP-induced apoptosis and DNA synthesis and is increased in Alzheimer's disease brain. J. Cell Biol. 163: 27-33.

Chen Y, McPhie DL, Hirschberg J, Neve RL, 2000. The amyloid precursor protein-binding protein APP-BP1 drives the cell cycle through the S-M checkpoint and causes apoptosis in neurons. J. Biol. Chem. 275: 8929-8935.

Cheung ZH, Ip NY, 2011. Autophagy deregulation in neurodegenerative diseases - recent advances and future perspectives. J. Neurochem. 118: 317-325.

Chiu YH, Sun Q, Chen ZJ, 2007. E1-L2 activates both ubiquitin and FAT10. Mol. Cell 27: 1014-1023.

Cho JH, Johnson GV, 2003. Glycogen synthase kinase 3beta phosphorylates tau at both primed and unprimed sites. Differential impact on microtubule binding. J. Biol. Chem. 278: 187-193.

Ciechanover A, Brundin P, 2003. The ubiquitin proteasome system in neurodegenerative diseases: sometimes the chicken, sometimes the egg. Neuron 40: 427-446.

Conklin D, Holderman S, Whitmore TE, Maurer M, Feldhaus AL, 2000. Molecular cloning, chromosome mapping and characterization of UBQLN3 a testis-specific gene that contains an ubiquitin-like domain. Gene 249: 91-98.

Crouch PJ, Harding SM, White AR, Camakaris J, Bush AI, Masters CL, 2008. Mechanisms of A beta mediated neurodegeneration in Alzheimer's disease. Int. J. Biochem. Cell Biol. 40: 181-198.

Cuchillo-Ibanez I, Seereeram A, Byers HL, Leung KY, Ward MA, Anderton BH, Hanger DP, 2008. Phosphorylation of tau regulates its axonal transport by controlling its binding to kinesin. FASEB J. 22: 3186-3195.

Daoud H, Rouleau GA, 2011. A role for ubiquilin 2 mutations in neurodegeneration. Nat. Rev. Neurol. 7: 599-600.

de Pril, Fischer DF, Roos RA, van Leeuwen FW, 2007. Ubiquitin-conjugating enzyme E2-25K increases aggregate formation and cell death in polyglutamine diseases. Mol. Cell Neurosci. 34: 10-19.

Dehmelt L, Halpain S, 2005. The MAP2/Tau family of microtubule-associated proteins. Genome Biol. 6: 204.

Demand J, Alberti S, Patterson C, Hohfeld J, 2001. Cooperation of a ubiquitin domain protein and an E3 ubiquitin ligase during chaperone/proteasome coupling. Curr. Biol. 11: 1569-1577.

Deng HX, Chen W, Hong ST, Boycott KM, Gorrie GH, Siddique N, Yang Y, Fecto F, Shi Y, Zhai H, Jiang H, Hirano M, Rampersaud E, Jansen GH, Donkervoort S, Bigio EH, Brooks BR, Ajroud K, Sufit RL, Haines JL, Mugnaini E, Pericak-Vance MA, Siddique T, 2011. Mutations in UBQLN2 cause dominant X-linked juvenile and adult-onset ALS and ALS/dementia. Nature 477: 211-215.

Deng L, Wang C, Spencer E, Yang L, Braun A, You J, Slaughter C, Pickart C, Chen ZJ, 2000. Activation of the IkappaB kinase complex by TRAF6 requires a dimeric ubiquitin-conjugating enzyme complex and a unique polyubiquitin chain. Cell. 103: 351-361.

Dennissen FJ, Kholod N, van Leeuwen FW, 2012. The ubiquitin proteasome system in neurodegenerative diseases: culprit, accomplice or victim? Prog. Neurobiol. 96: 190-207.

Deveraux Q, Ustrell V, Pickart C, Rechsteiner M, 1994. A 26 S protease subunit that binds ubiquitin conjugates. J. Biol. Chem. 269: 7059-7061.

Diaz-Hernandez M, Valera AG, Moran MA, Gomez-Ramos P, varez-Castelao B, Castano JG, Hernandez F, Lucas JJ, 2006. Inhibition of 26S proteasome activity by huntingtin filaments but not inclusion bodies isolated from mouse and human brain. J. Neurochem. 98: 1585-1596.

Dikic I, Wakatsuki S, Walters KJ, 2009. Ubiquitin-binding domains - from structures to functions. Nat. Rev. Mol. Cell Biol. 10: 659-671.

Dil KA, Kito K, Abe Y, Shin RW, Kamitani T, Ueda N, 2003. NEDD8 protein is involved in ubiquitinated inclusion bodies. J. Pathol. 199: 259-266.

DiTella M, Feiguin F, Morfini G, Caceres A, 1994. Microfilament-associated growth cone component depends upon Tau for its intracellular localization. Cell Motil. Cytoskeleton. 29: 117-130.

Doi H, Mitsui K, Kurosawa M, Machida Y, Kuroiwa Y, Nukina N, 2004. Identification of ubiquitin-interacting proteins in purified polyglutamine aggregates. FEBS Lett. 571: 171-176.

Dou F, Netzer WJ, Tanemura K, Li F, Hartl FU, Takashima A, Gouras GK, Greengard P, Xu H, 2003. Chaperones increase association of tau protein with microtubules. Proc. Natl. Acad. Sci. U. S. A 100: 721-726.

Dubey M, Chaudhury P, Kabiru H, Shea TB, 2008. Tau inhibits anterograde axonal transport and perturbs stability in growing axonal neurites in part by

displacing kinesin cargo: neurofilaments attenuate tau-mediated neurite instability. Cell Motil. Cytoskeleton. 65: 89-99.

Duncan LM, Piper S, Dodd RB, Saville MK, Sanderson CM, Luzio JP, Lehner PJ, 2006. Lysine-63-linked ubiquitination is required for endolysosomal degradation of class I molecules. EMBO J. 25: 1635-1645.

Duyckaerts C, Delatour B, Potier MC, 2009. Classification and basic pathology of Alzheimer disease. Acta Neuropathol. 118: 5-36.

Dye RB, Fink SP, Williams RC, Jr., 1993. Taxol-induced flexibility of microtubules and its reversal by MAP-2 and Tau. J. Biol. Chem. 268: 6847-6850.

Ebneth A, Godemann R, Stamer K, Illenberger S, Trinczek B, Mandelkow E, 1998. Overexpression of tau protein inhibits kinesin-dependent trafficking of vesicles, mitochondria, and endoplasmic reticulum: implications for Alzheimer's disease. J. Cell Biol. 143: 777-794.

Elliott E, Laufer O, Ginzburg I, 2009. BAG-1M is up-regulated in hippocampus of Alzheimer's disease patients and associates with tau and APP proteins. J. Neurochem. 109: 1168-1178.

Elliott E, Tsvetkov P, Ginzburg I, 2007. BAG-1 associates with Hsc70.Tau complex and regulates the proteasomal degradation of Tau protein. J. Biol. Chem. 282: 37276-37284.

Evans RJ, Schwarz N, Nagel-Wolfrum K, Wolfrum U, Hardcastle AJ, Cheetham ME, 2010. The retinitis pigmentosa protein RP2 links pericentriolar vesicle transport between the Golgi and the primary cilium. Hum. Mol. Genet. 19: 1358-1367.

Falsone SF, Kungl AJ, Rek A, Cappai R, Zangger K, 2009. The molecular chaperone Hsp90 modulates intermediate steps of amyloid assembly of the Parkinson-related protein alpha-synuclein. J. Biol. Chem. 284: 31190-31199.

Farah CA, Perreault S, Liazoghli D, Desjardins M, Anton A, Lauzon M, Paiement J, Leclerc N, 2006. Tau interacts with Golgi membranes and mediates their association with microtubules. Cell Motil. Cytoskeleton 63: 710-724.

Feng Y, Walsh CA, 2001. Protein-protein interactions, cytoskeletal regulation and neuronal migration. Nat. Rev. Neurosci. 2: 408-416.

Finder VH, 2010. Alzheimer's disease: a general introduction and pathomechanism. J. Alzheimers. Dis. 22 Suppl 3: 5-19.

Finney N, Walther F, Mantel PY, Stauffer D, Rovelli G, Dev KK, 2003. The cellular protein level of parkin is regulated by its ubiquitin-like domain. J. Biol. Chem. 278: 16054-16058.

Finsterer J, 2011. Parkinson's syndrome and Parkinson's disease in mitochondrial disorders. Mov Disord. 26: 784-791.

Fischer D, Mukrasch MD, Biernat J, Bibow S, Blackledge M, Griesinger C, Mandelkow E, Zweckstetter M, 2009. Conformational changes specific for pseudophosphorylation at serine 262 selectively impair binding of tau to microtubules. Biochemistry 48: 10047-10055.

Flajolet M, He G, Heiman M, Lin A, Nairn AC, Greengard P, 2007. Regulation of Alzheimer's disease amyloid-beta formation by casein kinase I. Proc. Natl. Acad. Sci. U. S. A 104: 4159-4164.

Frydman J, 2001. Folding of newly translated proteins in vivo: the role of molecular chaperones. Annu. Rev. Biochem. 70: 603-647.

Gao F, Cheng J, Shi T, Yeh ET, 2006. Neddylation of a breast cancer-associated protein recruits a class III histone deacetylase that represses NFkappaB-dependent transcription. Nat. Cell Biol. 8: 1171-1177.

Garcia-Sierra F, Jarero-Basulto JJ, Kristofikova Z, Majer E, Binder LI, Ripova D, 2011. Ubiquitin is Associated with Early Truncation of Tau Protein at Aspartic Acid(421) during the Maturation of Neurofibrillary Tangles in Alzheimer's Disease. Brain Pathol.

Agarwal-Mawal A, Qureshi HY, Cafferty PW, Yuan Z, Han D, Lin R, Paudel HK, 2003. 14-3-3 connects glycogen synthase kinase-3 beta to tau within a brain microtubule-associated tau phosphorylation complex. J. Biol. Chem. 278: 12722-12728.

Geetha T, Wooten MW, 2002. Structure and functional properties of the ubiquitin binding protein p62. FEBS Lett. 512: 19-24.

Gendron TF, Petrucelli L, 2009. The role of tau in neurodegeneration. Mol. Neurodegener. 4: 13.

Georgieff IS, Liem RK, Couchie D, Mavilia C, Nunez J, Shelanski ML, 1993. Expression of high molecular weight tau in the central and peripheral nervous systems. J. Cell Sci. 105 (Pt 3): 729-737.

Giese KP, 2009. GSK-3: a key player in neurodegeneration and memory. IUBMB. Life 61: 516-521.

Goedert M, Spillantini MG, Jakes R, Rutherford D, Crowther RA, 1989. Multiple isoforms of human microtubule-associated protein tau: sequences and localization in neurofibrillary tangles of Alzheimer's disease. Neuron 3: 519-526.

Goedert M, 2004. Tau protein and neurodegeneration. Semin. Cell Dev. Biol. 15: 45-49.

Goldbaum O, Oppermann M, Handschuh M, Dabir D, Zhang B, Forman MS, Trojanowski JQ, Lee VM, Richter-Landsberg C, 2003. Proteasome inhibition stabilizes tau inclusions in oligodendroglial cells that occur after treatment with okadaic acid. J. Neurosci. 23: 8872-8880.

Gong CX, Shaikh S, Wang JZ, Zaidi T, Grundke-Iqbal I, Iqbal K, 1995. Phosphatase activity toward abnormally phosphorylated tau: decrease in Alzheimer disease brain. J. Neurochem. 65: 732-738.

Gong P, Canaan A, Wang B, Leventhal J, Snyder A, Nair V, Cohen CD, Kretzler M, D'Agati V, Weissman S, Ross MJ, 2010. The ubiquitin-like protein FAT10 mediates NF-kappaB activation. J. Am. Soc. Nephrol. 21: 316-326.

Grunwald D, Singer RH, Rout M, 2011. Nuclear export dynamics of RNA-protein complexes. Nature 475: 333-341.

Gu Y, Oyama F, Ihara Y, 1996. Tau is widely expressed in rat tissues. J. Neurochem. 67: 1235-1244.

Haapasalo A, Viswanathan J, Bertram L, Soininen H, Tanzi RE, Hiltunen M, 2010. Emerging role of Alzheimer's disease-associated ubiquilin-1 in protein aggregation. Biochem. Soc. Trans. 38: 150-155.

Haase C, Stieler JT, Arendt T, Holzer M, 2004. Pseudophosphorylation of tau protein alters its ability for self-aggregation. J. Neurochem. 88: 1509-1520.

Hampel H, Prvulovic D, Teipel SJ, Bokde AL, 2011. Recent developments of functional magnetic resonance imaging research for drug development in Alzheimer's disease. Prog. Neurobiol. 95: 570-578.

Hanger DP, Anderton BH, Noble W, 2009. Tau phosphorylation: the therapeutic challenge for neurodegenerative disease. Trends Mol. Med. 15: 112-119.

Hardy J, Selkoe DJ, 2002. The amyloid hypothesis of Alzheimer's disease: progress and problems on the road to therapeutics. Science 297: 353-356.

Hartl FU, Bracher A, Hayer-Hartl M, 2011. Molecular chaperones in protein folding and proteostasis. Nature 475: 324-332.

Hartl FU, Hayer-Hartl M, 2002. Molecular chaperones in the cytosol: from nascent chain to folded protein. Science 295: 1852-1858.

Hartl FU, Hayer-Hartl M, 2009. Converging concepts of protein folding in vitro and in vivo. Nat. Struct. Mol. Biol. 16: 574-581.

Hartmann-Petersen R, Gordon C, 2004. Integral UBL domain proteins: a family of proteasome interacting proteins. Semin. Cell Dev. Biol. 15: 247-259.

He Y, Delaere P, Duyckaerts C, Wasowicz M, Piette F, Hauw JJ, 1993. Two distinct ubiquitin immunoreactive senile plaques in Alzheimer's disease: relationship with the intellectual status in 29 cases. Acta Neuropathol. 86: 109-116.

Heng MY, Duong DK, Albin RL, Tallaksen-Greene SJ, Hunter JM, Lesort MJ, Osmand A, Paulson HL, Detloff PJ, 2010. Early autophagic response in a novel knock-in model of Huntington disease. Hum. Mol. Genet. 19: 3702-3720.

Hernandez F, Perez M, de Barreda EG, Goni-Oliver P, Avila J, 2008. Tau as a molecular marker of development, aging and neurodegenerative disorders. Curr. Aging Sci. 1: 56-61.

Hernandez F, Gomez de BE, Fuster-Matanzo A, Lucas JJ, Avila J, 2010. GSK3: a possible link between beta amyloid peptide and tau protein. Exp. Neurol. 223: 322-325.

Hernandez-Ortega K, Quiroz-Baez R, Arias C, 2011. Cell cycle reactivation in mature neurons: a link with brain plasticity, neuronal injury and neurodegenerative diseases? Neurosci. Bull. 27: 185-196.

Herrmann J, Lerman LO, Lerman A, 2007. Ubiquitin and ubiquitin-like proteins in protein regulation. Circ. Res. 100: 1276-1291.

Hershko A, Ciechanover A, 1998. The ubiquitin system. Annu. Rev. Biochem. 67: 425-479.

Hicke L, 2001. Protein regulation by monoubiquitin. Nat. Rev. Mol. Cell Biol. 2: 195-201.

Hicke L, Schubert HL, Hill CP, 2005. Ubiquitin-binding domains. Nat. Rev. Mol. Cell Biol. 6: 610-621.

Hiltunen M, Lu A, Thomas AV, Romano DM, Kim M, Jones PB, Xie Z, Kounnas MZ, Wagner SL, Berezovska O, Hyman BT, Tesco G, Bertram L, Tanzi RE, 2006. Ubiquilin 1 modulates amyloid precursor protein trafficking and Abeta secretion. J. Biol. Chem. 281: 32240-32253.

Hipp MS, Raasi S, Groettrup M, Schmidtke G, 2004. NEDD8 ultimate buster-1L interacts with the ubiquitin-like protein FAT10 and accelerates its degradation. J. Biol. Chem. 279: 16503-16510.

Hirokawa N, Shiomura Y, Okabe S, 1988. Tau proteins: the molecular structure and mode of binding on microtubules. J. Cell Biol. 107: 1449-1459.

Hongisto V, Vainio JC, Thompson R, Courtney MJ, Coffey ET, 2008. The Wnt pool of glycogen synthase kinase 3beta is critical for trophic-deprivation-induced neuronal death. Mol. Cell Biol. 28: 1515-1527.

Hooper C, Killick R, Lovestone S, 2008. The GSK3 hypothesis of Alzheimer's disease. J. Neurochem. 104: 1433-1439.

Hort J, O'Brien JT, Gainotti G, Pirttila T, Popescu BO, Rektorova I, Sorbi S, Scheltens P, 2010. EFNS guidelines for the diagnosis and management of Alzheimer's disease. Eur. J. Neurol. 17: 1236–1248.

Hosono T, Tanaka T, Tanji K, Nakatani T, Kamitani T, 2010. NUB1, an interferon-inducible protein, mediates anti-proliferative actions and apoptosis in renal cell carcinoma cells through cell-cycle regulation. Br. J. Cancer 102: 873-882.

Howarth JL, Kelly S, Keasey MP, Glover CP, Lee YB, Mitrophanous K, Chapple JP, Gallo JM, Cheetham ME, Uney JB, 2007. Hsp40 molecules that target to the ubiquitin-proteasome system decrease inclusion formation in models of polyglutamine disease. Mol. Ther. 15: 1100-1105.

Hur EM, Zhou FQ, 2010. GSK3 signalling in neural development. Nat. Rev. Neurosci. 11: 539-551.

Hurley JH, Lee S, Prag G, 2006. Ubiquitin-binding domains. Biochem. J. 399: 361-372.

Ingelson M, Vanmechelen E, Lannfelt L, 1996. Microtubule-associated protein tau in human fibroblasts with the Swedish Alzheimer mutation. Neurosci. Lett. 220: 9-12.

Ittner LM, Ke YD, Delerue F, Bi M, Gladbach A, van EJ, Wolfing H, Chieng BC, Christie MJ, Napier IA, Eckert A, Staufenbiel M, Hardeman E, Gotz J, 2010. Dendritic function of tau mediates amyloid-beta toxicity in Alzheimer's disease mouse models. Cell 142: 387-397.

Ittner LM, Gotz J, 2011. Amyloid-beta and tau--a toxic pas de deux in Alzheimer's disease. Nat. Rev. Neurosci. 12: 65-72.

Jana NR, Nukina N, 2005. BAG-1 associates with the polyglutamine-expanded huntingtin aggregates. Neurosci. Lett. 378: 171-175.

Johnson GV, Stoothoff WH, 2004. Tau phosphorylation in neuronal cell function and dysfunction. J. Cell Sci. 117: 5721-5729.

Jones J, Wu K, Yang Y, Guerrero C, Nillegoda N, Pan ZQ, Huang L, 2008. A targeted proteomic analysis of the ubiquitin-like modifier nedd8 and associated proteins. J. Proteome. Res. 7: 1274-1287.

Joo Y, Ha S, Hong BH, Kim J, Chang KA, Liew H, Kim S, Sun W, Kim JH, Chong YH, Suh YH, Kim HS, 2010. Amyloid precursor protein binding protein-1 modulates cell cycle progression in fetal neural stem cells. PLoS. One. 5: e14203.

Jope RS, Johnson GV, 2004. The glamour and gloom of glycogen synthase kinase-3. Trends Biochem. Sci. 29: 95-102.

Kaganovich D, Kopito R, Frydman J, 2008. Misfolded proteins partition between two distinct quality control compartments. Nature 454: 1088-1095.

Kalveram B, Schmidtke G, Groettrup M, 2008. The ubiquitin-like modifier FAT10 interacts with HDAC6 and localizes to aggresomes under proteasome inhibition. J. Cell Sci. 121: 4079-4088.

Kamitani T, Kito K, Fukuda-Kamitani T, Yeh ET, 2001. Targeting of NEDD8 and its conjugates for proteasomal degradation by NUB1. J. Biol. Chem. 276: 46655-46660.

Kampinga HH, Hageman J, Vos MJ, Kubota H, Tanguay RM, Bruford EA, Cheetham ME, Chen B, Hightower LE, 2009. Guidelines for the nomenclature of the human heat shock proteins. Cell Stress. Chaperones. 14: 105-111.

Kanai Y, Hirokawa N, 1995. Sorting mechanisms of tau and MAP2 in neurons: suppressed axonal transit of MAP2 and locally regulated microtubule binding. Neuron 14: 421-432.

Kang Y, Zhang N, Koepp DM, Walters KJ, 2007. Ubiquitin receptor proteins hHR23a and hPLIC2 interact. J. Mol. Biol. 365: 1093-1101.

Keck S, Nitsch R, Grune T, Ullrich O, 2003. Proteasome inhibition by paired helical filament-tau in brains of patients with Alzheimer's disease. J. Neurochem. 85: 115-122.

Keller JN, Hanni KB, Markesbery WR, 2000. Impaired proteasome function in Alzheimer's disease. J. Neurochem. 75: 436-9.

Kelley LA, Sternberg MJ, 2009. Protein structure prediction on the Web: a case study using the Phyre server. Nat. Protoc. 4: 363-371.

Kermer P, Krajewska M, Zapata JM, Takayama S, Mai J, Krajewski S, Reed JC, 2002. Bag1 is a regulator and marker of neuronal differentiation. Cell Death. Differ. 9: 405-413.

Kerscher O, Felberbaum R, Hochstrasser M, 2006. Modification of proteins by ubiquitin and ubiquitin-like proteins. Annu. Rev. Cell Dev. Biol. 22: 159-180.

Kim SH, Shi Y, Hanson KA, Williams LM, Sakasai R, Bowler MJ, Tibbetts RS, 2009. Potentiation of amyotrophic lateral sclerosis (ALS)-associated TDP-43 aggregation by the proteasome-targeting factor, ubiquilin 1. J. Biol. Chem. 284: 8083-8092.

Kleijnen MF, Shih AH, Zhou P, Kumar S, Soccio RE, Kedersha NL, Gill G, Howley PM, 2000. The hPLIC proteins may provide a link between the ubiquitination machinery and the proteasome. Mol. Cell 6: 409-419.

Klein C, Kramer EM, Cardine AM, Schraven B, Brandt R, Trotter J, 2002. Process outgrowth of oligodendrocytes is promoted by interaction of fyn kinase with the cytoskeletal protein tau. J. Neurosci. 22: 698-707.

Ko HS, Uehara T, Tsuruma K, Nomura Y, 2004. Ubiquilin interacts with ubiquitylated proteins and proteasome through its ubiquitin-associated and ubiquitin-like domains. FEBS Lett. 566: 110-114.

Kopito RR, 2000. Aggresomes, inclusion bodies and protein aggregation. Trends Cell Biol. 10: 524-530.

Kril JJ, Patel S, Harding AJ, Halliday GM, 2002. Neuron loss from the hippocampus of Alzheimer's disease exceeds extracellular neurofibrillary tangle formation. Acta Neuropathol. 103: 370-376.

Kudo N, Wolff B, Sekimoto T, Schreiner EP, Yoneda Y, Yanagida M, Horinouchi S, Yoshida M, 1998. Leptomycin B inhibition of signal-mediated nuclear export by direct binding to CRM1. Exp. Cell Res. 242: 540-547.

Kumar P, Ambasta RK, Veereshwarayya V, Rosen KM, Kosik KS, Band H, Mestril R, Patterson C, Querfurth HW, 2007. CHIP and HSPs interact with beta-APP in a proteasome-dependent manner and influence Abeta metabolism. Hum. Mol. Genet. 16: 848-864.

Kumar S, Tomooka Y, Noda M, 1992. Identification of a set of genes with developmentally down-regulated expression in the mouse brain. Biochem. Biophys. Res. Commun. 185: 1155-1161.

Kuusisto E, Salminen A, Alafuzoff I, 2001. Ubiquitin-binding protein p62 is present in neuronal and glial inclusions in human tauopathies and synucleinopathies. Neuroreport 12: 2085-2090.

LaFerla FM, Green KN, Oddo S, 2007. Intracellular amyloid-beta in Alzheimer's disease. Nat. Rev. Neurosci. 8: 499-509.

Lasker K, Förster F, Bohn S, Walzthoeni T, Villa E, Unverdorben P, Beck F, Aebersold R, Sali A, Baumeister W, 2012. Molecular architecture of the 26S proteasome holocomplex determined by an integrative approach. Proc. Natl. Acad. Sci. USA. 109: 1380-7.

Lau KF, Miller CC, Anderton BH, Shaw PC, 1999. Expression analysis of glycogen synthase kinase-3 in human tissues. J. Pept. Res. 54: 85-91.

Lee DH, Goldberg AL, 1998. Proteasome inhibitors: valuable new tools for cell biologists. Trends Cell Biol. 8: 397-403.

Lee G, 2005. Tau and src family tyrosine kinases. Biochim. Biophys. Acta 1739: 323-330.

Lee G, Rook SL, 1992. Expression of tau protein in non-neuronal cells: microtubule binding and stabilization. J. Cell Sci. 102 (Pt 2): 227-237.

Lee HG, Casadesus G, Zhu X, Castellani RJ, McShea A, Perry G, Petersen RB, Bajic V, Smith MA, 2009. Cell cycle re-entry mediated neurodegeneration and its treatment role in the pathogenesis of Alzheimer's disease. Neurochem. Int. 54: 84-88.

Lee JY, Nagano Y, Taylor JP, Lim KL, Yao TP, 2010. Disease-causing mutations in parkin impair mitochondrial ubiquitination, aggregation, and HDAC6-dependent mitophagy. J. Cell Biol. 189: 671-679.

Lee MR, Lee D, Shin SK, Kim YH, Choi CY, 2008. Inhibition of APP intracellular domain (AICD) transcriptional activity via covalent conjugation with Nedd8. Biochem. Biophys. Res. Commun. 366: 976-981.

Lee VM, Goedert M, Trojanowski JQ, 2001. Neurodegenerative tauopathies. Annu. Rev. Neurosci. 24: 1121-1159.

Lei P, Ayton S, Bush AI, Adlard PA, 2011. GSK-3 in Neurodegenerative Diseases. Int. J. Alzheimers. Dis. 2011: 189246.

Lewis SA, Ivanov IE, Lee GH, Cowan NJ, 1989. Organization of microtubules in dendrites and axons is determined by a short hydrophobic zipper in microtubule-associated proteins MAP2 and tau. Nature 342: 498-505.

Li T, Hawkes C, Qureshi HY, Kar S, Paudel HK, 2006. Cyclin-dependent protein kinase 5 primes microtubule-associated protein tau site-specifically for glycogen synthase kinase 3beta. Biochemistry 45: 3134-3145.

Li T, Santockyte R, Yu S, Shen RF, Tekle E, Lee CG, Yang DC, Chock PB, 2011. FAT10 modifies p53 and upregulates its transcriptional activity. Arch. Biochem. Biophys. 509: 164-169.

Lim CB, Zhang D, Lee CG, 2006. FAT10, a gene up-regulated in various cancers, is cell-cycle regulated. Cell Div. 1: 20.

Lim KL, Lim GG, 2011. K63-linked ubiquitination and neurodegeneration. Neurobiol. Dis. 43: 9-16.

Lin H, Vicini S, Hsu FC, Doshi S, Takano H, Coulter DA, Lynch DR, 2010. Axonal alpha7 nicotinic ACh receptors modulate presynaptic NMDA receptor expression and structural plasticity of glutamatergic presynaptic boutons. Proc. Natl. Acad. Sci. U. S. A 107: 16661-16666.

Liu F, Li B, Tung EJ, Grundke-Iqbal I, Iqbal K, Gong CX, 2007. Site-specific effects of tau phosphorylation on its microtubule assembly activity and self-aggregation. Eur. J. Neurosci. 26: 3429-3436.

Liu G, Xirodimas DP, 2010. NUB1 promotes cytoplasmic localization of p53 through cooperation of the NEDD8 and ubiquitin pathways. Oncogene 29: 2252-2261.

Liu J, Furukawa M, Matsumoto T, Xiong Y, 2002. NEDD8 modification of CUL1 dissociates p120(CAND1), an inhibitor of CUL1-SKP1 binding and SCF ligases. Mol. Cell 10: 1511-1518.

Liu YC, Pan J, Zhang C, Fan W, Collinge M, Bender JR, Weissman SM, 1999. A MHC-encoded ubiquitin-like protein (FAT10) binds noncovalently to the spindle assembly checkpoint protein MAD2. Proc. Natl. Acad. Sci. U. S. A 96: 4313-4318.

Lopes JP, Oliveira CR, Agostinho P, 2009. Cdk5 acts as a mediator of neuronal cell cycle re-entry triggered by amyloid-beta and prion peptides. Cell Cycle 8: 97-104.

Lovestone S, Reynolds CH, Latimer D, Davis DR, Anderton BH, Gallo JM, Hanger D, Mulot S, Marquardt B, Stabel S, 1994. Alzheimer's disease-like phosphorylation of the microtubule-associated protein tau by glycogen synthase kinase-3 in transfected mammalian cells. Curr. Biol. 4: 1077-1086.

Lovestone S, Hartley CL, Pearce J, Anderton BH, 1996. Phosphorylation of tau by glycogen synthase kinase-3 beta in intact mammalian cells: the effects on the organization and stability of microtubules. Neuroscience 73: 1145-1157.

Lovestone S, Davis DR, Webster MT, Kaech S, Brion JP, Matus A, Anderton BH, 1999. Lithium reduces tau phosphorylation: effects in living cells and in neurons at therapeutic concentrations. Biol. Psychiatry 45: 995-1003.

Low P, 2011. The role of ubiquitin-proteasome system in ageing. Gen. Comp Endocrinol. 172: 39-43.

Lucas JJ, Hernandez F, Gomez-Ramos P, Moran MA, Hen R, Avila J, 2001. Decreased nuclear beta-catenin, tau hyperphosphorylation and neurodegeneration in GSK-3beta conditional transgenic mice. EMBO J. 20: 27-39.

Luk KC, Mills IP, Trojanowski JQ, Lee VM, 2008. Interactions between Hsp70 and the hydrophobic core of alpha-synuclein inhibit fibril assembly. Biochemistry 47: 12614-12625.

Lukasiak S, Schiller C, Oehlschlaeger P, Schmidtke G, Krause P, Legler DF, Autschbach F, Schirmacher P, Breuhahn K, Groettrup M, 2008. Proinflammatory cytokines cause FAT10 upregulation in cancers of liver and colon. Oncogene 27: 6068-6074.

Luo W, Sun W, Taldone T, Rodina A, Chiosis G, 2010. Heat shock protein 90 in neurodegenerative diseases. Mol. Neurodegener. 5: 24.

Mackenzie IR, Neumann M, Bigio EH, Cairns NJ, Alafuzoff I, Kril J, Kovacs GG, Ghetti B, Halliday G, Holm IE, Ince PG, Kamphorst W, Revesz T, Rozemuller AJ, Kumar-Singh S, Akiyama H, Baborie A, Spina S, Dickson DW, Trojanowski JQ, Mann DM, 2009. Nomenclature for neuropathologic subtypes of frontotemporal lobar degeneration: consensus recommendations. Acta Neuropathol. 117: 15-18.

Magdesian MH, Carvalho MM, Mendes FA, Saraiva LM, Juliano MA, Juliano L, Garcia-Abreu J, Ferreira ST, 2008. Amyloid-beta binds to the extracellular cysteine-rich domain of Frizzled and inhibits Wnt/beta-catenin signaling. J. Biol. Chem. 283: 9359-9368.

Mah AL, Perry G, Smith MA, Monteiro MJ, 2000. Identification of ubiquilin, a novel presenilin interactor that increases presenilin protein accumulation. J. Cell Biol. 151: 847-862.

Martin L, Latypova X, Terro F, 2011. Post-translational modifications of tau protein: implications for Alzheimer's disease. Neurochem. Int. 58: 458-471.

Martinez-Vicente M, Cuervo AM, 2007. Autophagy and neurodegeneration: when the cleaning crew goes on strike. Lancet Neurol. 6: 352-361.

Mattson MP, Magnus T, 2006. Ageing and neuronal vulnerability. Nat. Rev. Neurosci. 7: 278-294.

Meng L, Mohan R, Kwok BH, Elofsson M, Sin N, Crews CM, 1999. Epoxomicin, a potent and selective proteasome inhibitor, exhibits in vivo antiinflammatory activity. Proc. Natl. Acad. Sci. U. S. A 96: 10403-10408.

Merlet J, Burger J, Gomes JE, Pintard L, 2009. Regulation of cullin-RING E3 ubiquitin-ligases by neddylation and dimerization. Cell Mol. Life Sci. 66: 1924-1938.

Mizuno Y, Amari M, Takatama M, Aizawa H, Mihara B, Okamoto K, 2006. Immunoreactivities of p62, an ubiqutin-binding protein, in the spinal anterior horn cells of patients with amyotrophic lateral sclerosis. J. Neurol. Sci. 249: 13-18.

Moreno-Gonzalez I, Soto C, 2011. Misfolded protein aggregates: mechanisms, structures and potential for disease transmission. Semin. Cell Dev. Biol. 22: 482-487.

Mori F, Nishie M, Piao YS, Kito K, Kamitani T, Takahashi H, Wakabayashi K, 2005. Accumulation of NEDD8 in neuronal and glial inclusions of neurodegenerative disorders. Neuropathol. Appl. Neurobiol. 31: 53-61.

Mori F, Tanji K, Odagiri S, Toyoshima Y, Yoshida M, Ikeda T, Sasaki H, Kakita A, Takahashi H, Wakabayashi K, 2012. Ubiquilin immunoreactivity in cytoplasmic and nuclear inclusions in synucleinopathies, polyglutamine diseases and intranuclear inclusion body disease. Acta Neuropathol. 124:149-51.

Morishima Y, Gotoh Y, Zieg J, Barrett T, Takano H, Flavell R, Davis RJ, Shirasaki Y, Greenberg ME, 2001. Beta-amyloid induces neuronal apoptosis via a mechanism that involves the c-Jun N-terminal kinase pathway and the induction of Fas ligand. J. Neurosci. 21: 7551-7560.

Morris M, Maeda S, Vossel K, Mucke L, 2011. The many faces of tau. Neuron 70: 410-426.

Muchowski PJ, Wacker JL, 2005. Modulation of neurodegeneration by molecular chaperones. Nat. Rev. Neurosci. 6: 11-22.

Muller R, Heinrich M, Heck S, Blohm D, Richter-Landsberg C, 1997. Expression of microtubule-associated proteins MAP2 and tau in cultured rat brain oligodendrocytes. Cell Tissue Res. 288: 239-249.

Muller T, Meyer HE, Egensperger R, Marcus K, 2008. The amyloid precursor protein intracellular domain (AICD) as modulator of gene expression, apoptosis, and cytoskeletal dynamics-relevance for Alzheimer's disease. Prog. Neurobiol. 85: 393-406.

Multhaup G, 2006. Amyloid precursor protein and BACE function as oligomers. Neurodegener. Dis. 3: 270-274.

N'Diaye EN, Hanyaloglu AC, Kajihara KK, Puthenveedu MA, Wu P, von ZM, Brown EJ, 2008. The ubiquitin-like protein PLIC-2 is a negative regulator of G protein-coupled receptor endocytosis. Mol. Biol. Cell. 19: 1252-1260.

N'Diaye EN, Kajihara KK, Hsieh I, Morisaki H, Debnath J, Brown EJ, 2009. PLIC proteins or ubiquilins regulate autophagy-dependent cell survival during nutrient starvation. EMBO Rep. 10: 173-179.

Nagashima Y, Kowa H, Tsuji S, Iwata A, 2011. FAT10 protein binds to polyglutamine proteins and modulates their solubility. J. Biol. Chem. 286: 29594-29600.

Nijholt DA, van Haastert ES, Rozemuller AJ, Scheper W, Hoozemans JJ, 2011. The unfolded protein response is associated with early tau pathology in the hippocampus of tauopathies. J. Pathol. 226: 693-702.

O'Brien RJ, Wong PC, 2011. Amyloid precursor protein processing and Alzheimer's disease. Annu. Rev. Neurosci. 34: 185-204.

Oddo S, 2008. The ubiquitin-proteasome system in Alzheimer's disease. J. Cell Mol. Med. 12: 363-373.

Otero JH, Lizak B, Hendershot LM, 2010. Life and death of a BiP substrate. Semin. Cell Dev. Biol. 21: 472-478.

Otvos L, Jr., Feiner L, Lang E, Szendrei GI, Goedert M, Lee VM, 1994. Monoclonal antibody PHF-1 recognizes tau protein phosphorylated at serine residues 396 and 404. J. Neurosci. Res. 39: 669-673.

Panda D, Goode BL, Feinstein SC, Wilson L, 1995. Kinetic stabilization of microtubule dynamics at steady state by tau and microtubule-binding domains of tau. Biochemistry 34: 11117-11127.

Pandey UB, Nie Z, Batlevi Y, McCray BA, Ritson GP, Nedelsky NB, Schwartz SL, DiProspero NA, Knight MA, Schuldiner O, Padmanabhan R, Hild M, Berry DL, Garza D, Hubbert CC, Yao TP, Baehrecke EH, Taylor JP, 2007. HDAC6 rescues neurodegeneration and provides an essential link between autophagy and the UPS. Nature 447: 859-863.

Pankiv S, Clausen TH, Lamark T, Brech A, Bruun JA, Outzen H, Overvatn A, Bjorkoy G, Johansen T, 2007. p62/SQSTM1 binds directly to Atg8/LC3 to facilitate degradation of ubiquitinated protein aggregates by autophagy. J. Biol. Chem. 282: 24131-24145.

Parfitt DA, Michael GJ, Vermeulen EG, Prodromou NV, Webb TR, Gallo JM, Cheetham ME, Nicoll WS, Blatch GL, Chapple JP, 2009. The ataxia protein sacsin is a functional co-chaperone that protects against polyglutamine-expanded ataxin-1. Hum. Mol. Genet. 18: 1556-1565.

Phinney AL, Calhoun ME, Wolfe DP, Lipp HP, Zheng H, Jucker M, 1999. No hippocampal neuron or synaptic bouton loss in learning-impaired aged β-amyloid precursor protein-null mice. Neuroscience. 90: 1207-1216.

Plattner F, Angelo M, Giese KP, 2006. The roles of cyclin-dependent kinase 5 and glycogen synthase kinase 3 in tau hyperphosphorylation. J. Biol. Chem. 281: 25457-25465.

Plowey ED, Chu CT, 2011. Synaptic dysfunction in genetic models of Parkinson's disease: a role for autophagy? Neurobiol. Dis. 43: 60-67.

Pooler AM, Hanger DP, 2010. Functional implications of the association of tau with the plasma membrane. Biochem. Soc. Trans. 38: 1012-1015.

Pooler AM, Usardi A, Evans CJ, Philpott KL, Noble W, Hanger DP, 2012. Dynamic association of tau with neuronal membranes is regulated by phosphorylation. Neurobiol. Aging 33: 431-438.

Porzig R, Singer D, Hoffmann R, 2007. Epitope mapping of mAbs AT8 and Tau5 directed against hyperphosphorylated regions of the human tau protein. Biochem. Biophys. Res. Commun. 358: 644-649.

Qian W, Shi J, Yin X, Iqbal K, Grundke-Iqbal I, Gong CX, Liu F, 2010. PP2A regulates tau phosphorylation directly and also indirectly via activating GSK-3beta. J. Alzheimers. Dis. 19: 1221-1229.

Raasi S, Schmidtke G, Groettrup M, 2001. The ubiquitin-like protein FAT10 forms covalent conjugates and induces apoptosis. J. Biol. Chem. 276: 35334-35343.

Raasi S, Varadan R, Fushman D, Pickart CM, 2005. Diverse polyubiquitin interaction properties of ubiquitin-associated domains. Nat. Struct. Mol. Biol. 12: 708-714.

Rademakers R, Neumann M, Mackenzie IR, 2012. Advances in understanding the molecular basis of frontotemporal dementia. Nat. Rev. Neurol. Advance online publication 26 June 2012.

Rani N, Aichem A, Schmidtke G, Kreft SG., Groettrup M, 2012. FAT10 and NUB1L bind to the VWA domain of Rpn10 and Rpn1 to enable proteasome-mediated proteolysis. Nat. Commun. **3**, 749

Rankin CA, Sun Q, Gamblin TC, 2008. Pre-assembled tau filaments phosphorylated by GSK-3b form large tangle-like structures. Neurobiol. Dis. 31: 368-377.

Regan-Klapisz E, Sorokina I, Voortman J, de KP, Roovers RC, Verheesen P, Urbe S, Fallon L, Fon EA, Verkleij A, Benmerah A, van Bergen en Henegouwen

PM, 2005. Ubiquilin recruits Eps15 into ubiquitin-rich cytoplasmic aggregates via a UIM-UBL interaction. J. Cell Sci. 118: 4437-4450.

Reiman EM, Chen K, Liu X, Bandy D, Yu M, Lee W, Ayutyanont N, Keppler J, Reeder SA, Langbaum JB, Alexander GE, Klunk WE, Mathis CA, Price JC, Aizenstein HJ, DeKosky ST, Caselli RJ, 2009. Fibrillar amyloid-beta burden in cognitively normal people at 3 levels of genetic risk for Alzheimer's disease. Proc. Natl. Acad. Sci. U. S. A 106: 6820-6825.

Reina CP, Zhong X, Pittman RN, 2010. Proteotoxic stress increases nuclear localization of ataxin-3. Hum. Mol. Genet. 19: 235-249.

Reitz C, Brayne C, Mayeux R, 2011. Epidemiology of Alzheimer disease. Nat. Rev. Neurol. 7: 137-152.

Rendon A, Jung D, Jancsik V, 1990. Interaction of microtubules and microtubule-associated proteins (MAPs) with rat brain mitochondria. Biochem. J. 269: 555-556.

Reyes-Turcu FE, Wilkinson KD, 2009. Polyubiquitin binding and disassembly by deubiquitinating enzymes. Chem. Rev. 109: 1495-1508.

Riederer BM, Leuba G, Vernay A, Riederer IM, 2011. The role of the ubiquitin proteasome system in Alzheimer's disease. Exp. Biol. Med. (Maywood.) 236: 268-276.

Rosen KM, Moussa CE, Lee HK, Kumar P, Kitada T, Qin G, Fu Q, Querfurth HW, 2010. Parkin reverses intracellular beta-amyloid accumulation and its negative effects on proteasome function. J. Neurosci. Res. 88: 167-178.

Ross CA, Poirier MA, 2005. Opinion: What is the role of protein aggregation in neurodegeneration? Nat. Rev. Mol. Cell Biol. 6: 891-898.

Ryves WJ, Harwood AJ, 2001. Lithium inhibits glycogen synthase kinase-3 by competition for magnesium. Biochem. Biophys. Res. Commun. 280: 720-725.

Safadi SS, Barber KR, Shaw GS, 2011. Impact of autosomal recessive juvenile Parkinson's disease mutations on the structure and interactions of the parkin ubiquitin-like domain. Biochemistry 50: 2603-2610.

Sahara N, Murayama M, Mizoroki T, Urushitani M, Imai Y, Takahashi R, Murata S, Tanaka K, Takashima A, 2005. In vivo evidence of CHIP up-regulation attenuating tau aggregation. J. Neurochem. 94: 1254-1263.

Sakata E, Yamaguchi Y, Kurimoto E, Kikuchi J, Yokoyama S, Yamada S, Kawahara H, Yokosawa H, Hattori N, Mizuno Y, Tanaka K, Kato K, 2003. Parkin binds the Rpn10 subunit of 26S proteasomes through its ubiquitin-like domain. EMBO Rep. 4: 301-306.

Saliba RS, Pangalos M, Moss SJ, 2008. The ubiquitin-like protein Plic-1 enhances the membrane insertion of GABAA receptors by increasing their stability within the endoplasmic reticulum. J. Biol. Chem. 283: 18538-18544.

Salminen A, Kaarniranta K, Haapasalo A, Hiltunen M, Soininen H, Alafuzoff I, 2012. Emerging role of p62/sequestosome-1 in the pathogenesis of Alzheimer's disease. Prog. Neurobiol. 96: 87-95.

Schmidtke G, Kalveram B, Groettrup M, 2009. Degradation of FAT10 by the 26S proteasome is independent of ubiquitylation but relies on NUB1L. FEBS Lett. 583: 591-594.

Schmidtke G, Kalveram B, Weber E, Bochtler P, Lukasiak S, Hipp MS, Groettrup M, 2006. The UBA domains of NUB1L are required for binding but not for accelerated degradation of the ubiquitin-like modifier FAT10. J. Biol. Chem. 281: 20045-20054.

Schneider A, Mandelkow E, 2008. Tau-based treatment strategies in neurodegenerative diseases. Neurotherapeutics. 5: 443-457.

Selkoe DJ, 2001. Alzheimer's disease: genes, proteins, and therapy. Physiol Rev. 81: 741-766.

Selkoe DJ, 2011. Resolving controversies on the path to Alzheimer's therapeutics. Nat. Med. 17: 1060-1065.

Sengupta A, Kabat J, Novak M, Wu Q, Grundke-Iqbal I, Iqbal K, 1998. Phosphorylation of tau at both Thr 231 and Ser 262 is required for maximal inhibition of its binding to microtubules. Arch. Biochem. Biophys. 357: 299-309.

Shang F, Taylor A, 2011. Ubiquitin-proteasome pathway and cellular responses to oxidative stress. Free Radic. Biol. Med. 51: 5-16.

Shen LN, Liu H, Dong C, Xirodimas D, Naismith JH, Hay RT, 2005. Structural basis of NEDD8 ubiquitin discrimination by the deNEDDylating enzyme NEDP1. EMBO J. 24: 1341-1351.

Shimura H, Schlossmacher MG, Hattori N, Frosch MP, Trockenbacher A, Schneider R, Mizuno Y, Kosik KS, Selkoe DJ, 2001. Ubiquitination of a new form of alpha-synuclein by parkin from human brain: implications for Parkinson's disease. Science 293: 263-269.

Shin RW, Kitamoto T, Tateishi J, 1991. Modified tau is present in younger nondemented persons: a study of subcortical nuclei in Alzheimer's disease and progressive supranuclear palsy. Acta Neuropathol. 81: 517-523.

Slifer MA, Martin ER, Bronson PG, Browning-Large C, Doraiswamy PM, Welsh-Bohmer KA, Gilbert JR, Haines JL, Pericak-Vance MA, 2006. Lack of

association between UBQLN1 and Alzheimer disease. Am. J. Med. Genet. B Neuropsychiatr. Genet. 141B: 208-213.

Smemo S, Nowotny P, Hinrichs AL, Kauwe JS, Cherny S, Erickson K, Myers AJ, Kaleem M, Marlowe L, Gibson AM, Hollingworth P, O'Donovan MC, Morris CM, Holmans P, Lovestone S, Morris JC, Thal L, Li Y, Grupe A, Hardy J, Owen MJ, Williams J, Goate A, 2006. Ann. Neurol. 59: 21-6.

Sokolow S, Henkins KM, Williams IA, Vinters HV, Schmid I, Cole GM, Gylys KH, 2011. Isolation of synaptic terminals from Alzheimer's disease cortex. Cytometry A.

Song S, Jung YK, 2004. Alzheimer's disease meets the ubiquitin-proteasome system. Trends Mol. Med. 10: 565-570.

Song S, Kim SY, Hong YM, Jo DG, Lee JY, Shim SM, Chung CW, Seo SJ, Yoo YJ, Koh JY, Lee MC, Yates AJ, Ichijo H, Jung YK, 2003. Essential role of E2-25K/Hip-2 in mediating amyloid-beta neurotoxicity. Mol. Cell 12: 553-563.

Sroka K, Voigt A, Deeg S, Reed JC, Schulz JB, Bahr M, Kermer P, 2009. BAG1 modulates huntingtin toxicity, aggregation, degradation, and subcellular distribution. J. Neurochem. 111: 801-807.

Stamer K, Vogel R, Thies E, Mandelkow E, Mandelkow EM, 2002. Tau blocks traffic of organelles, neurofilaments, and APP vesicles in neurons and enhances oxidative stress. J. Cell Biol. 156: 1051-1063.

Sun W, Qureshi HY, Cafferty PW, Sobue K, garwal-Mawal A, Neufield KD, Paudel HK, 2002. Glycogen synthase kinase-3beta is complexed with tau protein in brain microtubules. J. Biol. Chem. 277: 11933-11940.

Taelman VF, Dobrowolski R, Plouhinec JL, Fuentealba LC, Vorwald PP, Gumper I, Sabatini DD, De Robertis EM, 2010. Wnt signaling requires sequestration of glycogen synthase kinase 3 inside multivesicular endosomes. Cell 143: 1136-1148.

Tajes M, Gutierrez-Cuesta J, Folch J, Ferrer I, Caballero B, Smith MA, Casadesus G, Camins A, Pallas M, 2008. Lithium treatment decreases activities of tau kinases in a murine model of senescence. J. Neuropathol. Exp. Neurol. 67: 612-623.

Takashima A, Murayama M, Murayama O, Kohno T, Honda T, Yasutake K, Nihonmatsu N, Mercken M, Yamaguchi H, Sugihara S, Wolozin B, 1998. Presenilin 1 associates with glycogen synthase kinase-3beta and its substrate tau. Proc. Natl. Acad. Sci. U. S. A 95: 9637-9641.

Tanaka T, Kawashima H, Yeh ET, Kamitani T, 2003. Regulation of the NEDD8 conjugation system by a splicing variant, NUB1L. J. Biol. Chem. 278: 32905-32913.

Tanaka T, Yeh ET, Kamitani T, 2004. NUB1-mediated targeting of the ubiquitin precursor UbC1 for its C-terminal hydrolysis. Eur. J. Biochem. 271: 972-982.

Tanji K, Mori F, Kakita A, Zhang H, Kito K, Kamitani T, Takahashi H, Wakabayashi K, 2007. Immunohistochemical localization of NUB1, a synphilin-1-binding protein, in neurodegenerative disorders. Acta Neuropathol. 114: 365-371.

Tanji K, Mori F, Kito K, Kakita A, Mimura J, Itoh K, Takahashi H, Kamitani T, Wakabayashi K, 2011. Synphilin-1-binding protein NUB1 is colocalized with nonfibrillar, proteinase K-resistant alpha-synuclein in presynapses in Lewy body disease. J. Neuropathol. Exp. Neurol. 70: 879-889.

Tanji K, Tanaka T, Kamitani T, 2005. Interaction of NUB1 with the proteasome subunit S5a. Biochem. Biophys. Res. Commun. 337: 116-120.

Tanji K, Tanaka T, Mori F, Kito K, Takahashi H, Wakabayashi K, Kamitani T, 2006. NUB1 suppresses the formation of Lewy body-like inclusions by proteasomal degradation of synphilin-1. Am. J. Pathol. 169: 553-565.

Tateishi K, Omata M, Tanaka K, Chiba T, 2001. The NEDD8 system is essential for cell cycle progression and morphogenetic pathway in mice. J. Cell Biol. 155: 571-579.

Taylor JP, Tanaka F, Robitschek J, Sandoval CM, Taye A, Markovic-Plese S, Fischbeck KH, 2003. Aggresomes protect cells by enhancing the degradation of toxic polyglutamine-containing protein. Hum. Mol. Genet. 12: 749-757.

Tetzlaff JE, Putcha P, Outeiro TF, Ivanov A, Berezovska O, Hyman BT, McLean PJ, 2008. CHIP targets toxic alpha-Synuclein oligomers for degradation. J. Biol. Chem. 283: 17962-17968.

Thal DR, Rub U, Orantes M, Braak H, 2002. Phases of A beta-deposition in the human brain and its relevance for the development of AD. Neurology 58: 1791-1800.

Tian Q, Wang J, 2002. Role of serine/threonine protein phosphatase in Alzheimer's disease. Neurosignals. 11: 262-269.

Townsend M, Mehta T, Selkoe DJ, 2007. Soluble Abeta inhibits specific signal transduction cascades common to the insulin receptor pathway. J. Biol. Chem. 282: 33305-33312.

Trojanowski JQ, Schuck T, Schmidt ML, Lee VM, 1989. Distribution of tau proteins in the normal human central and peripheral nervous system. J. Histochem. Cytochem. 37: 209-215.

Upadhya SC, Hegde AN, 2007. Role of the ubiquitin proteasome system in Alzheimer's disease. BMC. Biochem. 8 Suppl 1: S12.

Utton MA, Noble WJ, Hill JE, Anderton BH, Hanger DP, 2005. Molecular motors implicated in the axonal transport of tau and alpha-synuclein. J. Cell Sci. 118: 4645-4654.

van der Spuy J, Cheetham ME, 2004. The Leber congenital amaurosis protein AIPL1 modulates the nuclear translocation of NUB1 and suppresses inclusion formation by NUB1 fragments. J. Biol. Chem. 279: 48038-48047.

van der Spuy J, Kim JH, Yu YS, Szel A, Luthert PJ, Clark BJ, Cheetham ME, 2003. The expression of the Leber congenital amaurosis protein AIPL1 coincides with rod and cone photoreceptor development. Invest Ophthalmol. Vis. Sci. 44: 5396-5403.

Vanier MT, Neuville P, Michalik L, Launay JF, 1998. Expression of specific tau exons in normal and tumoral pancreatic acinar cells. J. Cell Sci. 111 (Pt 10): 1419-1432.

Viswanathan J, Haapasalo A, Bottcher C, Miettinen R, Kurkinen KM, Lu A, Thomas A, Maynard CJ, Romano D, Hyman BT, Berezovska O, Bertram L, Soininen H, Dantuma NP, Tanzi RE, Hiltunen M, 2011. Alzheimer's disease-associated ubiquilin-1 regulates presenilin-1 accumulation and aggresome formation. Traffic. 12: 330-348.

Voges D, Zwickl P, Baumeister W, 1999. The 26S proteasome: a molecular machine designed for controlled proteolysis. Annu. Rev. Biochem. 68: 1015-1068.

Wang G, Sawai N, Kotliarova S, Kanazawa I, Nukina N, 2000. Ataxin-3, the MJD1 gene product, interacts with the two human homologs of yeast DNA repair protein RAD23, HHR23A and HHR23B. Hum. Mol. Genet. 9: 1795-1803.

Wang YJ, Zhou HD, Zhou XF, 2006. Clearance of amyloid-beta in Alzheimer's disease: progress, problems and perspectives. Drug Discov. Today 11: 931-938.

Watson IR, Irwin MS, Ohh M, 2011. NEDD8 pathways in cancer, Sine Quibus Non. Cancer Cell 19: 168-176.

Wei N, Deng XW, 2003. The COP9 signalosome. Annu. Rev. Cell Dev. Biol. 19: 261-286.

Weingarten MD, Lockwood AH, Hwo SY, Kirschner MW, 1975. A protein factor essential for microtubule assembly. Proc. Natl. Acad. Sci. U. S. A 72: 1858-1862.

Weissmann C, Reyher HJ, Gauthier A, Steinhoff HJ, Junge W, Brandt R, 2009. Microtubule binding and trapping at the tip of neurites regulate tau motion in living neurons. Traffic. 10: 1655-1668.

Wen Y, Planel E, Herman M, Figueroa HY, Wang L, Liu L, Lau LF, Yu WH, Duff KE, 2008. Interplay between cyclin-dependent kinase 5 and glycogen synthase kinase 3 beta mediated by neuregulin signaling leads to differential effects on tau phosphorylation and amyloid precursor protein processing. J. Neurosci. 28: 2624-2632.

Wilquet V, De SB, 2004. Amyloid-beta precursor protein processing in neurodegeneration. Curr. Opin. Neurobiol. 14: 582-588.

Wilson RC, Hughes RC, Flatt JW, Meehan EJ, Ng JD, Twigg PD, 2009. Structure of full-length ubiquitin-conjugating enzyme E2-25K (huntingtin-interacting protein 2). Acta Crystallogr. Sect. F. Struct. Biol. Cryst. Commun. 65: 440-444.

Woods YL, Cohen P, Becker W, Jakes R, Goedert M, Wang X, Proud CG, 2001. The kinase DYRK phosphorylates protein-synthesis initiation factor eIF2Bepsilon at Ser539 and the microtubule-associated protein tau at Thr212: potential role for DYRK as a glycogen synthase kinase 3-priming kinase. Biochem. J. 355: 609-615.

Wooten MW, Geetha T, Babu JR, Seibenhener ML, Peng J, Cox N, az-Meco MT, Moscat J, 2008. Essential role of sequestosome 1/p62 in regulating accumulation of Lys63-ubiquitinated proteins. J. Biol. Chem. 283: 6783-6789.

Wyttenbach A, Sauvageot O, Carmichael J, az-Latoud C, Arrigo AP, Rubinsztein DC, 2002. Heat shock protein 27 prevents cellular polyglutamine toxicity and suppresses the increase of reactive oxygen species caused by huntingtin. Hum. Mol. Genet. 11: 1137-1151.

Xie Y, 2010. Structure, assembly and homeostatic regulation of the 26S proteasome. J. Mol. Cell Biol. 2: 308-317.

Xirodimas DP, 2008. Novel substrates and functions for the ubiquitin-like molecule NEDD8. Biochem. Soc. Trans. 36: 802-806.

Xirodimas DP, Saville MK, Bourdon JC, Hay RT, Lane DP, 2004. Mdm2-mediated NEDD8 conjugation of p53 inhibits its transcriptional activity. Cell 118: 83-97.

Yancopoulou D, Spillantini MG, 2003. Tau protein in familial and sporadic diseases. Neuromolecular. Med. 4: 37-48.

Zhang DW, Jeang KT, Lee CG, 2006. p53 negatively regulates the expression of FAT10, a gene upregulated in various cancers. Oncogene 25: 2318-2327.

Zheng H, Koo EH, 2006. The amyloid precursor protein: beyond amyloid. Mol. Neurodegener. 1: 5.

Appendix A

Reagents source

Antibodies

Name	Catalogue number	Supplier	Location
Anti-FAT10	PW9680	Biomol Enzo Life Science	Exeter, UK
Anti-NEDD8	PW9340		
Anti-GSK3β	1212010	Cell signalling	Hertfordshire, UK
Pan-tau	A0024	Dako	Cambridgeshire, UK
Anti-Ubiquitin	Z0458		
Swine anti-rabbit polyclonal	E0353		
Alexa Fluor® 488 anti-mouse	A11001	Invitrogen	Paisley, UK
Alexa Fluor® 488 anti-rabbit	A11008		
Alexa Fluor® 594 anti-mouse	A11005		
Alexa Fluor® 594 anti-rabbit	A11012		
Alexa Fluor® 647 anti-mouse	A21235		
Alexa Fluor® 647 anti-rabbit	A21244		
pS396	44752G		
Anti-Actin	A-5060	Sigma	Poole, UK
Anti-c-Myc	M4439		
Anti-FLAG	F1804		
Anti-GAPDH	G8735		
Mouse anti-HA	H9658		
Rabbit anti-HA	H6908		
Anti-tubulin	T4026		
AT8	MN1020	Thermo Scientific	Northumberland
GαM HRP	31430		
GαR HRP	31460		
Anti-NUB1	N/A	Genosys Biotechnology	Cambridge, UK

Molecular techniques

Name	Catalogue number	Supplier	Location
HISpeed Plasmid Midi kit	12643	QIAGEN	West Sussex, UK
Ampicillin	A1593	Sigma	Poole, UK
Kanamycin	60615		
Luria Broth media	L3522		
Agar	LP0013	OXOID	Hampshire, UK
JM109 competent cells	L1001	Promega	Southampton, UK
Petri dish	FB51506	Fisher Scientific	Loughborough, UK
Ethanol	101077Y	VWR	Lutterworth, UK
Isopropanol	102245K		
ON-TARGETplus Specificity-Enhanced small interfering RNA	N/A	Dharmacon, Thermo Scientific	Northumberland, UK

Cell culture

Name	Catalogue number	Supplier	Location
B27 ® supplement	0080085-SA	Invitrogen	Paisley, UK
DMEM	31331		
FBS	10108		
HBSS	14170		
L-Glutamine (GlutaMAX™)	35050038		
Lipofectamine ™	18324020		
Lipofectamine ® 2000	11668030		
Opti-MEM ®	31985-054		
Neurobasal ®-A media	12349		
Plus Reagent ®	11514015		
Penicillin-streptomycin	15140122		
Trypsin-EDTA	2530004		
Lithium Chloride (LiCl)	L4408	Sigma	Poole, UK
Corning® Costar® 12-well plates	3512		
T75 flask	353136	BD Falcon	Oxford, UK
6-well plates	351146		

Name	Catalogue number	Supplier	Location
DharmaFECT buffer I	T-2001-02	Thermo Scientific	Northumberland, UK
8-well Permanox chamber slide	17745	VWR	Lutterworth, UK
Coverslips glass 12 mm	734-1006		
SK-N-SH	86012802	ECACC	Salisbury, UK
SH-SY5Y cells	94030304		

Drugs

Name	Catalogue number	Supplier	Location
Cycloheximide	C7698	Sigma	Poole, UK
Epoxomicin	E3652		
Lactacystin	L6785		
Lithium Chloride (LiCl)	L0505		
DMSO	D4540		
MG132	BML-PI102-0025	Biomol Enzo Life Science	Exeter, UK

Common supplies

Name	Catalogue number	Supplier	Location
Glycerol	G6279	Sigma	Southampton, UK
BSA	A2153		
SDS	L4390		
Sodium pyrophosphate (Na_2HPO_4)	71321		
Tris-HCl	T3253		
Sodium phosphate (NaH_2PO_4)	567545	Merck	Middlesex, UK
PBS	BR0014G	OXOID	Hampshire, UK
Glycine	444495D	VWR	Lutterworth, UK
Methanol	20847.320		
Sodium chloride (NaCl)	102415K		

Immunohistochemistry

Name	Catalogue number	Supplier	Location
LSAB Dakocytomation kit	K0679	Dako	Cambridgeshire, UK
IMS	M/4400/17	Fisher Scientific	Loughborough, UK
Citric acid ($C_6H_8O_7$)	C0679	Sigma	Southampton, UK
DPX	44581		
Hydrogen peroxide (H_2O_2)	H-1009		
Sodium pyrophosphate (Na_2HPO_4)	S7907		
Normal Swine Serum	014.000.21	Stratech	Newmarket Suffolk, UK
Xylene	305 756	VWR	Lutterworth, UK

Immunocytochemistry

Name	Catalogue number	Supplier	Location
Dako mounting medium	S3023	Dako	Cambridgeshire, UK
DAPI	D9564	Sigma	Poole, UK
Glutaraldehyde	G6257		
Normal Goat serum	G9023		
Sodium borohydride ($NaBH_4$)	71321		
IGEPAL-CA630 (NP-40)	I3021		
Triton X-100	T8787		
PFA	F017	TAAB	Berks, UK

Biochemical assays

Name	Catalogue number	Supplier	Location
Protein Ladder	SM1811	Fermentas	York, UK
Acrylamide/Bisacrylamide 30%	EC-890-1	Fisher Scientific	Loughborough, UK
SDS PAGE Buffer	ELR-330-010Q		
Tris-glycine transfer buffer	ELR-322-010L		
ECL Plus reagent	RPN2132	GE Healthcare	Buckinghamshire, UK
Dynabeads	100.04D	Invitrogen	Paisley, UK
Super RX X-Ray Fuji film	JTS010	Labtech	East Sussex, UK
Ammonium persulphate (APS), $(NH_4)_2S_2O_8$	A 3678	Sigma	Southampton, UK
β-Mercaptoethanol	M3148		
Dithiothreitol (DTT)	D0632		
EGTA	E8145		
Magnesium Chloride ($MgCl_2$)	63068		
PhIC	P0044		
PIC	P8340		
PIPES	P-6757		
Ponceau-S	P3504		
Sodium Deoxycholate ($C_{24}H_{39}NaO_4$)	D6750		
TEMED	T92-81		
Tween -20	P9416		
BCA Protein Assay Kit	23 227	Thermo Scientific	Northumberland, UK
Acetic acid (glacial)	64-19-7	VWR	Lutterworth, UK
Bromophenol blue	44 305		
Nitrocellulose membrane	732 4007		

Appendix B

Solutions and buffers

Block solution for ICC

Goat serum	10 % (v/v)
BSA	3 % (w/v)
In PBS	

Block solution for IHC

Swine serum	10 % (v/v)
BSA	2 % (w/v)
In PBS	

BSA solution for antibody in IHC

BSA	0.1 % (w/v)
In PBS	

BSA-T block solution for immunoprecipitation

BSA	0.2 % (w/v)
Tween 20	0.02% (v/v)
In PBS	

Glutaraldehyde fixation

Glutaraldehyde	0.3 % (v/v)
Nonidet P-40 (NP-40)	0.5% (v/v)
In PEM	

Glycine solution

Glycine	0.1 M
In PBS	

2x Laemli buffer

Glycerol	10 % (v/v)
SDS	2.5 % (w/v)
Tris-HCl (pH 6.8)	60 mM
DTT	1 M
In ddH2O	

Lithium Chloride (LiCl)

LiCl	10 mM
In ddH2O	

Luria-Bertani Broth (LB) medium

Luria Broth	25 g/l
In ddH_2O, autoclaved	

LB agar

Luria Broth	25 g/l
Agar	15 g/l
In ddH_2O, autoclaved	

4X loading buffer

β-Mercaptoethanol	10 % (v/v)
Glycerol	20 % (v/v)
SDS	5 % (w/v)
Tris-HCl (pH 6.8)	125 mM
In ddH_2O	

Mc Ilvane's buffer

Citric acid	0.1 M
Na_2HPO_4	0.2 M
In ddH_2O	

Paraformaldehyde (PFA) fixation

PFA	3.7- 4 % (v/v)
In PBS	

Phosphate buffered saline (PBS)

NaCl	145 mM
NaH_2PO_4	3.6 mM
Na_2HPO_4	10.5 mM
In ddH_2O	

PBS-T

Tween 20	0.01 % (v/v)
In PBS	

Permeabilisation

Triton X-100	0.1 % (v/v)
In PBS	

Pipes/EGTA/$MgCl_2$ buffer (PEM)

Pipes	80 mM
EGTA	5 mM
$MgCl_2$	1 mM

In ddH_2O, pH 6.8

Ponceau S solution

Ponceau S red dye	0.1% (w/v)
Acetic acid	5 % (v/v)

In ddH_2O

RIPA buffer

Sodium deoxycholate	1 % (w/v)
NaCl	150 mM
NP-40	1 % (v/v)
SDS	0.1 % (w/v)
Tris-HCl (pH7.5)	50 mM

In ddH_2O

RIPA-Tween (RIPA-T) buffer

Tween-20	0.02% (v/v)

In RIPA buffer

0.1% SDS buffer

NaCl	150 mM
SDS	0.1 % (v/v)
Tris-HCl (pH 8)	10 mM

In ddH_2O

SDS-PAGE resolving gel (10%)

Tris-HCl (pH 8.8)	375 mM
Acrylamide/Bis-acrylamide	10% (v/v)
Ammonium persulfate	0.1% (v/v)
SDS	0.1% (w/v)
TEMED	0.05% (v/v)

In ddH2O

SDS-PAGE stacking gel (3%)

Tris-HCl (pH 6.8)	125 mM
Acrylamide/Bis-acrylamide	3 % (v/v)
APS	0.05% (v/v)
SDS	0.1% (w/v)
TEMED	0.08% (v/v)

In ddH_2O

SDS-PAGE running buffer

Tris-HCl	25 mM
Glycine	190 mM
SDS	3.5 mM

Sodium borohydride ($NaBH_4$) solution

$NaBH_4$	10 mg/l
In PBS	

Transfer buffer

Tris-HCl	25 mM
Glycine	192 mM
SDS	0.1% (w/v)
Methanol	20 % (v/v)

Appendix C

Supplementary figure

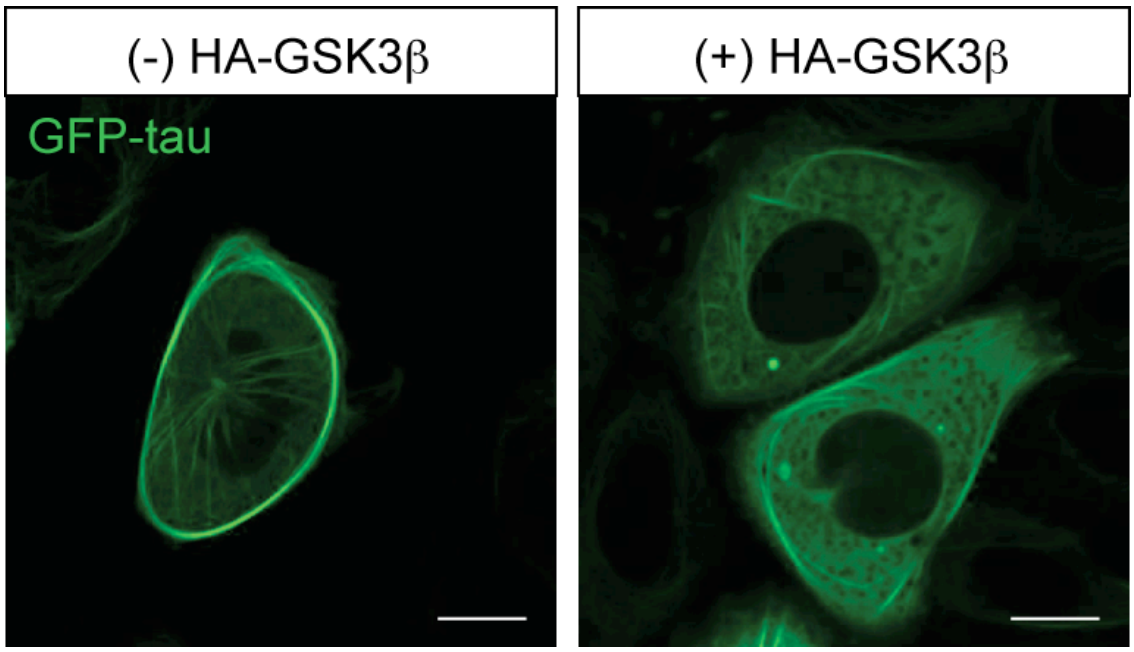

Supplementary Figure 1. *GFP-tau localisation with HA-GSK3β co-expression in live cells.* SK-N-SH cells were seeded on MatTek (MatTex Corp, MA, USA) slide dishes at a density of 600,000 cells/dish and after 24 hours were transfected with 100 ng of GFP-tau in the absence (-) or presence (+) of 150 ng of HA-GSK3β as described in chapter 2.3.2.2. Twenty-eight hours after transfection, cells were live imaged at 37°C with a Zeiss LSM510 confocal microscope (Carl Zeiss Ltd., Welwyn Garden City, Hertfordshire, UK). For FRAP measurements (not shown), a total of 40 images were acquired at one image per second. Supplementary figure 1 is a Z projection of the 40 images. Scale bar = 10 μm.